UNIVERSIDADE DE SÃO PAULO

UNIVERSITÉ DE STRASBOURG

Programa de Pós-Graduação Interunidades em Bioengenharia – EESC/FMRP/IQSC

École Doctorale de Physique et Chimie-Physique – ED 182

Caroline Faria Bellani

Biocompósitos Eletrofiados e Microfabricação 3D em Engenharia do Tecido Ósseo

São Carlos

Strasbourg

2018

CAROLINE FARIA BELLANI

Programa de Pós-Graduação Interunidades em Bioengenharia – EESC/FMRP/IQSC

École Doctorale de Physique et Chimie-Physique – ED 182

Biocompósitos Eletrofiados e Microfabricação 3D em Engenharia do Tecido Ósseo

Tese apresentada ao Programa de Pós-Graduação Interunidades em Bioengenharia - EESC/FMRP/IQSC, Universidade de São Paulo (Brasil) e para o Programa de Pós-Graduação em Física e Físico-Química - EDD 182, Université de Strasbourg (França), como requerimento para obtenção do título de Doutora em Ciências e Química, com ênfase em Bioengenharia e Química de Polímeros.

Orientadora: Dra. Ana Maria Minarelli Gaspar

Co-orientadores: Dr. Guy Schlatter; Dra. Márcia Cristina Branciforti

VERSÃO CORRIGIDA

São Carlos

Strasbourg

2018

CAROLINE FARIA BELLANI

Programa de Pós-Graduação Interunidades em Bioengenharia – EESC/FMRP/IQSC

École Doctorale de Physique et Chimie-Physique – ED 182

Electrospun Biocomposites and 3D Microfabrication for Bone Tissue Enginneering

Thesis presented to the Interunity Postgraduate Program in Bioengineering (EESC/FMRP/IQSC), University of São Paulo (Brazil) and to the Doctoral College of Physics and Chemistry-Physics (ED 182), Univ as fulfillment requirement of the degree of Doctor of Philosophy in Sciences and Chemistry, Université de Strasbourg (France) with emphasis in Bioengineering and Polymers Chemistry.

Supervisor: Dra. Ana Maria Minarelli Gaspar

Co-supervisors: Dr. Guy Schlatter; Dra. Márcia Cristina Branciforti

CORRECTED VERSION

São Carlos

Strasbourg

2018

Ficha catalográfica elaborada pela Biblioteca Prof. Dr. Sérgio Rodrigues Fontes da EESC/USP com os dados inseridos pelo(a) autor(a).

Bellani, Caroline
B436b Biocompósitos Eletrofiados e Microfabricação 3D para Engenharia do Tecido Ósseo / Caroline Bellani; orientador Ana Maria Minarelli Gaspar; coorientador Guy Schlatter. São Carlos, 2018.

Tese (Doutorado) - Programa de Pós-Graduação Interunidades em Bioengenharia e Área de Concentração em Bioengenharia -- Escola de Engenharia de São Carlos; Faculdade de Medicina de Ribeirão Preto; Instituto de Química de São Carlos, da Universidade de São Paulo, 2018.

1. Engenharia Tecidual. 2. Osso. 3. Biocompósitos. 4. Electrospinning. 5. Biofabricação. 6. Vascularização. 7. Enxertos Vasculares. I. Título.

FOLHA DE JULGAMENTO

Candidato(a): Caroline Faria Bellani

Título: " Electrospun biocomposites and 3D microfabrication for bone tissue engineering"

Data da defesa: 10/09/2018

Comissão Julgadora	Assinatura	Resultado
Prof(a). Dr(a). Marcia Cristina Branciforti (Coorientador(a)) EESC/USP		APROVADA
Prof(a). Dr(a). Guy Schlatter Université de Strasbourg p/		APROVADA
Prof(a). Dr(a). João Manuel Domingos de Almeida Rollo EESC/USP		APROVADA
Prof(a). Dr(a). Carlos Alberto Fortulan EESC/USP		Aprovada
Prof(a). Dr(a). Cecília Amélia de Carvalho Zavaglia UNICAMP	C A Zavaglia	Aprovada

DEDICATION

In Memory of Nilza Longhitano and Maria Helena Faria Martins.

ACKNOWLEDGMENTS

I would like to thank to my parents to have teach me how to persist with my dreams and my studies, and that some madness can be good.

To my beloved fiancé Lucas, for his unconditional love and supporting along all these years. For encouraging me to do this PhD, and, mostly important, for his patience during the time I was abroad and during the inevitable crises that comes together with someone who does a thesis.

To my advisor Dr. Ana Minarelli Gaspar to have accepted to advise me, for her valuable advices and to inspiring me to run a half marathon, and to my co-advisor Dr. Marcia Branciforti to always advise me, since I was undergrad, for all the knowledges in Materials Sciences, to her advices, and to introduce me to Electrospinning. I was blessed to work with these amazing women.

To my co-advisor Dr. Guy Schlatter, for all his dedication, to accept to advise me for my double degree and, mostly important, for always support my projects and always open his lab to me. He is a good example of scientist and professor (the best, actually!). This project it would be not possible without his guidance. Thank you!

To Dr. Ali Khademhosseini for the partnership of this thesis, for all the knowledges in advanced technologies, for his advices, and to his support to pursue my dreams and to push it forward. And for my colleagues at the time I made my PhD trainee on his lab: João Ribas, Zaya, Mahwish, Fabio, Marco, Valéria, Vinny and so many.

To Dr. Heloísa Selistre de Araujo, for keeping the doors of her lab opened, whenever I need to perform *in vitro* testing, for her kindness and advices, and for her students, to all supporting.

To my colleagues (and also friends) of the PolyFUN team: Florence, Domitille and Meng. I have learned a lot with them, and they made this PhD journey so much FUN.

To CAPES and to FAPESP (Process no. 2014/17939-0 and Process no. 2016/04418-8, Fundação de Amparo à Pesquisa do Estado de São Paulo) for the financial supporting.

“The size of your dreams must always exceed your current capacity to achieve them. If your dreams do not scare you, they are not big enough”- Ellen Johnson Sirleaf

“You gotta keep your ideals high/ You got to know that the sky belongs to no one” – Above & Beyond

“They did not know it was impossible, so they did it” – Mark Twain

ABSTRACT

BELLANI, Caroline F. **Electrospun Biocomposites and 3D Microfabrication for Bone Tissue Engineering**. 2018. 199f. Thesis (PhD in Sciences/ PhD in Chemistry) - São Carlos School of Engineering / École Doctorale de Physique et Chimie-Physique, Universidade de São Paulo/ Université de Strasbourg, São Carlos/ Strasbourg, 2018.

Bone tissue regeneration is still an important challenge in orthopedics and traumatology. Despite the natural ability of bone repair, a trauma beyond the critical limit (critical fracture) cannot be regenerated. Tissue Engineering is a multidisciplinary field that applies the principles of engineering and biological sciences to the development of biological substitutes that restore, maintain or improve the tissue function or of an organ as a whole. The aim of this work was to develop osteogenic and mechanically improved biomimetic scaffolds for bone tissue engineering; to improve the vascularization of a bone tissue engineered implant by the design and development of a suturable vessel graft embedded in hydrogels for 3D biofabrication. Biodegradable PCL membranes for guided bone regeneration, obtained by electrospinning, reinforced with various ratios of natural nanocomposites obtained from cellulose nanocrystals (CNCs) were produced. Results showed an improvement of mechanical properties, in the degree of crystallinity and in the melting temperature according to the ratio of cellulose nanocrystals. I employed Biosilicate® as bioactive phase into these membranes. The Biosilicate®, combined with the cellulose nanocrystals, considerably improved their mechanical properties. Osteoblasts were able to proliferate and biomineralize in these membranes. Thus, a biomimetic and biodegradable membranes, with osteogenicity and improved mechanical properties for guided bone regeneration and bone tissue engineering were developed. In order to improve the vascularization of bone tissue engineering constructs, new GelMA-CNC composites were developed. Cell-laden GelMA-CNC hydrogels with endothelial cells were biofabricated. Endothelial cells were able sprout and to organize in tubules. As rapid vascularization strategy, a rapid degrading biomimetic suturable graft obtained from electrospun membranes fusing, in order to allow endothelial cell migration from the vascular graft to the bone-like grafts and, following, new capillary formation, was manufactured. A porous pattern over the suturable grafts was fabricated by laser micromachining. The obtained elastic scaffolds were suturable and supported stress and recoil. The scaffolds are autoclavable and possess no *in vitro* toxicity. The porous patterned created on the suturable grafts allowed the endothelial cell towards the 3D culture of osteoblasts in GelMA, and 3D structures formed from the interaction of endothelial cells and osteoblasts were observed. Therefore, this strategy can potentially be employed to enhance the size and the survival biofabricated bone implants, accelerating the clinical translation of bone tissue engineering.

Keywords: Tissue Engineering. Bone. Biocomposites. Electrospinning. Biofabrication. Vascularization.

RESUMO

BELLANI, C. F. **Biocompósitos Eletrofiados e Microfabricação 3D para Engenharia do Tecido Ósseo**. 2018. 199f. Tese (Doutorado em ciências/ Doutorado em química) - Escola de Engenharia de São Carlos/ École Doctorale de Physique et Chimie-Physique, Universidade de São Paulo/ Université de Strasbourg, São Carlos/ Estrasburgo, 2018.

A regeneração do tecido ósseo ainda é um desafio importante em ortopedia e traumatologia. Apesar da capacidade natural de reparo ósseo, um trauma além do limite crítico (fratura crítica) não pode ser regenerado. A Engenharia de Tecidos é um campo multidisciplinar que aplica os princípios da engenharia e ciências biológicas para o desenvolvimento de substitutos biológicos que restauram, mantêm ou melhoram a função do tecido ou de um órgão como um todo. O objetivo foi desenvolver *scaffolds* biomiméticos com propriedades osteogênicas e mecânicas aprimoradas para a engenharia de tecidos ósseos; melhorar a vascularização do implante de engenharia de tecido pelo desenvolvimento de um enxerto vascular suturável a ser incorporado em hidrogéis para biofabricação 3D. Membranas biodegradáveis de PCL para regeneração óssea guiada reforçadas com diferentes proporções de nanocompósitos naturais obtidos a partir de nanocristais de celulose foram produzidas. Os resultados mostraram uma melhora nas propriedades mecânicas, no grau de cristalinidade e na temperatura de fusão, de acordo com a proporção de nanocristais de celulose. Como fase bioativa, empregou-se o Biosilicato®: combinado com os nanocristais de celulose, o Biosilicato® melhorou consideravelmente suas propriedades mecânicas. Os osteoblastos foram capazes de proliferar e biomineralizar nas membranas biodegradáveis. Membranas biomiméticas e biodegradáveis, com melhores propriedades mecânicas para regeneração óssea guiada e engenharia de tecido ósseo foram produzidas. A fim de melhorar a vascularização das construções de engenharia de tecido ósseo, foram desenvolvidos novos compósitos GelMA-CNC. Hidrogéis GelMA-CNC incorporados com células endoteliais foram biofabricados e, neles, as células endoteliais foram capazes de se organizar em túbulos. Baseada na estratégia de vascularização rápida, produziu-se um enxerto biomimético suturável de degradação rápida obtido a partir da fusão de membranas eletrofiadas. Um padrão poroso sobre os enxertos suturáveis foi fabricado por microusinagem a laser, com o objetivo de permitir a migração de células endoteliai, permitindo a formação de uma rede de capilares. Os *scaffolds* elásticos tubulares obtidos são resistentes à sutura, autoclaváveis e não possuem toxicidade *in vitro*. O padrão poroso criado nos enxertos suturáveis permitiu que células endoteliais fluíssem em direção à cultura 3D dos osteoblastos em GelMA, e estruturas 3D formadas a partir da interação de células endoteliais e osteoblastos foram observadas. Portanto, essa estratégia pode ser empregada para aumentar o tamanho e a sobrevivência dos implantes ósseos biofabricados, acelerando a translação clínica da engenharia do tecido ósseo.

Palavras-Chave: Engenharia Tecidual. Osso. Biocompósitos. Eletrofiação. Biofabricação. Vascularização.

RÉSUMÉ

BELLANI, Caroline F. **Biocomposites Electrofilés e Microfabrication 3D pour l'Ingénierie des Tissus Osseaux**. 2018. 199f. Thèse (Doctorat em Sciences/ Doctorat en Chimie) – École d'Ingénierie de São Carlos/ École Doctorale de Physique et Chimie-Physique, Université de São Paulo/ Université de Strasbourg, São Carlos/ Strasbourg, 2018.

La régénération des tissus osseux reste un défi important en orthopédie et en traumatologie. Malgré la capacité naturelle de la réparation osseuse, un traumatisme au-delà de la limite critique (fracture critique) ne peut pas être régénéré. L'ingénierie tissulaire est un domaine multidisciplinaire qui applique les principes de l'ingénierie et des sciences biologiques pour le développement de substituts biologiques qui restaurent, maintiennent ou améliorent la fonction tissulaire ou d'un organe dans son ensemble. Les objectives étaient de développer des *scaffolds* biomimétiques avec des propriétés ostéogéniques et mécaniques améliorés pour l'ingénierie des tissus osseux ; vasculariser des implants obtenus par l'ingénierie tissulaire osseuse, par la conception et le développement d'un greffon sanguin suturable intégrée dans des hydrogels pour la biofabrication 3D. Des membranes biodégradables en PCL pour la régénération osseuse guidée, obtenues par *electrospinning*, renforcées par différents rapports de nanocomposites naturels obtenus à partir de nanocristaux de cellulose, ont été fabriquées. Les résultats ont montré une amélioration des propriétés mécaniques, du degré de cristallinité et de la température de fusion en fonction de l'ajoute des nanocristaux de cellulose. Comme phase bioactive, le Biosilicate® a été utilisé. Combiné avec les nanocristaux de cellulose, le Biosilicate® a considérablement amélioré leurs propriétés mécaniques. Les ostéoblastes étaient capables de proliférer et de se bio-minéraliser dans ces membranes. Afin d'améliorer la vascularisation dans les greffons obtenues pour le tissu osseux, de nouveaux composites GelMA-CNC ont été développés. Des hydrogels GelMA-CNC remplis de cellules endothéliales ont été biofabriqués. Les cellules endothéliales étaient capables de germer et de s'organiser en tubules. En tant que stratégie de vascularisation rapide, un greffon biomimétique suturable à dégradation rapide obtenue par fusion de membranes électrofilées a été fabriqué. Des motifs poreux sur les greffes suturables ont été fabriqué par micro-usinage au laser pour permettre la migration des cellules endothéliales vers le greffon osseux. Les *scaffolds* tubulaires élastiques obtenus étaient suturables, supportaient le stress et le recul, sont autoclavables et ne possèdent aucune toxicité *in vitro*. Les motifs poreux créés sur les greffes suturables ont permis aux cellules endothéliales migrer vers la culture 3D des ostéoblastes dans GelMA, et des structures 3D formées à partir de l'interaction des cellules endothéliales et des ostéoblastes ont été observées. Par conséquent, cette stratégie peut être utilisée pour améliorer la taille et la survie des implants osseux biofabriqués, en accélérant la traduction clinique de l'ingénierie du tissu osseux.

Mots Clés : Ingénierie Tissulaire. Os. Biocomposites. *Electrospinning*. Biofabrication. Vascularisation.

FIGURES

TABLES

ABBREVIATIONS

PCL	Polycaprolactone
CNC	Cellulose Nanocrystals
GelMA	Gelatin Methacryloyl
ECM	Extracellular Matrix
FDA	Food and Drug Administration
ICPEES	Institut of Chimie et Polymères pour l'Énergie, l'Environnement et la Santé (Français)
SEM	Scanning Electron Microscopy
BioSiO-g-PCL	Biosilicate® grafted with Polycaprolactone
CNC-g-PCL	Cellulose Nanocristals grafted with Polycaprolactone
TEM	Transmission Electron Microscopy
CTI	Centro de Technologia da Informação "Renato Archer" (Portuguese)
GelMA-CNC	Gelatin Methacryloyl-Cellulose Nanocrystals composites
HUVEC	Human Umbilical Vein Endothelial cells
MG-63	*Homo sapiens* Bone Osteosarcoma cells
PGS	Poly (Glycerol Sebacate)
PVA	Polyvinyl Alcohol
PTFE	Polytetrafluoroethylene
PCR-rt	Polymerase Chain Reaction (Real Time)
3D	Three dimensions
PLA	Poly (lactic acid)
PGA	poly (glycolic acid)
CNTs	Carbon Nanotubes
ROP	Ring-Opening Polymerization
TGA	Thermogravimetric Analysis
DMA	Dynamic Mechanical Analysis
DSC	Differential Scanning Calorimetry
FT-IR	Infrared Spectroscopy
DCM	Dichloromethane
DMF	*N, N*-dimethyl formamide
PVB	polyvinyl butyral
DMEM	Dulbecco's Modified Eagle Medium

PBS	Phosphate Buffer Saline
BSA	Bovine Serum Albumin
FBS	Fetal Bovine Serum
dH2O	distilled water
XRD	X-Ray Diffraction
IR	Infra-Red
NMR H+	Proton Nuclear Magnetic Resonance
TMSPMA	3- (trimethylsilyl) propyl methacrylated
DPBS	Dulbecco's Phosphate Buffer Saline
EBM-2	Endothelial Cell Growth Basal Medium
EGM-2	Endothelial Growth Media
GFP	Green Fluorescent Protein
VEGF	Vascular Endothelial Growth Factor
hFGF-B	Human Basic Fibroblast Growth Factor
IGF-1	Insulin-like Growth Factor

TABLE OF CONTENTS

INTRODUCTION

BONE

Bone is a specialized, complex and highly organized connective tissue. It is composed of an external layer, referred to as cortical or compact bone, and an internal layer, referred to as cancellous or spongy bone Figure 1. Cortical bone makes up to ~80% of the total bone mass in adults (SIKAVITSAS; TEMENOFF; MIKOS, 2001). It is extremely dense, with low porosity (20%) and high mechanical strength (130–190MPa) (TURNER; WANG; BURR, 2001). Cancellous bone accounts for the other 20% of the total bone mass and is highly porous (50%–90%), with ~10% of the mechanical strength of cortical bone (SIKAVITSAS; TEMENOFF; MIKOS, 2001). Osteons are functional units within the cortical bone structure and contain central Haversian canals, which house nerves and blood vessels (HILLIER; BELL, 2007). In contrast, cancellous bone does not contain osteon units, as its high porosity and surface area allows for better penetration of vasculature (RODAN, 1992). Although cortical and cancellous layers are quite different in structure, they both contain a highly vascularized network. The presence of a vascular network is essential to supply nutrients and remove waste products.

Figure 1. Bone Anatomy

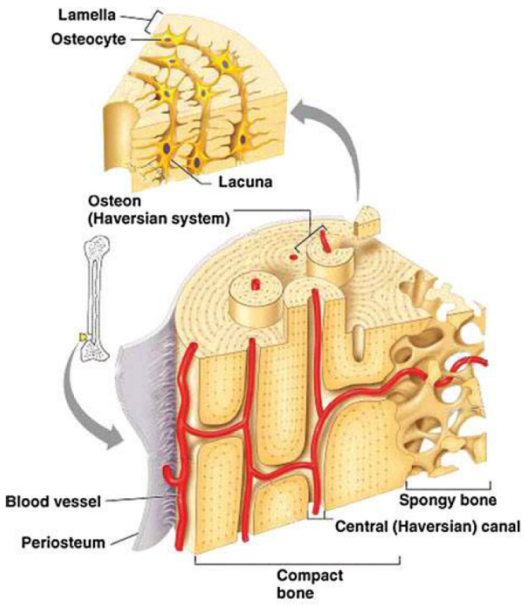

Source : NGUYEN et al. (2012a)

EXTRACELLULAR MATRIX (ECM)

The extracellular matrix (ECM) is a three-dimensional, non-cellular structure that is present in all tissues and is essential for life. Every organ has an ECM with unique composition that is generated in early embryonic stages. The function of the ECM goes beyond providing physical support for tissue integrity and elasticity: it is a dynamic structure that is constantly remodeled to control tissue homeostasis(HYNES, 2009). As a matter of fact, the ECM is formed by the secreted product of resident cells within each tissue and organ and is composed of a mixture of structural and functional proteins arranged in a three-dimensional ultra-structure. Most of these molecules are well recognized and they form a complex mixture of proteins, glycosaminoglycans, glycoproteins and small molecules arranged in a structural support matrix. Fiber proteins, like collagens, give the matrix strength and resilience and form structures to which cells can be anchored (CANCEDDA, 2009). ECM metabolism plays a central role in the development of skeletal tissues and in their repair/regeneration in most orthopedic diseases and trauma such as bone fracture, osteotomy, cartilage damage, arthritis, and congenital skeletal deformity (Figure 2). During development or disease, specific genes must be expressed in order to make a new or to repair an existing ECM. Formation of the ECM is essential also for processes like tissue growth, wound healing, fibrosis, tumor invasion and metastasis (OSTADAL et al., 1995).

Figure 2. Hierarchical organization of bone at different magnifications. The bone has a strong external compacted calcified layer (a), which comprises several Harversian canals (b). The membrane of resident cells has a layer of receptors that respond to specific binding sites (c) and to the characteristic architecture of the surrounding ECM (d).

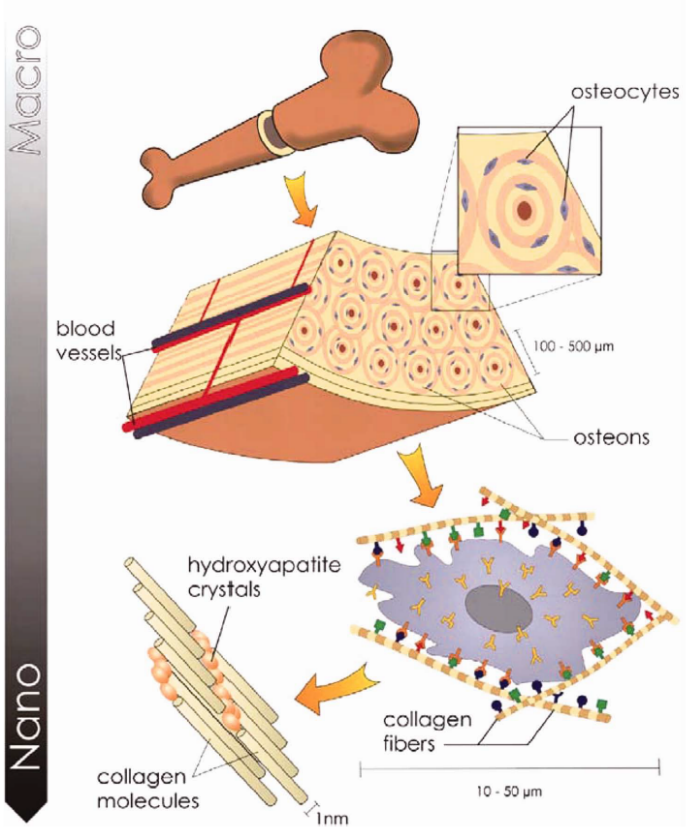

Source: Adapted from STEVENS (2008)

The regeneration of the bone tissue is still an important challenge in orthopedics and craniofacial surgery. Despite the natural ability of bone repair, a trauma beyond the critical limit (critical fracture) cannot be regenerated. Many traumas and pathologies, such as osteoporosis, osteoarthritis, imperfect osteogenesis and Paget's disease, can prevent normal bone function and consolidation of fractures and lead to immobility, deformity and severe pain, leading to the need for bone grafting or the insertion of biomaterials or prostheses (FERNANDEZ-YAGUE et al., 2015). Moreover, advances in medicine over the past century have resulted in a dramatic rise in the ageing population worldwide. As such, there is an increasing need for new treatments for patients with musculoskeletal diseases as evidenced by bone being the next most transplanted tissue after blood (LEACH; MOONEY, 2004; ORYAN et al., 2014). The bone transplanted tissue can be in the form of an autograft (harvested from the patient), an allograft or xenograft (obtained from a donor or animal). Moreover, the use of an engineered synthetic or biomaterial substitute can be also employed (GIBBS et al., 2014).

Autologous bone graft (bone tissue transplanted from the patient's own body) is still the most commonly used procedure for reconstruction of defects and bone fractures (KURIEN; PEARSON; SCAMMELL, 2013). However, this technique has some

disadvantages, such as limited availability, graft loss or resorption, short-term instability in the case of large areas affected, complications associated with the second surgery, and failure rates exceeding 50% in sites of difficult consolidation (BAJAJ; WONGWORAWAT; PUNJABI, 2003; CLAVERO; LUNDGREN, 2003; KURIEN; PEARSON; SCAMMELL, 2013). In elderly patients, autologous or allogenous bone transplantation is an expensive and painful procedure, presents additional risks associated with additional surgical procedures for autologous grafts, and presents a high risk of disease transmission and rejection to allogeneic grafts (MEHTA et al., 2012; ROSE; OREFFO, 2002). As an alternative to transplants and grafts, there are prostheses of various materials and architectures. Although many artificial prosthetic devices are available, few can completely replace all complex biological functions (ARMENTANO et al., 2010; ASGHARI et al., 2017; FREED et al., 1994).

Therefore, there is a need for new solutions to remedy the limitations of current prostheses and bone graft treatments. Currently, the idea of reconstruction of laboratory-created organs and tissues is widely disseminated and investigated worldwide. As a multidisciplinary science in regenerative medicine, these studies involve knowledge in the fields of biology, health sciences, engineering and materials science (GRIFFITH; NAUGHTON, 2002; LANGER; VACANTI, 1993).

TISSUE ENGINEERING

Tissue Engineering is a multidisciplinary field that applies the principles of engineering and biological sciences to the development of biological substitutes that restore, maintain or improve the tissue function or of an organ as a whole (LANGER; VACANTI, 1993), by the combination of cells, engineering methods and biochemical factors in order to improve or substitute biological functions (FREED et al., 1994; LANGER; VACANTI, 1993). The development of tissue engineering is based on the *in vitro* culture of scaffolds associated progenitor cells, which must mimic the extracellular matrix (ECM), forming a suitable medium or microenvironment for the cells to organize into structures functionally similar to the tissue (GRIFFITH; NAUGHTON, 2002; LANGER; VACANTI, 1993)

BONE TISSUE ENGINEERING

The aim of bone tissue engineering is to create clinically relevant grafts that can be used therapeutically. Bone tissue engineering is a complex and dynamic process that initiates with migration and recruitment of osteoprogenitor cells followed by their proliferation, differentiation, matrix formation along with remodeling of the bone. Major advances in bone tissue engineering with scaffolds are achieved through growth factors, drugs and gene deliveries. Bone scaffolds are typically made of porous degradable materials that provide the mechanical support during repair and regeneration of damaged or diseased bone (LEACH; MOONEY, 2004). Therefore, Bone Tissue engineering, involving the use of relevant scaffolds, appropriate growth factors, and/or cells, has developed in recent times to meet this demand for new therapies. Such approaches have in some cases improved graft incorporation, osteoconductivity, osteoinductivity and osseointegration (FERRIS; GILMORE; WALLACE, 2013).

BONE TISSUE ENGINEERING SCAFFOLDS

An essential component in tissue engineering is the development of porous 3D structures - scaffolds - that will provide to the cells the necessary support to guide bone formation. Many materials have been investigated; however, despite significant advances in the area, the development of synthetic structures capable of fully sustaining the capacity for bone regeneration and self-remodeling is still a major challenge (LI et al., 2013). There are many physical and biological properties that an ideal scaffold for bone tissue engineering needs to possess, among them: (i) a porous matrix with interconnected pores and surface suitable for cell growth and proliferation and transport of nutrients and metabolic waste; (ii) reabsorption rate and remodeling synchronized with osteogenic activity, with the production of only metabolically acceptable substances; (iii) releasing a controlled cascade (in time and space) of signaling to guide cell differentiation and promote tissue regeneration; (iv) mechanical properties appropriate to those of the host tissue by means of a concise and stable material-tissue interface which must persist during the time of resorption of the implant; (v) have no risk of rejection or reaction of the immune system by foreign body; and (vi) have good adaptation with the host tissue environment. Possessing these properties, the implant can replace, at least temporarily, the natural tissue, providing a resistance and rigidity necessary to prevent fractures even under the physiological loads, besides providing a structure necessary for the body to build the new bone tissue (FERNANDEZ-YAGUE et al., 2015). However,

only the manufacturing process of the scaffold itself is not enough to manufacture an ideal scaffold. In this sense, nanotechnology provides tools to project the internal surfaces of the scaffolds (NICHOL; KHADEMHOSSEINI, 2009; PECK et al., 2011; RIDLEY et al., 2003).

Scaffolds typically consist of a solid support structure with an interconnected pore network, which matrices are often hydrogels containing encapsulated cells. Both forms must support cell colonization, proliferation, differentiation and migration. Additionally, they should possess appropriate physicochemical properties (such as strength, stiffness, biodegradability, surface chemistry) that are necessary for tissue formation as well as being capable of withstanding and responding to mechanical stresses (TANG et al., 2016). Cells associated with bone should be directed to recognize and respond appropriately to form bone ECM that is analogous to the native bone matrix (JANG; CASTANO; KIM, 2009 et al., 2009).Therefore, there is a preference for the design and engineering of materials with structure, composition and properties similar to bone ECM (SHIN; JO; MIKOS, 2003). Materials that mimic bone should play a key role in assisting cells to follow processes that are effective in bone formation and, most importantly, in the synthesis and incorporation of nanocrystals (mostly bioactives) between the organic matrix (OLSZTA et al., 2007).

ELECTROSPINNING

In recent years, the electrospinning process and the nanofibrous matrices have gained great interest in tissue engineering, mainly due to the structural similarity with the ECM (being possible to manufacture fibers of nanometric to micrometric dimensions), to the possibility of working with a great variety of materials as well such as to the simplicity of assembly and operation at a low cost (BARNES et al., 2007; BELLANI et al., 2016; NEDJARI et al., 2014; PHAM; SHARMA; MIKOS, 2006; SILL; VON RECUM, 2008). In bone reconstruction, electrospun fibers have also attracted attention, and suitable materials had been identified and explored for electrospinning matrices for bone tissue engineering and guided regeneration, and it has been identified compositions of suitable materials and exploiting them for electrospinning (ASHAMMAKHI et al., 2007; CASTILLO-DALI et al., 2014; CHAPPUIS et al., 2017; RETZEPI; DONOS, 2010; YOSHIMOTO et al., 2003). In general, it is believed that a fibril matrix that can be produced by electrospinning is able to retain the components of the ECM and to be designed to modulate surrounding microenvironments throughout the conditions of bone tissue engineering ex vivo or *in vivo* (LUTOLF; HUBBELL, 2005; RETZEPI; DONOS, 2010).

The electrospinning process consists of the application of electricity to disperse a liquid. A high voltage is applied to a liquid through an emitter, or spinneret, which is usually a small diameter glass or metal needle or capillary (INGAVLE; LEACH, 2013). The liquid remains at the tip of the spinneret by the liquid surface tension, and an electric charge is induced at the surface of the solution by a high voltage at the spinneret (Figure 3, A and B). The mutual repulsion of the charges produces a force directly opposite to the surface tension (TEO; INAI; RAMAKRISHNA, 2011.). When the electric field reaches a critical value in which the repulsive electric force exceeds the force of the surface tension, the Taylor Cone is formed (Figure 3, C), which emits the liquid from its tip. An instability is formed in the space between the capillary tip and the collector, leading to solvent evaporation and deposition of the polymer (Figure 3, D)(ADOMAVIČIŪTĖ; MILAŠIUS, 2007; TAYLOR, 1969).

Figure 3. Electrospinning process, represented by: (A) Electrospinning equipment; (B) schematic diagram of the production of nanofibers using syringe, needle, collector and high voltage; (C) Taylor cone; (D) morphology of poly (ε-caprolactone) nanofibers viewed by Scanning Electron Microscopy (SEM).

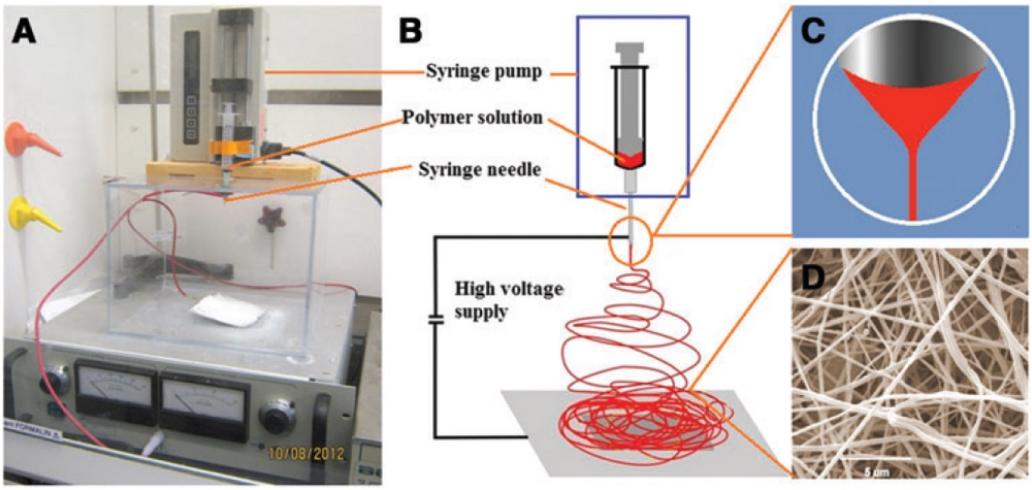

Source: Adapted from INGAVLE; LEACH (2013).

Due to the possibility of controlling the composition, fiber diameter and orientation, electrospun fiber mats are ideal substrates for use in bone tissue engineering (INGAVLE; LEACH, 2013) and in guided bone regeneration (RETZEPI; DONOS, 2010). Because bone-associated cells present early adhesion responses to their environment similar to those of other tissues which are anchorage-dependent, as well as their stem/progenitor cells, the nanofibrilic substrate of these membranes can provide favorable conditions for cell adhesion and growth.

The electrospinning of biodegradable polymers, both of synthetic origin and natural origin, was first reported to generate bone cell matrices. The flexibility and variety of the

polymeric materials gives them great potential in the area of bone regeneration (JANG; CASTANO; KIM, 2009). Among various polymeric materials, a group of poly (α-hydroxyacids) such as poly (lactic acid) (PLA), poly (glycolic acid) (PGA) and poly (ε-caprolactone) (PCL) and their copolymers are extensively investigated for electrospun membranes for tissue regeneration, including bone (BURG; PORTER; KELLAM, 2000).

POLY (Ɛ-CAPROLACTONE)

PCL is biodegradable, hydrophobic and semi-crystalline polymer and FDA approved (Figure 4). The first suggested application of PCL was its use in electrospun membranes for bone regeneration (YOSHIMOTO et al., 2003). The good solubility of PCL, its low melting point (59-64 ° C) and excellent compatibility with blends have stimulated extensive research into its potential application in the biomedical field (CHANDRA; RUSTGI, 1998; NAIR; LAURENCIN, 2007; OKADA, 2002). PCL has superior viscoelastic and rheological properties over many resorbable polymers and is easy to handle in the manufacture of various types of scaffolds (HUANG et al., 2007; LUCIANI et al., 2008; MARRAZZO; DI MAIO; IANNACE, 2008; ZEIN et al., 2002). The degradation of PCL compared to PLA, PGA and its copolymers is slow, making PCL more suitable for long-term degradation applications (WOODRUFF; HUTMACHER, 2010), as guided bone regeneration.

Figure 4. Poly (caprolactone) – PCL

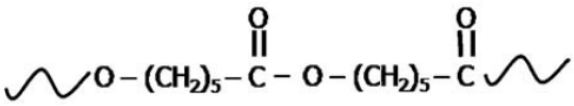

Fonte: WOODRUFF; HUTMACHER (2010)

However, there are still some challenges that need to be overcome in the application of PCL as a biomaterial, including effects caused by its hydrophobicity, which can prevent cell adhesion and mobility, and tune its mechanical properties according to the target tissue and/or application (GHASEMI-MOBARAKEH et al., 2008), which can be accomplished by reinforcing PCL scaffolds/mats with suitable fillers (VENUGOPAL et al., 2008), obtained suitable composites for bone tissue engineering applications.

BIOCOMPOSITES

Composites are composed of two (or more) different constituents, where one is usually the matrix and the other, fibers or particles (EICHHORN et al., 2010). Basically, the bone ECM itself is a type of biocomposite whose structural integrity is guaranteed primarily by collagen fibers integrated with bioceramic nanocrystals (hydroxyapatite). In order to mimic bone ECM, an engineered scaffold should combine the optimal properties of both matrix (polymer) and reinforcement (fiber or particle) (OLSZTA et al., 2007). To date, there are no synthetic biomaterials with the same hierarchical structure of bone (Figure 2), even though the message of nature is clear: unique mechanical properties can be achieved by combining mechanisms acting at various scales(INGAVLE; LEACH, 2013). In this context, the design of performing scaffolds requires the incorporation of a hierarchical design that also comprises several scales, from the nano level - in order to provide greater resistance (for example, mimic the deformation of hydroxyapatite and collagen crystals) - until the level of microstructure to provide rigidity. Therefore, an optimal scaffold must combine many materials and techniques to achieve the desired mechanical and biodegradation responses (LI et al., 2013).

A considerable part of the bone ECM contains mineral phases of calcium-phosphates, which requires a mineralization step that is essential in the process of bone regeneration. The existence of bioactive inorganic components among biomaterials generally favor bone mineralization and osteogenic differentiation. Thus, many studies have focused on the introduction of a range of inorganic phases between electrospun scaffolds and membranes in order to provide both specific bone bioactivity and improvement in mechanical properties. Modulation of a polymer interface with materials that are active for bone cells is an example of a strategy for biomaterials for bone regeneration. Bioactive inorganic materials, including hydroxyapatite and bioactive ceramics or glasses, as glass-ceramics as well, are excellent choices of materials for reconstruction of rigid tissues (LI et al., 2013).

In practice, electrospinning of inorganic materials is well documented (KIM; KIM, 2006; LU et al., 2009; WU et al., 2004; XIA; ZHANG; CHANG, 2007). However, despite their great bone bioactivity, the employment of pure inorganic materials may lead to materials with limited mechanical properties for use as matrices or scaffolds for bone regeneration. In this context, advanced knowledges and technologies need to be developed in order to overcome the disadvantages of pure inorganic fibers and to identify suitable materials. Thus,

the inorganic materials as fillers for the production of composite scaffolds with degradable polymers are investigated (KIM; LEE; CHUN, 2008).

BIOSILICATE®: A BIOACTIVE CERAMIC GLASS

Bioactive glasses and glass-ceramics belong to the third generation of biomaterials. Among all synthetic biomaterials available for the treatment of bone lesions, bone substitution or any other application where bone regeneration is needed, bioactive glasses show the best clinical outcome. The best known bioactive glass is Bioglass® 45S5, developed by Larry Hench in the late 1960s, which has a composition of $24.5Na_2O–24.5CaO–45SiO_2–6P_2O_5$ (wt.%) (HENCH, 2003). This glass exhibits the highest bioactivity index ($I_B = 12.5$) and is still considered the gold standard of bioactive materials (CROVACE et al., 2016). However, despite its excellent bioactive properties, the major disadvantages of bioactive glasses are their low mechanical strength and low fracture toughness. These characteristics restrict their use to a few applications. To improve the mechanical performance, bioactive glass-ceramics have been developed. Biosilicate® is a glass ceramic from the quaternary system $SiO\text{-}Na_2O\text{-}CaO\text{-}P_2O_2$, with high bioactivity and improved mechanical properties (CROVACE et al., 2016). The potential of Biosilicate® in the consolidation of bone fractures has been proven in several studies. Among them, we highlight the work from GRANITO et al., 2009, which showed that bone defects in tibia of rats filled with Biosilicate® particles (180-210μm) have mechanical properties similar to that of healthy bones (GRANITO et al., 2009); BOSSINI et. al. demonstrated the osteogenic capacity of Biosilicato® implants associated or not with Low Intensity Laser in rats (BOSSINI et al., 2011); and MOURA et. al. demonstrated that Biosilicate® is more bioactively effective than Bioglass 45S5® (MOURA et al., 2007). Several situations involving bone loss may be benefited by the osteogenic properties of Biosilicate®, including the possibility of selecting its granulometric range to achieve optimum conditions of a specific application (CROVACE et al., 2016).

CELLULOSE NANOCRYSTALS

Essentially, the hierarchical structure of cellulose comprises repeated crystal structures to form microfibrils to generate cellulose fibers from vegetables, which also aggregates into large macroscopic fibers. Thus, the cellulose is composed of an amorphous and crystalline phase. The highly crystalline structure of the cellulose can be extracted in the form of nanocrystals (or nanowiskers) (Figure 5) from the plant material through controlled acid

hydrolysis, which hydrolyses the amorphous region of the cellulose and leaves crystals of pure cellulose with high aspect ratio (length by diameter). The dimensions of cellulose nanocrystals (CNC) depend on the source of cellulose. In general, their length varies between 100 and 300 nm (EICHHORN et al., 2010).

Figure 5. Transmission Electron Microscopy of Cellulose Nanocrystals obtained from balsa wood.

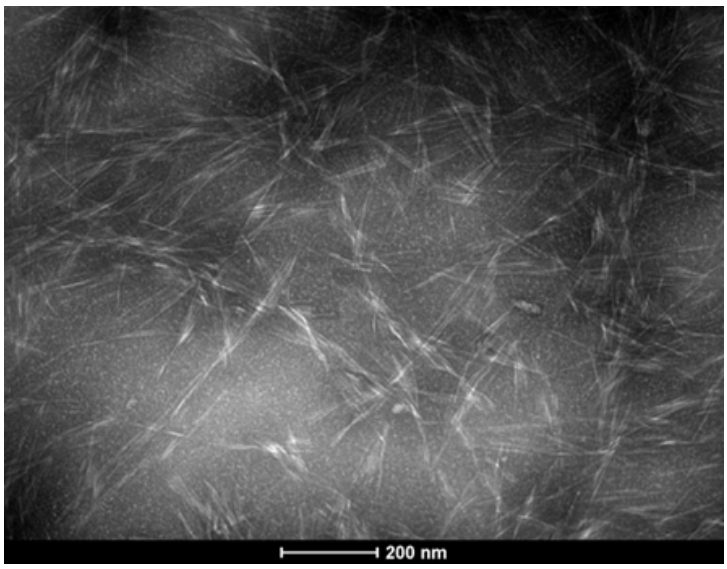

Source: MORELLI et al. (2012).

CNCs can be produced from a variety of cellulose sources, including wood, cotton, sisal, ramie, tunicates, fungi or bacteria (O'SULLIVAN, 1997). It has previously been shown that the addition of biodegradable and non-toxic cellulose nanocrystals in polymer matrices improves the mechanical properties of scaffolds according to the proportion thereof. Thus, it is possible to adapt the mechanical properties of scaffolds according to the proportion of CNC incorporated, according to the desired application (BELLANI et al., 2016).

In addition, CNCs have several advantages: their cost of production is simple and cheap and, most importantly, they are biocompatible and biodegradable (JACKSON et al., 2011; LAM et al., 2012; MAHMOUD et al., 2010); In addition, CNCs has been used as reinforcing phase in biomaterials due to their remarkable mechanical properties (Table 1) (ZOPPE et al., 2009a).

Table 1. Engineering materials modulus compared with crystalline cellulose.

Material	*Modulus (GPa)*	*Density (Mg m^{-3})*	*Specific Modulus (GPa Mg^{-1} m^3)*
Aluminum	69	2,7	26
Steel	200	7,8	26
Glass	69	2,5	28
Crystalline Cellulose	138	1,5	92

Source: Adapted from EICHHORN et al. (2010).

The main problem associated with the manufacture of effective nanocomposites is related to the particles dispersion in synthetic polymer matrices and organic solvents. CNCs and Biosilicate® exhibit strong interactions with polar surface groups and therefore a significant tendency for self-association in organic solvents (DE SOUZA LIMA; BORSALI, 2004), which may limit the extent of mechanical reinforcement (LJUNGBERG et al., 2005; SCHROERS; KOKIL; WEDER, 2004). An alternative to improve the dispersion of these fillers in organic solvents and synthetic polymer matrices is the modification of their surface (GOUSSÉ et al., 2002). The polymers can be polymerized directly from the particles using the hydroxyls of their surface as initiation sites for controlled polymerization (EICHHORN et al., 2010).

PCL GRAFTING FROM RING-OPENING

Polymeric chains grafting-from the surface of polysaccharides and inorganic particles have been reported (HABIBI et al., 2008; LABET; THIELEMANS, 2009a). The grafting-from particles in order to improve their dispersion in polymeric matrices is interesting because it provides a covalent link between the matrix and the particle. In addition, if the polymer chains and the matrix constitute the same material, a better compatibilization can be obtained thanks to the co-continuous phase that can be created (EICHHORN et al., 2010).

In the grafting-from method, the polymer chains are formed by the in-situ polymerization initiated on the surface from primers immobilized on the substrate Figure 6. PCL has traditionally been prepared by the ring-opening polymerization, by the cyclic monomer Ɛ-caprolactone. The ring-opening polymerization of lactones is the most common route of synthesis today. Tin (II) -ethyl hexanoate (Tin (II)) octoate is the most widely used catalyst today because of its high effectiveness and low toxicity (STOREY; SHERMAN, 2002).

Thus, as the ring-opening polymerization can be initiated by the hydroxyls present, there is no need for pretreatment to the grafting process, since the substrate has free hydroxyls (HABIBI et al., 2008).

Figure 6. Schematics from the polymerization reaction initiated from the CNC surface through the ring-opening polymerization.

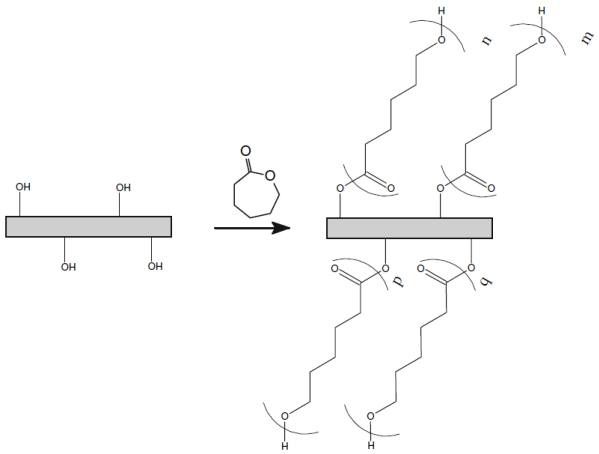

Adapted from HABIBI et al. (2008).

As Biosilicate® also possess free hydroxyl groups, we assume the PCL ring-opening polymerization from Biosilicate can also be achieved. By PCL grafting from CNC and Biosilicate®, we can yield better interaction between PCL and the CNC and Biosilicate®, which can lead to stronger hydrogen bonds between the polymeric and the reinforcement phases, improving the mechanical properties and osteoinduction properties of PCL electrospun membranes. Upon implantation, the Biosilicate® forms a biologically active hydroxyl carbonate apatite layer similar to the mineral phase in bone, which provides an excellent interfacial bonding with bone (HRISTOV et al., 2009; REZWAN et al., 2006). Thus, Biosilicate® can be tailored to deliver ions such as Si at levels capable of activating complex gene transduction pathways, improving cell differentiation and osteogenesis.

3D BIOFABRICATION TECHNOLOGIES

Despite the advances in scaffold fabrication, cell-based treatments are not yet available for clinical use. Currently, these top-down approaches, which consist in manufacturing of a scaffold, followed by cell manipulation and seeding are promising, but they rely on manual cell seeding and culturing of pre-fabricated scaffolds (FERRIS; GILMORE; WALLACE, 2013). This is time-consuming, inefficient and operator dependent,

reflecting the fact that current cell-based therapies are typically only applicable on a limited scale. This lack of cost-effectiveness has, to date, curtailed translation from the laboratory to clinical use as a mainstream therapeutic option. Furthermore, cell seeding of pre-fabricated scaffolds does not recreate the cellular organization of native tissues, nor does it address the issue of construct vascularization (TANG et al., 2016).

3D Biofabrication approaches enable the fabrication of biological constructs with precise control over the positioning of cells and biomaterials, which strategies can be applied to engineer 3D tissue models *in vitro* by mimicking the structure and function of native tissue through the precise deposition and assembly of materials and cells (Figure 7). This approach allows the spatiotemporal control over cell–cell and cell–extracellular matrix communication and thus the recreation of tissue-like structures (MORONI et al., 2018). Bioprinting and bioassembly constitute the two major biofabrication pillars, and various techniques have been developed. Bioprinting allows the spatial arrangement of cells, materials and biologically active factors, whereas bioassembly facilitates the automated assembly of cell containing building blocks (GROLL et al., 2016, p. 201). These techniques provide a high level of biomimicry by recreating the complexity of tissues and organs, and they can be upscaled for manufacturing and production. Importantly, biofabrication strategies allow the spatiotemporal modulation of cell–cell and cell–extracellular matrix (ECM) interactions (DAI et al., 2017; LIND et al., 2017) through the formulation and use of engineered materials, such as hydrogels, that enable cells to migrate and that can be remodeled for ECM deposition. The synthetic or natural materials used to recreate tissues are processed together with cells and/or biomolecules and are often termed bioinks, which refers to the material that incorporate cells. Historically, material formulations used in bioprinting have been dominated by materials that rapidly stabilize from a non-viscous state, for example, hydrogels (MORONI et al., 2018).

In particular, hydrogels for biomedical applications are designed to resemble the characteristics of native extracellular matrix (ECM) and to provide three-dimensional (3D) supports for cellular growth and tissue formation (ALGE; ANSETH, 2013). To this aim, hydrogels based on naturally occurring biopolymers have potential advantages over synthetic polymers, such as excellent biocompatibility, low immune response, and possible bioactive motifs encoded in their chemical structures (YUE et al., 2015).

Figure 7. Evolutionary Stages from 2D Cell Culture to the Development of 3D Tissue Analogs (A) 2D cell culture on plastic; (B) 3D cell culture inside hydrogel constructs; (C) bioprinting of 3D constructs; (D) biological maturation of the 3D bioprinted construct forming a tissue analog; and (E) implantation and integration of the tissue analog into the defect site

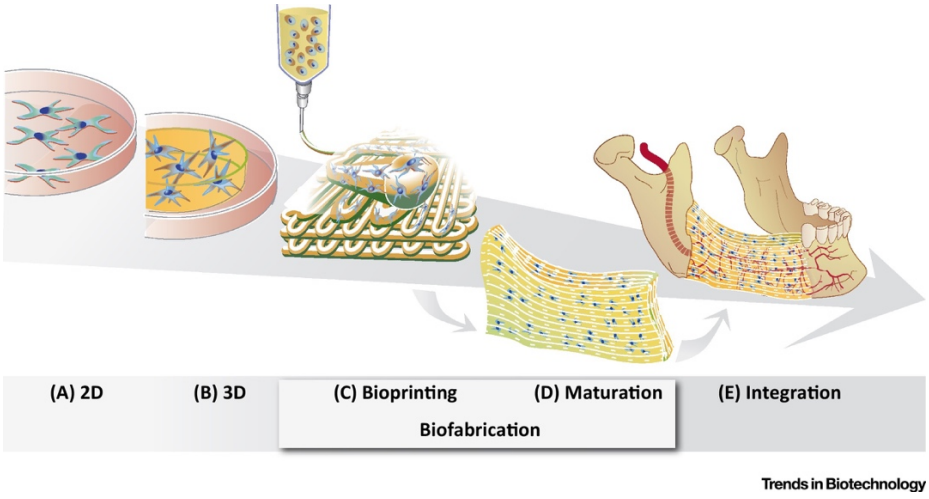

Source: KLOTZ et al. (2016).

GELATIN METHACRYLOYL (GELMA)

GelMA hydrogels have been widely used for various biomedical applications due to their suitable biological properties and tunable physical characteristics (ANNABI et al., 2014; HEO et al., 2014; NIKKHAH et al., 2012; TAN et al., 2013; ZHOU et al., 2014). GelMA hydrogels closely resemble some essential properties of native extracellular matrix (ECM) due to the presence of cell-attaching and matrix metalloproteinase responsive peptide motifs, which allow cells to proliferate and spread in GelMA-based scaffolds (YUE et al., 2015). GelMA is also versatile from a processing perspective. It crosslinks when exposed to light irradiation to form hydrogels with tunable mechanical properties. It can also be microfabricated using different methodologies including micromolding, photomasking, bioprinting, self-assembly, and microfluidic techniques to generate constructs with controlled architectures, as illustrated at Figure 8 (ANNABI et al., 2013; BERTASSONI et al., 2014; CHA et al., 2014; GAUVIN et al., 2012; HOSSEINI et al., 2014; TAMAYOL et al., 2015; ZAMANIAN et al., 2010).

Figure 8. Microfabrication techniques used to produce GelMA hydrogels constructs. (A) Schematic representation of photopatterning of GelMA using a pre-patterned photomask. (B) Stacked layers of patterned GelMA hydrogels fabricated using a micro-mirror projection stereolithography system. (C) Schematic representation of a fiber-assisted micromolding technique for production of parallel microgrooved surfaces that serve as a template for micropatterning GelMA. (D) Schematic representation of the self-assembly of microgels fabricated by photopatterning. (E) Examples of the microfluidics of GelMA hydrogels microfabrication. (i) Schematic representation of the method for coating microchannels with GelMA hydrogel. (ii) Fabrication of

spherical GelMA microhydrogels using a microfluidic flow-focusing device. (F) Schematic representation of the bioprinting method for fabricating microchannels inside a GelMA hydrogel using an agarose template. (G) Biotextile techniques as applied to the microfabrication of hybrid alginate and GelMA fibers and their assembly; (i) a representative SEM image of fabricated fiber; (ii) picture and micrograph of a typical woven fabric; (iii) a braided construct from NIH 3T3 fibroblasts, HUVECs, and hepatocytes (HepG2) as a liver model

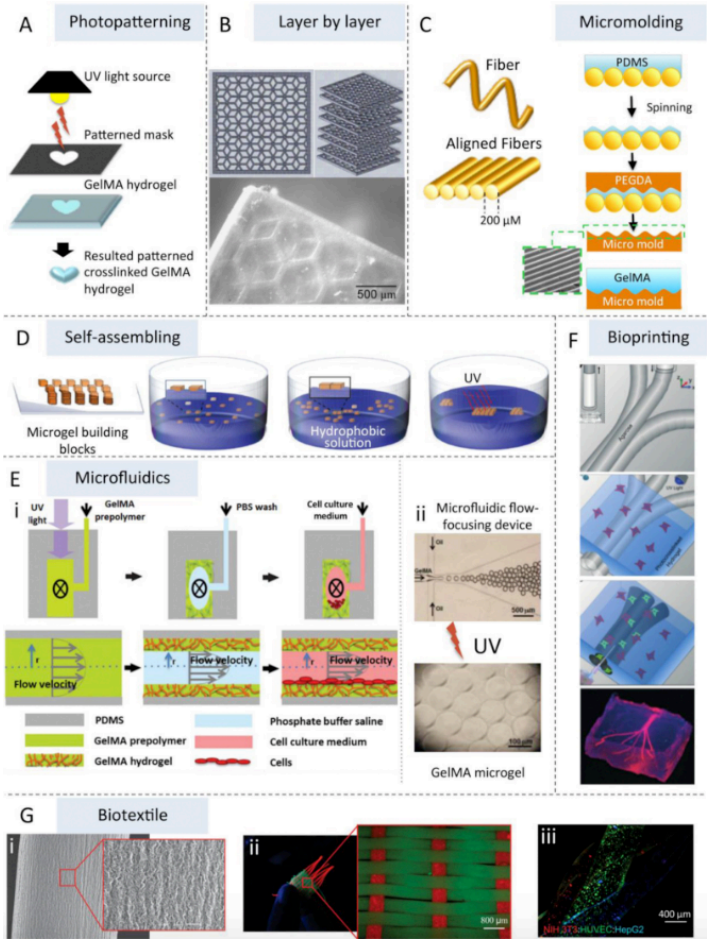

Source: YUE et al. (2015).

Briefly, GelMA is synthesized by the direct reaction of gelatin with MA in phosphate buffer (pH = 7.4) at 50 °C. This reaction introduces methacryloyl substitution groups on the reactive amine and hydroxyl groups of the amino acid residues. GelMA undergoes photoinitiated radical polymerization (i.e. under UV light exposure with the presence of a photoinitiator) to form covalently crosslinked hydrogels. As the hydrolysis product of collagen, the major component of ECM in most tissues, gelatin contains many arginine-glycine-aspartic acid (RGD) sequences that promote cell attachment (VAN DEN BULCKE et al., 2000).

Hybrid hydrogel systems can also be formed by mixing GelMA with nanoparticles such as carbon nanotubes (SHIN et al., 2012) and graphene oxide, and other polymers to form

networks with desired combined properties and characteristics for specific biological applications (YUE et al., 2015). Recent research has demonstrated the proficiency of GelMA-based hydrogels in a wide range of tissue engineering applications including engineering of bone, cartilage, cardiac, and vascular tissues, among others (ANNABI et al., 2014; HEO et al., 2014; NIKKHAH et al., 2012; TAN et al., 2013; ZHOU et al., 2014).

VASCULARIZATION IN TISSUE ENGINEERING: MATTER OF SURVIVAL

After construct implantation, delivery of nutrients to cells on a biomaterial is limited to approximately 200μm and occurs via interstitial fluid diffusion (ARONSON, 1994; CARMELIET, 2000; JAIN et al., 2005; KANNAN et al., 2005). Most bone tissue regeneration applications are considerably larger, at the case after tumor surgery. In addition, similar to most other tissues and organs, the bone is interlaced with blood vessels (KNESER et al., 2006; ROUWKEMA; RIVRON; VAN BLITTERSWIJK, 2008; SMITH et al., 2004). The vascular ingrowth is limited to several tenths of micrometers per day, which is too slow to provide adequate nutrients to cells in the interior part of implant, leading to the compromised healing results (JAFARIAN et al., 2008). Therefore, vascularization remains the principle obstacle that impedes the translation of most bone tissue engineered constructs to clinical practice (SALGADO; COUTINHO; REIS, 2004). As such, it is one of the main research topics in the tissue engineering community.

Two processes can be distinguished during the formation of a natural vascular network: vasculogenesis and angiogenesis. Vasculogenesis is the process that takes place during early embryonic development where angioblasts differentiate into endothelial cells, and proliferate within a previously avascular tissue to form a primitive capillary network (RISAU; FLAMME, 1995). Vasculogenesis can also occur in adults to revascularize a tissue following extensive damage or during tumor growth (BALAJI et al., 2013; BROWN, 2014).

Angiogenesis is defined as the formation of new vessels from an existing vascular network. These vessels can be formed by sprouting angiogenesis, where endothelial cells form sprouts starting from pre-existing vessels, or intussusceptive angiogenesis, where tissue pillars are inserted within existing capillaries to split the vessels (PATEL-HETT; D'AMORE, 2011). Angiogenesis is mainly driven by the need to supply tissues with sufficient nutrients and oxygen. As such, angiogenesis is regulated to a large extent by oxygen levels within tissues. Hypoxic tissues secrete growth factors and chemokines that activate vascular growth

and remodeling (FRAISL et al., 2009). Endothelial cells are stimulated to break out of their stable position in the vessel wall and jointly coordinate sprouting, branching, and new lumenized network formation (PHNG; GERHARDT, 2009). When perfusion of the tissue has increased and the supply of oxygen meets the demand, quiescence can be re-established resulting in a stable vascular network.

One strategy used to create vascular structures in GelMA is to prepare hollow channels within hydrogel matrices, which can be seeded with vascular cells to form a predesigned pattern of vascular structures. Multiple methods have been reported to create hollow channels in polymeric biomaterial scaffolds, including the use of multi-material 3D deposition (LUO; LODE; GELINSKY, 2013; MORONI et al., 2006), by directing printing or biofabricating the vessels during the 3D biofabrication process. It is clear that approaches that focus on the active patterning of vascular cells within engineered tissues provide the highest level of control over the initial organization of vascular structures, and therefore have the potential to result in the most naturally organized vascular networks at the initial stage of tissue culture (ROUWKEMA; KHADEMHOSSEINI, 2016). However, a question regarding this approach is how can a preformed vascular network in hydrogels be anastomosed to the vasculature of the patient in pre-vascularized tissue engineering? Microsurgical anastomosis is preferable because it will result in instantaneous perfusion, but this is generally not achievable due to insufficient organization and mechanical properties of the engineered vascular network (ROUWKEMA; KHADEMHOSSEINI, 2016).

A key challenge of vascular grafts is that they need to withstand a mechanically challenging environment immediately upon implantation (WU; ALLEN; WANG, 2012a). Thus, the classic approaches to arterial substitutes use strong materials. This is reflected in autografts, synthetic grafts and many tissue-engineered grafts (DAHL et al., 2011; HASHI et al., 2010; ISENBERG; WILLIAMS; TRANQUILLO, 2006; KAUSHAL et al., 2001; L'HEUREUX et al., 2006a; NIKLASON et al., 1999; WEINBERG; BELL, 1986). The host may be a good source of cells and a more efficient 'bioreactor' than the current *in vitro* tissue-engineering paradigm. Thus, it is possible to take advantage of the body's regenerative capacity to remodel cell-free synthetic grafts with an open porous structure that accelerates cell infiltration and remodeling (Figure 40)(WU; ALLEN; WANG, 2012a). The success of an implantable tissue engineered vascular graft is governed, among other factors, by the development of a scaffold that mimics the ECM(BARNES et al., 2007). It is well known that in natural tissues the ECM is a three-dimensional (3D) network of 50–500 nm diameter structural fibers(HASAN et al., 2014). Electrospun scaffolds, are known to be good

candidates for tissue engineering applications because of their ability to mimic the ECM of vascular tissue (HASAN et al., 2014; JIA et al., 2013; SHIN, 2013).

Rapid remodeling of a synthetic graft to a neoartery would most likely offer efficient integration with host tissue, a non-thrombogenic lumen and mechanical properties matching native vessels because it reduces the duration of host exposure to foreign materials (WU; ALLEN; WANG, 2012a).

POLY (GLYCEROL SEBACATE) (PGS)

PGS is a fast degrading elastomer, which is prepared by polycondensation of glycerol and sebacic acid, and degrades rapidly *in vivo* into glycerol and sebacic acid, metabolites naturally exist in the body, minimizing the duration of host inflammatory response (WU; ALLEN; WANG, 2012a, p. 20). PGS exhibits biocompatibility and biodegradability, both highly relevant properties in biomedical applications. PGS also involves cost effective production with the possibility of up scaling to industrial production. In addition, the mechanical properties and degradation kinetics of PGS can be tailored to match the requirements of intended applications by controlling curing time and curing temperature. Because of the flexible and elastomeric nature of PGS, its biomedical applications have mainly targeted soft tissue replacement and the engineering of soft tissues, such as endothelial tissue (RAI et al., 2012; WANG et al., 2002). PGS has been employed in order to successful produce vascular grafts with porous structure, which includes fabrications approaches that mimics the ECM, as electrospinning (GAHARWAR et al., 2014; HEYDARI et al., 2018; HU et al., 2017; JEFFRIES et al., 2015; SANT et al., 2011b).

Even though these approaches have been successful in generating well-organized endothelialized vascular networks, these structures are generally bordered by a dense, impenetrable layer of biomaterial, limiting further vascular remodeling and nutrient transport.

LASER ABLATION

Laser ablation is considered a promising tool to rapidly process and create complex structures on electrospun scaffolds (LEE et al., 2012; LIM et al., 2011; MCCULLEN et al., 2011). One of the benefits of laser ablation is that material is removed with minimal thermal damage (LEE et al., 2012; SRINIVASAN, 1986). This technique removes selective regions

of the scaffold and introduces micro-structured features including pores of a uniform size, specific global porosity, and preferential routes for cell and vascular tissue infiltration. Laser ablation possesses the ability for precise material processing with clean surface and reduced thermal damage in order to create controlled porous pattern to allow rapid endothelial cell infiltration and, thus, rapid endothelialization from tubular polymeric scaffolds employed as vascular graft. This is of crucial importance for tissue engineering scaffolds as the addition of controlled pores in the scaffold can provide many additional benefits including enhanced diffusion properties for mass transport of nutriments and cells during *in vitro* and *in vivo* expansion.

WHAT IS STILL MISSING TO CLINICAL TRANSLATE BONE TISSUE ENGINEERING CONSTRUCTS?

Bone Tissue Engineered grafts can improve osteogenicity and graft incorporation by incorporating grown factors, cells and performing materials. They can be molded to match the defect site using 3D printing and biofabrication techniques and avoid donor site morbidity, in comparison with the most currently employed strategy to heal critical size bone defects, i.e., autografts. However, bone is a complex tissue, and some drawbacks needs to be resolved: limited mechanical properties, limited osteogenicity, unknown immune response and poor vascularization, leading to poor graft integration and failure of engineered substitutes in clinical trials. In this work, we aimed to overcome these issues by employing fabrication techniques to produces proper substrates that mimics the extracellular matrix, incorporating biocompatible and bioactive composites with improved compatibility, using FDA approved synthetic biodegradable polymers for guided bone regeneration; and employing the combination of advanced biofabrication techniques and microfabrication approaches in order to immediately provide blood perfusion in 3D fabricated bone constructs. Therefore, by combining multiple strategies simultaneously, we aimed to be able to produce bone replacements that more closely recapitulate human physiology, and to accelerate the clinical translation of bone tissue engineering.

OBJECTIVES

The main scope of this thesis is dedicated to the development of solutions for Bone Tissue Engineering.

This manuscript is divided in **two parts**. The **first part** concerns to the development of electrospun membranes for Guided Bone Regeneration. The **main objective** of this part was:

- To produce biomimetic, bio-absorbable membranes with suitable mechanical properties and increased osteoconductivity for Guided Bone Regeneration.

The **specific objectives** of this first part were:

- To obtain biodegradable, biocompatible nanocomposites from cellulose nanocrystals and polycaprolactone in order to tune the mechanical properties of the biodegradable membranes obtained from electrospinning;
- To synthesize new bioactive and biodegradable composites from Biosilicate® and polycaprolactone in order to increase the osteoconductivity of these membranes.

The **second part** of this manuscript is devoted to new strategies in 3D microfabrication for bone constructs. The **main objective** of this part was:

- To design a new strategy of rapid vascularization of 3D microbiofabricated bone grafts

The **specific objectives** of the second part were:

- To obtain new nanocomposites from cellulose nanocrystals and Gelatin Methacryloyl (GelMA) in order to tune the mechanical properties of microbiofabricated constructs;
- To manufacture a small, biomimetic, suturable vessel graft from electrospinning, that can be embedded in microbiofabricated bone constructs and anastomosed with the host blood stream;

- To increase the porosity of the vascular grafts to allow the flow of vascular cells and precursors towards the microbiofabricated bone-like construct in order to nurture the construct, increase its size and improve its osteogenesis.

MORPHOLOGICAL, THERMAL AND MECHANICAL PROPERTIES OF POLY(E-CAPROLACTONE)/POLY(E-CAPROLACTONE)-GRAFTED-CELLULOSE NANOCRYSTALS MATS PRODUCED BY ELECTROSPINNING

INTRODUCTION

The use of biomaterials has attracted special interest and played an important role in biomedical applications, as tissue engineering (TIAN et al., 2012), an interdisciplinary and multidisciplinary research field involving the use of living cells cultivated into polymeric scaffolds for development of functional substitutes for damaged tissue or organs (BURG; PORTER; KELLAM, 2000; LANGER; VACANTI, 1993). A key goal of this area is to develop scaffolds with similar properties to those of extracellular matrices (ECMs) in order to help the tissue construction (FREED et al., 1994; LANGER; VACANTI, 1993).

Tissue engineering scaffolds, as ECM, should contain nanophase elements in order to mimic the nano/microsize scale of fibrous proteins (SILL; VON RECUM, 2008). Electrospinning is regarded as a simple and versatile top-down approach for the fabrication of uniform sub-micrometric fibers with long length scales in a continuous process (SUN et al., 2014; TAMAYOL et al., 2013). Electrospun matrices are able to support the attachment and proliferation of a wide variety of cell types (SILL; VON RECUM, 2008). A broad range of materials such as synthetic and renewable polymers, including collagens, chitosan, hyaluronic acid, poly(lactic acid), poly(glycolic acid), and poly(ε-caprolactone) (PCL) have been used for this purpose (AGARWAL; WENDORFF; GREINER, 2009; SUN et al., 2014; WANG; DING; LI, 2013).

PCL-based materials have emerged as a class of biomaterials of growing interest for applications in surgery as sutures, devices for bone fracture internal fixation, drug delivery and scaffolds for the regeneration of tissues or organs (KIM et al., 2013; RUCKH et al., 2010). However, few issues need to be overcome to enlarge the use of PCL, as its limited mechanical strength which can be too low to ensure scaffold structural integrity for specific applications (GHASEMI-MOBARAKEH et al., 2008; TAMAYOL et al., 2013; ZOPPE et al., 2009b), such as bone tissue engineering (BOSE; ROY; BANDYOPADHYAY, 2012; DIBA et al., 2012; WOODRUFF; HUTMACHER, 2010). Therefore, enhancing mechanical properties of PCL-based scaffolds is desirable for biomedical applications, because the materials have to meet controllable mechanical requirements for handling implants and

supporting the process of tissue regeneration and structure degradation (TAMAYOL et al., 2013; WANG; DING; LI, 2013).

The use of carbon nanotubes (CNTs) to improve mechanical properties of PCL-based scaffolds has been largely reported (CROWDER et al., 2013; D. DESHPANDE et al., 2012; MATTIOLI-BELMONTE et al., 2012; MCKEON-FISCHER; FLAGG; FREEMAN, 2011; PAN et al., 2012). Although the introduction of CNTs yielded composite fibers with increased mechanical properties, such types of composites can be quite costly (DE VOLDER et al., 2013). In addition, CNTs possess some degree of *in vivo* and *in vitro* toxicity (KAYAT et al., 2011; LIU et al., 2013; ZHAO; LIU, 2012).

Cellulose nanocrystals (CNC) are short particles with high crystallinity in a length of micro to nanometers scale with an estimated Young's modulus of 138 GPa and strength in the order of 7 GPa (NISHINO; TAKANO; NAKAMAE, 1995; SHI et al., 2012). Excellent chemical and thermomechanical properties of CNC/polymer nanocomposites have been reported (RESCIGNANO et al., 2014; SIQUEIRA et al., 2013; XIANG; JOO; FREY, 2009). Nevertheless, the most important drawback related to the use of cellulose nanocrystals for polymer nanocomposites is their inherent difficulty to disperse in non-polar medium, because of their polar surface (OKSMAN et al., 2006). Hence, the nanocrystal-matrix interface is usually the weakest point in nanocomposites, which limits the global performance of the corresponding composite due to the fiber pull-out, rather than nanofiber break (ZOPPE et al., 2009b). To overcome such effect and increase the compatibility with the polymeric matrix, chemical treatments must be performed on the cellulose surface, using different techniques and molecules (HABIBI, 2014; HABIBI et al., 2008; KROUIT; BRAS; BELGACEM, 2008; LÖNNBERG et al., 2011; RESCIGNANO et al., 2014; XIANG; JOO; FREY, 2009).One of the main drawbacks to the use of CNC in tissue engineering is their non-degradability, at best, slow degradability, by human body due to the lack of adequate cellulose enzymes (cellulases). However, researchers demonstrated that the degree of degradability can be influenced by the crystallinity of cellulose, and can be enlarged through oxidation steps (LIN; DUFRESNE, 2014). Moreover, CNC hold many advantages compared with CNT, since CNC are less expensive, simple to produce, largely available and, most importantly, biocompatible and more biodegradable (JACKSON et al., 2011; KÜMMERER et al., 2011; LAM et al., 2012; MAHMOUD et al., 2010), making them suitable candidates as nano-reinforcements in biomaterials.

In this study, low-molar mass PCL chains were grafted by ring-opening polymerization (ROP) from the surfaces of CNC, which were obtained from eucalyptus wood by acid hydrolysis, in an effort to improve their compatibility with the PCL continuous phase. Afterwards, nanocomposites of PCL-grafted CNC incorporated into PCL were produced by electrospinning aiming to improve the mechanical properties of electrospun PCL mats. Finally, the morphology, the thermal and mechanical properties of the electrospun nanocomposites were characterized. The produced electrospun mats have potential uses in biomaterial application as drug delivery, substitute implants, tissue repair, and also as medium for cells culture because of its morphology, high porosity and biological properties of their constituents.

MATERIALS AND METHODS

Cellulose nanocrystals (CNC) were extracted from eucalyptus wood in the laboratories of the Federal University of Minas Gerais, Brazil, according to a previously described procedure based on acid hydrolysis by aqueous solution of sulfuric acid (DE MESQUITA et al., 2011), yielding CNC typically 160 nm long and 5 nm thick. The ε-caprolactone monomer (99%) was purchased from Acros Organics© and was dried 48h over calcium hydride, distilled under reduced pressure and stored under nitrogen atmosphere prior to use. PCL (Mn = 57 kg/mol, D = 1.8, determined by size-exclusion chromatography in chloroform with polystyrene standards) was provided by Perstorp© (commercial name CAPA™ 6806). Toluene RE (99.5%), n-heptane RE (99%) and *N, N*-dimethyl formamide (DMF) RE (99.9%) were purchased from Carlo Erba©. Anhydrous toluene is obtained by refluxing over sodium and distillation. (DCM) RE (99.8%), tin (II) ethyl hexanoate (Sn $(Oct)_2$) catalyst, and uranyl acetate dihydrate (98%) were purchased from Sigma Aldrich and were used as received, without further purification.

ε-caprolactone ring opening polymerization from cellulose nanocrystals

Cellulose nanocrystals (CNC) were grafted with PCL chains by ROP, in a procedure adapted from the work of Habibi *et al.*[32] and sketched in Figure 9. Lyophilized CNC (1g) were placed in a three-neck flask, maintained under argon atmosphere. An amount of 50 ml of anhydrous toluene was added into the flask directly on the CNC. To improve dispersion, the suspension of CNC in toluene was maintained in a sonication bath during 5 minutes. Then, an azeotropic distillation of toluene was carried out in order to remove residual water. After this distillation, the required volume of anhydrous toluene (50 ml), previously distillated ε-caprolactone monomer (8ml, with density of 1.03g/ml) and tin (II) ethyl hexanoate (Sn

$(Oct)_2$) (200µl) were added into the flask. The polymerization proceeded for 24h under magnetic stirring at 120°C, and a few drops of aqueous HCl (1M) were added to stop the reaction. The modified CNC were recovered by precipitation in heptane and then filtered. In order to remove any non-grafted PCL chains (free PCL), the resulting PCL-grafted CNC were purified by Soxhlet extraction with toluene and then with dichloromethane (DCM).

Figure 9. Ring-opening polymerization of ε-caprolactone from the CNC surface.

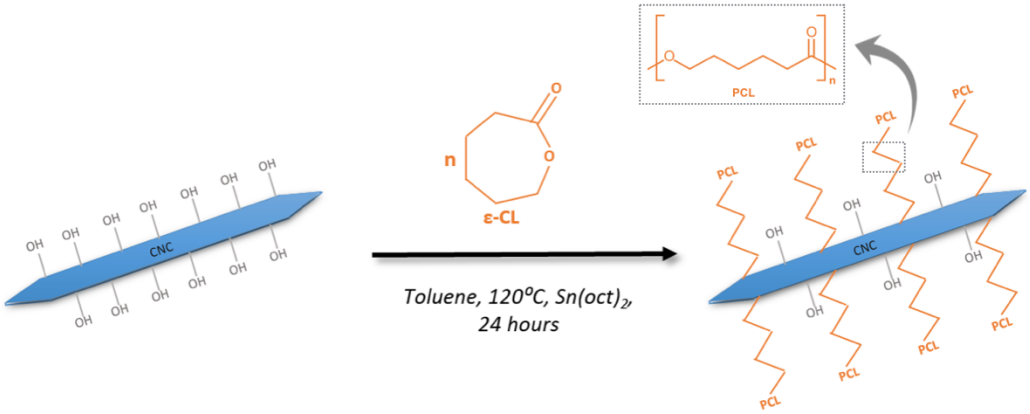

Source: Own authorship.

Fabrication of electrospun nanofiber mats

Preparation of the electrospinning solutions

The electrospinning solutions were prepared with final PCL concentration of 19% w/w (considering the amount of PCL grafted onto CNC) in 60/40 v/v DCM/DMF solvents mixture. Desired quantities of PCL-grafted CNC were dispersed at loadings of 1, 3 and 5wt.% of CNC in PCL. All solutions were sonicated for 5 minutes prior to electrospinning.

Electrospinning

Electrospun nanofibrous scaffolds of neat PCL, and PCL reinforced with PCL-grafted CNC were produced at room temperature and 80% humidity, with a voltage of 30kV applied through a positive electrode connected to the tip of a needle (15kV) plugged to a plastic syringe and syringe pump, and a negative electrode (-15kV) attached to a grounded static

collector plate covered with aluminum foil. All mats were electrospun for 20 minutes at a flow rate of 1.2 ml/h and a tip-to-collector distance of 15 cm.

Characterization

Infrared Spectroscopy (FT-IR)

Unmodified CNC, PCL-grafted CNC and neat PCL samples were characterized using a PerkinElmer infrared spectrometer model Spectrum 1000. The spectra were taken in the range 4000-750cm^{-1} using 32 scans and a scanning resolution of 4cm^{-1}. The samples were previously dried for 24 hours at 30°C in a vacuum oven.

Scanning Electron Microscopy (SEM)

The morphology of the nanofiber mats was observed in a Philips model XL30 scanning electron microscope, operating at 20kV. Prior to observation, parts of all electrospun nanomats, collected on aluminum foil, were glued on a stub using a double-face carbon adhesive and gold-sputtered. Average diameter of the nanofibers (D) was measured using the Image-Pro Plus 4.5 software. Approximately 50 measurements per sample were performed to calculate the average values.

Transmission Electron Microscopy (TEM)

Drops of aqueous dispersions of unmodified CNC and PCL-grafted CNC (0.01% w/v) were deposited on carbon-coated grid for electron microscope. Thin pieces of electrospun nanofibers were placed directly on copper grids. These samples were stained with uranyl acetate solution (2wt.%) for 2 min, and then allowed to dry. The samples were observed in a FEI Magellan model 400L, with acceleration voltage of 30kV.

Dynamic Mechanical Analysis (DMA)

The mechanical properties of the nanofiber mats were characterized using a dynamic-mechanical analyzer (DMA) model 8000 from Perkin-Elmer, in the controlled force mode, with a pre-load of 0.010N and load rate of 0.5N/min at room temperature. The glass transition temperature (Tg) of the nanocomposites was determined using constant frequency of 1Hz, temperature range from -100 to 40°C and heating ramp of 3°C/min. The DMA samples were carefully peeled off from the surface of the aluminum foil and placed between weighting

papers to avoid any damage. The sample dimensions were 10mm in length, 8mm in width and 0.10-0.15mm in thickness. Three samples were used to characterize each material.

Differential Scanning Calorimetry (DSC)

The thermal properties of the electrospun mats were analyzed by differential scanning calorimetry (DSC), using DSC8000 equipment from PerkinElmer, under a nitrogen flow of 20mL/min. The mat samples were first heated from -70°C to 100ºC, maintained at100ºC during 3 min and then cooled down to room temperature using a rate of 10ºC/min. From the heat of fusion (ΔH_m), the degree of crystallinity (Xc) of the samples was determined by using the equation bellow:

$$Xc = \Delta H_m / w\ (\Delta H_m{}^o 100\%) * 100 \qquad (1)$$

Where w is weight fraction of the polymeric matrix in the nanocomposite (without CNC) and $\Delta H_m{}^o 100\%$ is the heat of fusion of a 100% crystalline PCL, 139.4J/g (CRESCENZI et al., 1972).

Thermogravimetric Analysis (TGA)

The thermal stability of the samples was analyzed by thermogravimetric analyses (TGA) using a PerkinElmer thermo analyser model Pyris 1. Thermograms were recorded from room temperature to 600 or 800ºC at a heating rate of 10ºC/min under nitrogen flow of 20 ml/min.

RESULTS AND DISCUSSION

The thermogravimetric analysis under nitrogen of the unmodified cellulose nanocrystals (CNC), Figure 10 (a), indicated first a mass loss of 6% probably due the water and volatile products between 30 - 100ºC. A second mass loss with an onset degradation temperature of 260°C and a maximum degradation temperature at approximately 314°C typical of cellulose nanocrystals (SEGAL et al., 1959) was observed. A third degradation peak, with a maximum at 398°C and a mass loss of about 10% was also observed. The residue at 650ºC of the CNC was about 18%. These last two results are related to the hydrolysis time with sulfuric acid during the extraction process of the CNC. Regions of CNC which did not bind to sulfate groups have greater thermal stability. The sulfate groups on the CNC surface tend to promote the CNC thermal degradation and remain as residue after the thermal analysis under nitrogen (GREINER; WENDORFF, 2007; TEODORO et al., 2011). On the other hand,

the thermogravimetric analysis of the grafted cellulose nanocrystals (PCL-grafted CNC), Figure 10(b), displayed an onset degradation temperature around 295°C and a maximum degradation temperature at 382°C, consistent with the temperature range for lower molar mass due to PCL degradation. The residue at 650ºC was about 2%. As described above, the CNC had an 18% residue; and on the premise that the thermodegradation of PCL has no residue, the CNC content in the grafted cellulose nanocrystals could be calculated. This content was found to be between 10 and 12%. This result shows the grafting process was effective.

Figure 10. TGA thermograms of (a) cellulose nanocrystals (CNC) and (b) PCL-grafted CNC.

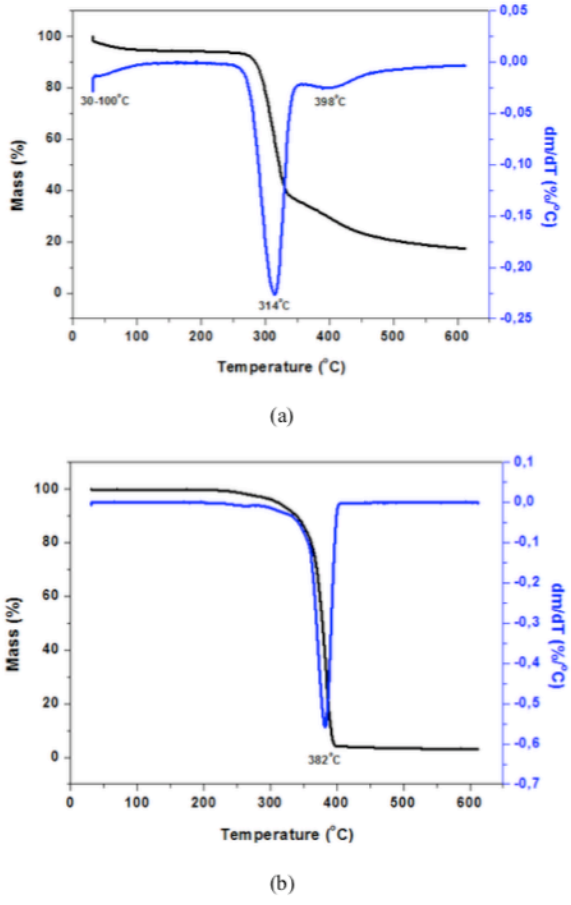

Source : Own autorship

The PCL grafting process onto cellulose nanocrystals was also confirmed by FT-IR analyses. The FT-IR spectra of the unmodified cellulose nanocrystals (CNC), PCL-grafted CNC nanocrystals and neat PCL are shown in Figure 11. In comparison with the pure cellulose nanocrystals spectra, the PCL-grafted CNC spectrum shows, even after Soxhlet extraction, the presence of the band at 1730cm^{-1}, characteristic of the axial deformation of the

carbonyl (C=O) group from PCL. Moreover, a lower band intensity of the axial deformation of the OH bonds at 3330cm^{-1} was also observed, suggesting the effective grafting of PCL at the surface of the CNC. These results are in accordance with the patterns of FT-IR spectra previously obtained by Habibi *et al.* (HABIBI et al., 2008).

Figure 11. FT-IR spectrum of cellulose nanocr O título da figura deve ser acima dela ystals (CNC), PCL-grafted CNC and neat PCL

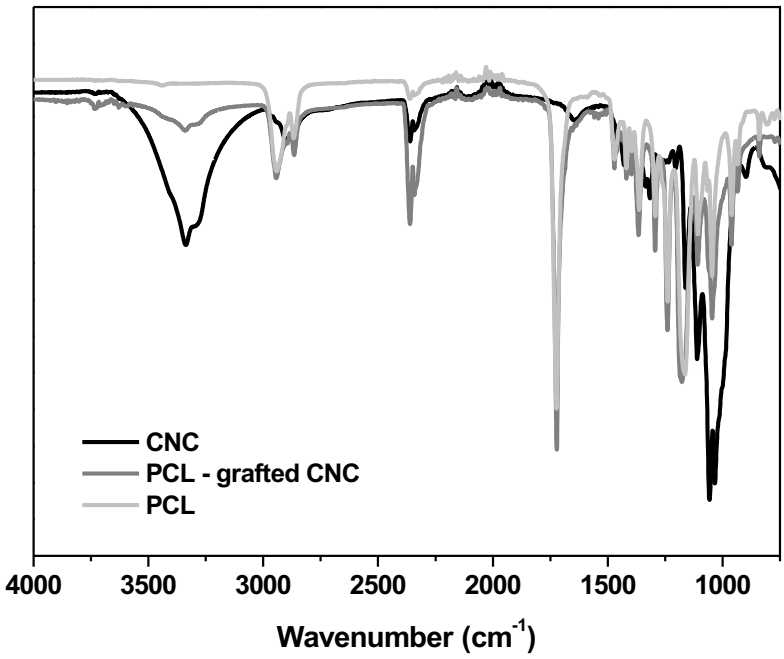

Source: Own authorship.

Figure 12 shows SEM images obtained for the electrospun mats of (a) neat PCL, (b) PCL with 1wt.%, (c) with 3wt.%, and (d) with 5wt.%of PCL-grafted CNC. The global appearance and morphology of the corresponding mats were preserved, even after the addition of PCL-grafted CNC. However, it can be observed that the average fiber diameter (D) decreases when adding the PCL-grafted CNC (Figure 12 and Table I). Indeed, in the present work, the diameter of the nanofibers produced under the same conditions decreased from 640 nm for the neat PCL to 180 nm for the PCL + 1wt. % PCL-g-CNC fibers and 165 nm for the PCL + 2wt. % and 5 wt. % PCL-g-CNC fibers. This diameter reduction can be probably attributed to the addition of the PCL-g-CNC leading to an increase of the electrospinning solution conductivity. This observation clearly corroborates the previous works of Shi *et al.* (SHI et al., 2012) and Xiang *et al*. (XIANG; JOO; FREY, 2009), which

have studied the morphology of electrospun nanofibers of poly (lactic acid) reinforced with cellulose nanocrystals. The authors observed an increase in the electrical conductivity of the solution due to the presence of sulfate ester groups on the CNC surface, resulting in a higher charge density on the surface of ejected jet, which promote the formation of higher elongation forces and thus, producing fibers with smaller diameter.

Figure 12. SEM images of electrospun mats of (a) neat PCL, and PCL with (b) 1wt.% (c) 3wt.% and (d) 5wt.% PCL-grafted CNC.

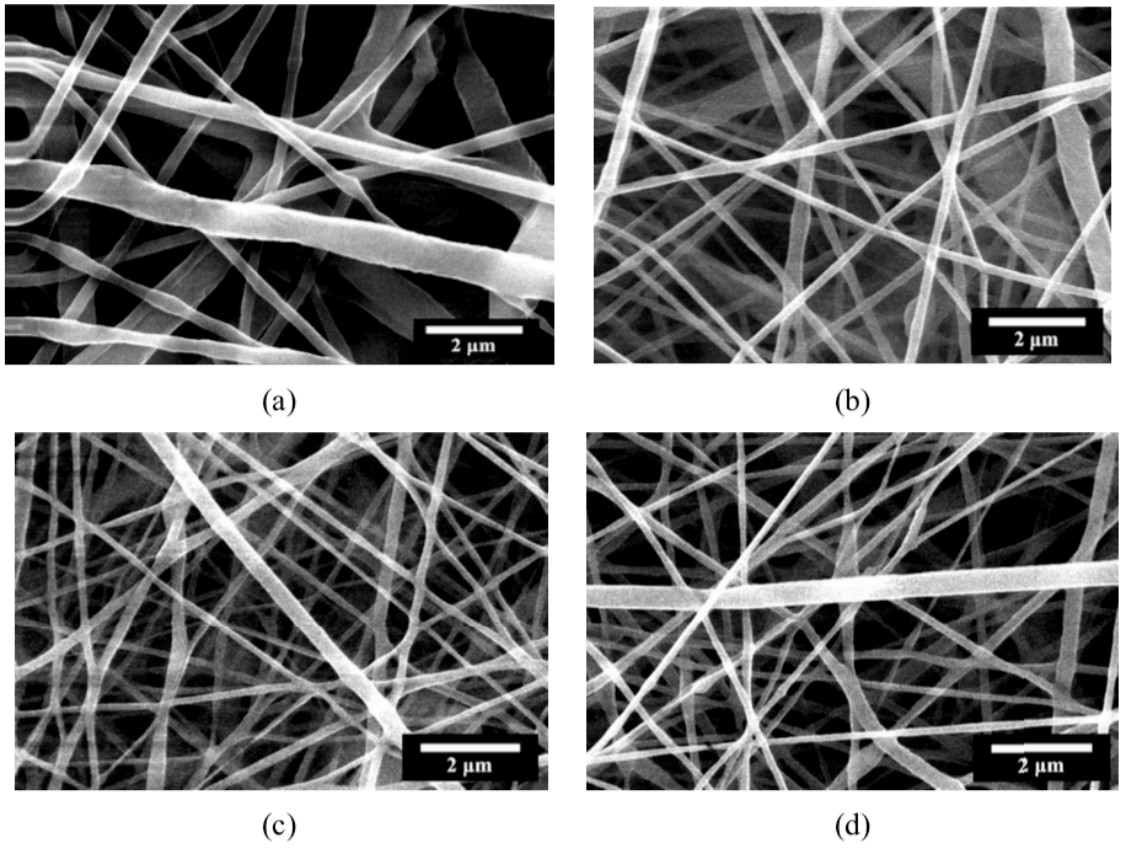

Source: Own authorship

Table 2. Average fibers diameter (D), thermal properties and degree of crystallinity (Xc) of the samples.

Sample	D (nm)	Tm (ºC)	ΔHm (Jg^{-1})	Tc (ºC)	Xc (%)	Tg (ºC)
PCL	636.9 ± 62.1	60.0 ± 2.1	80.9 ± 0.1	41.3 ± 1.4	58.0 ± 0.1	-60.0 ± 1.5
PCL + 1wt.% PCL-g-CNC	182.1 ± 11.9	62.8 ± 1.8	81.7 ± 0.1	41.4 ± 1.8	59.2 ± 0.1	-60.5 ± 2.2
PCL + 3wt.% PCL-g- CNC	164.7 ± 8.9	66.2 ± 2.3	82.5 ± 0.2	44.3 ± 1.4	61.0 ± 0.2	-60.8 ± 2.5
PCL + 5wt.% PCL-g- CNC	166.4 ± 7.5	67.8 ± 1.5	84.4 ± 0.2	46.7 ± 2.0	63.2 ± 0.2	-61.3 ± 1.8

Source: Own authoship.

In order to analyze the effect of the incorporation of PCL-grafted CNC into the PCL matrix, the corresponding mats were observed by TEM. In Figure 13, micrographs of (a) neat PCL nanofibers, (b) PCL + 1wt.%, (c) PCL + 3wt.% and (d) PCL + 5wt.% of PCL-grafted CNC are shown. The slightly dark regions observed in Figure 13 (a) are due to PCL fibers overlapping. In Figure 13(b)-(d), the PCL-grafted CNC domains are visualized as denser lines (dark) indicated by arrows, while the less dense areas (brighter) represent the PCL domains. The PCL-grafted CNC domains show a thin and aligned shape with good distribution within PCL fibers. The TEM analysis showed the PCL-grafted CNC were incorporated into the PCL matrix, and the corresponding nanocomposites were successfully obtained while preserving the global appearance and general morphology of nanofiber mats, as previously shown by the SEM analysis (Figure 12).

Figure 13. TEM images of electrospun mats of (a) neat PCL, and PCL with (b) 1wt.% (c) 3wt.% and (d) 5wt.% PCL-grafted CNC. Arrows are pointing to some PCL-grafted domains.

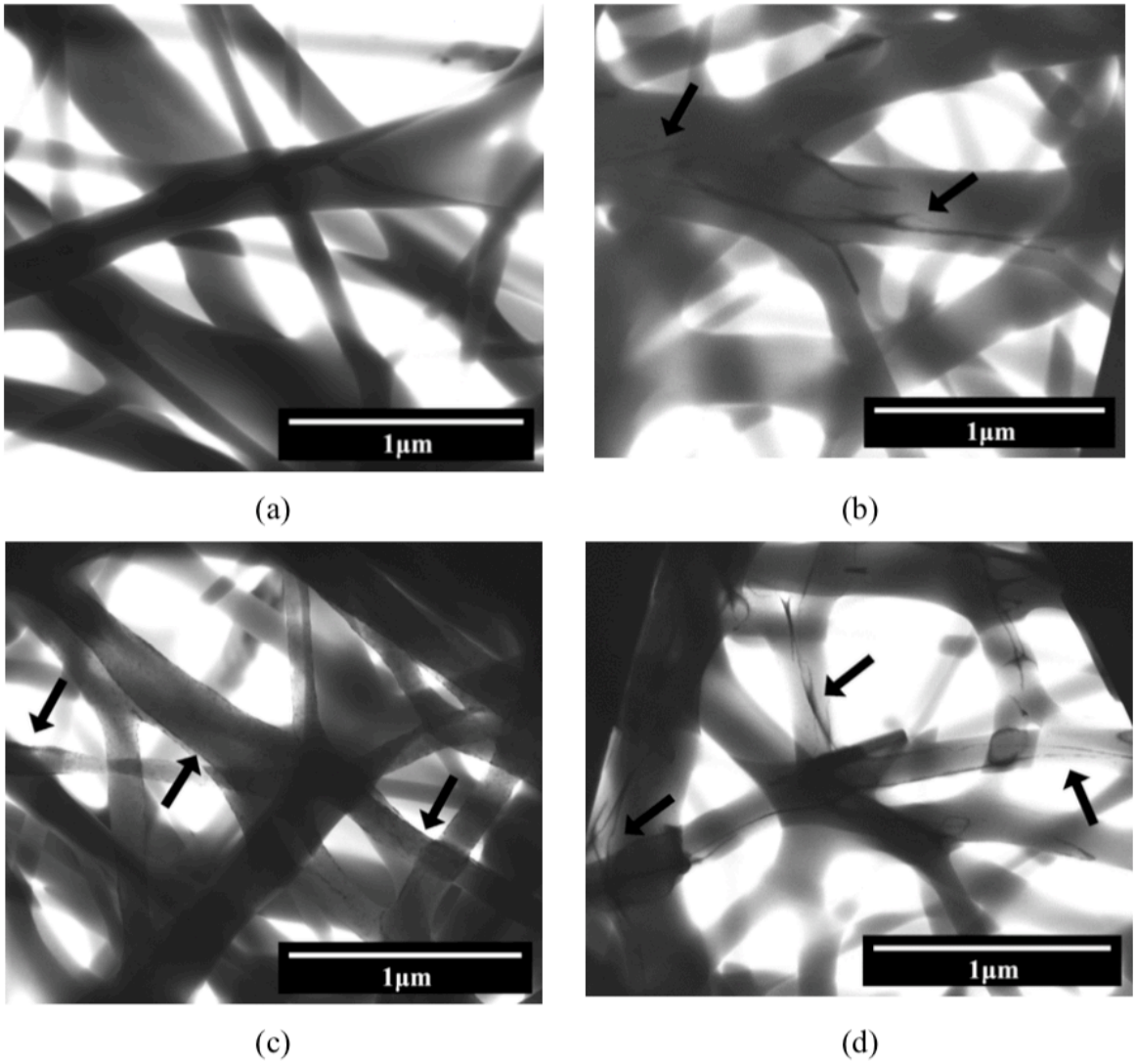

Source: Own authorship

DSC experiment were performed on the fibrous mats in the temperature range of -70°C to 100°C. In this temperature range, no specific degradation of the PCL-g-CNC can occur as previously shown by TGA analysis. From the first heating curves, Figure 14 (a), the melting temperature (Tm) and the degree of crystallinity (Xc) of the sample were obtained (Table I). There was an increase in Tm with the PCL-grafted CNC addition, indicating the production of more perfect crystallites. The degree of crystallinity of the samples also increased with the PCL-grafted CNC addition. Such a result was also observed by Habibi *et al*. (HABIBI et al., 2008) with PCL casting films and unmodified or modified (PCL-grafted) cellulose nanocrystals. They noted the grafting procedure contributes considerably to increase the degree of crystallinity of the corresponding bionanocomposite. The crystallization temperature of the samples (Tc) was obtained from the cooling curve, Figure 14 (b), after erasing the previous thermal history. An increase in the Tc of the nanocomposites with an

increase in the amount of PCL-grafted CNC was observed, which means the filler surface probably acts as nucleation sites for the PCL chains crystallization under quiescent conditions. The main relaxation temperature which can be associated with glass transition temperature (Tg) of the nanocomposites, determined from DMA curves, not shown here, was not affected by the incorporation of PCL-grafted CNC (Table I), indicating the CNC did not interfere with the relaxation of the PCL amorphous phase.

Figure 14. DSC (a) heating and (b) cooling thermograms of neat PCL, and PCL with 1wt.%, 3wt.% and 5wt.% PCL-grafted CNC electrospun mats.

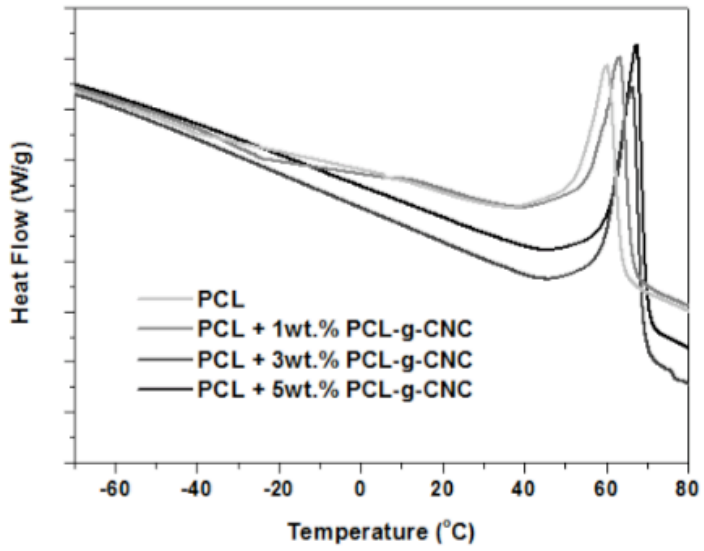

(a)

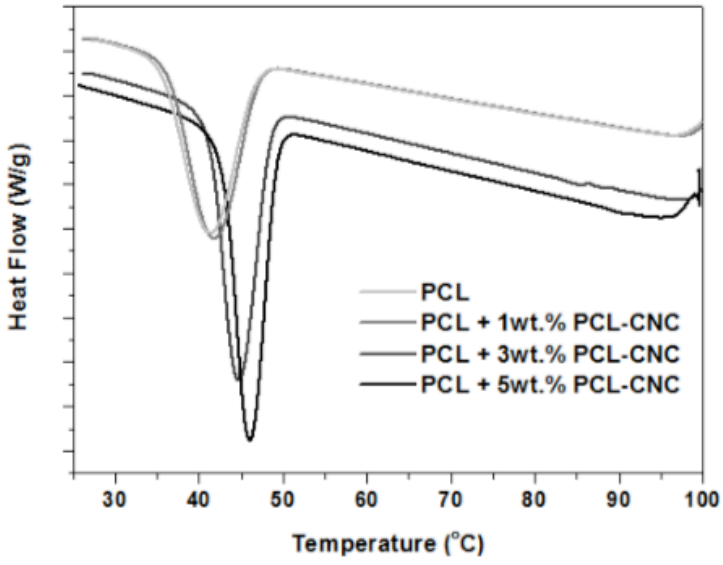

(b)

Source: Own authorship

Figure 15shows the results of the thermogravimetric analyses for the electrospun mats formed of neat PCL and PCL with 1wt.%, 3wt.% and 5wt.% of PCL-grafted CNC. These results clearly indicate a decrease in the thermal stability of the PCL mats with increasing content of PCL-grafted CNC in the bionanocomposites, as expected due to the lower thermal stability of the PCL-grafted CNC as already described. The neat PCL mat shows a maximum degradation temperature at approximately 450°C and no residue. As showed above (Figure 10), the PCL-grafted CNC shows a maximum degradation temperature around 380°C. The lower temperature observed for the PCL-grafted CNC is likely due to shorter chains (lower molar masses) of the PCL grafts compared to the commercial PCL matrix (with Mn of 57 Kg/mol). The neat PCL mat had a maximum degradation temperature of approximately 50°C higher than the bionanocomposites with 3wt.% and 5wt% of PCL-g-CNC. Therefore, the thermal degradation of the two components in the bionanocomposites is not independent; as the PCL-g-CNC thermal degradation occurs first, thus the thermal degradation of the PCL matrix tends to occur at lower temperature.

Figure 15. TGA thermograms of neat PCL, and PCL with 1wt.%, 3wt.% and 5wt.% PCL-grafted CNC electrospun mats.

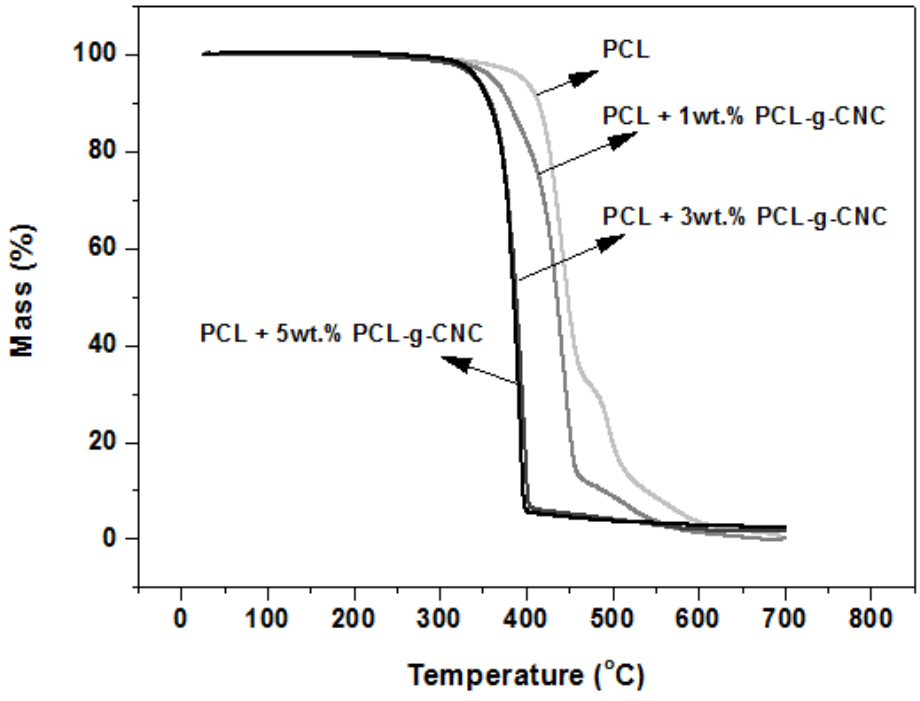

Source: own authorship

As shown in Figure 16, the Young's modulus (E) and the tension at break (σ_b) of the PCL nanomats increased when the PCL-grafted CNC was added, indicating that stiffer and more performing nanomats were obtained. The addition of 5wt.% of PCL-grafted CNC increased the elastic modulus by over 50%. However, with increased PCL-grafted CNC content, the elongation at break (ε_b) of the bionanocomposite mats decreased. These results indicated a good dispersion and interface between the PCL-grafted CNC and the PCL matrix was developed. The spread in the data is fairly typical reflecting variations in the randomly deposited electrospun mats.

Mechanical properties of non-woven electrospun mats are influenced by several factors related to processing and solution conditions. THOMAS et al., 2006 studied the mechanical and morphological properties of PCL electrospun mats fabricated at different collector rotation speeds. They observed that the mechanical properties (modulus and tensile strength) of the mats increased gradually with increasing collector rotation speed. This behavior was attributed to the increased fiber alignment and packing and the decrease in interfiber pore size at higher collector rotating speeds. In our case, a static collector was used. Zoppe *et al*. have demonstrated that the mechanical behavior of nanocomposites formed of PCL incorporated with unmodified and modified (PCL-grafted) cellulose nanocrystals are intimately related to the reinforcing effect of the CNC filler and also to the nanofiber diameter (ZOPPE et al., 2009b). The density of entanglements and its distribution are better in fibers with smaller diameters due to the higher surface area. In the work of Lönnberg *et al.* the highest mechanical properties of PCL bionanocomposite reinforced with grafted microfibrillated cellulose (MFC) were obtained for the longest PCL graft length and with a high loading in MFC (10wt.%) (LÖNNBERG et al., 2011).

Figure 16. Elastic modulus (E), tension at break (σ_b) and elongation at break (ε_b) of the electrospun mats samples.

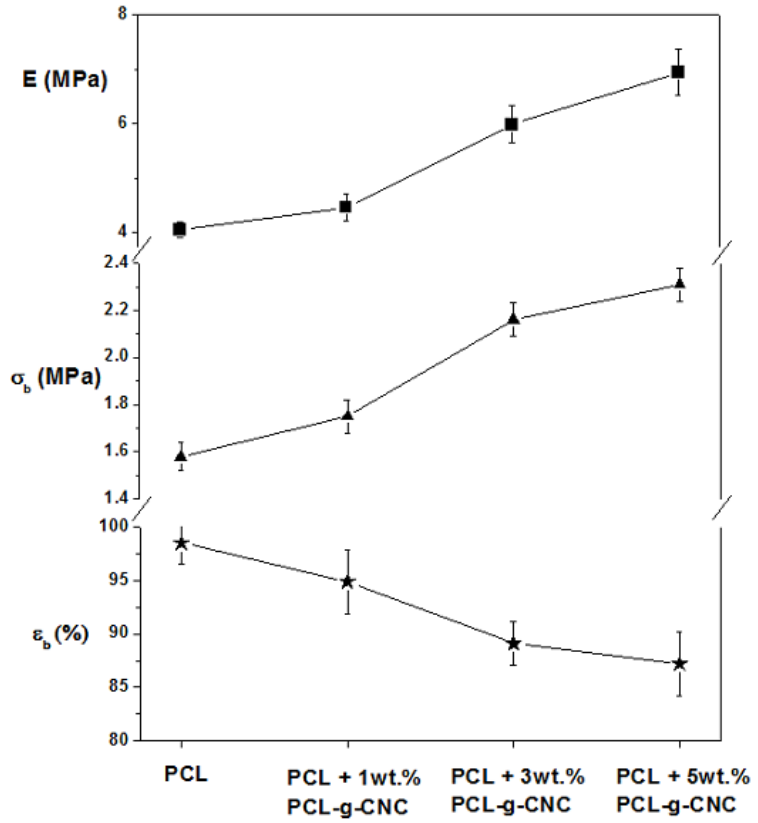

Source: Own authorship.

Therefore, according to our results, the incorporation of PCL-grafted CNC, even in small amounts, increased considerably the mechanical properties of PCL nanofiber mats. The improvements in mechanical behavior can be attributed to the addition of PCL-grafted CNC to the fiber and to respective decrease in the fibers diameter. Thus, from these analyses, it is clear the grafting procedure contributed to rise (even slightly) the degree of crystallinity and to considerably increase the mechanical strength and stiffness of the bionanocomposites.

CONCLUSION

In order to reinforce biodegradable membranes for Guided Bone Regeneration from Poly(ε-caprolactone) (PCL), we employed natural and biodegradable cellulose nanocrystals (CNC) as reinforcement phase. To improve the compatibility within the hydrophilic cellulose nanocrystals and the hydrophobic phase (PCL), the PCL grafting from cellulose shows to be a simple and effective technique: PCL chains grafting from cellulose nanocrystals was successfully obtained via *in-situ* ring opening polymerization reaction, and the resulting Poly(ε-caprolactone)/ Poly(ε-caprolactone)-Grafted cellulose nanocrystals were successfully dispersed into hydrophobic PCL/DCM/DMF dissolution. Electrospun mats of PCL/PCL-

grafted CNC have been produced, with homogeneous nanofibers, and the average fiber diameter decreases with the addition of PCL-grafted CNC.

The grafting procedure contributes considerably to increase the degree of crystallinity and also to increase the mechanical strength of the nanocomposite by significant increasing the melting temperature (Tm) and the melt crystallization temperature (Tc) in the electrospun PCL by adding the CNCs. Also, a rising in the degree of crystallinity of the scaffolds with PCL-grafted CNC indicates a better compatibility between the matrix and the filler.

The incorporation of PCL-grafted CNC, even in a small amount, increases considerably the mechanical properties of PCL nanofiber mats, with significant improvements in Young's Modulus in Strain at Break. The reinforcement effect is attributed to PCL-grafted CNC within the fiber (intrinsic strength) and to more fibers entanglements due to the fiber diameter decreasing. Therefore, it become clear the potential of cellulose nanocrystals as reinforcement in biodegradables membranes for Guided Bone Regeneration, as for many tissue engineering applications according mechanical requirements. In order to improve the bone regeneration, these membranes can be embedded with an osteogenic phase, as it will be discussed in the following chapter.

DEVELOPMENT OF SCAFFOLDS OF POLY(ε-CAPROLACTONE) INCORPORATED WITH BIOSILICATO® AND CELLULOSE NANOCRISTALS FOR BONE GUIDED REGENERATION AND TISSUE ENGINEERING

INTRODUCTION

Despite the natural regeneration capacity of bone tissue, many traumas and pathologies can impede normal bone function, leading to the need for bone grafting or prostheses (AMINI; LAURENCIN; NUKAVARAPU, 2012; MANSOUR et al., 2017). However, these techniques may lead to complications related to a second surgery and limited availability (for autologous grafts) or undesirable immune responses (for halogen grafts)(DAMIEN; PARSONS, 1991; DELLOYE et al., 2007).

Tissue engineering is an interdisciplinary field that applies the principles of engineering and biological sciences in the development of biological substitutes that recover, maintain or restore tissue function (ASGHARI et al., 2017; LANGER; VACANTI, 1993). The methodology in tissue engineering is based on scaffolds, or tridimensional matrices which, according to their intrinsic properties, modulate and guide cell differentiation and proliferation, leading to the reconstruction of different tissues, such as bone tissue (WINKLER et al., 2018). The general criteria for developing appropriated scaffolds for bone tissue engineering are based on the type of material used, as well as its architecture and porosity, surface chemistry and mechanical properties appropriate to the bone tissue (WINKLER et al., 2018).

The Guided Bone Regeneration treatment concept advocates that regeneration of osseous defects is predictably attainable via the application of occlusive membranes, which mechanically exclude non-osteogenic cell populations from the surrounding soft tissues, thereby allowing osteogenic cell populations originating from the parent bone to inhabit the osseous wound (RETZEPI; DONOS, 2010). Guided Bone Regeneration membranes are occasionally utilized with dental implant (CHAPPUIS et al., 2017; PIATTELLI; SCARANO; PAOLANTONIO, 1996) or bone grafting materials (GUESS; KRATCHMAN; KIM, 2018). The exposed implant or material filled area is covered by the membrane (RETZEPI; DONOS, 2010). In the market, conventional materials for guided bone regeneration membranes are non-degradable, as the expanded—polytetrafluoroethylene (ePTFE: Gore-Tex®)(SCHNEIDER et al., 2014). Although ePTFE membranes have achieved excellent

clinical results, second surgery procedure is required to remove the membranes after new bone generation. Biodegradable guided bone regeneration membranes have a benefit to avoid second surgery, which prevent the discomfort of the patient and extra surgical procedures. However, there are still challenges related to (1) barrier of tissue invasion associated with rapid degradation of membranes, (2) osteoinduction and osteoconductivity to achieve large area repair and (3) mechanical stability of membrane to sustain surgery treatment (SCHNEIDER et al., 2014).

Electrospinning is a fabrication technique which leads to the production of membranes and scaffold from various polymers, including biodegradable polymers, as Poly (Caprolactone) (ATTIA et al., 2018; HAJIALI; TAJBAKHSH; SHOJAEI, 2018; YAO et al., 2017). Electrospinning consists in the application of an electric current to the polymeric solution, leading to the creation of a jet, where occur the rapid evaporation of the solvent and, consequently, to the production of polymeric fibers (KISHAN; COSGRIFF-HERNANDEZ, 2017; PHAM; SHARMA; MIKOS, 2006). Membranes produced by electrospinning have architecture and porosity that mimics the ECM (KISHAN; COSGRIFF-HERNANDEZ, 2017), being a suitable material for scaffolds for tissue engineering. Moreover, electrospinning membranes can be employed as physical barrier, mainly in the form of a membrane (CHAPPUIS et al., 2017; RETZEPI; DONOS, 2010), preventing the fast-growing fibroblasts from migrating into the wound site and keeping a space for the slow-growing bone tissue to regenerate(CASTILLO-DALI et al., 2014).Therefore, Electrospinning is an ideal technique to produce polymeric guided bone regeneration membranes and scaffolds for tissue engineering.

Poly(ε-caprolactone) (PCL) is a known biocompatible polyester, having the advantage that its degradation products are not acidic. A major disadvantage of synthetic membranes is that they generally lack osteoinductive capacity to allow bone growth along their surface and promote bone healing or regeneration (RETZEPI; DONOS, 2010; SIMIAN et al., 1999).

Tuning the mechanical properties of biodegradable materials and composites according to the application is a priority in the research of electrospinning membranes for bone tissue engineering and bone guided regeneration. Previously, we demonstrated the addition of cellulose nanocrystals-PCL nanocomposites led to improved mechanical properties of electrospun membranes based on PCL (BELLANI et al., 2016). However, we are still concerned to the osteoinduction of the material in order to improve the bone regeneration at the injury site.

Biosilicate® is a recently developed glass ceramic with excellent bioactivity. Studies had shown Biosilicate® significantly improved osteoblasts proliferation *in vitro* (CROVACE et al., 2016; MOURA et al., 2007; RENNO et al., 2010) and osteoinduction *in vivo* (CROVACE et al., 2016; GRANITO et al., 2009; RENNO et al., 2010) and is currently being applied in medical and dental areas (CROVACE et al., 2016). Through the combination of PCL electrospun mats and Biosilicate®, scaffolds can be produced with bioactive properties provided by bioceramics, while the polymer phase of PCL increases the degree of flexibility of the material, reducing its fragility. However, because it is difficult to control the Biosilicate® particles size (RENNO et al., 2013), it may be challenging to predict the mechanical properties of the obtained composite.

Cellulose nanocrystals (CNC) are constituted by short, nanometric and hydrophilic rod-shaped crystalline chains. It has previously been shown that the addition of biodegradable and non-toxic cellulose nanocrystals in polymer matrices improves the mechanical properties of scaffolds according to their proportion (BELLANI et al., 2016; SIMÃO; BELLANI; BRANCIFORTI, 2017). In this context, it is possible to adapt to the mechanical properties of scaffolds according to the proportion of CNC incorporated, according to the desired application.

The incorporation of Biosilicate® and cellulose nanocrystals in PCL scaffolds obtained by electrospinning is innovative in the area of biomaterials for bone regeneration. This approach may allow better restoration of the structure, function, behavior, biochemical metabolism and biomechanical performance of these tissues.

However, the interfacial adhesion between both CNC and Biosilicate® and the PCL is low as the low polar PCL and the high polar CNC and Biosilicate® are thermodynamically immiscible, resulting in particles aggregations, limiting their mechanical reinforcing (DE SOUZA LIMA; BORSALI, 2004; LJUNGBERG et al., 2005; SCHROERS; KOKIL; WEDER, 2004). By PCL grafting from CNC and Biosilicate®, we can yield better interaction between PCL and the CNC and Biosilicate®, which can lead to stronger hydrogen bonds between the polymeric and the reinforcement phases, improving the mechanical properties of PCL electrospun membranes.

In this work, we produced composites from Biosilicate® and cellulose nanocrystals, and PCL, by PCL grafting-from both particles in order to increase their compatibility with the PCL matrix. The resulting BioSiO-g-PCL and CNC-g-PCL composites particles, respectively, were incorporated into PCL electrospun membranes, creating the bioactive/reinforcement and

the controllable reinforcement phase. Morphological, thermal and mechanical properties of nanocomposite scaffolds were characterized. *In vitro* testing with the composite mats and osteoblasts-like cells were performed to assess the cell proliferation and viability, and the biomineralization assay to investigate the effect of the Biosilicate® addition in the *in vitro* mineralization. We expected to obtain degradable PCL electrospun membranes with controlled reinforcing and osteoinductive properties for potential applications in bone tissue engineering and guided bone regeneration.

MATERIALS AND METHODS

Biosilicate® Milling

The Biosilicate® was supplied by the Laboratory of Vitreous Materials (LaMaV) of the Federal University of São Carlos (UFSCar), with particle size distribution between 25 and 54μm. In order to reduce the size and improve the distribution of the particles, improving thus the incorporation of these particles among the fibers of the PCL scaffolds, the particles were milled in low energy (rotation) for 48 hours and then in a vibratory mill for 24 hours.

In a polystyrene cylindrical shell, with zirconia beads, with total volume of 300 ml, and work volume of 80 ml, it was added:

• 64 ml (49.92 g) of isopropyl alcohol (density = 0.78, Labsynty Ltda.), corresponding to 80% of the work volume;

• 16 ml (45.056 g) of Biosilicate® (density = 2.816 g / cm 3) as supplied, corresponding to 20% of the work volume;

• 0.045 g of polyvinyl butyral (PVB) resin (Butvar B-98) as powder, considering 0.1% of the volume of Biosilicate®, previously dissolved in part of the of the isopropyl alcohol required for milling, in order to facilitate the dispersion of the PVB in content.

The Biosilicate® particles were milled for 48 hours at 108 revolutions per minute. At the end of this period, it was noticed the suspension inside the jar was more viscous than desired. Following, more 100 ml of isopropyl alcohol and 0.02% of PVB were added in order to decrease the shear stress and thus optimize the milling process (HOTZA et al., 1998). A sample of the obtained suspension was removed for particle size characterization. Then, the jar was placed on a vibrating platform and the milling was held for more 24 hours. Part of the suspension obtained after vibratory milling was also characterized.

Cellulose Nanocrystals

Cellulose nanocrystals (CNC) was as a generous donation from the Department of Materials Engineering, UFSCar. The material was extracted from microcrystalline cellulose (Avicel® PH-101, Sigma Aldrich®) by acid hydrolysis with sulfuric acid solution, using previously reported procedures (MORELLI et al., 2012) and lyophilized after extraction.

PCL Grafting by ε-CL Opening Ring Polymerization from Cellulose Nanocrystals and Biosilicate®

In order to allow the CNC and the Biosilicate® to be dispersed in PCL matrix and, thus, improving the reinforcement of PCL scaffolds with the nanoparticles by a correct interfacial connection between the matrix and the particles, the CNC and Biosilicato® grafting procedure was performed from the PCL through the ring opening of the ε-CL based on the works of HABIBI et. al. (HABIBI et al., 2008) and BELLANI et. al. (BELLANI et al., 2016), with some adaptations.

Prior to this procedure, Ɛ-caprolactone monomer (99%, 1.03 g / ml density, Acros Organics®) was dried over calcium hydroxide for 48 hours, then distilled under reduced pressure and finally maintained under argon atmosphere until the time of use. The lyophilized cellulose nanocrystals and Biosilicate® were dried in a vacuum oven at 50°C for 12 hours in order to minimize water or solvent residues and, following, they were maintained under an argon atmosphere until the grafting. Besides, all the glassware used for the experiments was previously dried in an oven at 60˚C for 24 hours until the time of its use. All these procedures were strictly followed in order to minimize, as much as possible, the presence of water, since the grafting starts from free hydroxyl groups.

The required amount of toluene (100 ml for CNC and 50 ml for Biosilicate®, whose volumes of solvent based on particle volumes) (99.5%, Carlo Erba®) was distilled twice and, then, dispersed with a syringe and needle in a round bottom flask with three sealed exits containing 1 g of lyophilized and dried CNC or Biosilicate®, which were previously placed in these flasks with a magnetic bar inside and kept under argon atmosphere, as mentioned. The flasks were kept in an atmosphere of circulating argon for more 5 minutes, by injecting argon through a needle into one of the rubber sealed exits of the flask and, in order to circulate the argon, another needle was simple placed punching another flask exit sealed with a rubber cap. Again, this proceeding was performed to prevent any presence of free hydroxyl groups other than the ones over the CNCs and the Biosilicate®.

After adding the toluene, the flasks were then maintained for 5 minutes in sonication to improve the dispersion of the CNC or Biosilicate® in the solvent. In order to remove any azeotropes that would may be present between the CNC or Biosilicate® and toluene, the toluene was removed by a cold trap system, where the toluene was captured in a glass apparatus immersed in a thermal isolating cylinder, as shown in Figure 17, except that isopropanol and dry ice were used instead of liquid nitrogen.

Figure 17. “Cold Trap” solvent capture system.

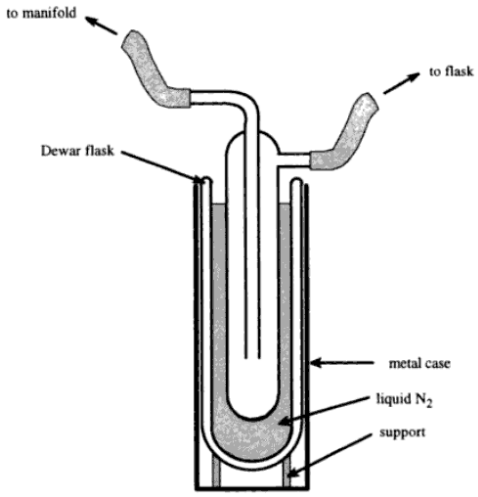

Source: ERRINGTON (1997).

During the toluene removal by this system, the reaction flask was kept in an oil bath at 250°C for 20 minutes and in hot air flow for a further 5 minutes to facilitate evaporation of the solvent and the exit of the vapors towards the "cold trap" and, for another 30 minutes, the vial was only connected to the system.

Subsequently, another 100 ml or 50 ml (for CNCs or Biosilicate®, respectively) of double distilled toluene, 8 ml of distillated caprolactone monomer (Ɛ-CL) and 200µL of Tin (II) 2-ethylhexanoate catalyst (previously stored under refrigeration) were added to the reaction flask. The reaction was kept under magnetic stirring in a paraffin oil bath at 120°C for 24 hours under an argon atmosphere. After this time, a few drops of 1M hydrochloric acid were added in order to stop the Ɛ-CL polymerization reaction.

The obtained biocomposites were recovered by precipitation: the flask contents were slowly poured into a high beaker containing 1000 ml heptane (99%, Carlo Erba®) for the CNCs or 500 ml for Biosilicate® (considering 10 times the amount of toluene added for the reaction) in strong magnetic stirring for 20 minutes. Then the contents were filtered on

cellulose filters under constant pressure. The final biocomposites were dried in a vacuum oven at 26 ° C overnight and kept in anhydrous glass vials with screw cap.

Electrospinning solutions

The electrospinning solutions were prepared in two steps, by first preparing matrix solutions and then obtaining the final solutions by mixing the matrix solutions at different ratios, according to the described.

For the matrix solutions, we employed:

• 100 ml dichloromethane (DCM, 99.8%, Sigma Aldrich®) and N, N-dimethylformamide (DMF, 99.9%, Carlo Erba®) system solvent at a ratio 60/40 % (v/v), respectively;

• 30 g of poly (Ɛ-caprolactone) solution (PCL, density = molar mass = 57 kg/mol, polydispersity index = 1.8, as measured by size exclusion chromatography on polystyrene standards, CAPA ™ 6806, Perstorp®) at 20% (w/w) in DCM/DMF, being, thus, 6 grams of PCL and 24 g of solvent;

• 10 g of 12% (w/w) CNC grafted with PCL (CNC-g-PCL) solution in DCM/DMF, or 1.2 g of CNC-g-PCL and 8.8 g of solvent;

• 10 g of 12% (w/w) PCL-grafted Biosilicate® (BioSiO-g-PCL) solution in DCM / DMF, or 1.2 g of CNC-g-PCL and 8.8 g of solvent.

All solutions were kept under magnetic stirring for at least 24 hours to electrospinning. For the preparation of 10 g of each of the final electrospinning solutions, the matrix solutions were mixed according to Table 3 respecting the ratio of 19% PCL (w/v) to the solvent (or 13.94% w/w) and the desired ratio of biocomposites to the PCL. The solvent mass already added in the matrix solutions and the mass of PCL present in the biocomposites (based on the final mass yield of the grafted composites) were taken into account:

• Final mass of the obtained CNC-g-PCL: 9.83 g; where it was employed 1 g of CNC and 8.83 g of PCL, hence 89.83% of PCL;

• Final mass of the obtained BioSiO-g-PCL: 10.12 g; where: 1g of Biosilicate® and 9.12g of PCL, therefore, 90.11% of PCL.

Finally, 3% (w/w) of each biocomposite was added according to the scaffold composition to be manufactured. This proportion has been previously investigated for the CNC in a work on the development of poly (Ɛ-caprolactone) scaffolds obtained by electrospinning incorporated with CNC-g-PCL, which were manufactured under the same conditions (BELLANI et al., 2016). After preparation, the solutions were kept in magnetic stirring until the electrospinning.

Table 3. Required mass from the matrix solutions to the final solutions preparations (10 g each) according to the electrospun membrane composition.

Electrospun membrane composition	*Amount of PCL matrix solution (g)*	*Amount of CNC-g-PCL matrix solution (g)*	*Amount of BioSiO-g-PCL matrix solution (g)*	*Amount of solvent (DCM/DMF) (g)*
PCL	6,97	-	-	3,03
PCL + 3% CNC-g-PCL	6,77	0,042	-	3,188
PCL + 3% BioSiO-g-PCL	6,77	-	0,042	3,188
PCL + 3% CNC-g-PCL + 3% BioSiO-g-PCL	6,59	0,042	0,042	3,326

Source: Own authorship

Electrospinning

A laboratory-scale electrospinning equipment was employed, which consists of a high voltage source connected to the tip of a needle with a 1mm diameter hole, an electronic injector (PHD 2000 Programmable, Harvard Apparatus®), grounded, and a flat collector 16 cm in diameter connected to ground wire as shown in Figure 18.

Prior to electrospinning, all solutions were kept in an ultrasonic bath for 5 minutes in order to improve the dispersion of their components. The solution was placed in a plastic syringe connected to the needle by a silicone tube, allowing perpendicular positioning of the needle-collector axis (vertical) in relation to the injector (horizontal) as seen at Figure 18 (a).

To avoid possible attraction between the biocomposites and the injector due to the static electricity present in the equipment, the syringe was attached to an internal plastic support placed inside the electrospinning chamber, connected to the injector by a stick (Figure 18(a)). The plate collector was positioned 15 cm of distance from the needle (spinneret) and the fibers were collected in aluminum foil. We manufactured electrospun membranes of PCL, PCL + 3% CNC-g-PCL (w/w), PCL + 3% BioSiO-g-PCL (w/w) and PCL + 3% de CNC-g-PCL + 3% of BioSiO-g-PCL (w/w).

Figure 18. Electrospinning equipment employed, composed of a plate collector, a spinneret (needle)(a) connected to power supply and the syringe pump (c) with programmable platform (d).

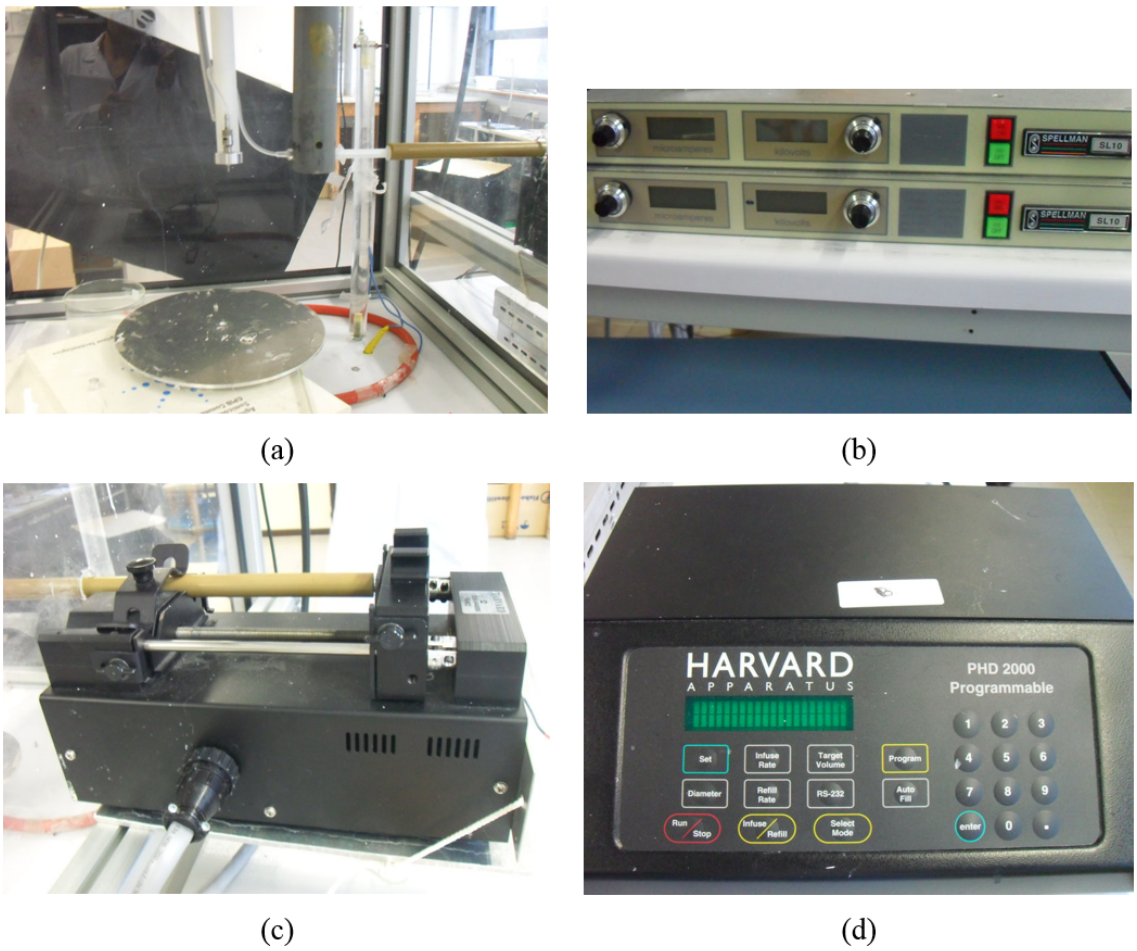

(a) (b)

(c) (d)

Source: Own authorship

Characterization

Biosilicate® particles size distribution

Biosilicate® particles were dispersed in isopropyl alcohol and evaluated in a particle analyzer, in order to characterize the particle size distribution and to compare the results obtained after milling in a low energy mill and in a vibratory mill, respectively.

Infrared Spectroscopy

Samples of cellulose nanocrystals (CNC) and Biosilicate® particles without modification and after the grafting process were analyzed in FT-IR with the purpose of investigating the effectiveness of the procedure.

Transmission Electronic Microscopy (TEM)

TEM analysis from the particles and electrospun mats composites were performed in order to visualize the morphology of the scaffolds obtained, as well as the particle domains that were incorporated. The particles were suspended in isopropyl ethanol, then drops of this suspension were placed over a metal grid suitable for TEM analysis. For the electrospun membranes, a piece of the peripheral part of the blankets was peeled off, with employment of ethanol absolute to detach the polymeric sample from the aluminum foil, in order to remove a sample as thin as possible and, then, the removed sample was transferred to a MET metal grid and allowed to dry. The particles were analyzed in a TEM model FEI TECNAI 2^2 F20 HRTEM, while the electrospun mats were examined in a TEM model CM 120 (Phillips®).

Scanning Electron Microscopy (SEM)

In order to evaluate the morphology of Biosilicate® particles processed by milling, prior to the electrospinning process, solutions of Biosilicate® particles in isopropyl alcohol were analyzed in Scanning Electron Microscopy (SEM). A few drops of these solutions were placed on small pieces of aluminum foil and kept on absorbent paper at room temperature until the specimens dried. The specimens were glued with double-sided carbon tape on SEM stub, metallized with gold and analyzed in the VEGA3 model VEGA3, Tescan®, using 5 kV acceleration voltage. From the images obtained, Biosilicate® particles measurements were made with the intuit to corroborate with the measurements obtained in the particle size analyzer.

Samples of electrospun mats were also analyzed in SEM in order to observe the overall morphology of the fibers. Samples from different electrospun mats were cut, then glued with double-sided carbon tape on SEM aluminum stub. Specimens were carbon coated and analyzed by an Inspect ™ F-50, FEI ™ Electronic Microscope, with 10 kV acceleration voltage. An Energy Dispersive X-ray detector (EDX) module of the equipment was also used to detect BioSiO-g-PCL particles. The images obtained were analyzed in the ImagePRO® software, in order to perform the average fiber diameter measurements. Thirty measurements were taken from each micrograph and then the average diameters and standard error of the meaning were calculated.

Mechanical Testing

The mechanical properties of the nanofiber mats were characterized using a dynamic-mechanical analyzer (DMA), in the tensile force mode, with a pre-load of 0.010 N and speed of 100 μm/s at room temperature. The DMA samples were obtained by carefully peeled off them from the surface of the aluminum foil. The sample dimensions were 10mm in length and 5mm in width. The thickness of the membranes was measured by high precision caliper. Four samples were used to characterize each material. DMA tensile testing was carried until sample rupture.

in vitro characterization

Cell Proliferation/Viability

In order to understand the *in vitro* behavior of osteoblasts in contact with the electrospun mats developed, and also to investigate if these mats have any cytotoxic effects to osteoblasts, we performed cell proliferation and viability essays.

Human osteoblast-like MG-63 cells, provided from a generous donation of INSERM, Strasbourg, France, were maintained in DMEM medium (Vitrocell®, Embriolife™) supplemented with 10% fetal bovine serum, 1% penicillin, and 1% streptomycin (100 mg/mL) at 37 °C in an atmosphere supplemented with 5% CO2.

We obtained samples by cutting the electrospun membranes using an 18mm diameter leather cutter. The samples were then sterilized with ultra violet during 20 minutes at each side of mats. Since the polymeric samples tend to float over the media, we employed Matrigel® (Corning™ Cat. Nº 354234) to keep PCL samples at the bottom of the wells. To prepare the experimental plate, frozen Matrigel® was left at 8˚C overnight. Each well, from a 24-well cell culture plate, dedicated to the experiments was washed with cell culture media, to improve the spread of the non-polymerized Matrigel®. Following, we put 50 μl of cold Matrigel® per well, and then we've kept the plate over ice (to keep Matrigel® liquid) and the samples were placed over liquid Matrigel®. The Matrigel® was allowed to polymerize at 37˚C for 30 minutes. As control, we employed wells with only Matrigel®. It is noteworthy this amount of Matrigel® is not enough to cover the bottom of the well, so mostly of the control well surface was still a 2D surface. Besides, for the test wells, this amount was enough to only keep an interface within the electrospun scaffolds and the place surface, not

compromising the PCL electrospun surface. The 24-well plate was kept in 37ºC to polymerize the Matrigel® and, thus, to "cement" the electrospun samples on bottom of the wells. For the cell proliferation assay, the cells were trypsinized, counted and seeded at 1×10^4 per well in a 24-well TCPS plate. The cell medium was changed every two days.

AlamarBlue® staining (Life Technologies™) was used for cell proliferation assay, which quantitatively measures cell proliferation on several human and animal cell lines, bacteria or fungi. Continuous cell growth maintains a reduced environment (fluorescent, red). Inhibition of cell growth maintains an oxidized environment (non-fluorescent, blue) (CZEKANSKA, 2011). The cell proliferation assay was performed at 3, 7, 14 and 21 days after cell seeding. We had chosen these time points in order to understand the cell proliferation behavior during the period we will assess the osteoblast *in vitro* biomineralization. We employed four specimens of each sample per test, and three independent essays. At each point in time, the medium was aspirated, and 600µl of fresh medium containing 10% of AlamarBlue® (v/v) was applied into each well that contained samples; two empty wells were used as reagent blanks (control of AlamarBlue®). The cells were incubated at 37 °C for 4 h. After incubation, 100µL of medium was transferred into a 96-well TCPS plate, and 100µL of 100% reduced AlamarBlue® (obtained by autoclaving 10% AlamarBlue® solution in cell culture medium for 15 minutes) was used as a positive control of the AlamarBlue®. Wells with only cell medium were used as the negative control of the AlamarBlue®.

Fluorescence was measured at an excitation wavelength of 544 nm and an emission wavelength of 590 nm on a Spectra Max Gemini XS instrument from Molecular Devices™. Finally, cell proliferation was quantified in terms of percentage reduction in AlamarBlue®, according to the Equation 1 bellow:

Equation 1: Relative Fluorescence calculation for the AlamarBlue® cell viability essay

$$Relative\ Fluorescence\ (\%) = \frac{(sample\ value - negative\ control\ of\ alamarBlue®)}{(Positive\ control\ of\ alamarBlue® - negative\ control\ of\ alamarBlue®)} \times 100$$

The higher the relative fluorescence, the bigger the number of viable cells.

Epi-fluorescence microscopy imaging from MG-63 on electrospun membranes

In order to visualize osteoblasts-like MG-63 over the PCL electrospun membranes through fluorescence, electrospun samples were obtained by electrospinning over round glass slides (10 mm) placed over the plate collector covered by aluminum paper. Samples were placed inside wells of a 24-well TCPS plate. Four specimens for each sample (PCL; PCL + CNC; PCL + Biosilicate®; PCL + CNC + Biosilicate®) were employed. MG-63 were trypsinized, counted and seeded at 1 x 10^4 per well. The cells were kept in DMEM + 10% of fetal bovine serum.

After 7 days, the cells were fixed with 4% of paraformaldehyde in PBS for 10 minutes and washed twice with PBS. To increase the permeability of the cells, a solution of 0.1% of triton x-100 in PBS was used for 5 minutes. The wells were washed two times with PBS, and DAPI (provided by Sigma-Aldrich) and Phalloidin (CytoPainter Phalloidin-iFluor 488, Cat. Nº 176753, Abcam™) staining was diluted in PBS with 1% of BSA as the manufacturer's recommendations.

After 10 minutes, the samples were washed twice with PBS, but, at the last wash, some PBS was left to prevent samples dehydration. The light and fluorescence images from samples were taken from a Zeiss Axio Vert.A1 inverted microscope with AxioCam software. The images were superimposed according to the desirable (DAPI and GFP filters and their superimposition with the light microscopy images). Noise reduction and contrast improvement filters were applied.

Mineralization *in vitro*

To identify the mineralization from osteoblasts-like cultured on the electrospun membranes, MG-63 were counted and seeded at 1 x 10^4 cells per well, employing 4 specimens per sample, as reported. MG-63 were stimulated by DMEM media (used as described) supplemented with 400μM of ascorbic acid, 5mM of β-glycerophosphate and 10nM of dexamethasone.

Alizarin Red is a dye that binds selectively calcium salts and is widely used for mineral staining (GREGORY et al., 2004). Nanofibrous scaffolds with MG-63 cells were washed twice with PBS and fixed in ice-cold 70% ethanol for 1 h. These constructs were then washed twice with dH_2O and stained with ARS (40 mm) for 20 min at room temperature.

After several washes with dH_2O (until the rinsed water was clear) the scaffolds were observed under a stereo zoom microscope.

Statistical Analysis

Statistical comparisons were performed using two-way ANOVA carried out with GraphPad Prism® software and the Bonferroni multiple comparisons test. P-values < 0.05 were considered statistically significant (n=4).

RESULTS AND DISCUSSION

Characterization

The Figure 19 and Figure 20 demonstrate the size distribution of Biosilicate® particles after milling in low energy and vibratory mill, respectively.

After milling in low energy (ball mill), the particle diameter distribution was between 0.3μm and 14μm (Figure 19), with the highest amount distributed to 1.8μm (about 9.5% of the particles). Considering the Biosilicate® particle size as provided ranged between 25 to 54μm, the particle size decreased substantially after the first milling step. Following the second milling (vibratory mill), the particle size distribution dropped to a range from 0.2 to 8μm (Figure 20), with the largest particle distributions around 2.33μm and 2μm (about 14% of the particles for both diameters). In addition, a better distribution was obtained for the particles around 1.8μm in diameter (about 10.5%) after milling in vibratory mill. It must be noted that, despite the considerable decrease in the size of Biosilicate® particles, the final size obtained after the two millings was not considered satisfactory to incorporate them into the electrospun fibers. Only a relatively small proportion of the particles (less than 5%) has a size smaller than 500 nm, the maximum size suitable for incorporation into the PCL fibers, for improvements in the mechanical properties by the incorporation of these particles and for better distribution of the ceramic into the polymeric phase (ARMENTANO et al., 2010; QIAO; BRINSON, 2009). In order to increase the proportion of particles of nanometric dimensions, it is proposed the combination of a longer milling time and also an increase of the liquid phase (isopropanol) and the deflocculant (PVB) in relation to the ceramic phase; or the synthesis of Biosilicate® by the sol-gel process, whereby it may be possible to obtain particles of about 200 nm (LUKOWIAK et al., 2013).

Figure 19. Particles size distribution (μm) after ball milling.

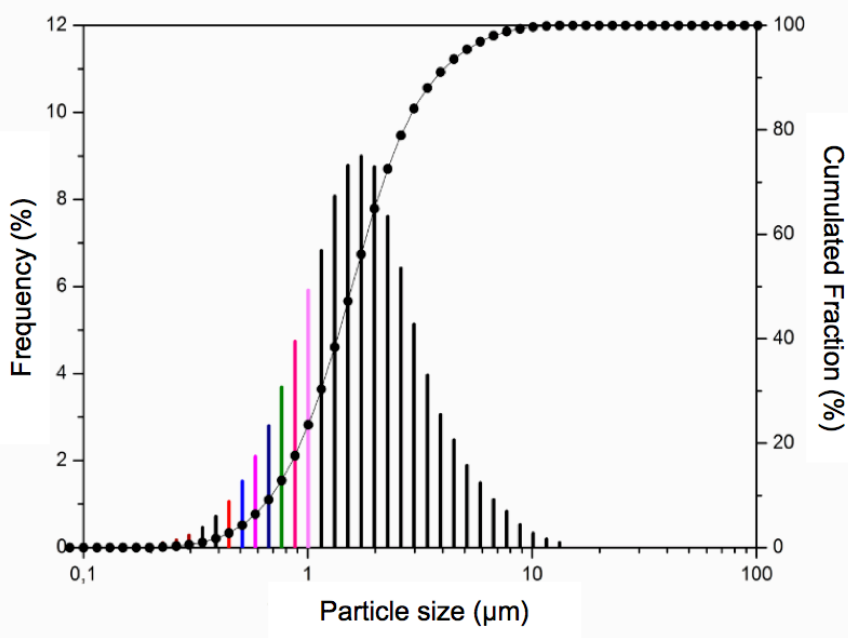

Source: Own authorship

Figure 20. Particles size distribution after ball milling and vibratory milling.

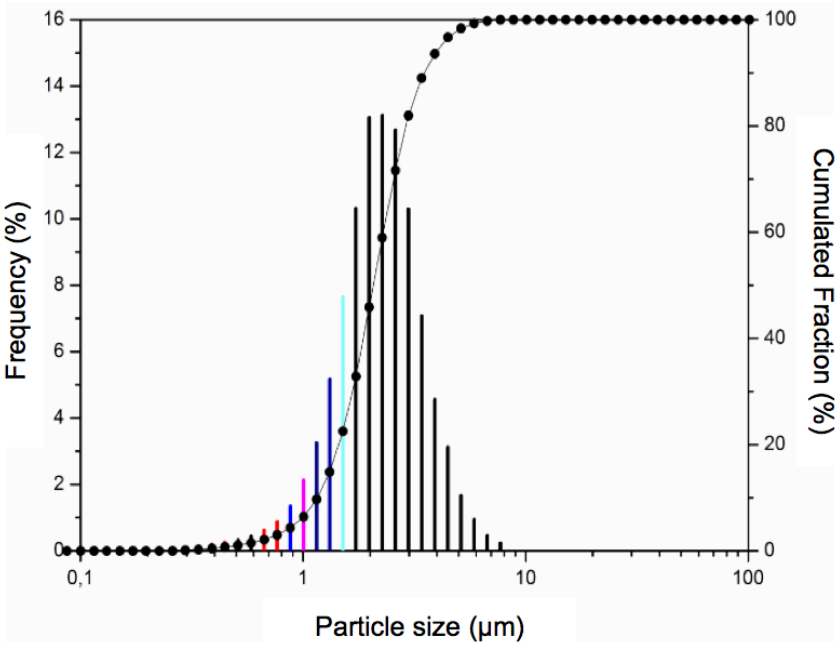

Source: Own autorship

The SEM images shown at Figure 21 reveals the irregular appearance of the particle surface, which is attributed to particle breakage due to shear forces in the ball mill (SHI; NAPIER-MUNN, 1999). The Figure 21 (c) and (d) also illustrate some measurements of the

particle diameters, ranging between 0.13 and 2.79μm, which corroborate the values found through the particle size analysis.

Figure 21. SEM images from the Biosilicate® particles. In (A) and (B), is show the overall aspect of the Biosilicate® particles as employed for the grafting and electrospinning into PCL electrospun matrices. Some particle diameter measures are shown in (C) and (D).

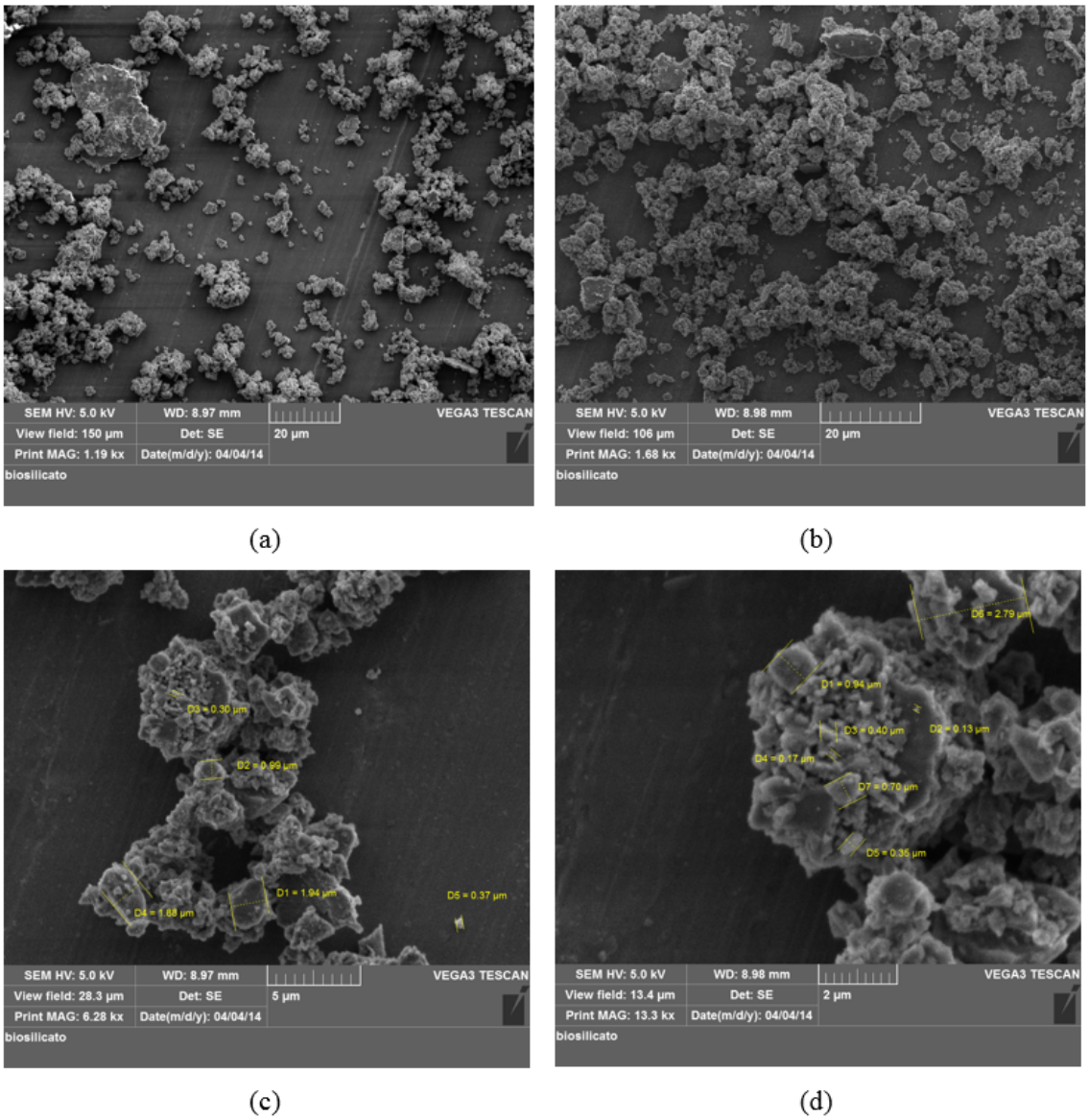

Source: Own authorship

On Figure 22, we can see Transmission Electronic Microscopy (TEM) pictures of raw Biosilicate®(A) and BioSiO-g-PCL (B) particles, which images show the overall aspect of both particles. The TEM image of BioSiO-g-PCL (B) is distinguished of the Biosilicate® one (A) as it has lighter surroundings that can be attributed to the interface Biosilicate®-PCL. To better investigate this interface, we employed the EDX analyses, as shown at Figure 23 for the

raw Biosilicate® and Figure 24, for BioSiO-g-PCL particles. At Figure 23 (C), we can see elements spectra of Na, Ca and Si (as the highest peak), typical of the Biosilicate® (CROVACE et al., 2016).

The interface Biosilicate®-PCL of the BioSiO-g-PCL was analyzed as illustrated in Figure 24. From (B), the EDX of the periphery of BioSiO-g-PCL (most likely to have a more important ratio of PCL/Biosilicate®) is showed in (C), while the XRD analysis of the center of the particle (where we believe the PCL/Biosilicate® ratio is smaller) is pictured in (D). In both regions (C, the periphery, and D, the center), we can see the presence of carbon (C) (exclusive of PCL) (NAGHIZADEH et al., 2014), oxygen (O) (which is composed by both PCL and Biosilicate® (CROVACE et al., 2016; NAGHIZADEH et al., 2014); and Sodium (Na) and Silicon (Si), exclusive of Biosilicate® (CROVACE et al., 2016). However, the carbon/oxygen, sodium, silicon ratio is higher in (C) than in (D), which means, thus, a higher PCL/Biosilicate® ratio in the periphery, indicating the PCL is successfully recovering the Biosilicate® surface. Therefore, the grafted Biosilicate® (BioSiO-g-PCL) can be dispersed and reinforce PCL matrixes, and, mostly important, confer the bioactivity feature to this material.

Figure 22. Transmission Electronic Microscopy of raw Biosilicate® particles (A) and PCL-grafted Biosilicate® (BioSiO-g-PCL) (B).

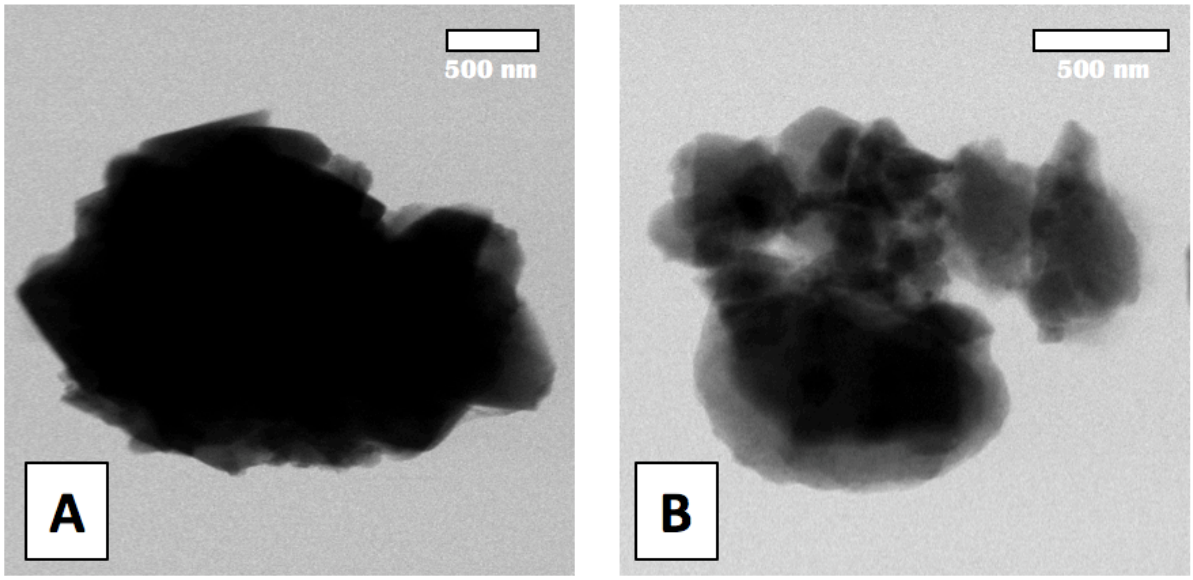

Source: Own authorship

Figure 23. Transmission Electronic Microscopy of a raw Biosilicate® particle (A) and the X-Ray Diffraction (XRD) shown in (C). The selected area for XRD is marked on (B).

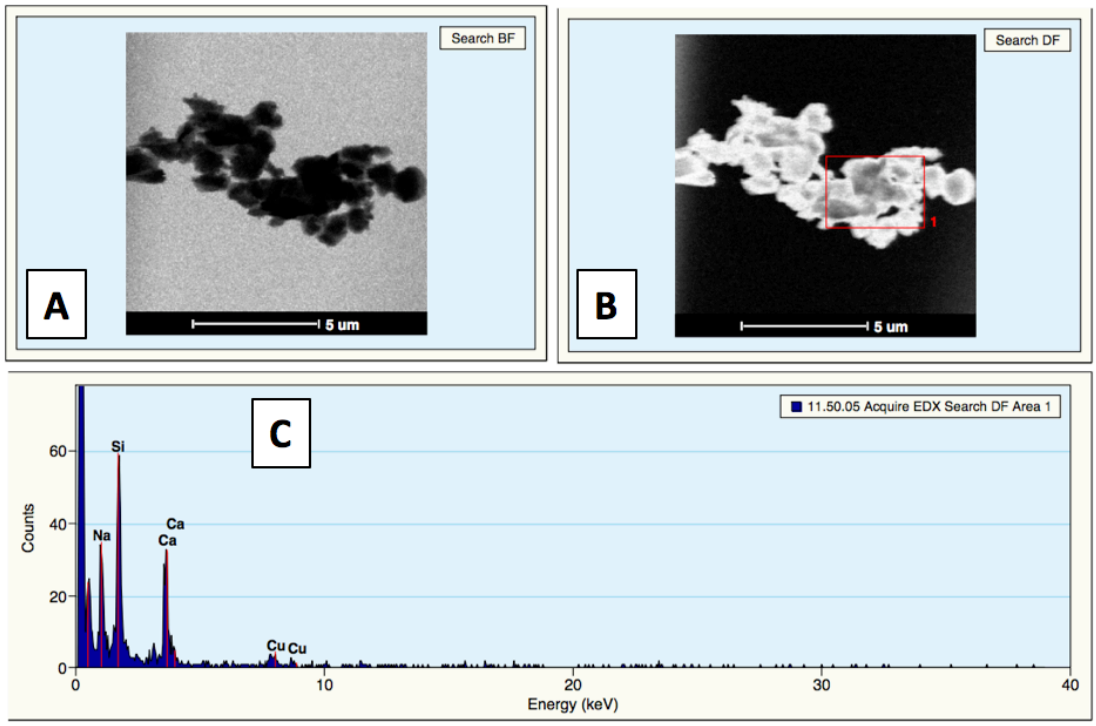

Source: Own authorship

Figure 24. Transmission Electronic Microscopy of a PCL-grafted Biosilicate® particle (BioSiO-g-PCL). In (B), the areas selected for XRD analysis: the area 1, peripheral, which XRD spectra is shown in (C), and the area 2, central, and its XRD spectra shown in (D).

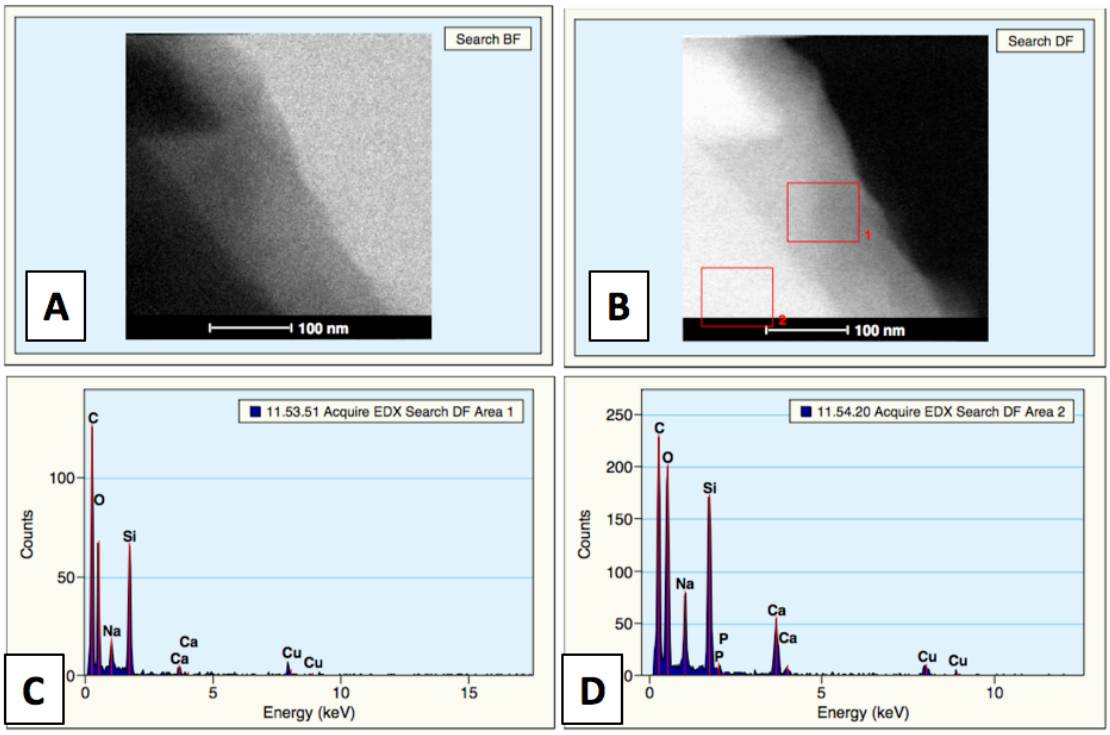

Source: Own authorship

The PCL grafting process from cellulose nanocrystals and Biosilicate® was confirmed by FT-IR analyzes in Figure 25 and in Figure 26. PCL, unmodified CNC and CNC-g-PCL, and Biosilicate® and CNC-g-BioSiO spectra are observed. At Figure 25, the FT-IR spectrum of CNC-g-PCL shows the presence of a band at 1750 cm-1, characteristic of the axial deformation of the carbonyl group (C = O) of the PCL. Moreover, a band of lower intensity of the axial deformation at 3330 cm^{-1}, attributed to the hydroxyl bonds, can also be observed, suggesting the effectiveness of the PCL grafting from the surface of the CNC. These results corroborate with the FT-IR spectrum patterns obtained by Habib et. al. (HABIBI et al., 2008) and Bellani et. al. (BELLANI et al., 2016) in studies of the synthesis of bionanocomposites of cellulose grafted with PCL by the ring-opening polymerization process. One can notice the same axial deformation peak of the carbonyl group (C = O) in the BioSiO-g-PCL spectrum (Figure 26), and an axial decrease of the band ranging from 1250 cm^{-1} to 750 cm^{-1} when comparing Biosilicate ® with the grafted Biosilicate® (CNC-g-BioSiO). In this region, the bands observed are typical of Si-O-Si type bonds to Biosilicate® (CROVACE et al., 2016). After grafting, this band was no longer accessible to IR radiation, indicating that the surface was functionalized and, thus, there was polymerization of PCL from Biosilicate®. Therefore, it is suggested that grafting was also successfully performed on the surface of Biosilicate®. However, to identify which type of bonding has occurred between the surface of Biosilicate®

and Ɛ-caprolactone, more detailed analyzes of these spectra should be performed or characterization of the material using other techniques, as NMR H^+ and Raman Spectroscopy.

Figure 25. FT-IR spectra of CNC (black line) and PCL grafted CNC – CNC-g-PCL (gray line). For comparison purposes, the PCL spectra is also show (dotted line).

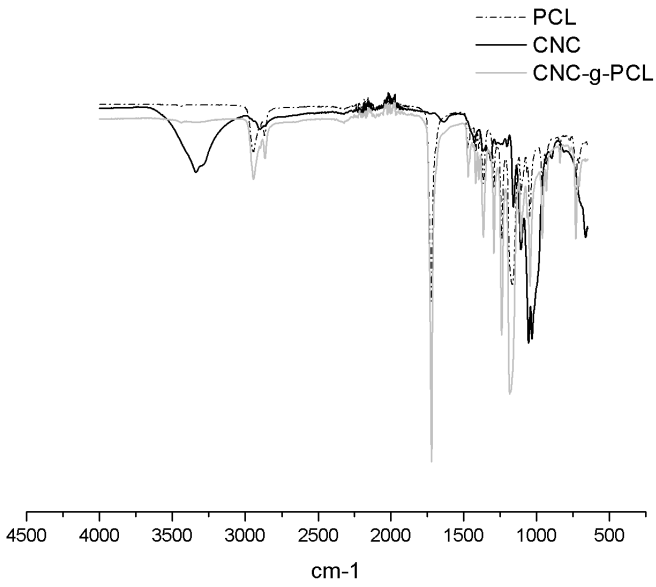

Source: Own Authorship

Figure 26. FT-IR spectra of Biosilicate® (black line) and PCL-grafted Biosilicate® - BioSiO-g-PCL (gray line). For comparison purposes, the PCL spectra is also show (dotted line).

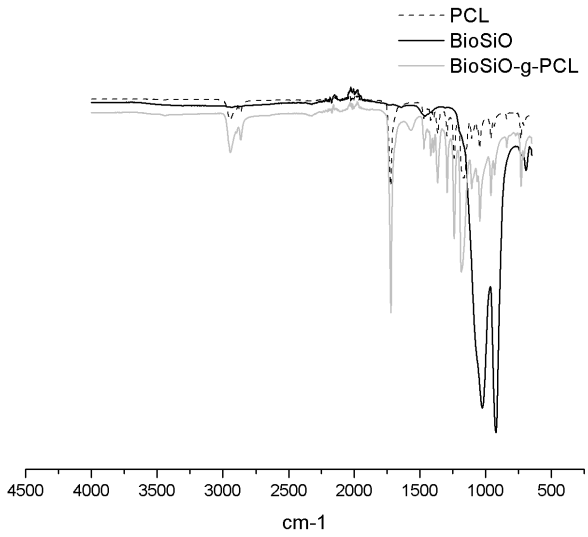

Source: Own Authorship

The Figure 27 shows the SEM images obtained from the electrospun membranes of PCL (a), PCL + 3% CNC-g-PCL (b), PCL + 3% BioSiO- and PCL + 3% CNC-g-PCL + 3% BioSiO-g-PCL. The black arrows indicate some domains of Biosilicate® particles (Figure 27 (c) and (d)), which were possible to be detected by the XRD mode of SEM (represented by brighter domains in comparison the fibers polymeric matrices). The micrographs reveal homogeneous, bead-free nanofibers for all scaffolds. PCL + CNC-g-PCL electrospun mats have uniform surface and diameters along the length of the fibers, whose general morphology is comparable to pure PCL scaffolds. These results corroborate with a work of synthesis of PCL scaffolds incorporated with CNC-g-PCL previously performed by the author (BELLANI et al., 2016). In addition, these micrographs show that CNC-g-PCL do not affect the surface appearance of the PCL + CNC-g-PCL + BioSiO-g-PCL electrospun membranes (Figure 27 (d)).

When the BioSiO-g-PCL is observed in the context of the scaffolds, it is noted that the particles of nanometric dimensions were mostly internally incorporated into the fibers (Figure 27 (c)). This is an interesting feature because, besides the expected mechanical improvements in mechanical properties, these dimensions of the BioSiO-g-PCL mimic the mineral crystals present in the bone tissue (KOKUBO et al., 2004; NIRMALA et al., 2010) as it can be seen in Figure 27 (d). However, it is also noticed the size of some other particles of BioSiO-g-PCL compared to the size of the nanofibers, a characteristic which was previously predicted. Although these larger particles were not internally incorporated into the fibers, due to the higher particle dimensions in comparison with the PCL fiber diameter, the PCL-grafted

Biosilicate® still may provide bioactive characteristics to the electrospun mats, thanks to the bioceramic phase in the scaffolds (JANG; CASTANO; KIM, 2009). It can be also observed the formation of bead-like structures where BioSiO-g-PCL bigger particles are inserted. Although this effect is undesirable in electro-spinning, the inclusion of beads in electrophilic scaffolds did not show any apparent negative effects on cellular function. In addition, a moderate surface roughness promotes initial adhesion and cell proliferation, as well as the ability of osteogenic differentiation of mesenchymal stem cells when compared to cells grown on uniform surfaces (LUO; STRIDE; EDIRISINGHE, 2012).

Regardless the incorporation of the particles within or between the fibers, both the bioceramics and the cellulose nanocrystals are dispersed in the electrospun mats. In other words, the formation of particles aggregates did not occur, thanks to the chains of PCLs connected to particles that improves the particle-PCL interfacial interaction (JIANG et al., 2018). Therefore, the grafting with PCL was fundamental to improve the dispersion of the biocomposites in the scaffolds and we expect it will improve their mechanical properties and bioactivity by loading those the CNC and Biosilicate®, respectively, enhancing their performance as biomaterial for guided bone regeneration.

From the evaluation of SEM micrographs and fiber measurements, the average fiber diameter (D) (Table 4) decreased considerably according to the addition of biocomposites (Figure 27 (a), (b), (c) and (d), and Table 4) for the electrospun PCL mats produced under the same conditions. According to the work of Greiner & Wendorff (GREINER; WENDORFF, 2007), this decreasing effect on fiber diameters can be attributed primarily to the charge density and the viscoelastic behavior of polymer solutions containing nanocomposites. Xiang et. al. (XIANG; JOO; FREY, 2009) and Shi et. al. (SHI et al., 2012) studied the morphology of CNC-reinforced poly (lactic acid) nanofibers and observed an increase in the viscosity and electrical conductivity of the electrochemical solution due to the presence of CNC, resulting in a higher charge density in the surface of the ejected jet and, consequently, the production of fibers with smaller diameter occurred. This observation corroborates the author's previously published work (BELLANI et al., 2016) and the publication of Zoppe et. al. (ZOPPE et al., 2009b). In these works, it is reported that the mechanical behavior of nanocomposites is closely related to the diameter of nanofibers. The density and distribution of entanglements between the fibers become larger when the fibers diameter decrease, due to the increasing on the fibers surface area. Moreover, an improvement in the mechanical properties can be attributed to the effect of decreasing the diameter of the nanofibers due to the addition of biocomposites (BELLANI et al., 2016).

Figure 27. SEM images of electrospun mats of PCL (a), PCL + 3% CNC-g-PCL (b), PCL + 3% m/m BioSiO-g-PCL (c) e PCL + 3% CNC-g-PCL + 3% BioSiO-g-PCL. Arrows indicates some of the electrospun brighter domains visualized through EDX, in (c) and (d).

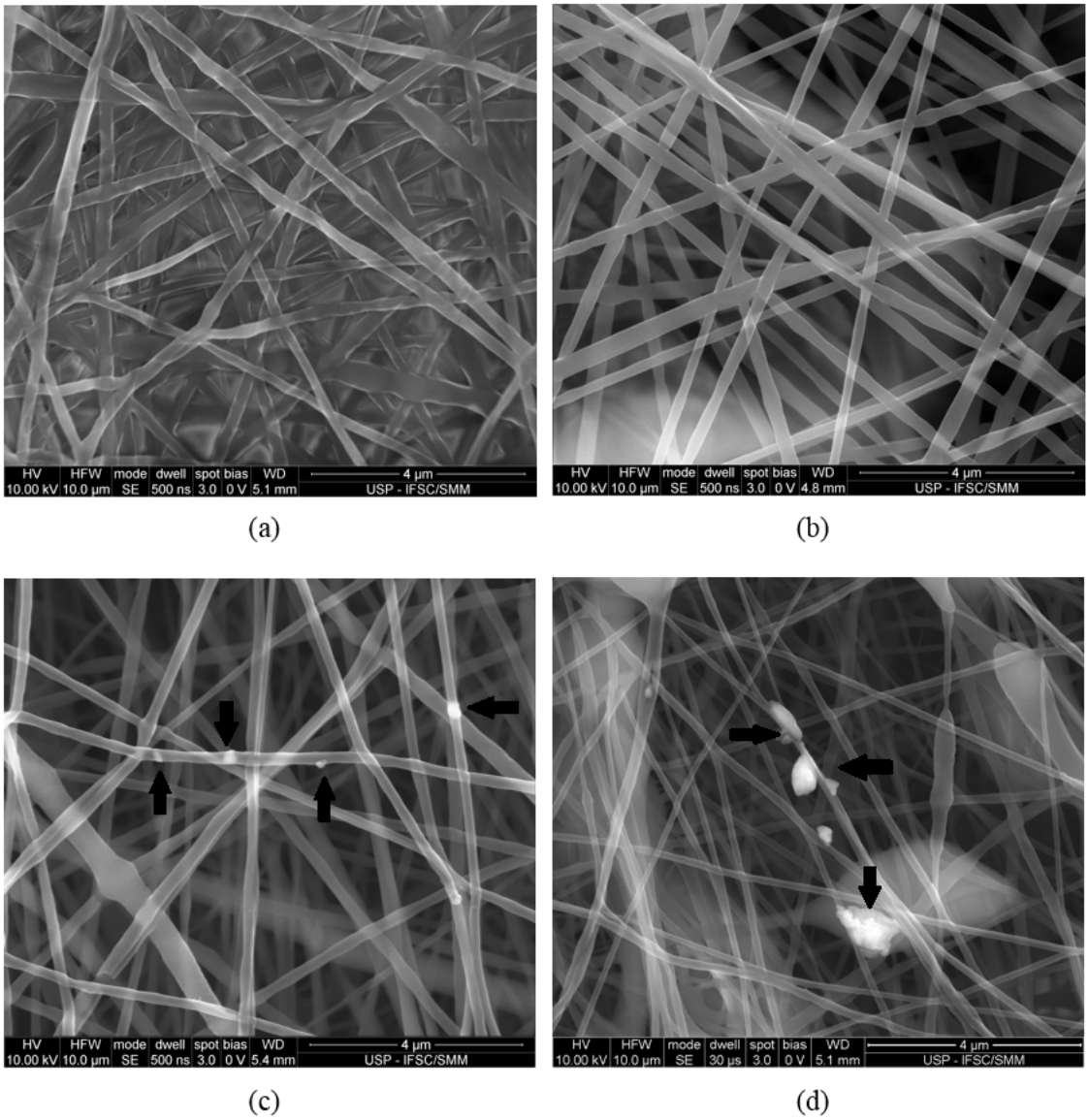

Source: Own authorship.

Table 4. Electrospun fibers average diameter (D) in nanometers (nm) ± standard error of the meaning.

SAMPLE	*AVERAGE DIAMETER (D) (NM)*
PCL	298,79 ± 13,88
PCL + 3% CNC-G-PCL	212,78 ± 10,18
PCL + 3% BIOSIO-G-PCL	205,05 ± 6,97
PCL + 3% CNC-G-PCL + 3% BIOSIO-G-PCL	143,83 ± 5,56

Source: Own authorship

In order to visualize the incorporation of CNC-g-PCL into the PCL matrix of the mats, as well the Biosilicate® domains (inside and within the fibers), we had analyzed the electrospun mats through Transmission Electronic Microscopy (TEM). At Figure 28, TEM micrographs of PCL (A), PCL + 3% CNC-g-PCL (B), PCL + 3% BioSiO-g-PCL (C) and of PCL + 3% CNC-g-PCL + 3% BioSiO-g-PCL (D) are shown. On Figure 28 (A), we can see the PCL fibers and the contrast of the superposed fibers. We can see CNC were successfully incorporated inside the fibers in (B) and (D): the CNC domains can be seen as thin, darker regions into the fibers (as pointed by the arrow). We are able to also confirm the incorporation of Biosilicate® within the fibers, as can be seen in (C) and (D) as bulk, irregular, almost black domains (also pointed by arrows), due to the higher density of Biosilicate® in comparison with PCL. Both CNC and Biosilicate® domains are highlighted on (D). Therefore, CNC-g-PCL and BioSiO-g-PCL were successfully incorporated into biodegradable and biocompatible PCL electrospun mats. Hence, the presence of these composites did not affect the overall aspect of the membranes.

Thus, from the TEM analysis, we can confirm we were able to produce novel PCL composites with osteogenic properties, which can be conferred by the Biosilicate®, and tunable mechanical properties by controlling the CNC ratio inside the mats according to the bone tissue engineering application, in addition to other tissues guided regeneration.

Figure 28. TEM images from electrospun scaffolds of PCL (A), PCL + 3 % w/w of CNC-g-PCL (B), PCL + 3% w/w of BioSiO-g-PCL (C) and PCL + 3% w/w of CNC-g-PCL + 3% w/w of BioSiO-g-PCL. The arrows indicate the CNC (from CNC-g-PCL) and the Biosilicate® (from BioSiO-g-PCL) domains.

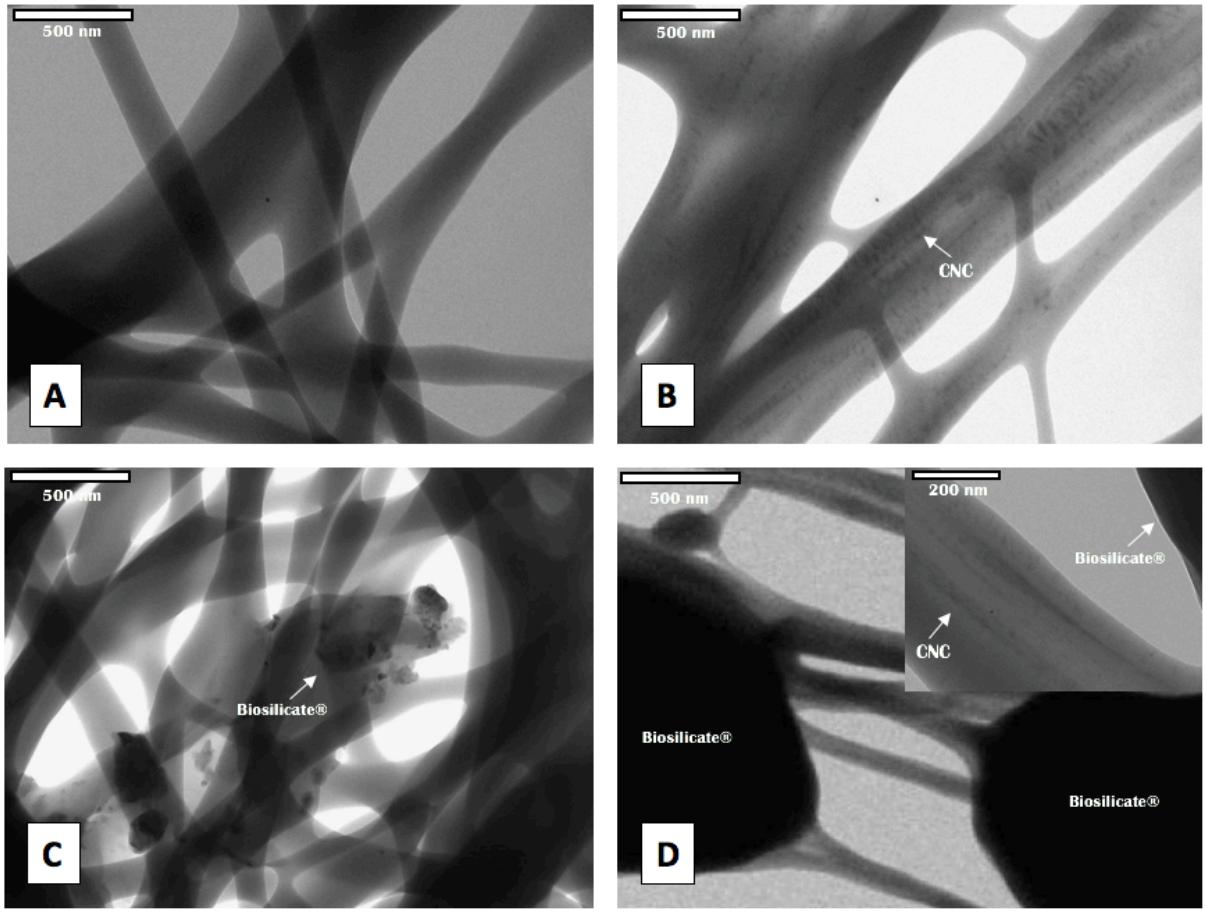

Source: Own authorship

Regarding the mechanical properties, as shown in Figure 29, the Young's modulus and the stress at break of the PCL electrospun mats increased when the PCL-grafted CNC was added, while the elongation at break decreased indicating that stiffer materials were obtained. This find is consistent with our previous published work about the reinforcement of PCL with cellulose nanocrystals, where the addition of only 3% (w/w) of CNC considerably increased the PCL electrospun mats mechanical properties (BELLANI et al., 2016).

Surprisingly, the same effect was observed for the BioSiO-g-PCL composites. We not expected a reinforcement effect for Biosilicate®-PCL composites as for CNC-PCL ones, because of the size of Biosilicate® particles, and their poor aspect ratio dimensions compared to the CNC. However, in this work, there is a critical step: the Biosilicate® particles were PCL-grafted prior to their employment within PCL fibers, as for the CNC as well. Moreover, when both CNC and Biosilicate were employed together, the elastic modulus increased three times in comparison with the neat PCL membranes, and doubled in comparison with the CNC-PCL ones. These findings highlight the importance to improve the compatibility of the matrix-particles in nanocomposites in order to proper predict and tune their mechanical

properties, as we have performed for the Biosilicate®. However, it is worth note this reinforcement effect may be due to the fiber diameter decreasing with the addition of the particles (Table 4). The decreasing in fibers diameter increase the fibers entanglements per area, as previously observed by us (BELLANI et al., 2016) and THOMAS et al., 2006.

The elongation at break (%) of the bionanocomposites mats decreased in comparison with the neat PCL. These results indicate a good dispersion and interface between the PCL-grafted CNC, Biosilicate® and the PCL matrix was developed. However, this decreasing was not proportional to the particles load, probably because the Biosilicate particles size is very variable (Figure 20).

Therefore, according to our results, the incorporation of PCL-grafted CNC and PCL-grafted Biosilicate® leaded to the mechanical properties increasing of PCL nanofiber mats. The improvements in mechanical behavior can be attributed to the addition of PCL-composites to the fiber and to respective decrease in the fibers diameter. Thus, from these analyses, it is clear the grafting procedure contributed to rise the compatibility between the PCL, and CNC and Biosilicate® loads.

Figure 29. Mechanical properties of PCL membranes and their composites (CNC [Cellulose Nanocrystals; BioSiO [Biosilicate®]; and CNC + BioSiO) at a 3% load.

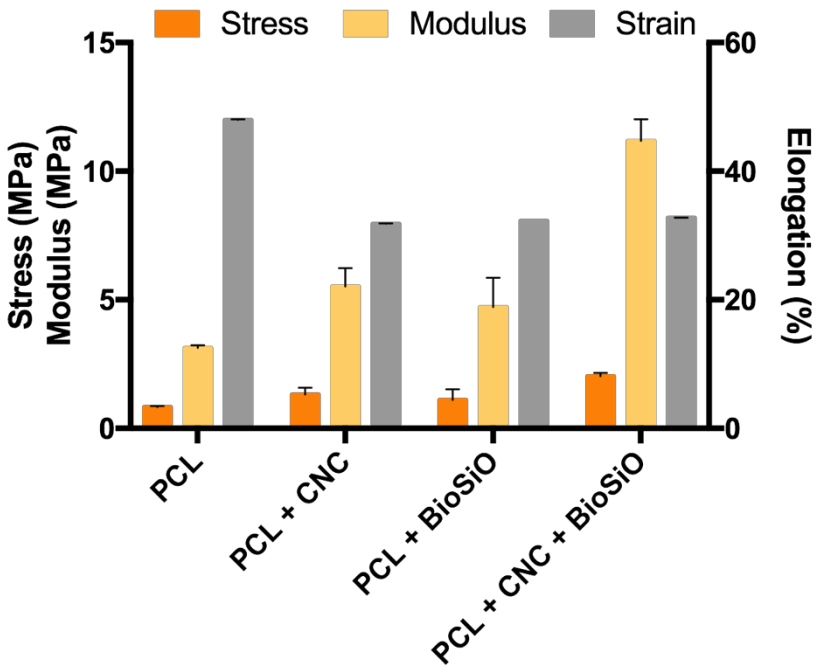

Source: Own authorship

***In vitro* essays**

Cell Proliferation

As shown in Figure 30, osteoblast-like MG-63 cells cultured on the samples PCL, PCL + CNC, PCL + BioSiO and PCL + CNC + BioSiO showed increasing proliferation throughout the time of analysis. There were no significant differences in osteoblasts proliferation in comparison with the control and the with the different samples, with the exception for 7 days after cell seeding, when the samples with CNC and Biosilicate® (BioSiO) presents a cell proliferation significant superior in comparison with the CNC and BioSiO alone samples. As this difference didn't persist for the other time points, we conclude this variance occurred during the stabilization of the cell culture. The wide error bars for 7 days and the smaller ones for the following time points corroborates this hypothesis. Therefore, from the cell viability essay we conclude all samples support cell proliferation, and thus do not show *in vitro* toxicity.

Figure 30. AlamarBlue® cell viability essay for the electrospun samples and their respective error bars. The higher the relative fluorescence, the bigger the number of viable cells. *n<0.05.

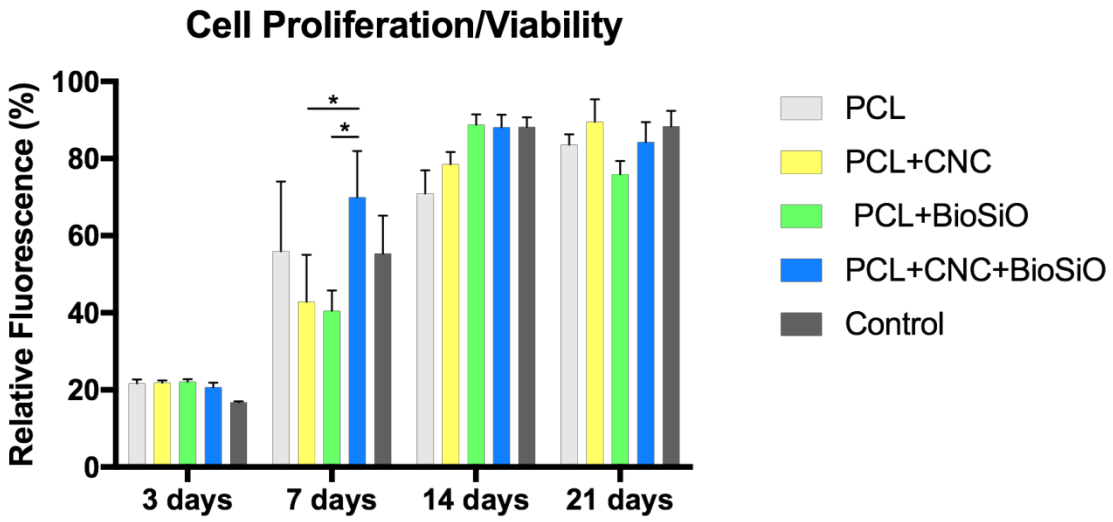

Source: Own authorship.

Fluorescent Microscope Images

On Figure 31, fluorescent images of MG-63 cultured on PCL (A), PCL + CNC (B), PCL + Biosilicate® (C) and PCL + CNC + Biosilicate® (D) are shown. In blue, they are evidenced cell nuclei (stained by DAPI) and, in green, the F-actin protein (stained by green phalloidin), present in cytoskeleton, in order to visualize the cell shape. From these images,

we can conclude MG-63 were able to proliferate and attach over all samples during the period of essay. Interestingly, at Figure 31(C), which were taken for the PCL + Biosilicate® samples, the MG-63 seems to possess increased nuclei size, in comparison with other samples be oriented at (C). It is worth note all images were taken at the same magnification. This increase could be attributed to the presence of Biosilicate®, which stimulates cell proliferation and viability (BOSSINI et al., 2011; CROVACE et al., 2016; GRANITO et al., 2009), however, this effect is not observed at samples with CNC + Biosilicate®. Because the MG-63 nuclei appear to be bigger, in comparison with the electrospun mats incorporated with the CNC, for the neat PCL samples, in fact, osteoblasts increased nuclei can be due to fibers diameter effect. Bashur et. al. noticed osteoblasts spreading diminished on the smaller fibers. They attributed this effect to the role of focal adhesion complexes in mediating cell adhesion to biomaterials. Thus, a smaller projected area may cause a smaller cell projection (BASHUR; DAHLGREN; GOLDSTEIN, 2006) and, consequently, smaller nuclei. However, the cell proliferation essay (Figure 30) indicated cells proliferated equally over all electrospun mats. This may affect cell on early days after seeding, as we took these pictures after 7 days of seeding, which corroborates with the work of Bashur et. al, as cited. Conversely, as the neat PCL fibers has a higher fiber diameter than the PCL + Biosilicate® mats (Table 4), the increasing in spreading for osteoblasts for the PCL + Biosilicate® membranes can be due to a positive effect attributed to the combination of superior fiber diameter plus the Biosilicate®.

However, it must be noted this is a qualitative analysis, and quantitative measurements must be made in order to better understand the role of fiber diameters and Biosilicate in cell spreading and proliferation on PCL + CNC + Biosilicate electrospun composites.

Figure 31. MG-63 cultured over electrospun membranes of PCL (A); PCL + 3 % CNC-g-PCL (B); PCL + 3% BioSiO-g-PCL (C); PCL + 3 % CNC-g-PCL + 3% BioSiO-g-PCL. MG-63 were stained with DAPI (blue), to show the nuclei, and with Green Phalloidin, which links to F-actin, present in the cell cytoskeleton. Images were taken after 7 days in culture. The arrow at (c) indicates the orientation sense of the osteoblasts over this sample.

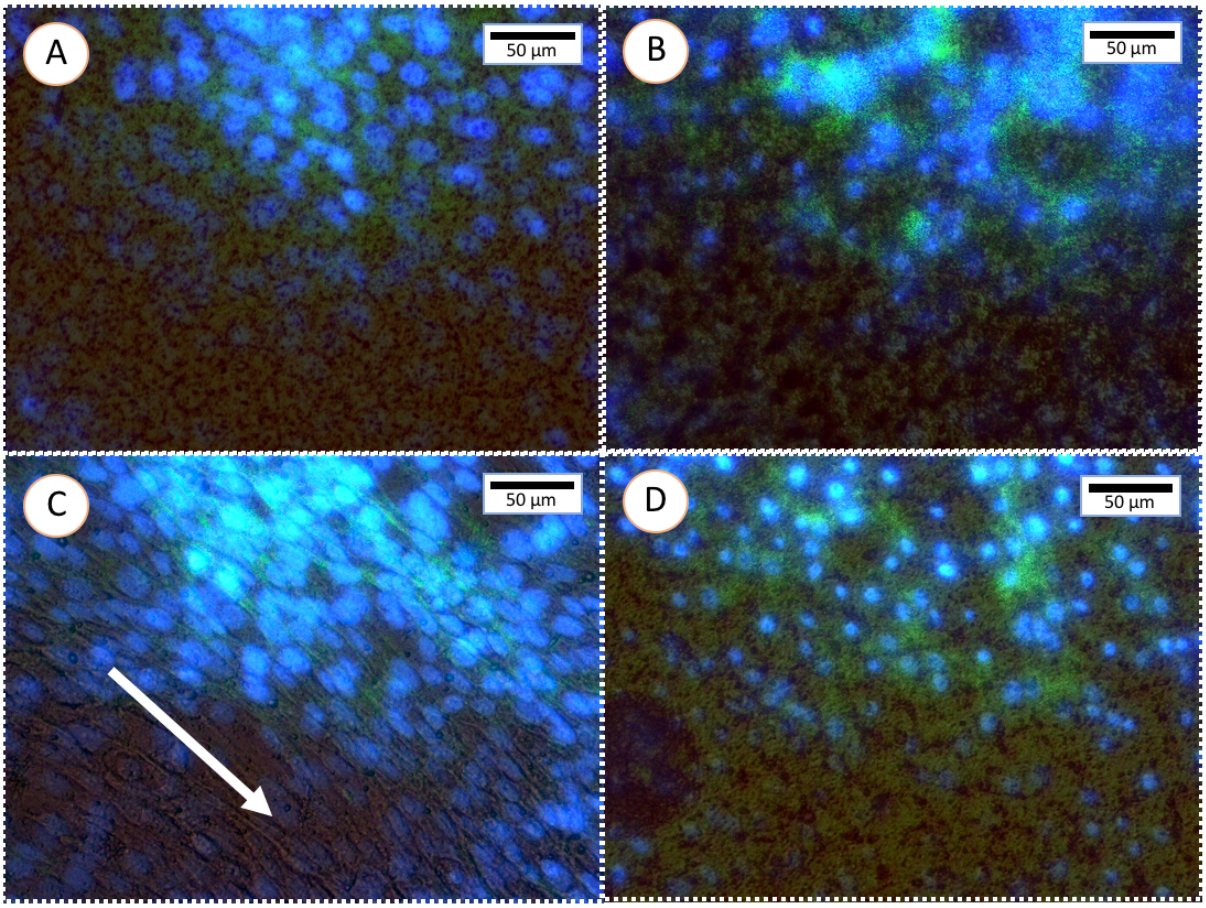

Source: Own authorship.

in vitro Mineralization

After 21 days of culture, the mineralization can be detected thanks to the alizarin red staining on the calcium exudations onto the membranes (Figure 32). Mineralization refers to cell-mediated deposition of extracellular calcium salts where anionic matrix molecules take up the Ca^{2+}, phosphate ions and serve as nucleation and growth sites leading to calcification (BOSKEY, 1998), and alizarin stains in red these depositions. By the gross observations, we can observe the mineral deposits in red over all the membranes, and thus, we can conclude all the membranes supports *in vitro* mineralization. These observations corroborate with the work of Joshi et. al., which reports PCL electrospun membrane with cellulose nanocrystals generated *in-situ* (JOSHI et al., 2015) and with various works of PCL/bioceramics composites obtained by electrospinning (ENAYATI et al., 2018; GAHARWAR et al., 2014; SAJESH et al., 2016; VENUGOPAL et al., 2008; ZHANG et al., 2010a). However, quantitative analysis may seem to be necessary in order to stablish a correlation between the composites and the biomineralization *in vitro* to further predict the *in vivo* mineralization and, thus, the bone formation. Conversely, Hulsart-Billstrom, in a multicenter review of various *in vitro* and *in*

vivo data results of biological assessment of biomaterials for bone regeneration, from a significant number of publications, stablished a poor correlation between *in vitro* and vivo testing of biomaterials, including calcium deposition *in vitro* and *in vivo*, and *in vitro* calcium deposition and *in vivo* biocompatibility. He found a correlation value (R^2) <0.1 (HULSART-BILLSTRÖM et al., 2017). Thus, in order to assess the mineralization from these membranes, *in vivo* analyses are required in order to stablish a correlation.

Figure 32. Light microscopy images obtained by Stereo Zoom microscopy of Alizarin Red Staining essay, after 21 days of cell seeding, for the mineralization in MG-63 cells cultured over the electrospun membranes: (A) PCL; (B) PCL + CNC; (C) PCL + Biosilicate®; (D) PCL + CNC + Biosilicate®.

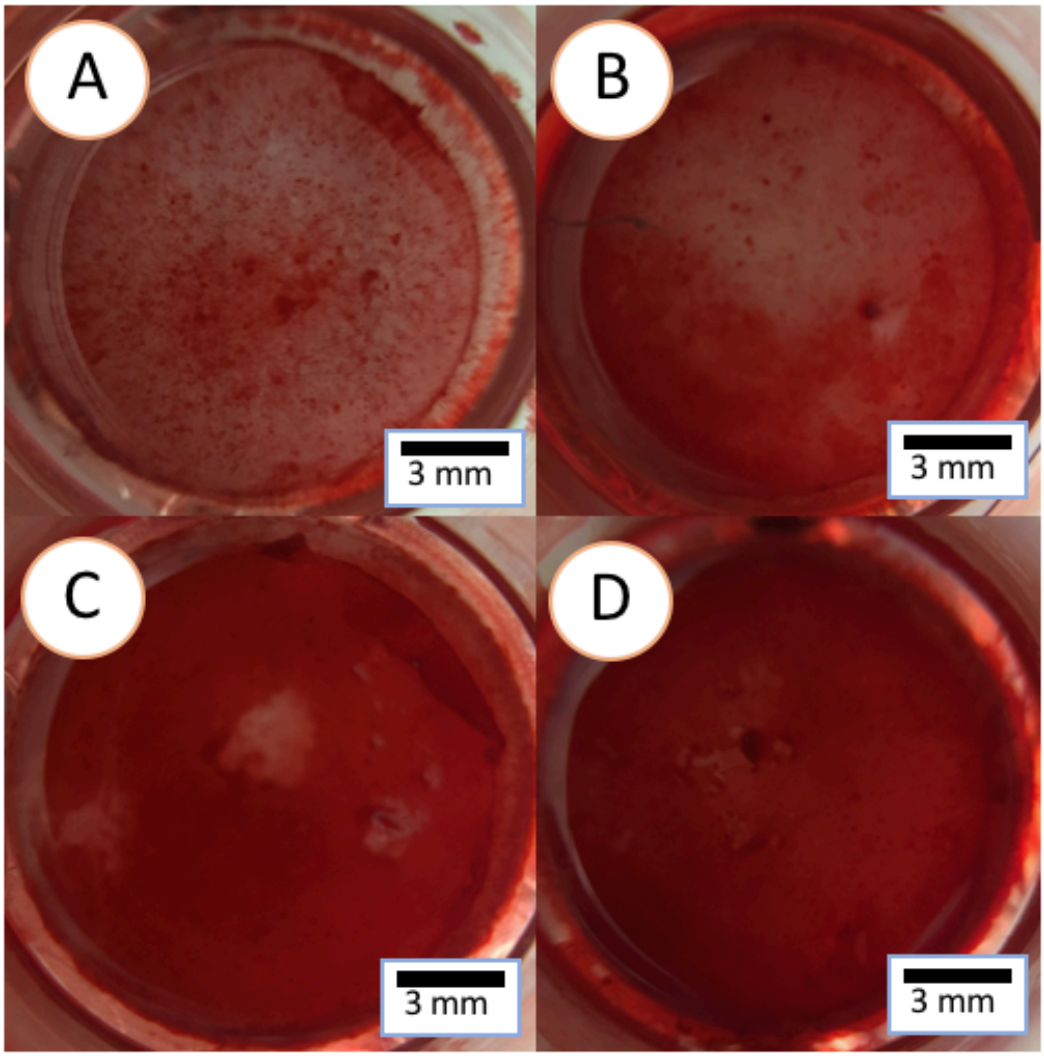

Source: Own authorship.

CONCLUSION

As the main objective of this chapter was to improve the bioactivity of the reinforced biodegradable membranes for Guided Bone Regeneration described at the first part of this work, we employed Biosilicate® as osteogenic phase. To improve the compatibility with the polymeric phase and the osteogenic phase, we employed the same strategy as discussed at the previous chapter, which is the in-situ polymerization by ring-opening of ε-caprolactone) from the previously milled Biosilicate® particles, creating the new PCL-g-Biosilicate® (PCL-g-BioSiO) composites with success and the PCL grafted CNCs (PCL-g-CNC). However, the interaction occurred within the Biosilicate® and the PCL cannot be elucidated. As for the cellulose nanocrystals (CNC), the PCL grafting from approach shows to be effective to improve the compatibility within the Biosilicate® and the PCL. Both composites can be incorporated into the PCL biodegradable membranes obtained by electrospinning. All membranes present a homogeneous and typical morphology, with reduced fibers diameters according with the addition of composites. The CNCs significantly improve the mechanical properties of the PCL membranes, as expected from the previous part. Moreover, the Biosilicate® also increased some of the mechanical properties. When both composites are employed together, they may increase the Young's Modulus in up to three times and up to two times the stress at break in comparison with the neat PCL membranes. The *in vitro* essays have showed osteoblasts are able to attach and to grow in all membranes, with an increase in cell spreading for Biosilicate® membranes. Cell proliferation essay demonstrated all membranes supports cell proliferation over time, and showed no *in vitro* toxicity. All the membranes can stand the biomineralization from osteoblasts, however, a correlation with the composition of membranes and the rate of biomineralization *in vitro* cannot be stablished, but can be determined by a further *in vivo* assessment of these materials. These results highlight the potential of these membranes for guided bone regeneration and tissue engineering. Moreover, the obtained biocomposites can reinforce another materials and scaffolds, employing different fabrication technics to produce scaffolds with improved mechanical properties and osteogenicity.

We suggest, as the next phase of this work, the clinical translation of these membranes and, thus, an indispensable step will be the *in vivo* assessment of these membranes in critical bone defect models.Besides the Guided Bone Regeneration as strategy to heal critical size bone injuries, by employing bone grafts associated with porous membranes, another technique that is currently being subject of many studies in bone regeneration and tissue

engineering is the biofabrication, that has the advantage to produce personalized bone grafts on demand, as it will be following discussed.

RAPID VASCULARIZATION IN GELMA-CNC COMPOSITE 3D CONSTRUCTS: PRELIMINARY PROOF OF CONCEPTS

INTRODUCTION

Over the past decade, cell culture research has witnessed a paradigm shift into the third dimension. The emerging field of biofabrication has as its aim the automated generation of biologically functional, hierarchical 3D constructs using living cells, bioactive molecules, biomaterials, cell aggregates, or hybrid cell-material and their subsequent maturation (GROLL et al., 2016). This advanced technology, which encompasses both bioassembly and bioprinting, allows for the generation of architecturally complex tissue analogs, which comprise a spatially organized assembly of various cell types potentially mimicking the native situation (KLOTZ et al., 2016).

The photocrosslinkable Gelatin Methacryloyl (GeIMA) consists of a biocompatible hydrogel platform, capable of interacting with and encapsulating cells during photopolymerization, allowing tissue formation in three dimensions (NGUYEN et al., 2012a; SHIN et al., 2012). In addition, it is possible to construct porous structures in a microscale of GeIMA, with adjustable mechanical properties (SHIN et al., 2012). GelMA has recently gained increasing attention because it satisfies the requirements of biofunctionality and mechanical tunability to a reasonable extent, particularly compared with other available hydrogel-forming biomaterials (BERTASSONI et al., 2014; LEVATO et al., 2014; LIN et al., 2014, 2013; OCCHETTA et al., 2015). By using this 3D cell culture platform, not only is the natural extracellular environment represented, but it also provides the possibility to generate well-defined 3D tissue constructs (BILLIET et al., 2014; MELCHELS et al., 2014; SCHUURMAN et al., 2013).

While current synthetic hydrogels are often still too reductionist compared with biopolymers and, therefore, lack important biological cues (BENTON et al., 2009; EHRBAR et al., 2007), biological materials generally lack the necessary strength and precise mechanical tunability. In present day biomaterial research, there is a strong need for a merger of both biologically active and physicochemically tailorable hydrogels (BENTON et al., 2009). It is desirable to control their mechanical properties so that they match the properties of the tissue they are aiming to emulate (brain, muscle, bone, etc.)(KUMACHEV et al., 2011). The mechanical properties of hydrogels can be controlled by a number of parameters such as the density and chemistry of the crosslinks and the concentration, and molecular weight of the

precursors. However, it is observed that highly cross-linked 3D hydrogel environments have high stiffnesses but limited cell proliferation, migration, and morphogenesis (ENGLER et al., 2006; HUTSON et al., 2011; NICHOL et al., 2010; PATEL et al., 2005). Therefore, a method that enhances the mechanical properties of hydrogels without affecting their beneficial properties is needed for advanced engineered tissue constructs.

Cellulose nanocrystals (CNC) are constituted by short hydrophilic rod-shaped crystalline chains whose length varies from micro to nanometer, with Young's modulus estimated at 138 GPa, and rupture strain estimated at 7 GPa (NISHINO; TAKANO; NAKAMAE, 1995). In addition, it has been demonstrated previously that the addition of biodegradable and non-toxic cellulose nanocrystals in polymer matrices improves the mechanical properties of scaffolds according to their proportion of them (BELLANI et al., 2016; HABIBI et al., 2008; RESCIGNANO et al., 2014; SIQUEIRA et al., 2013; XIANG; JOO; FREY, 2009). Therefore, it is possible to adjust the mechanical properties of scaffolds according to the desired application.

Vascularization remains the principle obstacle that impedes the translation of most bone tissue engineered constructs to clinical practice. Currently, bioengineering studies of vascular networks have been widely used employing natural hydrogel scaffolds. Several microfabrication techniques lead to the creation of vascular capillaries from GelMA (BERTASSONI et al., 2014; LIN et al., 2013; ROUWKEMA; KHADEMHOSSEINI, 2016). However, how to connect this delicate vascular network to host blood with important caliber, in order to assure a correct blood flow inside the biofabricated construct?

Various procedures of pre-vascularization have demonstrated their efficacy for new bone regeneration and rapid capillary network formation throughout the implants: the prevascularization procedures demonstrated the advantages to provide instantaneous perfusion after the graft is implanted, which can dramatically decrease the time required for capillary ingrowth (KLENKE et al., 2008; SMITH et al., 2004; UNGER et al., 2007a; YU et al., 2009). Thus, rapid vascularization of bone graft materials is a key step for early and long-term effective osteogenesis.

The success of an implantable tissue engineered vascular graft is governed, among other factors, by the development of a scaffold that mimics the ECM (BARNES et al., 2007). The electrospinning technique is based on the stretching of a viscoelastic solution into nano/microfibers using a high electrostatic force (HASAN et al., 2014). Engineered synthetic, cell-free electrospun vessels with fast degradation properties can enable rapid *in vivo*

remodeling into neo-artery (WU; ALLEN; WANG, 2012b). Several studies have fabricated scaffolds for vascular tissue grafts by using synthetic materials. For example, Gottlieb et al. used non-woven scaffolds composed of polyglycolic acid (PGA) and poly-l-lactic acid (PLLA). Despite promising results *in vitro*, these scaffolds stiffened *in vivo* over time (GOTTLIEB et al., 2010; HOERSTRUP et al., 2000). Khademhosseini et. al. recently fabricated elastic fibrous scaffolds containing random fibers by electrospinning PGS and poly(caprolactone)(PCL) to produce vascular constructs (MASOUMI et al., 2014; SANT et al., 2011a, 2013) . A fabricated electrospun PGS/PCL scaffold had an elastic modulus in the range of 8.5MPa that mimicked the mechanical stiffness of the native heart valve (SANT et al., 2011a).

The aim of the project was to propose a concept of rapid vascularization in biofabrication for bone tissue engineering by developing a cell-laden, suturable, integrated vascular/bone construct for segmental bone defect repair, with tunable mechanical properties. GelMA-CNC composites were produced, and 3D constructs from HUVEC cells and GelMA-CNC were biofabricated. A PCL/PGS tubular scaffold and PCL/PGS membranes were manufactured by electrospinning. The electrospun membranes were processed by laser ablation, and a 3D construct from electrospun membranes and GelMA were manufactured, in order to assess the endothelial cell migration from the scaffold to GelMA. We expect to develop a microenvironment, with suitable mechanical proprieties, that promotes vascular morphogenesis in tissue engineering.

METHODS, RESULTS AND DISCUSSION

CNC-GelMA Synthesis

In order to improve the mechanical properties of the hydrogels, cellulose nanocrystals (CNC) were added to the GelMA hydrogels. However, due to the presence of gelatin, nanocrystals precipitated in the matrixes, resulting in agglomeration of the nanoparticles. In order to improve the dispersion of the CNC, the CNC was methacrylated with the gelatin. Briefly, GelMA and GelMA + CNC (1 % w/w of the gelatin weight) was synthesized by the direct reaction of gelatin (previously diluted to 10% in saline buffer (PBS, pH = 7.4 for one hour at 50 ° C) with the methyl acrylate in PBS at 50°C for two hours (Figure 33). The CNC were pre-diluted in 1%. The polymerization reaction was stopped by 5-fold dilution of the product in PBS. The mixture was dialyzed in deionized water (12-14kDa membrane) for

removal of the low molecular weight impurities (free methyl acrylate). The dialysis was carried out for 5 days at 60°C and, following, the solution was lyophilized and stored at room temperature until the time of use. The final lyophilized product was diluted at 5% in a basal culture medium (EBM-2; Lonza ®) at 60°C, and then the 0.1% w/v of photoinitiator (2-Hydroxy-4′-(2-hydroxyethoxy)-2-methylpropiophenone, Sigma-Aldrich®) was added to the GelMA + EBM medium solution. This GelMA solution was kept at 37°C until the subsequent encapsulation of the cells. The material needs to be analyzed to confirm the methacrylation of the CNC, but a significant improvement in the CNC dispersion in the matrices has already been noticed.

Figure 33. Schematics of GelMA and GelMA-CNC synthesis.

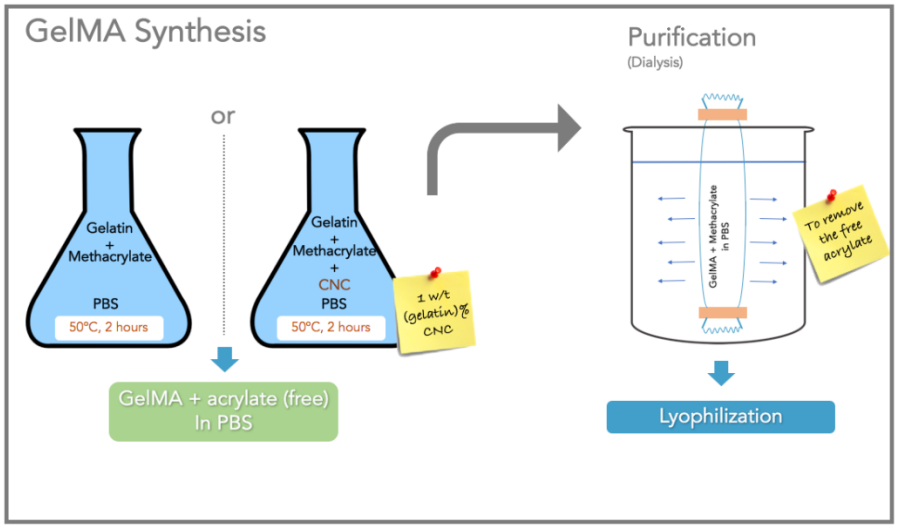

Source: Own authorship.

HUVEC Cell culturing and encapsulation

Human umbilical cord endothelial cells (HUVEC) GFP-expressing (ATCC, Manassas, VA, USA) were cultured in EBM-2 basal medium supplemented with bullet kit (EGM-2; Lonza) until reaching confluence. Then the cells were trypsinized, centrifuged, and the cell pellet was resuspended in the GelMA solution. For the 3D fabrication of the hydrogel, 10µL of the GelMA + cell suspension was introduced between two spacers 50µm in height, and the suspension was covered with a 3- (trimethylsilyl) propyl methacrylate (TMSPMA) functionalized coverslip. The hydrogels were then polymerized with cells encapsulated by ultraviolet light (UV) 6.9mW/ cm 2, 360-480nm. The exposure time to UV light was 15 seconds. Hydrogels were maintained in DMEM culture medium supplemented with Lonza bullet kit + 10% fetal bovine serum (Figure 34).

Figure 34. Schematics of 3D HUVEC cell encapsulation in GelMA.

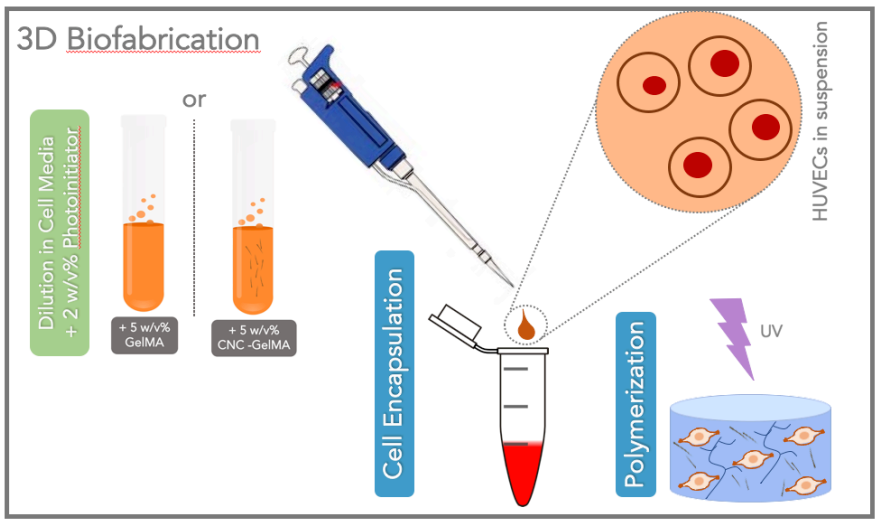

Source: Own authorship

After 1, 3 and 5 days, the hydrogels were fixed in 4% paraformaldehyde in DPBS and stained with DAPI (Invitrogen®) according to the manufacturer's instructions. The images were obtained using an inverted fluorescence microscope (Nikon TE 2000-U, Nikon, USA).

Figure 35 shows light microscopy images of HUVEC cells encapsulated in GelMA hydrogels (medium grade methacrylation and 0.1% photoinitiator) and GelMA + CNC (1%) after 1 and 3 days of culture. A slight increase in the number of cells in the images corresponding to the hydrogels with cellulose nanocrystals is observed, however, it must be ascertained whether the increase is significant, in addition to comparing the alignment of the cells in both samples (indicative of the vasculogenesis process). After 5 days, encapsulated HUVECs proliferated, organized in tubules and sprout in both hydrogels (Figure 36).

Figure 35. Light microscopy images of HUVECs 3D culturing in GelMA and GelMA + CNC (1 wt.%), after 1 and 3 days of encapsulation.

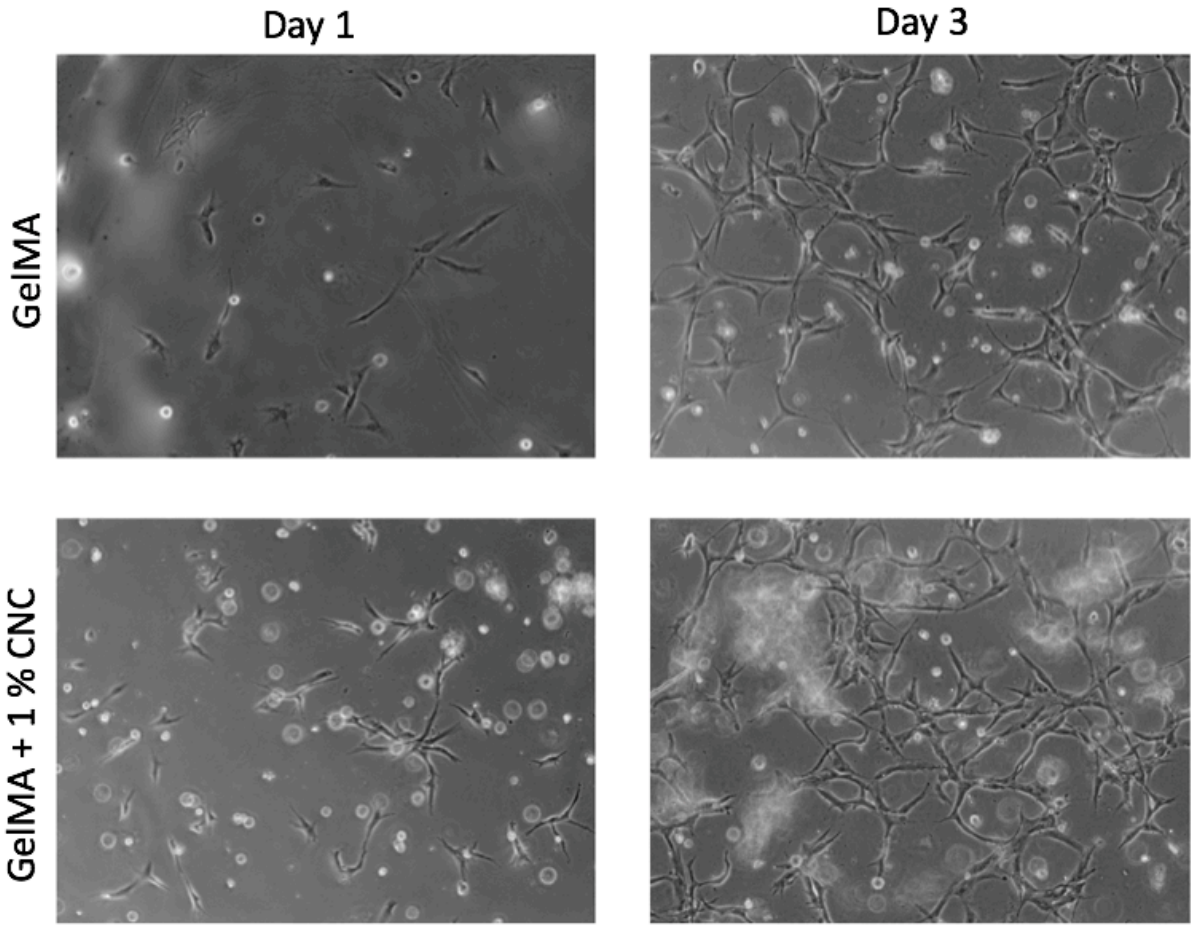

Source: Own authorship

Figure 36. Epifluorescent images of HUVECs 3D culture in GelMA and GelMA + CNC (1 wt.%), after 5 days of encapsulation. In green, the GFP expressed by the cells and, in blue, the nuclei stained with DAPI. Scale bar = 100 μm.

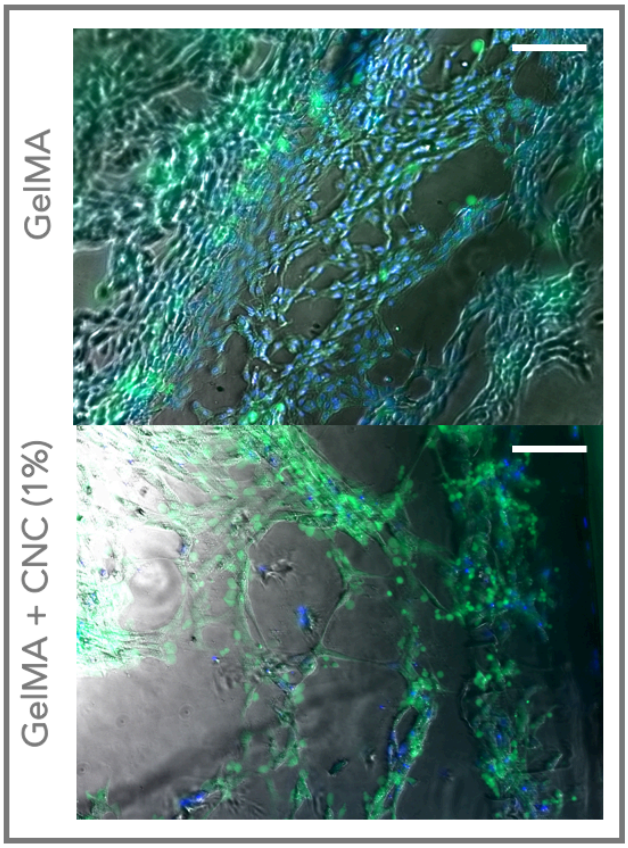

Source: Own authorship.

Tubular scaffold fabrication

The manufacture of tubular scaffolds (vascular grafts) was performed by electrospinning. The materials employed, after an exhaustive optimization step, consisted of a 1: 1 poly (caprolactone) - PCL and pre - poly (glycerol sebacate) - pPGS blend. For the scaffold mold, a gelatin coated copper tube connected to a single motor was used.

Figure 37 shows some images of one of the scaffolds. The scaffold possess a satisfactory macroscopic appearance. However, it was not possible to perform the synthesis of new scaffolds with the same properties. Besides, it was not possible to execute the polymerization of PGS after the synthesis, because there were degradation of PCL and loss of the material. Furthermore, as reported below, the pores of the scaffolds are too small to allow passage of the cells Figure 39, being a problem for the migration of endothelial cells and the consequent remodeling of the scaffold in neoartery, in addition to preventing neovascularization from perfused cells from the lumen of the scaffold and the anastomosis from an *in vivo* system, in future applications.

Figure 37. Gross pictures of the PGS/PCL (1:1) scaffold and of the fabrication process of the tubular scaffolds.

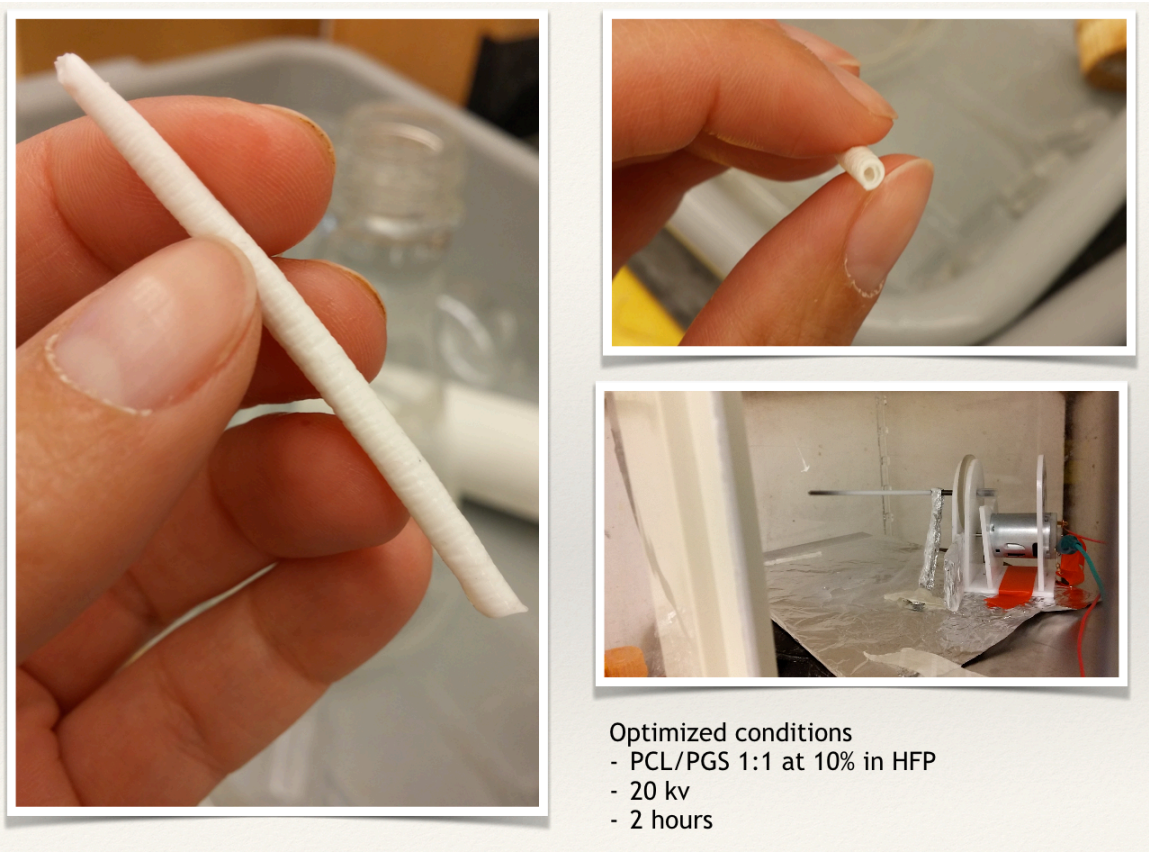

Source: Own authorship.

As it is necessary to analyze whether the vascular scaffolds allow the passage and proliferation of the cells from the scaffolds (so that new blood vessels are formed), a transmigration experiment was performed. The HUVECs were grown on pieces of electrospun membranes mounted on a small device containing a plastic frame filled with GelMA (Figure 38) in two different configurations: with micro holes (made in laser printer) and without the micro holes. After three days of culture, GeIMA (Gelatin replaced by Methacryloyl) was polymerized on the opposite side of the culture. After 7 days, the samples were fixed, treated with fluorescent dyes and analyzed under a microscope, in order to visualize if the cells passed through the scaffolds. The objective was to evaluate if the created porous structures facilitates endothelial migration.

Figure 38. Details of the assembly of the transversing assay devices (A and B).

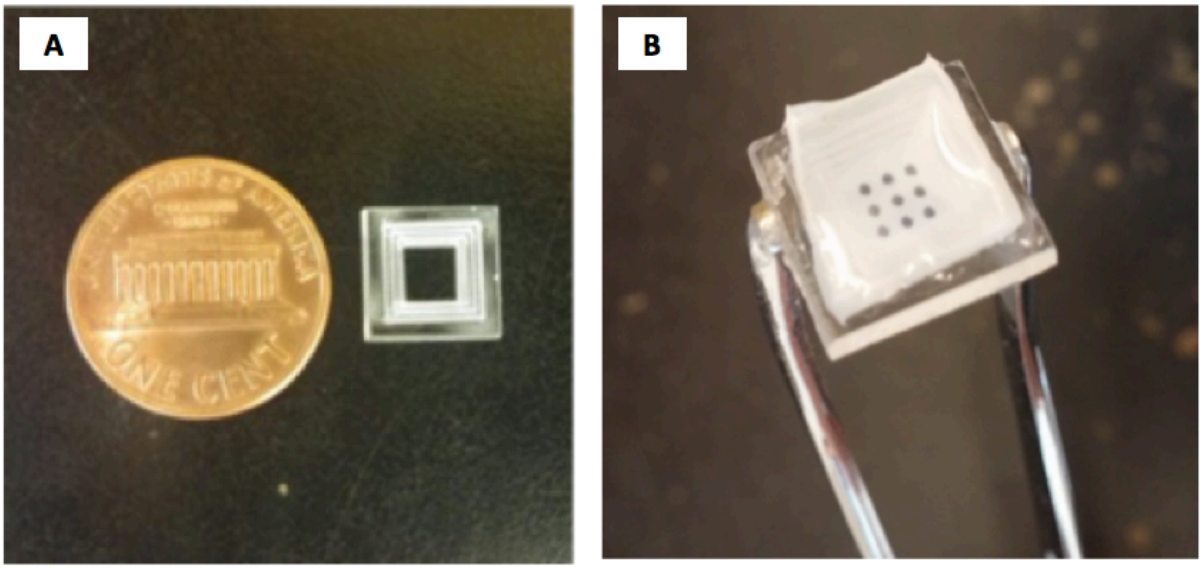

Source: Own authorship.

In Figure 39, it is possible to visualize the HUVEC cells cultured on the assembled 3D construct made from electrospun mats and GelMA, on the face of the scaffolds (A and B) and on the face of the hydrogel (GelMA) (C and D) and after 7 days of seeding (scale not shown). It is noticed that the cells multiplied and presented good morphology on the face of the nanofibrilic mats. However, although the size of the orifice in the scaffolds is considerably larger than HUVECs, allowing the passage of them, the cells did not grow in the hydrogel part of the orifices. After several attempts of this assay, the degree of methacrylation of the hydrogels (high) and the amount of photoinitiator (2-hydroxy-4- (2-hydroxyethoxy) -2-methylpro) at 1% were noted to be toxic the cells. Thus, it was decided to perform the synthesis of hydrogels with a medium degree of methacrylation and use of the photoinitiator at 0.1%, obtaining softer hydrogels, as proposed. To ascertain the interaction of the cells in the new hydrogels, HUVEC cells were encapsulated in the hydrogels as reported above.

Figure 39. Traversing essay after 7 days of HUVEC seeding over 3D GelMA + laser ablated PCL/PGS membranes. In (A), epifluorescent images the membranes, where HUVECs can be seen; (B) the porous face, showing the GelMA; (C) the GelMA side bellow the electrospun membrane, after its removal; (D) the magnified pore side.

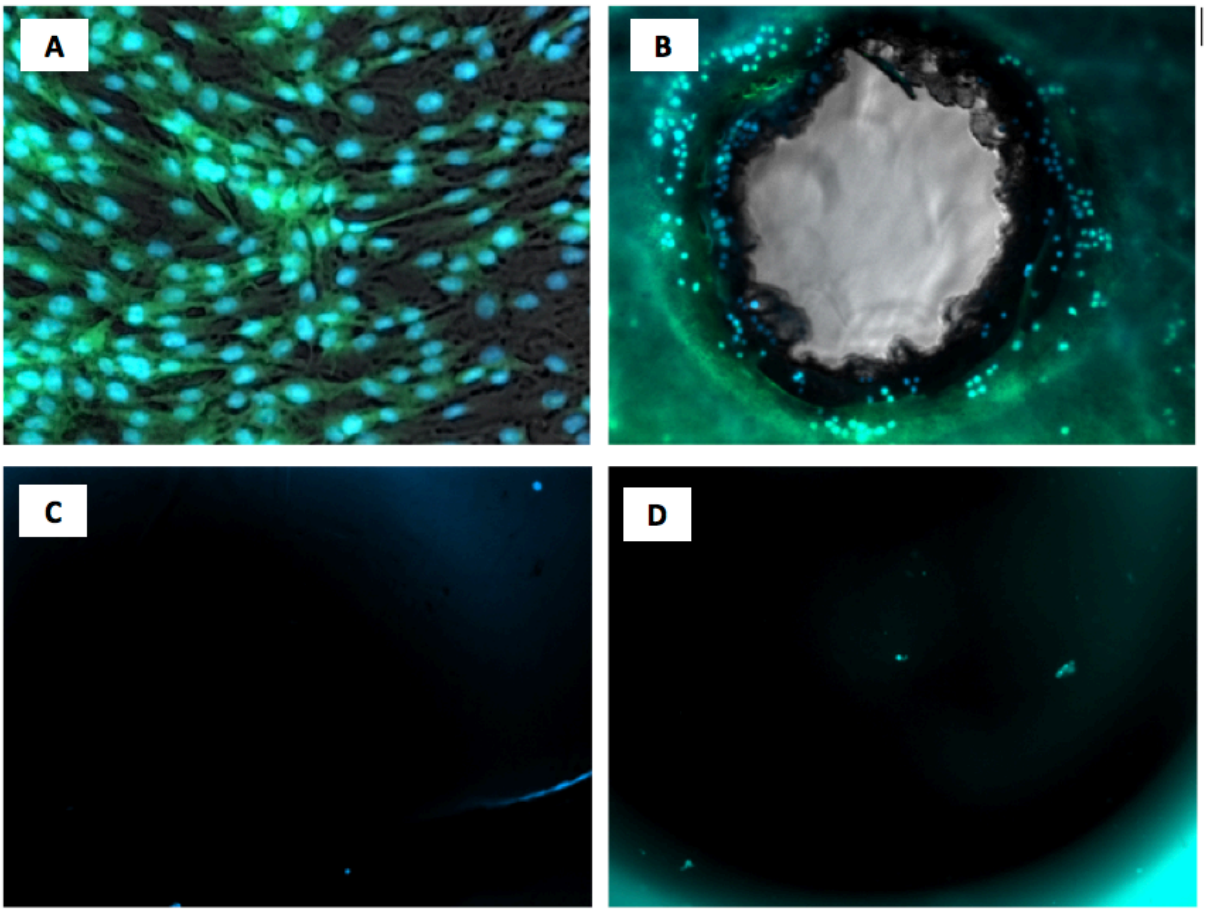

Source: Own authorship.

CONCLUSION

At this part of the thesis, we aimed to develop vascularization strategies for bone tissue engineering, in order to improve the size and survival of tissue engineered bone-like constructs. Gelatin Methacryloyl (GelMA) hydrogels were employed as vascular microfabrication platform, and cellulose nanocrystals (CNCs) were chosen as reinforcement phase, in order to tune the mechanical properties of GelMA, in such manner these properties become suitable as possible for the injury site, without compromising the liquid phase of GelMA, essential for cell spreading. To avoid the precipitation of CNCs into the GelMA, novel Gelatin Methacryloyl (GelMA)-CNC nanocomposites were synthesized. These GelMA-CNC can be successfully incorporated into pre-GelMA solutions, generating suspensions with well distributed nanocomposites. HUVECs cells were encapsulated into the pre GelMA-CNC nanocomposite hydrogel, following by the crosslink of the hydrogel, generating a novel cell-laden nanocomposite hydrogel. HUVECs proliferated, organized in tubules and sprout in these hydrogels. Thus, these hydrogels can be potentially applied as platform to build a microvascular network, and the GelMA-CNC can be employed as natural nanocomposites to

possibly tune the mechanical properties of these constructs, that can be microfabricated within biofabricated bone grafts and, then, employed as channel to transport nutriments and oxygen to the grafts by the blood. However, the key question is how to connect this micronetworking – that, though they can be reinforced, they will may not be tough sufficient to stand the suture and burst pressure. Thus, following, another strategy conceived from this part was the rapid vascularization approach, by embedding tubular scaffolds obtained by electrospinning of a fast degradation elastomer, the PGS, in order to enable the rapid remodeling of the tubular graft into a neo-artery. PCL/pPGS tubular grafts, produced by electrospinning, cannot be crosslinked due to melting point of the carrier polymer employed (PCL), which is bellow of the PGS one, and, thus, pPGS remains. PCL/pPGS membranes were also produced and laser ablated to assess cell migration from the electrospun membranes to GelMA. HUVEC cells successfully proliferated over the electrospun membranes, but they did not migrate to GelMA, and we attribute this to the concentration of the photoinitiator, toxic for cells. The GelMA was then produced with a lower concentration of photoinitiator, and it was employed at the next part of this work. Overall, the results from this part demonstrated the potential of the cellulose nanocrystals as reinforcing phase of hydrogels for 3D biofabrication, and allowed to develop a concept of rapid vascularization that has a potential to improve tissue engineering implants survival. A strategy to overcome the issue with the carrier polymer, with the objective to crosslink the PGS, is discussed at next part of this thesis.

SUTURABLE VESSEL GRAFTS FROM ELECTROSPUN TUBES FOR RAPID VASCULARIZATION OF BONE TISSUE ENGINEERED CONSTRUCTS

INTRODUCTION AND JUSTIFICATION

Generating healthy bone for the replacement of diseased or missing bone tissue has been one of the major objectives of tissue engineering scientists in the last years (NGUYEN et al., 2012b). Vascularization remains the principle obstacle that impedes the translation of most bone tissue engineered constructs to clinical practice (SALGADO; COUTINHO; REIS, 2004). After construct implantation, delivery of nutrients to cells on a biomaterial is limited to approximately 200μm and occurs via interstitial fluid diffusion (ARONSON, 1994; CARMELIET, 2000; JAIN et al., 2005; KANNAN et al., 2005). Most bone tissue regeneration applications are considerably larger, at the case after tumor surgery. In addition, similar to most other tissues and organs, the bone is interlaced with blood vessels (KNESER et al., 2006; ROUWKEMA; RIVRON; VAN BLITTERSWIJK, 2008; SMITH et al., 2004). The vascular ingrowth is limited to several tenths of micrometers per day, which is too slow to provide adequate nutrients to cells in the interior part of implant, leading to the compromised healing results (JAFARIAN et al., 2008).

Therefore, rapid vascularization of bone graft materials is a key step for early and long-term successful osteogenesis, and the degree of angiogenesis is related to the stimuli present in surrounding tissues that allow preexisting vessels to start budding into the freely applied grafts and the graft material itself (KIM; KIM; PARK, 2010). Pre-vascularization of large constructs has great potential to improve functional vasculature throughout the scaffold to rapidly facilitate integration with the surrounding tissue and circumvent necrosis in the core of the scaffold (KANG et al., 2015). Various procedures of prevascularization have demonstrated their efficacy for new bone regeneration and rapid capillary network formation throughout the implants: the prevascularization procedures demonstrated the advantages to provide instantaneous perfusion after the graft is implanted, which can dramatically decrease the time required for capillary ingrowth (KLENKE et al., 2008; SMITH et al., 2004; UNGER et al., 2007a; YU et al., 2009). Furthermore, the new formed capillaries can anastomose with the host vasculature after implantation and supply blood to the biomaterial construct (CORREIA et al., 2011).

A key challenge of vascular grafts is that they need to withstand a mechanically challenging environment immediately upon implantation (WU; ALLEN; WANG, 2012a). Thus, the classic approaches to arterial substitutes use strong materials. This is reflected in autografts, synthetic grafts and many tissue-engineered grafts (DAHL et al., 2011; HASHI et al., 2010; ISENBERG; WILLIAMS; TRANQUILLO, 2006; KAUSHAL et al., 2001; L'HEUREUX et al., 2006a; NIKLASON et al., 1999; WEINBERG; BELL, 1986). The host may be a good source of cells and a more efficient 'bioreactor' than the current *in vitro* tissue-engineering paradigm. Thus, it is possible to take advantage of the body's regenerative capacity to remodel cell-free synthetic grafts with an open porous structure that accelerates cell infiltration and remodeling (Figure 40)(WU; ALLEN; WANG, 2012a).

Figure 40. Schematic representation of direct implantation of the cell-free graft and the proposed remodeling process of the graft into a biological neoartery.

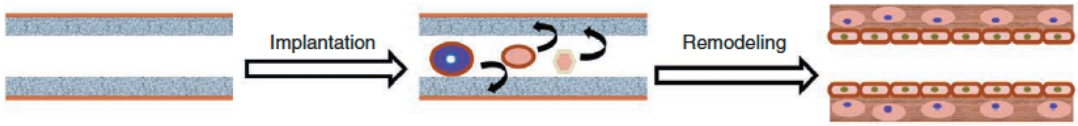

Source: *WU; ALLEN; WANG (2012a)*..

The success of an implantable tissue engineered vascular graft is governed, among other factors, by the development of a scaffold that mimics the ECM (BARNES et al., 2007). It is well known that in natural tissues the ECM is a three-dimensional (3-D) network of 50–500 nm diameter structural fibers (HASAN et al., 2014). Electrospun scaffolds are known to be good candidates for tissue engineering applications because of their ability to mimic the ECM of vascular tissue (HASAN et al., 2014; JIA et al., 2013; SHIN, 2013). The electrospinning technique, which process is based on the stretching of a viscoelastic solution into nano/microfibers using a high electrostatic force (HASAN et al., 2014), offers precise control over the composition, dimension and alignment of fibers that have impact on the architecture of scaffolds.

Poly(glycerol sebacate) (PGS), is a fast degrading elastomer and degrades rapidly *in vivo* into glycerol and sebacic acid, metabolites naturally exist in the body, minimizing the duration of host inflammatory response (RAI et al., 2012; WANG et al., 2002). However, to electrospin PGS is challenging (BETTINGER, 2011) for two reasons: (1) the insolubility of crosslinked PGS in organic solvents necessitates the use of the uncrosslinked PGS

prepolymer (pPGS); and (2) pPGS has a glass transition temperature (Tg) below room temperature causing the polymer to flow and fibers fuse into a nonporous sheet.

In several techniques (KENAR; KOSE; HASIRCI, 2010; SALEHI et al., 2014; YI; LAVAN, 2008), pPGS is blended with a carrier polymer that readily forms fibers to facilitate fiber formation. Though the use of poly(ε-caprolactone) (PCL) as carrier polymer has been reported (SANT et al., 2011b, 2013), the high temperature required to crosslink the pPGS (120°C) (WANG et al., 2002) will melt the PCL (melting temperature: 60°C) (LABET; THIELEMANS, 2009b), fusing the fibers. Unfortunately, if the carrier polymer is not removed or if pPGS is not crosslinked, the properties of the PGS scaffold would differ substantially from those of unaltered PGS (WANG et al., 2002). JEFFRIES et al., 2015 developed a simple and low-cost method for electrospinning PGS scaffolds that retains the mechanical properties of crosslinked PGS using poly (vinyl alcohol) (PVA) as the carrier. PVA does not melt during thermal crosslinking, and it is highly water-soluble, enabling safe removal by dissolution in water. Additionally, PVA is approved by the US Food and Drug Administration for applications in food chemistry and pharmaceuticals (CHAOUAT et al., 2008), and is also being investigated for use in contact lenses, wound dressing, coatings for sutures and catheters, and other tissue engineered scaffolds (CHAOUAT et al., 2008; HASSAN; PEPPAS, 2000).

It is highly desirable for scaffolds to possess an interconnected and open macroporous structure to facilitate cellular in-growth and neovascularization of regenerated tissue *in vivo* (KANG et al., 2013a). For this purpose, an ideal scaffold must present pore sizes in the range of a few tens to a few hundreds of micrometer tissue (MADDEN et al., 2010; SALGADO; COUTINHO; REIS, 2004). Electrospinning usually produces interconnected pores in the range of a few microns due to its dense network of fibers which present a barrier to the vascularization of the tissue (PARK et al., 2008; ZOPPE et al., 2009b). Various techniques to overcome this shortcoming have been investigated, including the incorporation of sacrificial fibers (BAKER et al., 2008), porogens (NAM et al., 2007), modification of fiber diameter (SOLIMAN et al., 2011), and or ultraviolet radiation treatment (YIXIANG et al., 2008) to increase pore size and overall porosity. Though interesting, these approaches does not offer a control of the pore patterning or size. Laser ablation is considered a promising tool to rapidly process and create complex structures on electrospun scaffolds (LEE et al., 2012; LIM et al., 2011; MCCULLEN et al., 2011). One of the benefits of laser ablation is that material is removed with minimal thermal damage (LEE et al., 2012; SRINIVASAN, 1986). This

technique removes selective regions of the scaffold and introduces micro-structured features including pores of a uniform size, specific global porosity, and preferential routes for cell and vascular tissue infiltration. Laser ablation possesses the ability for precise material processing with clean surface and reduced thermal damage in order to create controlled porous pattern to allow rapid endothelial cell infiltration and, thus, rapid endothelialization from tubular polymeric scaffolds employed as vascular graft. This is of crucial importance for tissue engineering scaffolds as the addition of controlled pores in the scaffold can provide many additional benefits including enhanced diffusion properties for mass transport of nutriments and cells during *in vitro* and *in vivo* expansion.

To fabricate tissue constructs similar to living tissues, one of the essential requirements is to generate organized assemblies of various types of cells to resemble the complex architectures of the targeting tissues *in vitro.* Hydrogels provide a versatile platform to include desired combinations of properties for designed applications (ANNABI et al., 2014). In particular, hydrogels for biomedical applications are designed to resemble the characteristics of native extracellular matrix (ECM) and to provide three-dimensional (3D) supports for cellular growth and tissue formation (ALGE; ANSETH, 2013).

Gelatin methacryloyl (GelMA) hydrogels have been widely used for various biomedical applications due to their suitable biological properties and tunable physical characteristics. GelMA hydrogels closely resemble some essential properties of native extracellular matrix (ECM) due to the presence of cell-attaching and matrix metalloproteinase responsive peptide motifs, which allow cells to proliferate and spread in GelMA-based scaffolds. GelMA crosslinks when exposed to light irradiation to form hydrogels with tunable mechanical properties, according to the time and intensity of UV exposure (YUE et al., 2015). Recently, several state-of-the-art microfabrication techniques, including 3D bioprinting, have been applied to control the 3D microstructure of GelMA hydrogels, and in return, to tune the cell–material interactions and cellular behaviors (ANNABI et al., 2013; BERTASSONI et al., 2014; CHA et al., 2014; GAUVIN et al., 2012; TAMAYOL et al., 2015; ZAMANIAN et al., 2010), from a variety of tissues, including bone (CUI et al., 2016; TIELENS et al., 2007; VISSER et al., 2015; ZUO et al., 2015). The biofabrication of GelMA with human osteoblast-like cells (MG-63) and human umbilical vein endothelial cells (HUVECs) as vascular bone model has been reported (ZUO et al., 2015). 3D bioprinting GelMA tissue constructs can precisely control the location of biomaterials and cells, making it an effective, comprehensive mechanism for fabricating complicated macro and microstructures, as the bone tissue interlaced with a vascular network (DERBY, 2012; DO et al., 2015; MURPHY; ATALA,

2014; O'BRIEN et al., 2014; ZUO et al., 2015). However, the main hurdle from bioprinting blood vessels from GelMA, as other hydrogels platforms, is how to connect this delicate vascular network to host blood with important caliber, in order to assure a correct blood flow inside the biofabricated construct (ROUWKEMA; KHADEMHOSSEINI, 2016). This issue can be resolved by embedding a suturable vascular graft with connected porous in order to provide an immediate blood supply into the fabricating construct.

The aim of this work was to develop a suturable vascular tubular scaffold for use in rapid vascularization of 3D constructs to heal critical size segmental bone defects. Tubular scaffolds from various diameters were obtained from poly (glycerol sebacate) - PGS and poly (vinyl alcohol) – PVA electrospun membranes, assembled and crosslinked into tubular scaffolds through an innovative method. To create a porous patterned network, the scaffolds were processed by laser ablation. The tubular porous scaffolds were embedded into GelMA in order to assembly the tubular scaffold/GelMA 3D construct. Finally, the construct was dynamically co-seeded with osteoblast-like cells (MG-63) and endothelial cells (HUVEC) from the tubular scaffold, aiming to fabricate a bone model with rapid endothelialization.

EXPERIMENTAL

pPGS Synthesis

We performed pPGS synthesis assisted by microwave. Briefly, a 1:1 molar ratio of glycerol (99%, Sigma-Aldrich) and sebacic acid (99%, Sigma-Aldrich) were mixed together, at room temperature, inside a glass balloon connected to a glass tube to allow the evaporation of the water and the glycerol which would be resulted from the pPGS synthesis. The mixture was placed in a microwave oven (Discover SP®, CEM™) and the synthesis was carried during 180 minutes at 180˚C. The obtained pPGS were allowed to cool and stored at room temperature.

Fibrous mats and fibrous tubular scaffolds manufacturing

Electrospinning

As the PGS is insoluble in most of the organic solvents, it is required the use of the pre-polymer of PGS (pPGS) to prepare an electrospinning solution (HU et al., 2017; JEFFRIES et al., 2015). However, the molecules of pPGS are not long enough to form

entanglements within them, in order to form fibers (DOSHI; RENEKER, 1995). Thus, the pPGS must be electrospinned with a carrier polymer that possess longer chains (in other words, a higher molecular weight). Since it is necessary to further crosslink the pPGS into PGS after electrospinning, the carrier polymer of choice must have the following criteria: melting temperature above of PGS crosslink temperature; dissolution in a solvent which is not common to the pPGS or PGS. As suggested in the work of JEFFRIES et al., 2015, we employed the PVA (Gohsenol®, Nippon Gohsei™, MW ≈ 20,000) because it has a higher melting point than the one required for the crosslink process of PGS, and it is easily removed by water. Additionally, if some PVA remains, it is a non-toxic and non-carcinogenic material (CHAOUAT et al., 2008). Finally, we employed the hexafluoroisopropanol (HFIP, Covachem, Ref. 12206-25) as the common solvent for both pPGS and PVA to prepare a solution for electrospinning.

We have prepared the electrospinning solution as suggested by JEFFRIES et al., 2015, with some modifications. The pPGS/PVA were diluted at a 55:45 (w/w) ratio at 10% (w/v) in HFIP, and the solution was kept in magnetic stirring at room temperature overnight, prior to electrospinning. We employed an electrospinning machine assembled in the house with a rotating collector (Figure 41, A). A voltage of 20kV has been applied through a positive electrode connected to the tip of the spinneret (electrospinning needle), and -1kV to the collector, which was positioned at 18 cm of distance from the spinneret. The solution was put inside a syringe which has been connected to the spinneret by a polytetrafluoroethylene (TPFE) tube. Because the TPFE tube is too rigid to be extended in order to be directed connected to the syringe and to the spinneret, we utilized some pieces of silicone tubes as connectors. The flow rate was kept by a syringe pump (Harvard Apparatus™) at 2 ml/hour.

The pPGS/PVA fibers were collected over parchment paper (Figure 41, B). This step is essential to assure the employment of almost the totality of the collected fibers to produce the tubular scaffolds, as it will be reported, because all the membrane can be detached. The standard time of collection for samples assembled in tubes was 30 minutes, but it varied depending on the kind of sample, as it will be discussed.

Figure 41. Equipment and materials. A. Electrospinning machine, with the rotating collector; B. Parchment paper used as collection substrate; C. Detaching a sample with its substrate from the collector.

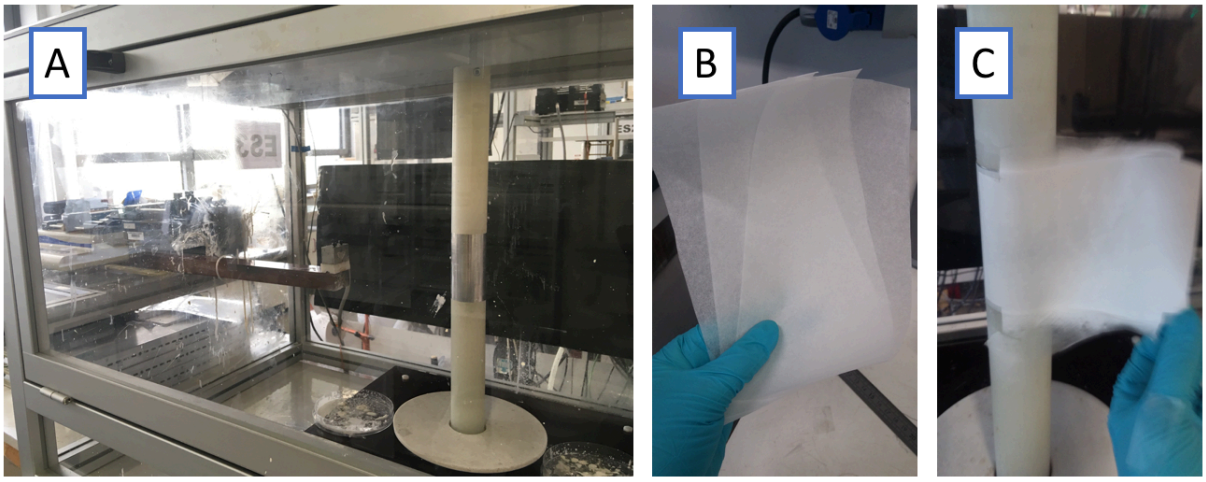

Source: Own authorship.

Assembly and Crosslink of the Scaffolds

We took advantage of the feature of the non-crosslinked pPGS to stick and to crosslink different layers of electrospun mats together to assembly tubular scaffolds by simply rolling the electrospun pPGS/PVA mats (10 cm width x 20 cm length) around PTFE mandrels of 0.75, 2 and 3 mm of diameter. Samples were obtained rolled around the PTFE rods while detaching them (Figure 42, B, C). The final tube was very stable, thanks to the ability of pPGS present to bond the different layers (Figure 42, D). In order to assess mechanical and *in vitro* testing, flat samples have been also crosslinked.

Finally, the assembled scaffolds obtained from the electrospun mats were placed in a vacuum oven (Heraeus, Thermo Scientific™), for 150˚C for 48 hours. We also crosslinked samples at 120˚C for 24h, then for 150˚C for 24h for some comparison purposes.

Figure 42. Assembly of tubular scaffolds. A. electrospun sheets and their parchment paper; B. The electrospun samples is easily detached from the paper; C: Rolling the electrospun sheet around the PTFE rod; D. The final pPGS/PVA fibrous construct, read to be cured into PGS/PVA tubular scaffold.

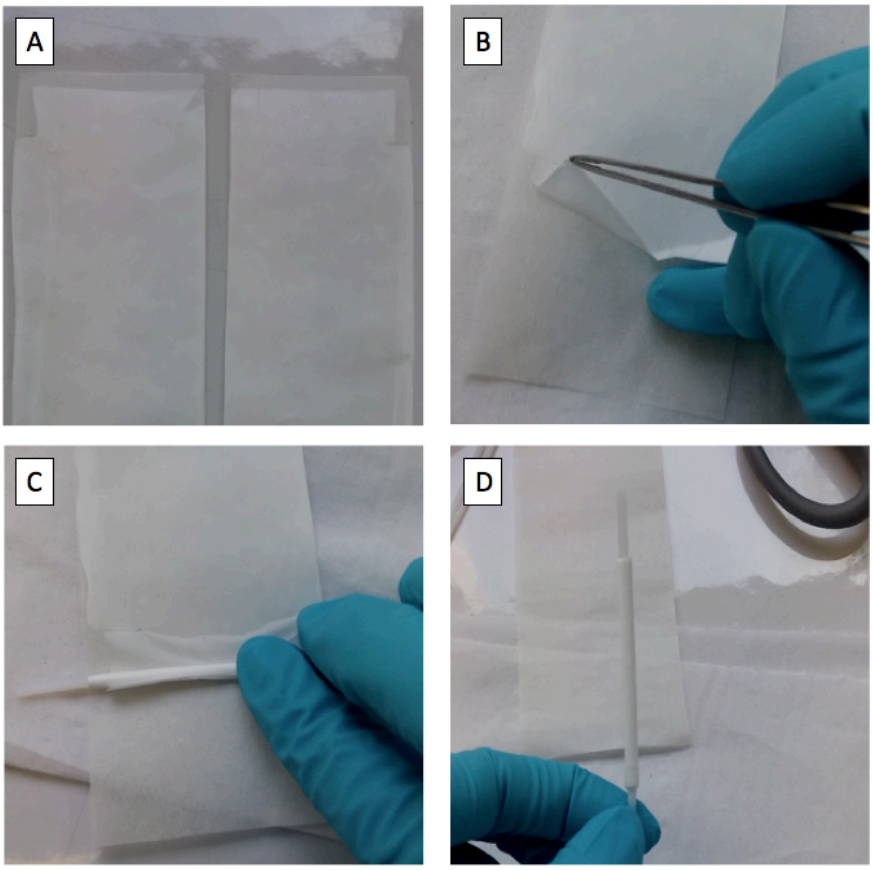

Source: Own authorship.

Samples for delamination essays

To test the interfacial adhesion of the electrospun layers, as employed for the tubular scaffolds, the samples for delamination essay was fabricated by direct electrospinning or stacking the electrospun membranes. For the direct electrospinning samples, the electrospinning membranes were collected over parchment paper for 20 minutes, then, a stripe of parchment paper was placed longitudinally to the collector over the sample. The electrospinning was carried for more 20 minutes. For the stacked samples, electrospun layers were stacked, with a parchment paper stripe between the layers. These samples were subject to curing with glass weight overt them, and with parchment paper between the weight and the samples. The samples were cured in a vacuum oven at 150˚C for 48h and then purified as described. Prior to mechanical testing, the parchment paper was removed and the samples obtained had at 3D T-shape.

Laser Micro-ablation

In order to pattern the tubular scaffolds with porous structures that allows cell migration, we employed a laser system (Optec Laser Systems) to perform laser ablation and

creation of the pores. Samples were loaded in rotor stage, and synchronized in a computer software, in order to fully pattern the tubular scaffold. The laser energy employed was 1.9W, with a frequency of 100kHz and laser beam scanning speed of 250mm/s.

Samples purification

In order to remove the PVA (the carrier polymer), the samples were washed by distillated water in room temperature for 24 hours, with gentle agitation. Following, to remove the non-crosslinked PGS (the pPGS), the samples were washed in ethanol 100%, then in distillated water. For storage and/or analyses, the samples were lyophilized.

Characterization

NMR analysis

In order to determine physical characteristics from a chemical indicator, i. e., the degree of esterification, as proposed by Li et. al., samples of the pPGS as synthesized were diluted in dimethyl sulfoxide (DMSO) and analyzed by ^{1}H NMR. The degree of esterification (DE) was calculated according the Equation 2 :

$$DE = \frac{I_E}{I_E + I_A}$$

Equation 2: Degree of Esterification

where I_E is the integration of the 2.28ppm peak, and the I_A is the integration of the 2.17ppm peak. The higher the degree of esterification, the more polymerized will be the PGS (LI et al., 2015). In our case, we aimed to achieve an ideal degree of esterification to possess a pre-polymer of PGS (pPGS), suitable for electrospinning.

Scanning Electron Microscopy (SEM)

We analyzed the morphologies of the electrospun mats and scaffolds by SEM Vega 3 TESCAN™. Samples were cut and placed over aluminum stubs with conductive adhesive tape, then they were coat with gold-palladium. The average fiber diameter was obtained by analysis at ImageJ (Wayne Hasband, National Institute of Health, USA). An average of 50 measures for each picture/condition was taken.

Mass Loss

We evaluate the removal of PVA and pPGS by mass loss. Samples were weighted after the crosslink, then after the different washing steps, and the mass was compared.

Mechanical Properties

Mechanical properties of electrospun PGS/PVA blends were measured by uniaxial tensile testing until their rupture in a Dynamic Mechanic Analyzer, with a pre-load of 0.010 N and speed of 50 μm/s at room temperature. Crosslinked and purified tubular samples were longitudinally opened, and carefully cut in order to obtain samples of 10 mm length and 4 mm width. Sample thickness was measure by a caliper. Four specimens of each sample were obtained and hydrated prior to the essays. The elastic modulus was calculated by determining the slope based on the applied load and scaffold deformation in the linear region of the stress–strain curve and the dimensions (thickness and width) of the samples.

Suture retention strength (SRS) was measured by inserting a 4-0 suture 2mm from the edge of the long axis of 4mm x 10mm samples and strained to rupture. Suture retention strength was calculated as maximum load/ (suture diameter x sample thickness) in N/mm^2. Delamination essay was performed on the hydrated T-peel samples (which manufacturing process was previously explained in "Assembly and Crosslink of the Scaffolds")

***In vitro* testing**

Cell seeding onto PGS/PVA membranes

In order to visualize the presence of HUVEC cells over the PGS membranes through fluorescence, autoclaved PGS/PVA membranes samples with 0.7 mm diameter were obtained by a punch cutter. In order to keep the PGS specimen on place, we employed 15 μl of Matrigel® (which was previously kept at 8˚C in order to melt) per well of a 96-well cell culture plate, kept over ice. The plate assembly with the PGS/PVA with Matrigel® was left under 37˚C for 20 minutes, in order to solidify the Matrigel®. HUVEC cells were trypsined, counted and seeded at 2 x 10^4 per well. The cells were kept in EBM-2 + bullet kit culture media.

After 3 days, the cells were fixed with 4% of paraformaldehyde in PBS for 10 minutes and washed twice with PBS. To increase the permeability of the cells, a solution of 0.1% of triton x-100 in PBS was used for 5 minutes. The wells were washed two times with PBS, and

DAPI (provided by Sigma-Aldrich) and Phalloidin (CytoPainter Phalloidin-iFluor 488, Cat. Nº 176753, Abcam™) staining was diluted in PBS with 1% of BSA as the manufacturer's recommendations. After 10 minutes, the samples were washed twice with PBS, but, at the last wash, some PBS was left to prevent samples dehydration. The light and fluorescence images from samples were taken from a Zeiss Axio Vert.A1 inverted microscope with AxioCam software. The images were superimposed according to the desirable (DAPI and GFP filters and their superimposition with the light microscopy images). Noise reduction and contrast improvement filters were applied.

In vitro testing

Cell proliferation/viability was measured by resazurin (Cat. No R7017, Sigma-Aldrich®). To prepare the resazurin solution, 1g of resazurin powder was diluted in 100 ml of ultrapure water in magnetic stirring overnight, producing the first resazurin stock solution. We diluted then the first stock solution at 10% in ultrapure water, then filtering it, creating a second stock solution, read to employ when diluted at 5% (v/v) in cell culture media.

The cell viability/cytotoxicity test was performed according the ISO 10993-5 standard, with biomaterials extract. The extract was prepared by incubating overnight 20 mg of autoclaved scaffolds per mL of cell culture media, at 37˚C. Human Umbilical Vein Endothelial Cells (HUVEC) were trypsinized, counted and resuspended at 1 x 104 cells/well. Cells were incubated in DMEM (Vitrocell®, EmbriolifeTM) supplemented with 10% fetal bovine serum, 1% penicillin, and 1% streptomycin (100 mg/mL) for 3 hours at 37˚C, 5% CO2. Following, cells were incubated with the scaffolds extract or DMEM only (negative control) or methanol (positive control for cytotoxicity). The extract, or cell medium or methanol was changed at each 2 days.

The cell proliferation essay was performed by incubation of resazurin final stock solution diluted at 5% in DMEM at 100 µL per well. We employed four wells for each PGS extract, positive and negative control, and three independent essays (triplicate). Two empty wells were used as reagent blanks (control of the resazurin). The cells were incubated at 37 °C in atmosphere supplemented with 5% of CO2 for 4 h. After incubation, 30 µL of medium was transferred into a 96-well TCPS plate, and 30 µL of 100% reduced (fluorescent) resazurin (obtained by autoclaving, as described) was used as reference of the essay. We measured the fluorescence according the Equation 2. The essay was done at 1, 3, 5 and 7 days after cell seeding.

GelMA 3D constructs

Pre-GelMA synthesis

The pre-GelMA (Gelatin Methacryloyl) was prepared as published before (YUE et al., 2015). Briefly, the pre-GelMA was fabricated by the direct reaction of the gelatin (previously diluted at 10% in PBS during one hour at 50˚C) with the methyl acrylate in PBS at 50˚C for two hours. The reaction was interrupted by diluting the obtained product 5 times in PBS. The solution was dialyzed in ultrapure water with a membrane of 12-14kDa to remove low molecular impurities (i. e. free methyl acrylate). The material was allowed to be dialyzed for 5 days, at 60˚C. Following, the solution was lyophilized and the GelMA was stored at -80˚C until utilization.

GelMA polymerization

Prior to the polymerization, the photoinitiator solution (PI) was prepared by adding 10 mg of 2-Hydroxy-4′-(2-hydroxyethoxy)-2-methylpropiophenone (Sigma-Aldrich 410896-10G) in 1 ml of ultrapure water, vortexing the solution and keeping it at 37˚C. Following, the pre-GelMA was diluted at 10% (m/v) in PBS, and this solution was also kept at 60˚C for, at least, 1 hour, in order to completely dissolve the pre-GelMA, creating the stock pre-GelMA. Following the dissolution steps, all solutions were kept at 37˚C. The final pre-GelMA solution was made by mixing the PI solution, the pre-GelMA stock solution and EBM-2 + bullet kit cell culture media, having a final pre-GelMA solution at pre-GelMA at 5% (m/v) with 0.1% (m/v) of PI read to employ. The pre-GelMA final solution was put inside the wells of a 96-well transparent TCPS plate (40 µl/well). The plate was place inside a UV curing chamber (375 nm, 36 w). The polymerization was proceeded for 15 minutes.

Endothelial Cells Seeding from the Vascular Graft: an *in vitro* model of bone vascularization from the PGS vascular grafts embedded in GelMA

HUVEC/MG-63 3D co-culture on GelMA

We created an *in vitro* model which simulates the rapid cell perfusion from the vascular scaffolds to an 3D bone construct, in order to observe how HUVECs can migrated and/or interact towards the osteoblasts on the 3D fabricated matrix. In order to determine which kind of interactions we must observe and/or expect from 3D co-culturing MG-63 and

HUVEC cells, though this interaction is widely reported (FUCHS; HOFMANN; KIRKPATRICK, 2007; KYRIAKIDOU et al., 2008; SHI et al., 2014; UNGER et al., 2007b; ZHANG et al., 2010b), we first made the direct osteoblasts and endothelial cells seeding on the previously polymerized GelMA, dynamically seeding these lineages over the GelMA as we performed for the GelMA + Tubular scaffolds 3D constructs. The GelMA was previously polymerized as described above. The osteoblasts were first seeded at 1 x 10^4 (suspended at 40 µl of EBM-2 bullet kit media), allowed to adhere on the GelMA for 1 hour and, then, the cell media was aspirated and the HUVEC cells were seeded at 2 X 10^4 cell/well (with the half of the cell concentration of the MG-63 because the HUVEC is a less proliferative cell lineage compared to the MG-63 (SHI et al., 2014)). This amount of HUVEC was, initially, suspended in 15 µl of media. They were allowed to attach for 30 minutes (to permit cell adhesion and, at the same time, to prevent cell dehydration) and, then, the wells were completed with 120 µl of cell culture media. These steps were made in order to keep the majority of HUVECs in the middle of the hydrogel, so we could create a gradient of HUVECs towards the osteoblasts. After 48, hours (accord to the structure development), the constructs were stained with DAPI and Phalloidin as previously explained, then observed by fluorescence microscope.

Endothelial Cells seeding from the PGS vascular grafts embedded in GelMA: co-culture dynamics of an *in vitro* vascularized bone model

For the *in vitro* model for rapid cell migration, the tubular scaffolds, transversal sections of non-processed by laser ablation and processed samples were and embedded inside non-crosslinked GelMA (pre-GelMA) on well of a 96 well-plate. The GelMA was allowed to crosslink for 15 minutes, fixing the tubular scaffold.

Suspended MG-63 were seeded at 1 x 10^4 per well (40 µl), outside the graft “well”. The MG-63 were allowed to adhere at GelMA substrates for 30 minutes prior to HUVEC seeding (2 x 10^4/well, suspended in 15 µl of cell culture media), creating again gradient of HUVECs and MG-63 (though HUVEC get out and MG-63 get in during seeding with, inevitably, which can be further avoided by encapsulating the cells). After 24, 48, and 120 hours (depending on the experiment), the constructs were fixed and stained with phalloidin and DAPI, as reported, and, then, observed by the fluorescence microscope.

RESULTS AND DISCUSSION

pPGS synthesis

The Figure 43 shows the Degree Esterification (DE) analysis of the synthesis of pPGS at 1:1 rate by Proton Nuclear Magnetic Resonance (H+ NMR) calculated according the Equation 2. A pPGS with a degree of esterification of 51% was obtained, with a soft wax aspect and no completely polymerized as described for LI et al. (2015).

Figure 43. NMR+ analysis of the pPGS (1:1 molar rate) employed. The degree of esterification obtained was 51%.

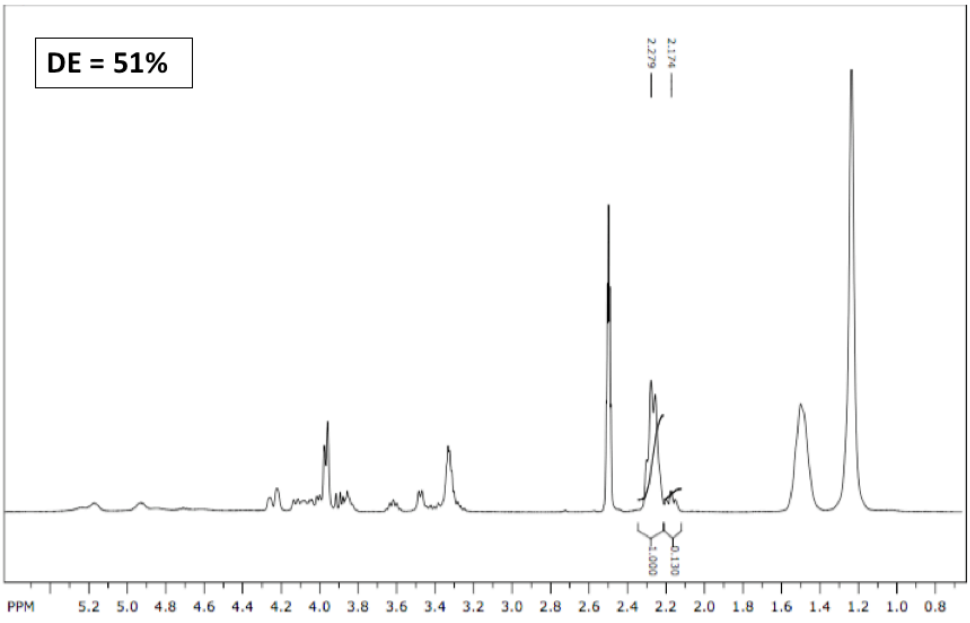

Source: Own authorship.

Fibrous mats and fibrous tubular scaffolds manufacturing

The morphology of the mats produced from pre-Poly (Glycerol Sebacate) and PVA at a 55:45, prior to crosslink, can be visualized through the SEM Micrographs shown at Figure 44. According to Jeffries et. al., the pPGS/PVA 55:45 ratio improves the fiber formation (due to considerable amount of PVA, the carrier polymer) at the same time the amount of pPGS can conserve the scaffold integrity, after the carrier removing. We can see the uniform, smooth aspect of the fibers, ranging at an average of 600 nm (Figure 47), with a few contact points within the fibers. The disposition of fibers of the mats is random, as it will also be further observed for the tubular scaffolds (Figure 50), since it was obtained by the assembly of the electrospun mats with fibers disposed in a random manner.

Figure 44. SEM images from the electrospun pPGS/PVA membranes, showing the overall morphologie of the fibers.

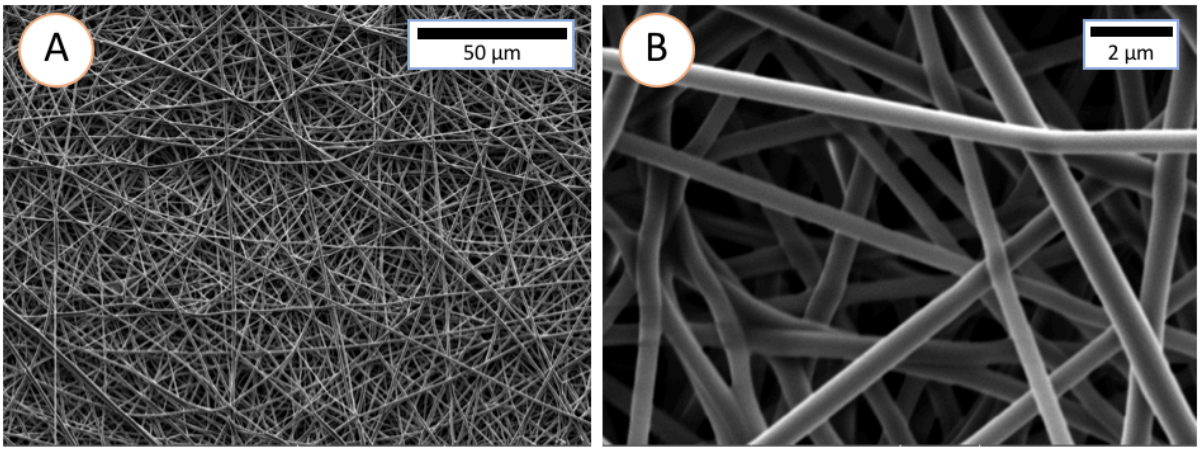

Source: Own authorship

Crosslink and Purification

The electrospun pPGS/PVA membranes and scaffolds were cured in a vacuum oven in order to crosslink the pre-polymer of PGS (pPGS), then washed in water in order to remove the PVA, following by series of ethanol washes in order to remove the non-crosslinked pPGS.

At the top left of the Figure 45, we can see typical morphology of an electrospun pPGS/PVA mats, with uniform and cylindrical fibers, as discoursed. We then cured the samples at 150˚C for 48 hours, in order to crosslink the PGS. It noteworthy that Jeffries et. al. (JEFFRIES et al., 2015) reported various conditions of crosslinking, concluding that the best condition, in terms of mechanical properties and integrity of fibers preservation, was 120˚C for 48h. We have submitted samples at these crosslink condition at our lab, and also at 120˚C for 24h, then for 150˚C for more 24 hours, as also investigated from Jeffries (JEFFRIES et al., 2015), but after the purification, we obtained a film or completely fused fibers, as can be seen at Figure 46. After curing the membranes at 150˚C for 48h, we obtained samples with a uniform morphology and preserved porosity. We also have tested crosslinking conditions with higher temperatures (170˚C 48 h), but the final membranes/scaffolds were too rigid (results not shown).

One can notice some of the fibers are fused, which is result from some of the PGS that melted and leaked from the fibers, filling some pores. This phenomenon may cause the impression the fibers diameter increased, but, as it can be seen at Figure 47, there was no significant fibers diameter increase or decrease. In any case, the porosity is still preserved,

which is one of the key points in order to possess a vascular scaffold similar to the ECM. Following the crosslinked, the samples were purified by water washing and ethanol washes, as described. The samples shown at the Figure 45 were lyophilized after each washing step (water and ethanol) so they could be visualized at SEM (in general, all the materials were only lyophilized after the complete purification). As can be observed at the Figure 45 again, we could not observe significant changes at the morphology of the fibers after the water washing, in comparison with the non-washed sample. However, after the subsequent ethanol washing, by a gross analysis, we can see an increasing in the porosity, in comparison with the crosslinked and the water washed sample, but, in other hand, it was not observed a significant decreasing in the fibers diameter, as shown in Figure 47.

As the purpose of the water washing is to remove the PVA (the carrier polymer) and the ethanol washes is to dissolve the non-crosslinked PGS, we can attribute the fibers fusion to the PGS that leaked, other than the PVA. Moreover, the PVA has a higher melting temperature than the one employed for the crosslinking (at least 200˚C (PEPPAS; MERRILL, 1976)), and thus, remains intact after the curing and/or interacting with the molecular structure of the PGS, as it will be discussed. However, after the purification, the fibers are still fused, resulted from the pPGS melting and the sequential curing, though the porosity and the overall fibers structure are preserved and, as can be seen, we obtained a final purified membrane which still has a similar structure as the ECM (HOREJS et al., 2016; SCHOEN et al., 2017; XU et al., 2004).

Figure 45. SEM pictures of the membranes as electrospun, crosslinked at 150˚C for 48 (pPGS/PVA into PGS/PVA), water washed (in order to remove the PVA, the carrier polymer) and subsequently washed by ethanol (to remove any non-crosslinked pPGS).

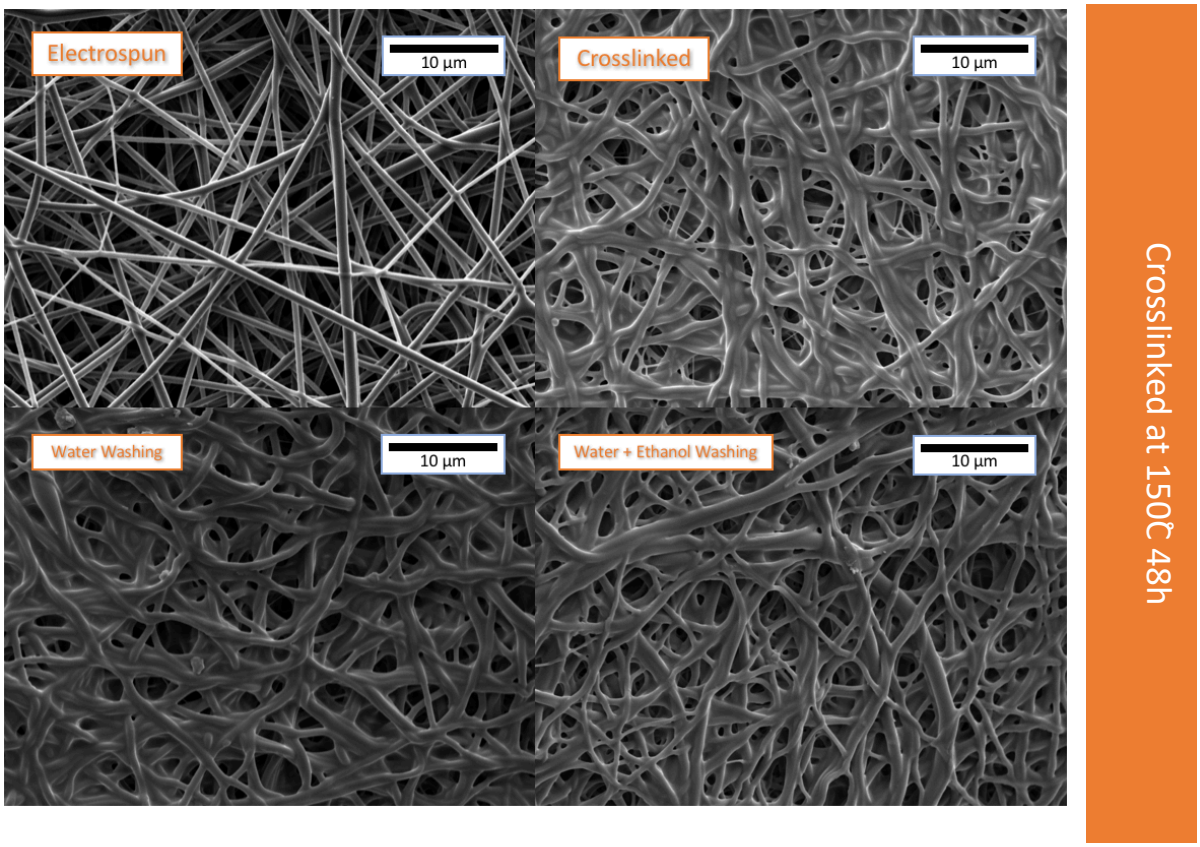

Source: Own authorship.

Figure 46. SEM images of the electrospun membranes after crosslinking at 120˚C for 24h, 150˚C 24h, and purified (after water and ethanol washes).

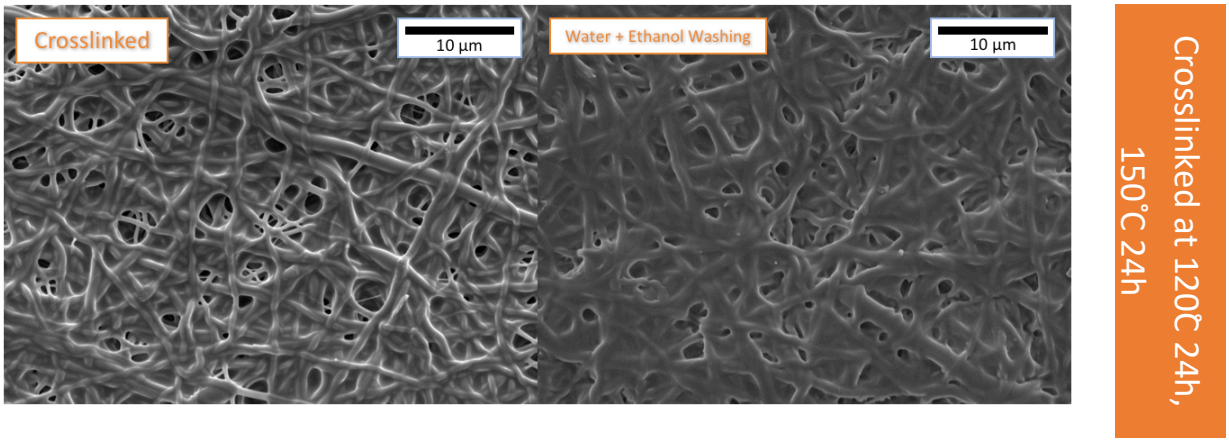

Source: Own authorship.

Figure 47. Diameter measure of the fibers from the electrospun membranes after electrospinning, curing, water washing and water + ethanol washing. The bars represent the average values after each step, and the alter bars

are the Standard Error of the Meaning (S.E.M.). The average fiber diameter for all samples is around 600 nm. No statistical differences were found. n=50.

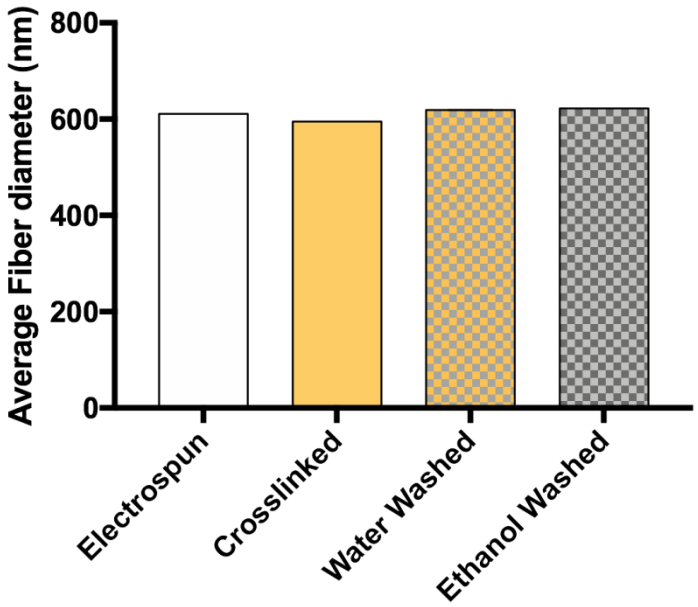

Source: Own authorship

Mass loss

We evaluate the removal of PVA and pPGS by mass loss after the different washes in comparison with the crosslinked samples. Because we have also investigated the crosslink condition proposed by Jeffries et. al. (JEFFRIES et al., 2015), in order to compare our results and stablish a relation between the crosslink conditions, and the fiber composition and morphology of the membranes, the mass loss investigation of both conditions are reported. Samples were weighted after the crosslink, then lyophilized after the different washing procedures, and the mass was compared.

From the Figure 48, we can see the remaining mass at 150ºC, 48 h condition is higher than for 120ºC 24 h; 150ºC, 24 h (condition employed by Jeffries et. al. (JEFFRIES et al., 2015), after both water and ethanol washes. For both crosslinking conditions, we can notice the most significant mass loss is after water washing, which most likely removes the PVA, due to this solubility in water. A significant higher amount of mass remaining after the water washing for the 150˚C 48h conditions in comparison with the first one. Considering we have employed 45% of PVA for the electrospun membranes manufacturing, but there is still around 75% of remaining mass, we may suppose still there was PVA remaining in the fibers. The temperature may contribute for PVA insolubility (HASSAN; PEPPAS, 2000) or crosslinking

with the residual carboxylic groups of the pPGS (JEFFRIES et al., 2015), but this must be confirmed by another analysis, as FT-IR spectra.

While for the first crosslink condition there was a significant mass loss after the ethanol washing, this is not observed for the second condition, which means most of pPGS was cured into PGS for the condition we employed. This explains why we obtained fibers with a regular structure and porosity only when curing the fibers at 150˚C for 48h (Figure 45), while, in other hand, the membranes crosslinked at 120˚C 24h, 150˚C 24h has been fused (Figure 46).

Moreover, we hypothesize more PVA remains for the second condition of crosslink not only because the temperature may improve the molecular interaction of the PVA with the PGS but, also, as the PGS crosslink, it may "traps" the PVA inside the fibers, during the curing, because the ratio of pPGS employed was higher than of the PVA. Thus, for the condition of 150˚C during 48 h (which was chose due the preserved integrity of fibers after washings), as more PGS is crosslinked at this condition, more PVA may be trapped inside. It is worth pointing out the remaining PVA is not harmful for cells (FATIH CANBOLAT et al., 2011; MAHMOUD et al., 2010; MATHEWS et al., 2008). PVA is non-toxic, biodegradable, and does not degrade in any harm compound to the cells (BAKER et al., 2012; BURSTEIN, 1980; DEMERLIS; SCHONEKER, 2003; WANG et al., 2008). Those are essential features, as we intend to use the scaffold as bioabsorbable vascular grafts.

Figure 48. Scaffolds purification efficiency calculated by the remaining mass (%) after each washing step (water washing and ethanol washing) in comparison with the crosslinked samples. The colored bars represent the average between the specimens (n=3), and the SEM (Standard Error of the Meaning) is imposed as alter bars. *n<0.05.

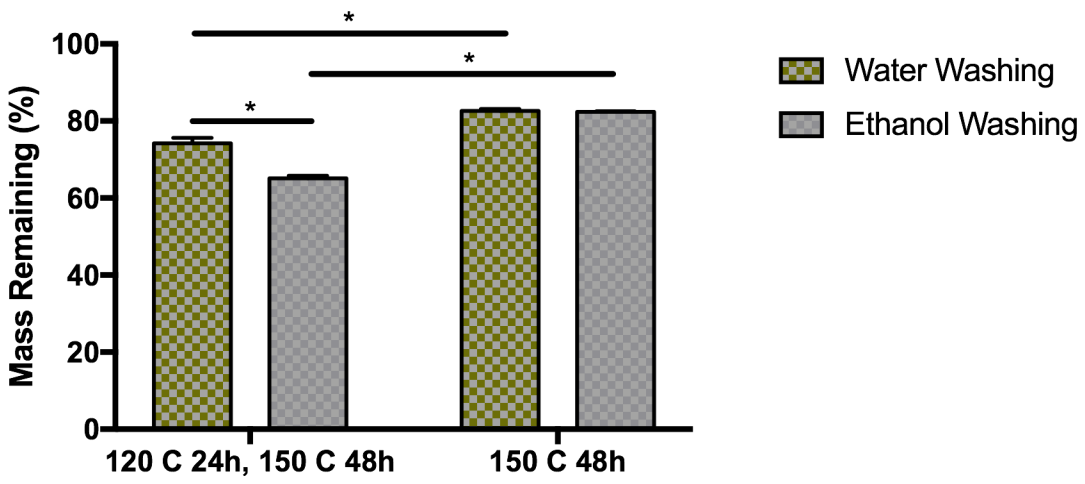

Source: Own authorship.

Tubular Scaffolds Assembly

Because the electrospun membranes constituted of pre-polymer of PGS (pPGS)/PVA can stick in different layers because of the employment of the pPGS, we took advantage of this feature together to assembly tubular scaffolds by simply rolling the electrospun pPGS/PVA mats (10 cm width x 20 cm length) around various PTFE mandrels with small diameters. Finally, the assembled scaffolds obtained from the electrospun mats were placed in a vacuum oven for 150˚C for 48 hours, as previously explained. Jeffries et. al. (JEFFRIES et al., 2015) also fabricated multilaminated scaffolds by stacking pPGS/PVA fibrous sheets between two PTFE blocks and crosslinking the constructs, besides tubular scaffolds from direct electrospinning. However, he did not fabricate tubular grafts from stacking electrospun layers around a TPFE mandrel. He described how he electrospun the fibrous sheets on aluminum paper. Once the pPGS/PVA membranes are fabricate over aluminum, these cannot be detached without leaving a lot of the product behind and, thus, producing a thin, non-uniform membrane which would be difficulty to assembly into a tubular construct and could lead to a non-uniform scaffold. Moreover, Jeffries et. al., in order to produce the electrospun tubular scaffolds employed an electrospinning technique which places a rotating mandrel, pre-coated with hyaluronic acid, between the spinneret connected to the charge and a needle as opposite charge, because, in the case of small diameters, the surface area is so small it does not attract the fibers. In this technique, the mandrel is covered with the fibers which are eventually trapped by it, however, most of the fibers goes out in the direction of the opposite charge. Though it is possible to produce a tubular scaffold from the accumulation of the fibers that are eventually trapped over the mandrel, this process is time and material consuming.

In other hand, our technique employed a rotating collector of 10 cm x 20 cm covered with parchment paper, directly connect to the opposite charge, which collects almost the totality of the fibers. The fibers can be easily detached from the parchment paper (*Figure 42*), and all of the electrospun membrane can be used in to the tubular scaffold manufacturing. Moreover, this technique does not require a pre-coating over the PTFE mandrel, and the scaffold, after the crosslink, can be effortlessly detached from the mandrel. Finally, the most important, this technique does not require any special mandrel, collector or setup. Any collector surface that can be covered by parchment paper can be employed, and it is very cheap. Though the parchment paper may isolate some charges, and we hypothesize it can be

more challenging to electrospin thicker membranes, this is not a constraint for this technique, because we stack various layers of electrospun membranes to create a scaffold.

According to the gross observations pictured at Figure 49, and also from the Scanning Electronic Microscopy (SEM) analysis Figure 51, from this technique, we successfully fabricated scaffolds with diameters raging 0.75 mm to beyond: the tubular scaffold inner diameter will depend only on the diameter of the PTFE mandrel. As the scaffolds illustrated here are prototypes, for most of the scaffolds samples we employed electrospun sheets of 10 cm, producing, thus, scaffolds of 10 cm length, which is considerate a clinical relevant length (L'HEUREUX et al., 2006b). Still, it is possible to employ larger electrospun membranes to obtain longer scaffolds. Moreover, it is possible to bond various sheets to create an unlimited long tubular scaffold, which can be cut and employed by the surgeon according to surgery site need. We created such scaffold, however, because it was difficulty to remove from the PTFE mold (we employed a PTFE tube as mold for the prototype), the results are not shown. To address this difficulty, in order to truly develop such product, we suggest fabricating a mold based on the device developed by SOHRABI et. al. (SOHRABI et al., 2016).

The thickness can be also controlled by the number of electrospun layers employed, customizing the tubular scaffolds according to injury site and/or the mechanical properties desirable, as it will be discussed further.

The ways to customize electrospun scaffolds fabricated from the technique described here are so extended that, in order to illustrate one (besides the tubular scaffolds in various diameters we produced), a bifurcated tubular scaffold, inspired on the GORE TEX® TPFE vascular grafts commercially available (which are neither biodegradable, nor mimics the native ECM), was easily produced, as it can be seen at Figure 49 (see also https://youtu.be/k7KW-xS_v0w and https://youtu.be/MSeoHkBzG6M). TPFE mandrel of 0.75, 2 and 3 mm were employed as molds for its fabrication. Tejeda-Alejandre et. al. (TEJEDA-ALEJANDRE et al., 2017) proposed an interesting fabrication process for bifurcated vascular graft obtained by electrospinning by using 3D fabricated mandrels in different sizes and shapes. However, the obtained scaffolds are limited in length, and the electrospinning setup requires motors with programmable axis turn. Zhang and Chang (ZHANG; CHANG, 2008) reported a method to produce 3D patterned electrospun tubular scaffolds with tubular, bifurcated, T and cross-shape, with the fascinating feature of controllable porous structures, thanks to the patterning of the mandrels. However, these scaffolds are also limited in length, with is a hindrance for their application as clinically

relevant vascular scaffolds. Here, the prototype of the bifurcated scaffolds produced presents an interesting and clinical relevant length (L'HEUREUX et al., 2006b), which can customizable in any diameter and thickness.

Mostly important, all the scaffolds illustrated on Figure 49 and Figure 51 are patent, and possess elastic recoil. It is worth note, though, the properties discussed are from the hydrated scaffolds, as they will keep hydrated in the organism.

This technique, therefore, offers new prospects to tissue engineers to develop 3D scaffolds from electrospinning. Thus, from these gross analyses, we project the tubular scaffolds produced from the assembly and curing of electrospun pPGS/PVA membranes have the potential to be applied as biodegradable vascular grafts, which can be highly customizable.

Figure 49. Gross images from various tubular scaffolds obtained by assembling and curing of electrospun PGS/PVA membranes. On the top left, a super small diameter (0.75 mm) tubular scaffold. On the top right, a lyophilized scaffold. At the bottom, a bifurcated scaffold obtained from the same technique. Their gross properties can be visualized at the links https://youtu.be/k7KW-xS_v0w and https://youtu.be/MSeoHkBzG6M.

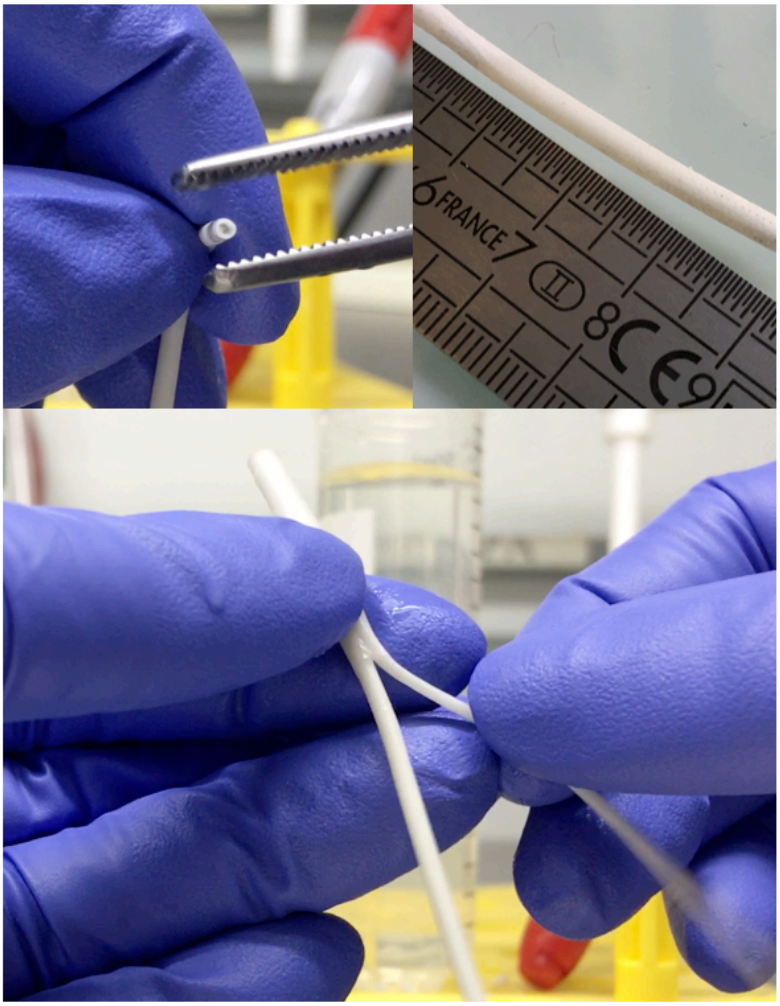

Source: Own authorship

At Figure 52, the abluminal (the external side of the scaffold) and the luminal (the inner side) surfaces of the tubular scaffold, analyzed by Scanning Electron Microscopy are show. From the abluminal side SEM pictures, it is noticed the fibrous architecture and the preserved porosity, typical features for crosslinked electrospun membranes. Conversely, when these pictures are compared with the crosslinked membranes (Figure 45), the fibers of the tubular scaffold surface are more fused. We assume this happened during the scaffold manufacturing, because the fibers were pressed, forcing some of the non-crosslinked PGS to flow outside. Despite this, the overall architecture of the fibers along the external scaffold is preserved, which still mimics the extracellular matrix.

From the luminal side, it is possible to observe a smooth, though porous, surface, in comparison with the abluminal side. The PGS flooded over the TPFE mandrel and was molded and crosslinked according the rod surface. Though we expected to possess equally porous structures from both abluminal and luminal sides of the scaffolds, however, the

smooth surface of the luminal side can be an interesting feature, since the scaffolds are intended to be immediate employed as vascular grafts, the smooth surface on the inner, luminal side can help to prevent turbulent blood flow after the first days from the graft implantation (KOONS et al., 2015).

To confirm the electrospun layers were fused during the fabrication and curing of the tubular PGS/PVA scaffold, the transversal sections of the scaffolds were also analyzed by SEM. At Figure 51, there are illustrated the variety of scaffolds produced, with their diameters, as discussed. At Figure 52, it is magnified a detail of the scaffold wall, where its inner diameter, wall thickness and wall detail are shown. From the wall detail, there are highlighted the layers connections which happened thanks to the pPGS flow and crosslinking during curing. These connections created a unique scaffold from the electrospun membranes stacked. Moreover, the SEM images of the scaffolds transversal section show the inner porosity of the wall, which is crucial for water, physiological signaling and nutrients exchange (HUTMACHER; WOODFIELD; DALTON, 2015).

The SEM images, shown at Figure 53, from a section a tip of a crosslinked and purified tubular scaffold, suggest how the interfacial adhesion between the layers occurs. At the tip of the scaffold, the last layer can be seen because the scaffold manufacturing is manual, them it is natural if a layer shift occurs. Because this is the last layer, and there is no a perpendicular mechanical force from the parallel layers, as occurs at the layers bellow, the last layer tends to conserve the plane form, as how it was electrospun. However, even with this mechanical event, the layers are linked, and one can see the interfacial fibers linking the parallel layers.

Therefore, we have successfully obtained tubular scaffolds from electrospun membranes of bioabsorbable and biodegradable polymers, with an architecture that resembles the native extracellular matrix. Thanks to the employment of the pre-PGS and its ability to stick the layers of the electrospun sheets, these layers were successfully fused during the crosslink of the assembled scaffolds. This allows the free-form fabrication of scaffolds in a diversity of forms, with relevant clinical sizes, for a diversity of applications. Still, as we intended to use these tubular grafts for rapid vascularization in tissue engineering, create porous structures with a relevant porous size that allows endothelial cell migration and anastomosis from the new formed vascular network was the key step.

Figure 50. Abluminal (on the left) and luminal (on the right) surfaces of the assembled and crosslinked tubular PGS/PVA scaffolds obtained from electrospun pPGS/PVA membranes.

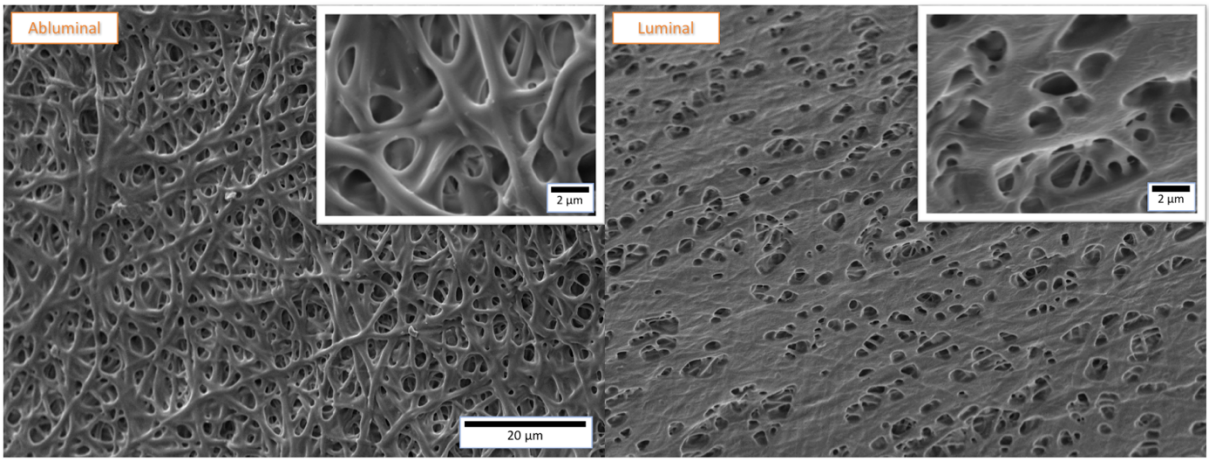

Source: Own authorship.

Figure 51. Transversal cuts of tubular scaffolds obtained from electrospun membranes, with various inner diameters, according to the TPFE rod employed: A. 1.75 mm; B. 1.35 mm; C. 1.12 mm; C; 0.73 mm.

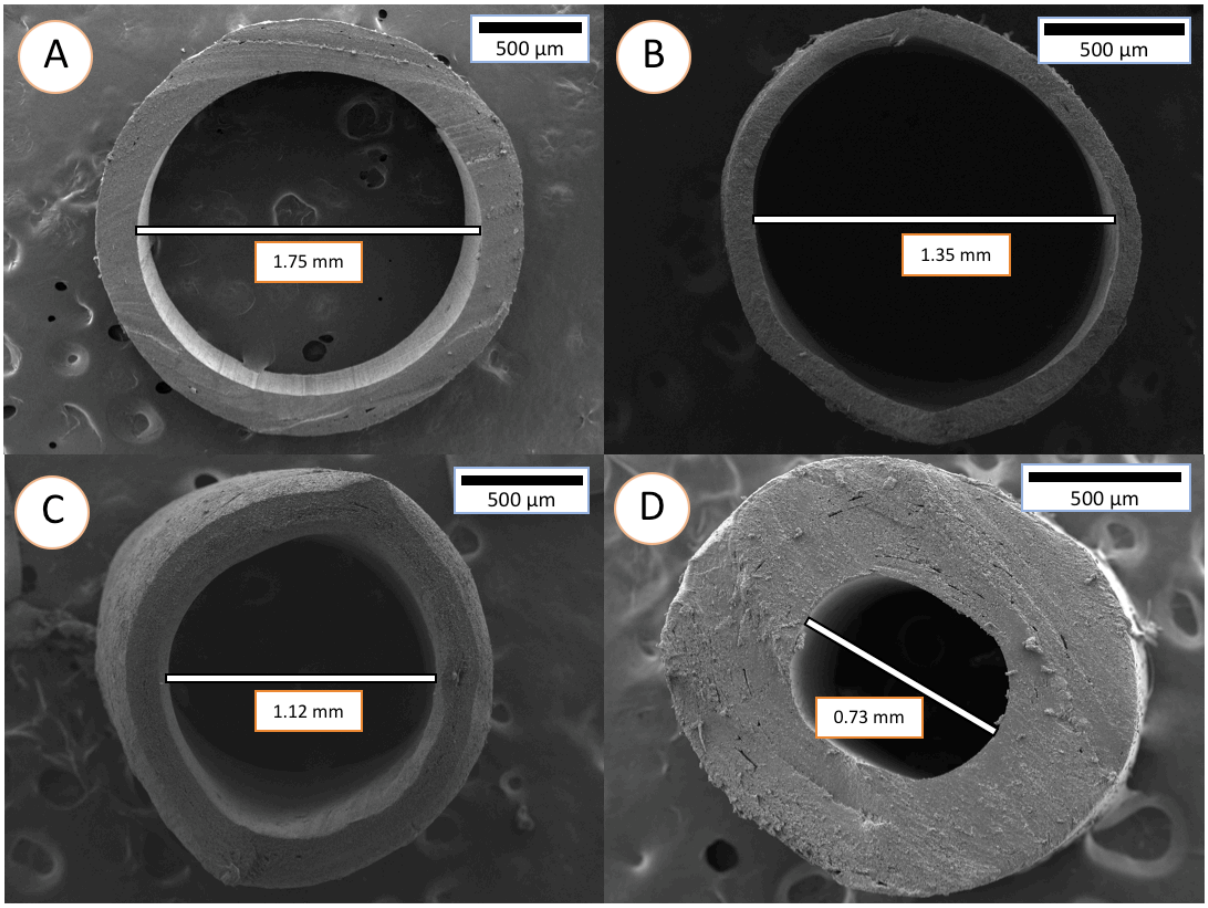

Source: Own authorship.

Figure 52. Wall detail from a transversal cut of a tubular PGS/PVA scaffold, in order to show the inner diameter, the wall thickness and the interlayer connection between the layers, highlighted in red dashed line.

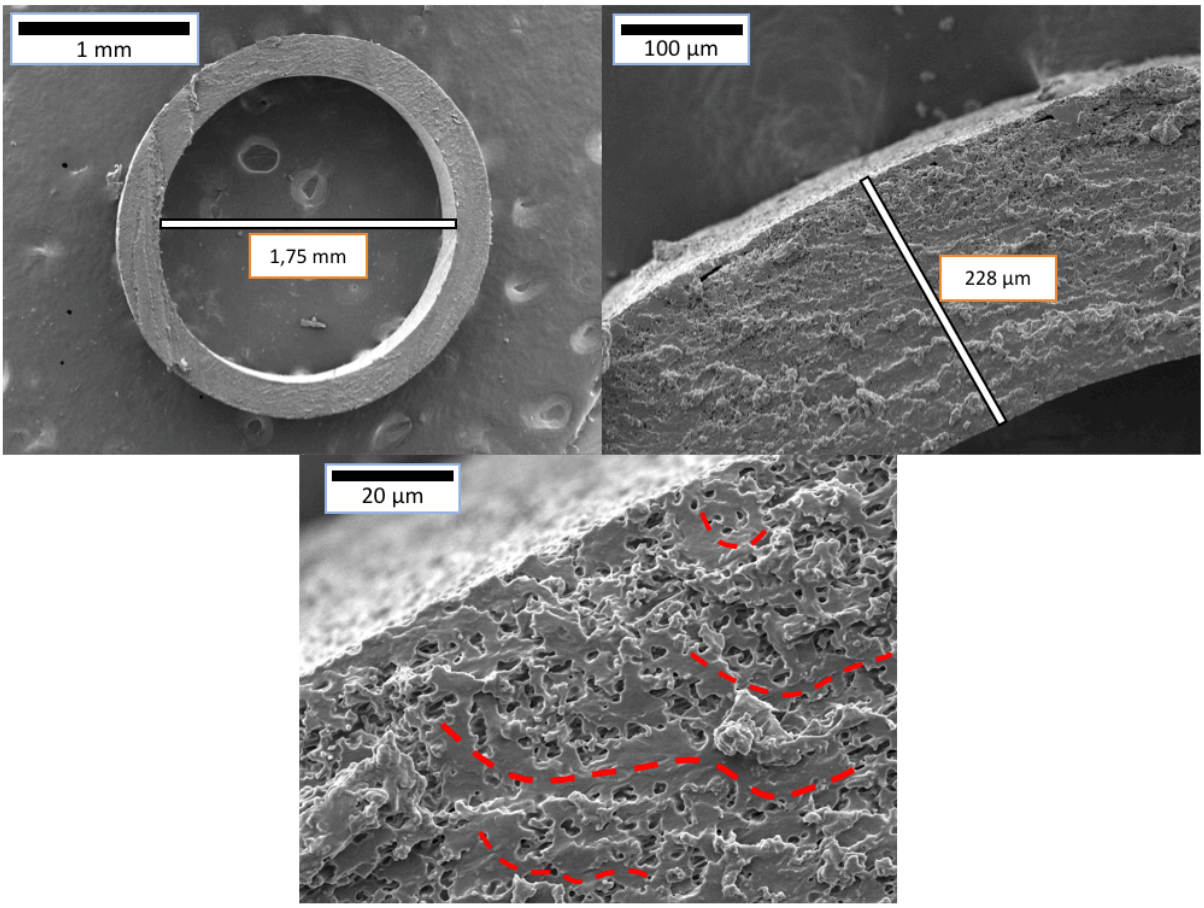

Source: Own authorship.

Figure 53. SEM images of the end section of a crosslink tubular scaffold, evidencing the interlayer adhesion at last electrospun layer of the scaffolds. This region is composed of both loose fibers and, most important, of fibers that are clearly connecting the last and the immediately inferior layer.

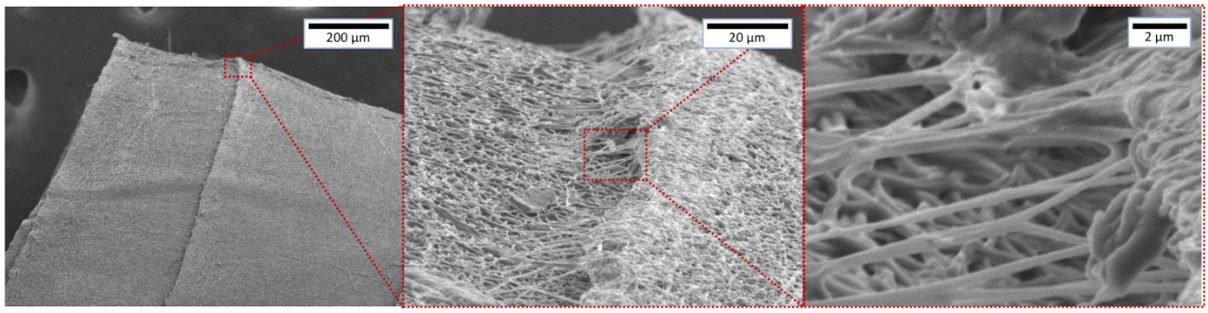

Source: Own authorship.

Delamination Mechanical Testing

Besides the SEM images, layers bonding force is shown at Figure 54. In comparison with the directly electrospun samples, stacked samples did not present significant differences in layer bond ultimate force, being both of around 4mN per mm. Therefore, laminated scaffolds, when properly manufactured, can stand the same forces as the directly electrospun ones. This approach opens new 3D fabrication approaches from electrospun membranes, is extremely simple and possess an enormous potential to 3D form control of electrospun scaffolds and only requires the employment of a material that costs around 1 euro: the parchment paper used to collect the electrospun fibers.

Figure 54. Delamination or layer bonding strength measured by the maximum force/width values from uniaxial tensile mechanical testing for T-peel samples obtained from directly electrospun and stacking layers.

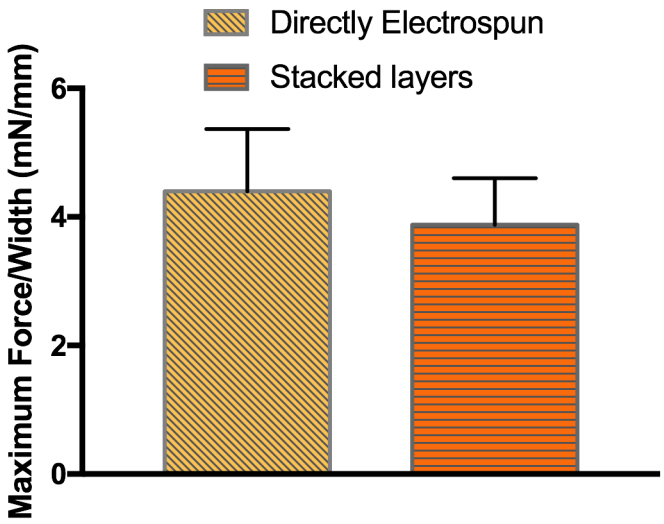

Source: Own authorship.

Femtosecond laser ablation

The gross images at Figure 55, shows the macroscopic aspect of hydrated PGS/PVA tubular scaffolds after laser ablation. From them, a patterned and elastic scaffold that does not tear can be seen. A better visualization of the scaffold elasticity can be seen at https://youtu.be/WltBTDnthIw.

The SEM images at Figure 56, shows a highly structured and patterned tubular scaffold. The porous distances obtained are 0.45 mm for the parallel pores, and 0.6 mm for

the congruent pores (B). For the prototype described in this work, this distance where chosen in order to allow optimal cell infiltration from the scaffolds to the tissue engineering fabricated construct. At Figure 56 (C), there is an overall view of a longitudinal section of the patterned tubular scaffold, where is possible to see the luminal side and it patterned pores. Therefore, both sides possess a patterned structure which can allow, thus, endothelial cell infiltration for rapid vascularization. At Figure 56 (A) and (B), they are illustrated the overall aspect from a transversal section of the patterned scaffold.

The obtained final shape created from the laser ablation is highlighted by a dashed contour at Figure 57 (A). The pore diameter, as shown, is 150µm, which we assume it will allow blood flow and endothelial cell migration, since endothelial cells have $13.2 \pm 4.1 \mu$m width and $25.8 \pm 8.5 \mu$m length (GARIPCAN et al., 2011). We expected to obtain a perfectly circular pore shape, however, for almost all pores, the final pore shape resembles a drop, which may be caused by the laser trajectory over a curved surface. Still, we hypothesize this will not be a constraint for cell migration. From Figure 58 (B), is shown in detail the abluminal surface/pore interface that confirms the laser ablation does not melt the polymer or compromise the architecture of the scaffolds.

A curious characteristic is the pore diameter at the abluminal side is larger (150 µm) than at this end at the luminal surface (130 µm), probably because the laser trajectory in angled, conical, which may also explain why the scaffold pore is a drop-shape. Through the Figure 57 (D), that shows a SEM image from a transversal section of the patterned scaffold, it is evidenced its slightly conical shape. At the same SEM image, it is pointed by arrows some vestiges of polymer that remained after the laser ablation, which may not affect neither the cell migration, nor the overall properties of the patterned tubular scaffolds.

Another interesting feature of the pores is their inner porous structures, as can be seen at Figure 58 (D) which may improve endothelial cell adhesion and migration, since it provides attaching sites for the cells (HOLLISTER, 2005). Moreover, because the laser ablation provides a transversal section view of the obtained scaffolds, one can confirm the preserved inner porosity inside the scaffold, while the electrospun layers are connected Figure 58 (C).

Therefore, the PGS/PVA tubular scaffolds machined by laser possess two major levels of porosity: the micro-porosity allows the nutrients and growth factors exchange (NGADIMAN et al., 2017), while the macro porous allows cell migration (HOLLISTER, 2005; LEE et al., 2012). However, it is worth to questioning how the vascular grafts with the

patterned pores will behave once is connected to the host vasculature in order to allow the angiogenesis inside the fabricated tissue engineering construct? As, for further studies, we will soak these tubular scaffolds in heparin, an anticoagulant that prevents blood coat formation as natural response from the organism at the implant site and also enhances endothelial cell recruitment (SARKAR et al., 2007), we hypothesized that, as the blood flows outside and goes in contact with the external tissue, it will coagulate the pores anyways, but the coagulum formation makes part of the dynamics of angiogenesis (BROWDER; FOLKMAN; PIRIE-SHEPHERD, 2000).

From converging the promising techniques of electrospinning and laser microablation, we successfully produced a porous pattern in tubular fibrous scaffolds, without damaging the fibrous structures of the scaffold. The porous structure will potentially improve the cell migration and angiogenesis from a prospected vascular graft to a biofabricated tissue, enhancing its viability and survival.

Figure 55. Gross images of the tubular scaffolds machined by laser microablation, taken by a camera coupled with a macro lens. A: the overall aspect of the machined tube, with its pores. B: the scaffold stretched.

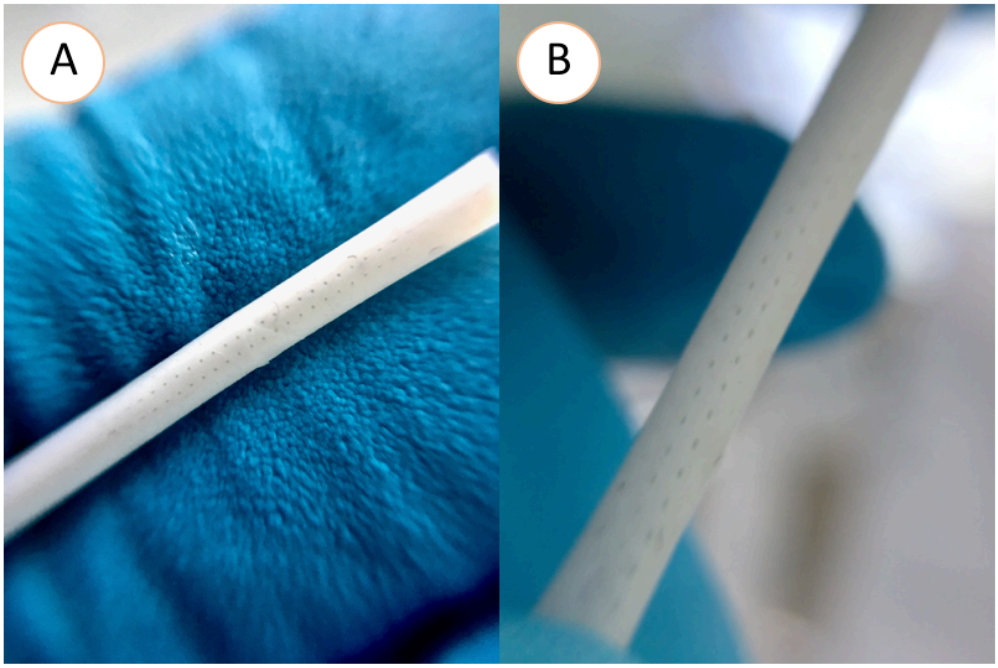

Source: Own authorship.

Figure 56. SEM images of the tubular scaffold processed by laser microablation. A: the scaffold seen by the external (or the abluminal) side. B: The porous distances, where is shown the distance between the opposites porous, in the same line (0.45 mm) and the porous distance in parallel lines, positioned in a congruent angle (0.6

mm). The values shown are approximated.

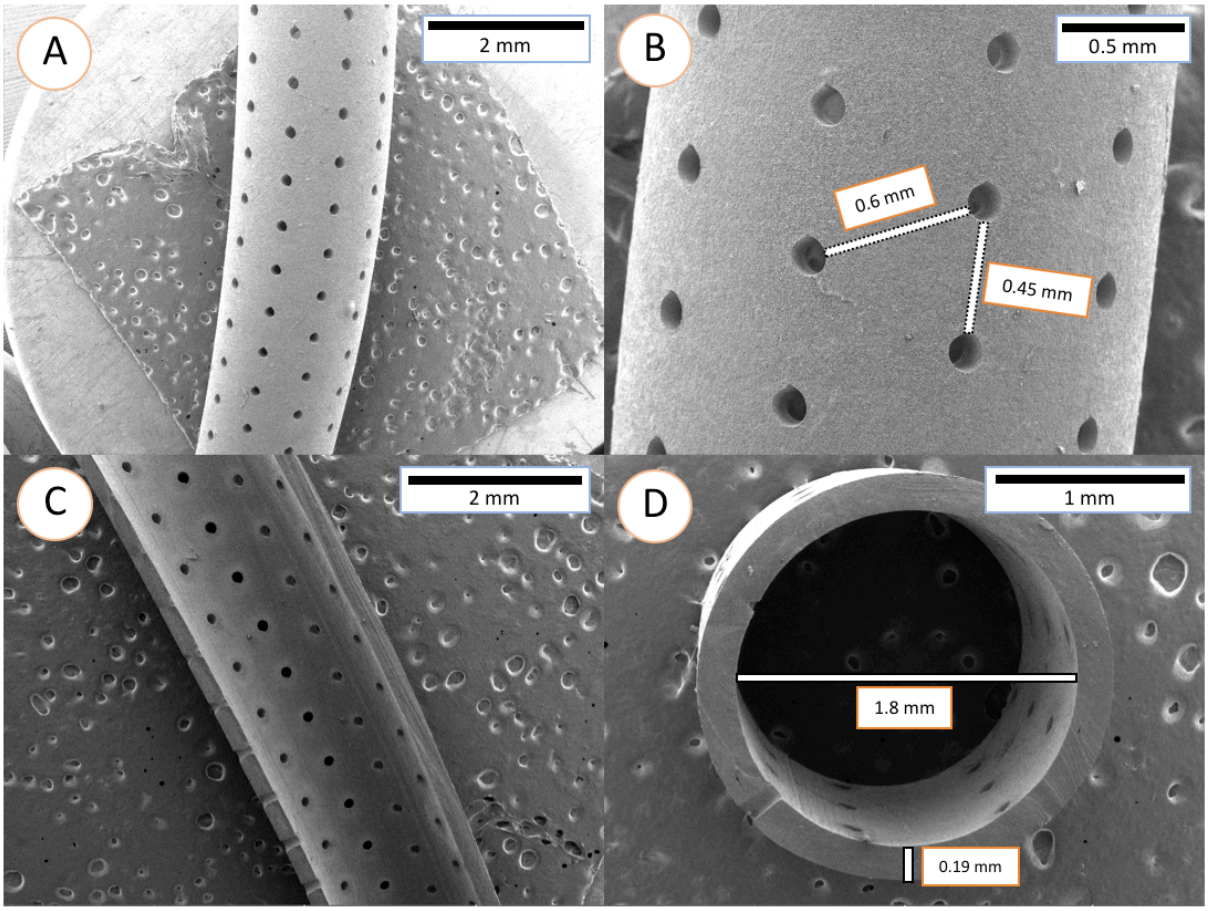

Source: Own authorship.

Figure 57. SEM images of the tubular scaffold processed by laser microablation, evidencing the pores created. The red dotted lines shown the pores shapes. A: the approximated pore size on the abluminal (external) scaffold side, with its shape. B: The pore-surface interface, showing the laser machining does not melt or fuse the polymer. C: The pore on the luminal (internal) surface, and its diameter measure and shape. D: The conical pore form, seen at a transversal section of the tubular scaffold. The arrows indicate some artefacts that may be residual polymers resulted from the laser ablation process.

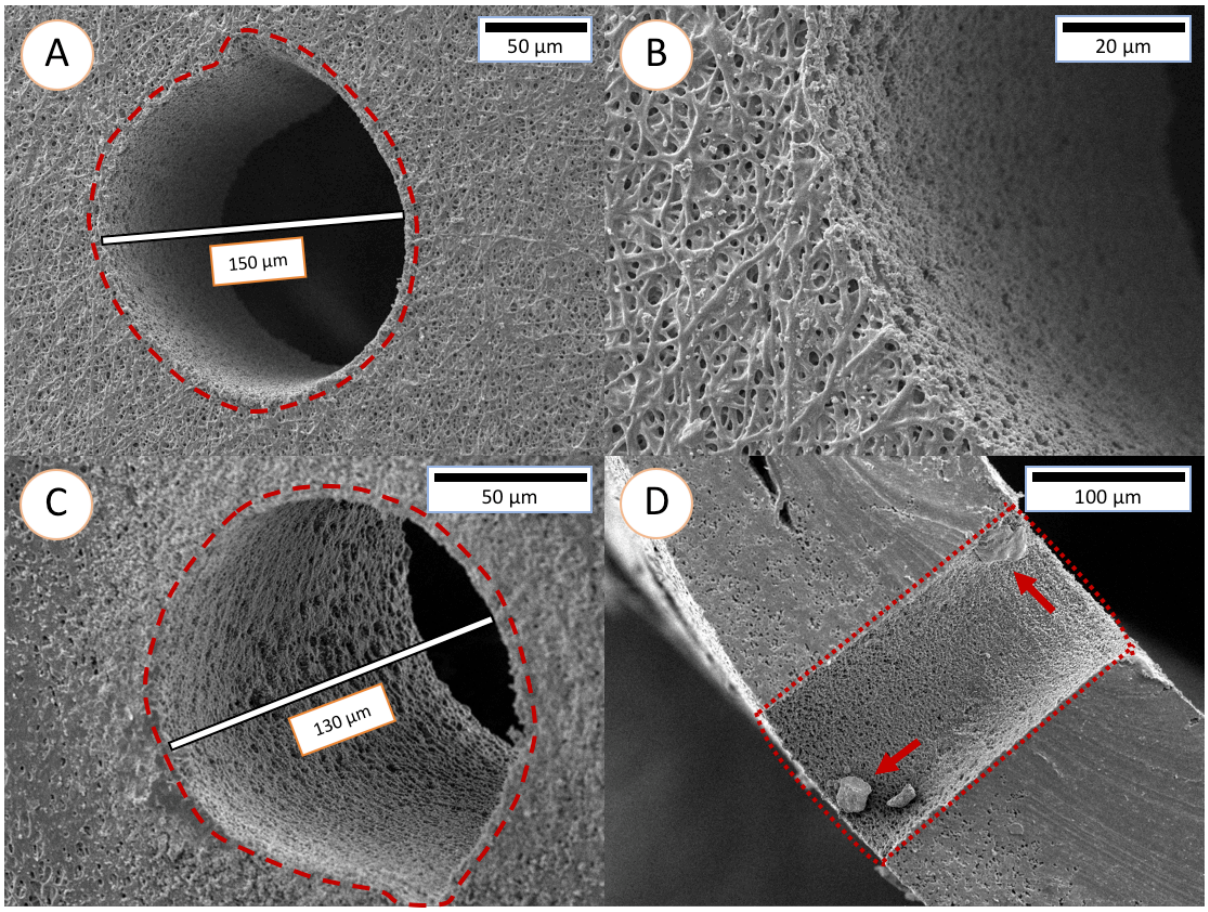

Source: Own authorship.

Figure 58. SEM details from the laser machined tubular scaffolds. A: luminal surface. B: abluminal side. C: transversal section. D: Transversal section of the created pore, which demonstrates the inner porosity of the tubular scaffolds.

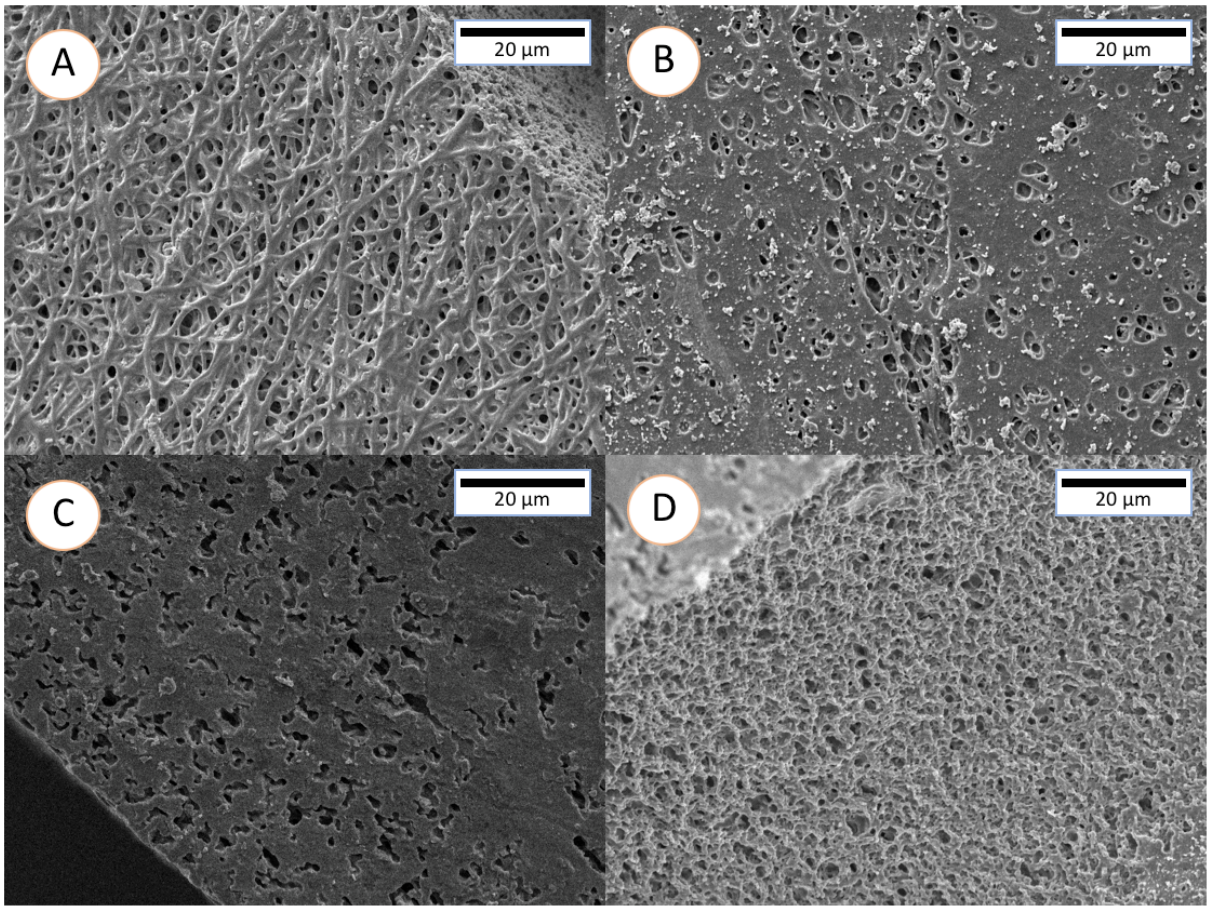

Source: Own authorship.

Thermogravimetric Analysis (TGA)

In order to evaluated the suitability of the PGS/PVA electrospun scaffolds for autoclaving, a widely and accessible sterilization method employed for medical devices, the weight loss characteristic of PGS/PVA scaffolds was evaluated by thermal gravimetric analysis (TGA), which result is show on Figure 59. The material degradation started at 200˚C, and its carbonization begins at around 430˚C. As the autoclave sterilize materials under a vapor temperature of 120˚C, the TGA analysis indicates the scaffolds are, thus, suitable for autoclaving and, then, this was our sterilization method of choice prior to the *in vitro* essays.

Figure 59. Thermogravimetric Analysis (TGA) of PGS/PVA scaffolds, after crosslink and purification.

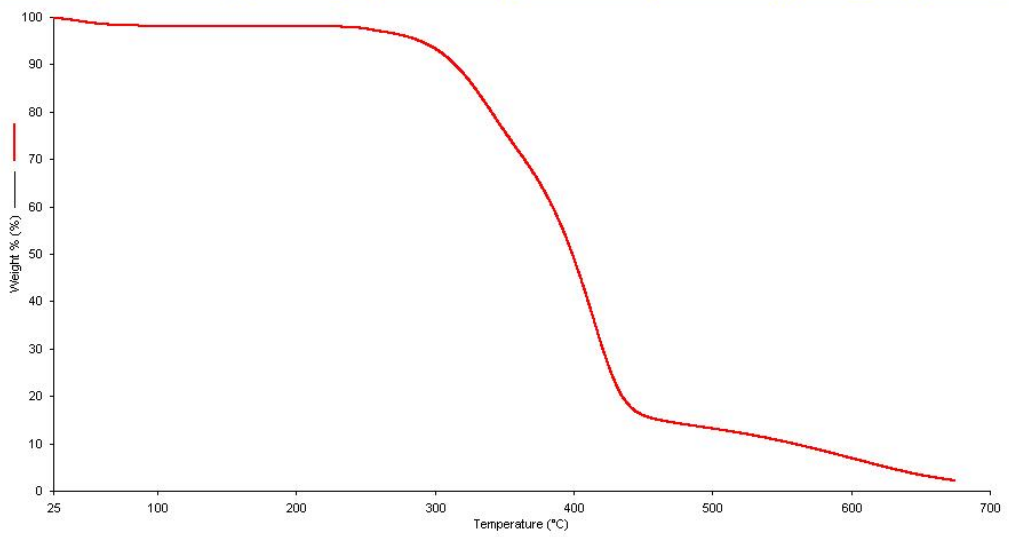

Source: Own authorship.

Mechanical Testing

In order to determine the mechanical properties of the obtained PGS/PVA tubular scaffolds, establish their suturability and verify the scaffold layers bond, comparing different samples and evaluating the influence of the laser ablation processing on these properties, we performed various mechanical testing by uniaxial tensile strength. Non-machined and machined samples did not presented differences regarding their ultimate tensile strain at rupture (Figure 60). All scaffolds are highly elastic, and elongated for more than 100% their original size. The elongation at the rupture of the ablated scaffolds varied from the control scaffold (non-ablated). We believe that the presence of holes changed the stress distribution and thus decreased the strength of the scaffolds. Consequently, the elastic modulus is smaller for the machined scaffolds.

Both non-machined and machined tubular scaffolds shown to be suturable (Figure 61). However, the suturability is smaller for the laser ablated scaffolds. We believe the porous structure facilitated the tearing due to force from the suture. However, the suture retention strength for the machined scaffolds is 4N/mm2. Thus, all scaffold can be employed as suturable vascular grafts. When embedded in fabricated tissue engineering constructs, the machined tubular scaffold can serve as anchor for their proper attachment by suture, while instantly providing a blood flow inside the biofabricated construct.

Figure 60. Mechanical properties of PGS/PVA tubular scaffold submitted to uniaxial tensile testing. Non-machined and machined samples by laser ablation stress (MPa), Young's Modulus (MPa) and sample elongation at rupture (% from the original size sample) results are shown.

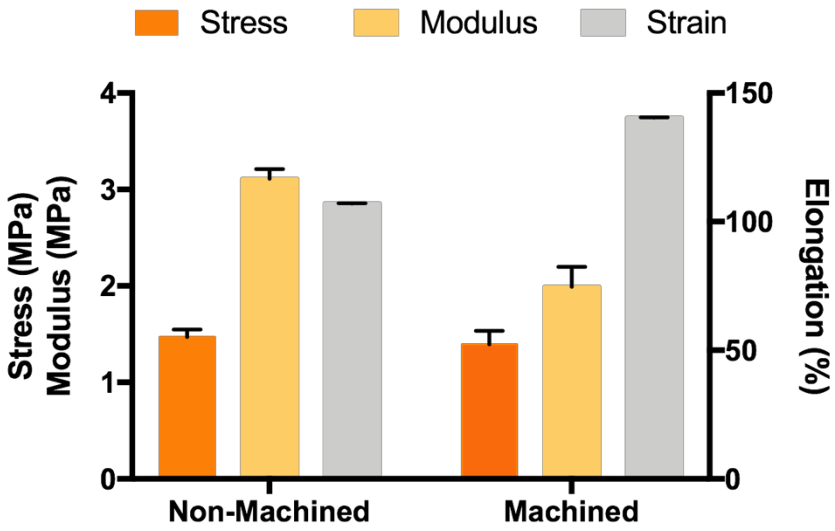

Source: Own authorship.

Figure 61. Suture retention strength of super small (0.75 mm), small (2mm) and small machined (2mm) PGS/PVA tubular grafts.

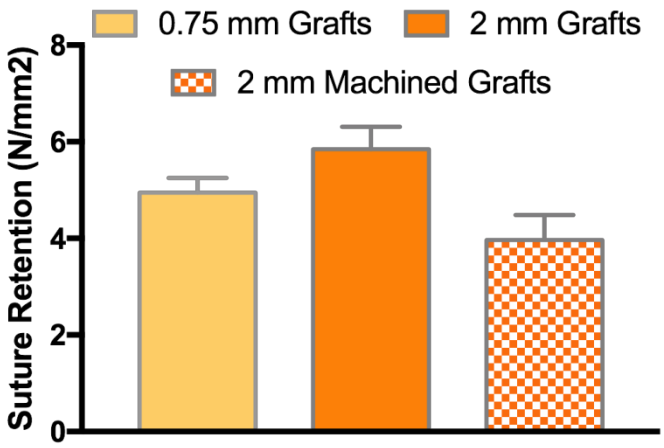

Source: Own authorship.

Scaffold sterilization

After the sterilization of the scaffolds in autoclave at 120˚C and pressure of 3 Bar for 15 minutes, samples were analyzed by scanning electron microscopy. The SEM images at Figure 62 shows the fiber morphology was not affected by the autoclaving sterilization and, thus, it preserves the architecture that mimics the extracellular matrix.

Figure 62. SEM pictures of the abluminal (external) surface of the autoclaved scaffolds, showing the intact

fibrous structure after the autoclaving procedure.

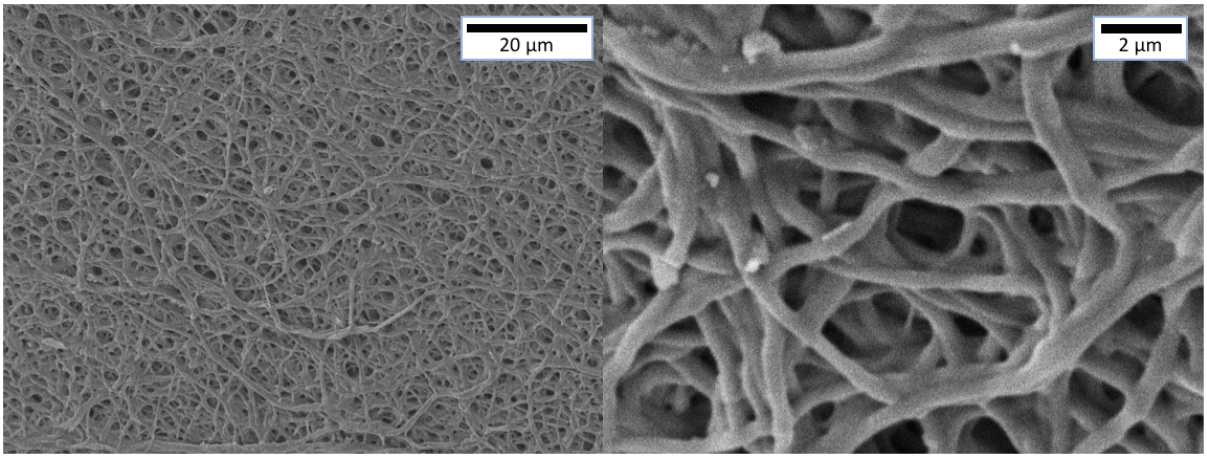

Source: Own authorship.

In vitro analysis

Though the PGS/PVA membranes block the light, at Figure 63, we can see the HUVEC cells proliferated and attached over the PGS membranes because some of the fluorescent light was able to pass. However, the PGS membranes also absorbed the fluorescence (specially the DAPI wavelength), which made the observation difficulty. On

Figure 63 (A), the overall aspect of the PGS membrane on bright field is shown. On

Figure 63 (B), the typical shape of the cytoskeleton of HUVEC cells can be seen thanks to the GFP fluorescent filter reflectance over green phalloidin, that attaches to the F-actin filaments presents on cytoskeleton. The circular shapes are the nuclei stained with DAPI, however, it is harder to be seen than the phalloidin staining due to the fluorescence of PGS. The overlay of

Figure 63 (A) and (B) is illustrated in (C). Therefore, from the epifluorescent images, we can conclude the HUVEC cells attached and proliferated over the PGS membranes, though Scanning Electronic Microscope analyses could be useful to see more clearly the morphology of the HUVEC cells cultured over the membranes.

Figure 63. Optical Microscopy Images: A. Bright field image of PGS membranes cultured with HUVEC cells. The HUVEC cells cannot being seen because the PGS membrane not allow the passage of the bright (white) light. B. The fluorescence could be detected by the microscope camera, and we can visualize the DAPI (lighter blue), phalloidin (green) and the fluorescence reflection of the PGS (darker blue). C. The A&B images merged.

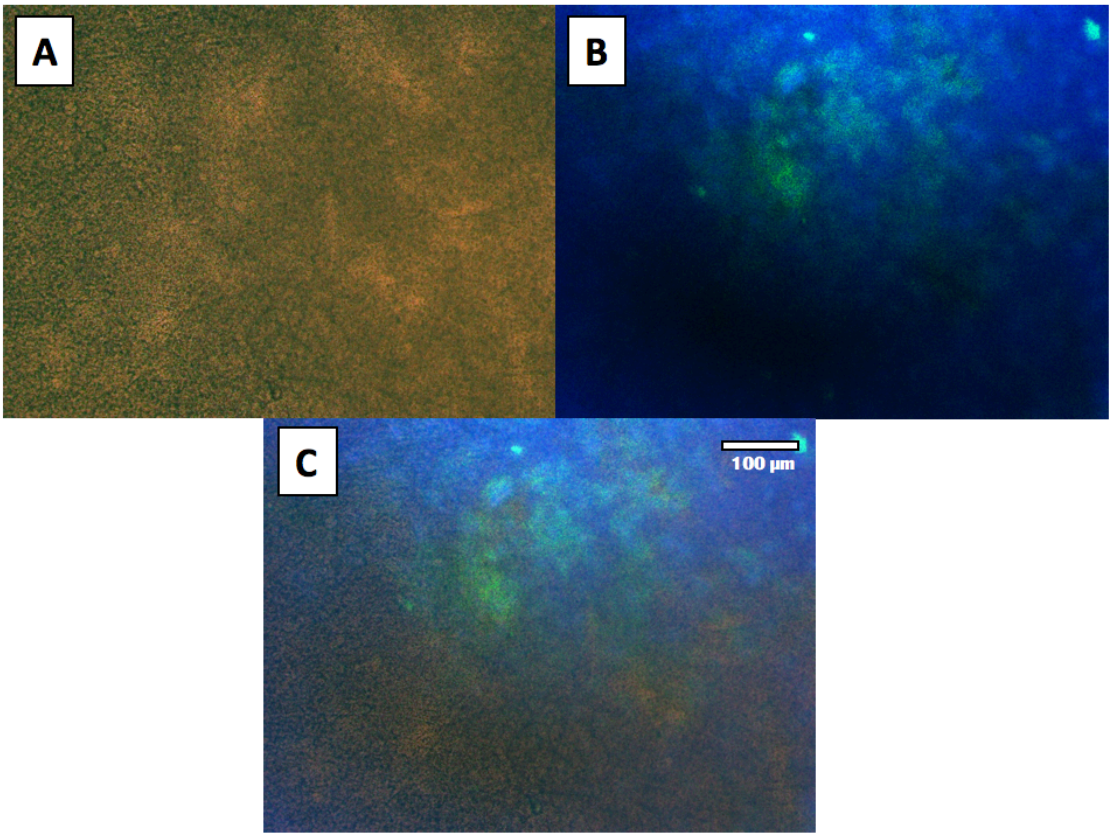

Source: Own authorship.

Cell proliferation/viability

From Figure 64, we can see the HUVECs proliferated over time with both PGS extracts and cell culture media, concluding the PGS does not release armful compounds and, therefore, has no cytotoxic effects, corroborating with the analysis of Jeffries et. al (JEFFRIES et al., 2015). At day 5 from cell seeding, however, the proliferation rate was significantly higher for the PGS extracts than control: the culture was maintained stable, which was expected for both PGS extracts and control, since we started with a relatively high cell density (1 x 10^4 cells/well from a 96-well plate). The causes of this increase in cell proliferation on cells treated with PGS extracts remains unclear. We can hypothesize that, during the extraction production at 37˚C, some PGS was degraded and dissociated into their compounds, which are the glycerol and the acid sebacic. These products are natural metabolites: the glycerol is used as energetic subtract by cells (ALBERTS et al., 2013), and probably the HUVECs took advantage from it. If this assumption is correct, the glycerol release from PGS scaffolds can be beneficial for cell proliferation and remodeling of the biodegradable PGS vascular graft, though this hypothesis must be verified by deeper investigations at molecular level.

At the day 7, once the HUVEC cells filled the well, it was expected the cell culture stabilized because of the limited space of the well. The HUVECs in control media continued to proliferate and reached a similar proliferation in comparison with the PGS extracts.

Figure 64. Resazurin cell viability essay for the HUVEC proliferation with PGS extracts and the control (cell culture media) with their respective error bars. The higher the relative fluorescence, the bigger the number of viable cells. *n<0.01.

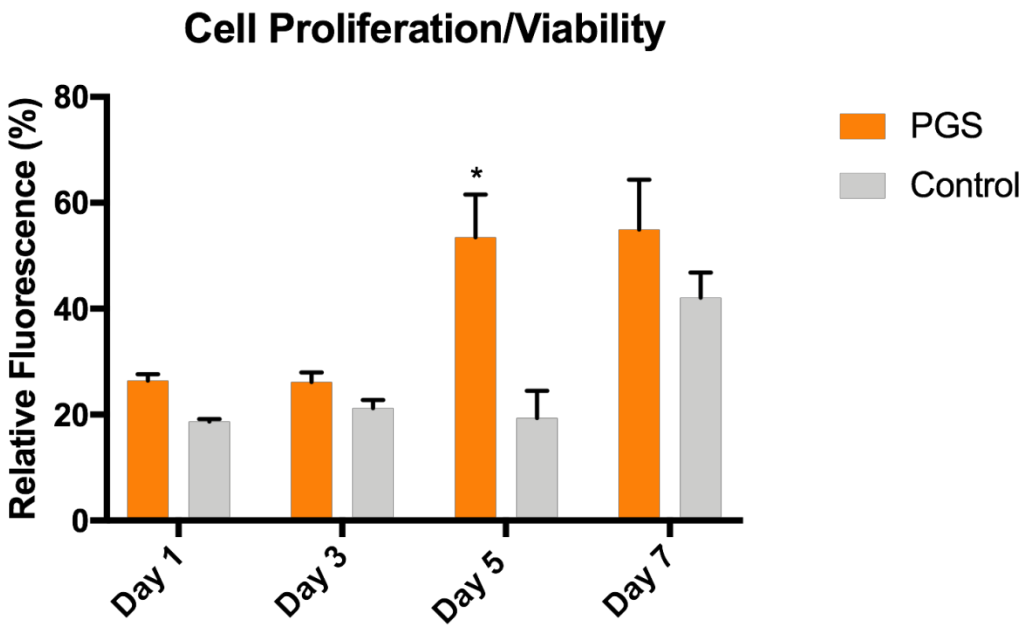

Source: Own authorship.

3D culture

Cell culture remarks for the 3D constructs experiments

All experiments were performed with EBM-2 media with exogenous growth factors (bullet kit EGM-2: hEGF, Hydrocortisone, VEGF, hFGF-B, R3, -IGF-1, ascorbic Acid, heparin) because these are *in vitro* models of what we can expect to happen inside the host organism, since the insertion of foreign construction can lead to inflammatory responses and the consequent secretion of exogenous growth factors (ALBERTS et al., 2013). Moreover, we not intend to investigate the VEGF paracrine signaling role of MG-63/HUVECs at this moment, because, thought is important to further understand the mechanisms of vascular network formation in general, this is not the aim of this project, but it can be for future projects.

Previously from the seeding, MG-63 osteoblasts were maintained in EBM-2 + bullet kit media because we wanted to verify if the MG-63 would survive in the same media of endothelial cells. After confirming by observations at microscopy the osteoblasts survived and proliferate on the habitual rates when cultured in DMEM media, which was checked by the frequency of the passages, after at least 4 passages, we proceed with the MG-63/HUVEC co-culture system with the EBM-2 culture media.

As one of the hypotheses of this work is that the porous structure created on the fibrous PGS/PVA scaffolds allows the endothelialization from the scaffold in a context of a rapid vascularization of a bone construct, and we aim to investigate preliminary the interaction with osteoblasts and endothelial cells thanks to the endothelial cell migration, we employed osteoblast-like MG-63 cells and HUVEC cells as osteoblasts and endothelial cells, respectively. MG-63 is derived from a malignant tumor and possess osteoblastic features (CLOVER; GOWEN, 1994), often employed for studies with different materials and it is a stable, immortal lineage, which is positive features for its use for *in vitro* essays (MASTERS, 2000). HUVEC cells are widely employed as angiogenesis model for vascularization *in vitro* (GOODWIN, 2007).

After the 3D co-culture settings, we employed periods of essay between 48h and 72h because, according to our prior co-culture observations, there is no 3D structures formation prior to 48h, and most of the formed structures fell apart after 72h, due to the *in vitro* environment, with limited space and limited in comparison with an *in vitro* model (ALBERTS et al., 2013; ARNAOUTOVA et al., 2009; GOODWIN, 2007). However, for some conditions, we report some results with 120 hours to see how the osteoblast/HUVEC interaction can affect the resilience of these structures.

For the treatment of the fluorescent images, microscopy pictures with no filter, yellow filter, then from the cells and/or structures stained with the fluorophores DAPI for the nuclei, and phalloidin for the f-actin (for the cytoskeleton) were taken. The images were superimposed as illustrated on the Figure 65, in order to obtain final microscopy images evidencing the structures stained (the nuclei and the cytoskeleton) and also with the contrast provided by the filter and no filter pictures.

Figure 65. Schematic of fluorescent images assembly, from the plate co-culture (2D) of HUVEC (endothelial cells) and MG-63 (osteoblasts). First, it was generated an image from the superimposition of a light picture with no filter, and one with a yellow filter (in order to create color contrast) from the specimen. Then, the fluorescent images from the nuclei, stained by DAPI, and from the F-actin, stained by phalloidin (Alexa Fluor) were

superimposed. Finally, the light and the fluorescent images were superimposed, obtaining the final pictures employed. It is worth note there is some difficulty in obtain fluorescent 2D microscopy images from fluorescent 3D structures, which were overlaid into a unique fluorescent signal in most of the cases. Thus, the superimposition of the fluorescent images and the white light images helped to define those 3D structures.

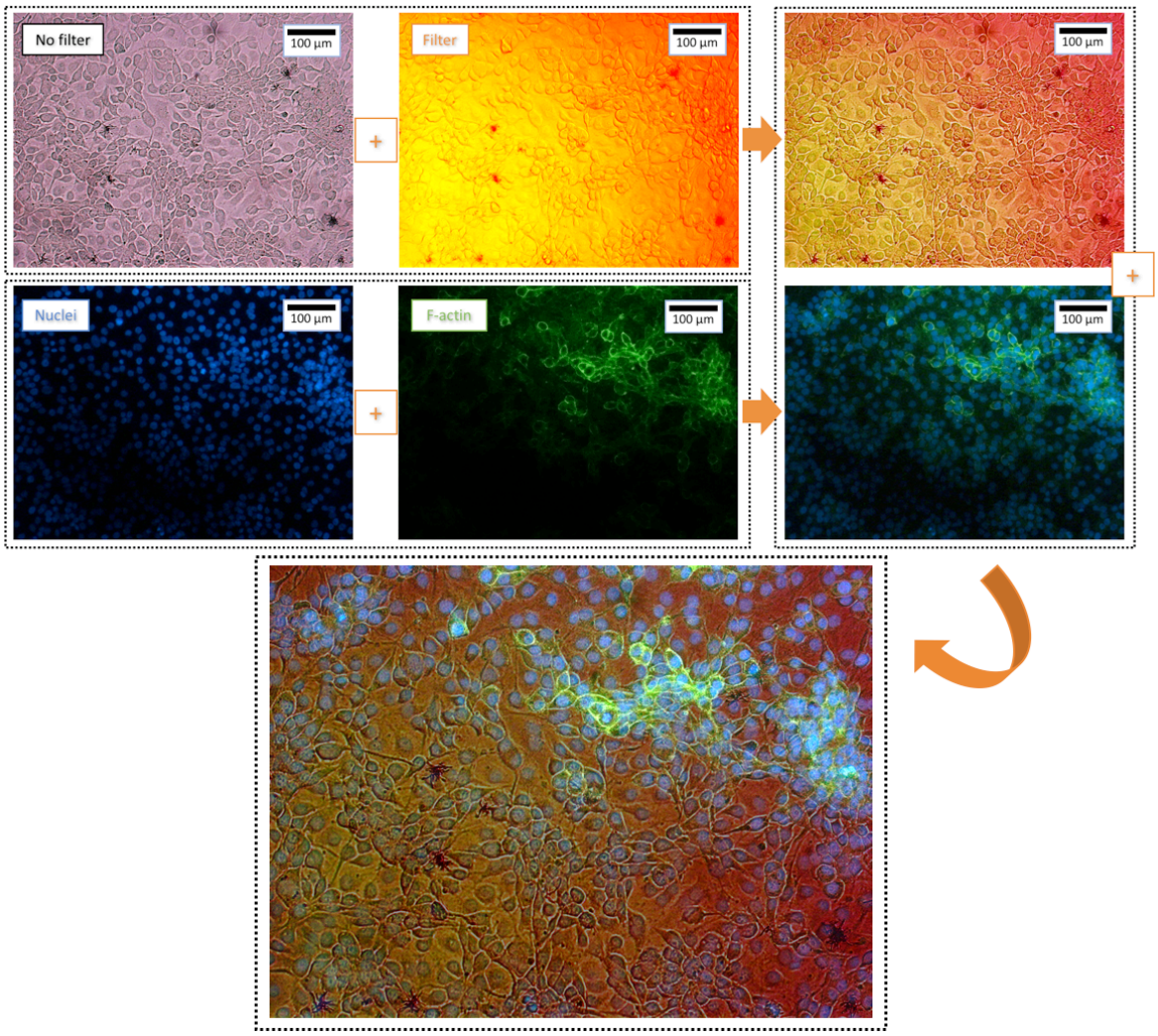

Source: Own authorship.

3D culture in GelMA

As we first intended to visualize and understand the *in vitro* behavior of the HUVEC (endothelial) and the MG-63 (osteoblasts-like) cultured in GelMA, so we could predict their behavior with the tubular scaffolds embedded in GelMA, HUVECs and MG-63 were 3D cultured on the scaffold-free GelMA. After 2 days of cell culture, HUVECs formed the typical tubular structure (ARNAOUTOVA et al., 2009) seen at Figure 66 (A), while the MG-63 were organized in spheroids (GRIGORE et al., 2014), as seen at Figure 66 (B). However, when in 3D co-culture, the HUVEC and MG-63 associated together in clusters Figure 66 (C),

interconnected by tubules Figure 66 (D), which corroborates with the works of Aguirre et. al. (BERTHIAUME; MAGUIRE; YARMUSH, 2011) and Fuchs et. al. (FUCHS; HOFMANN; KIRKPATRICK, 2007): the presence of MG-63 seems to influence the HUVEC cluster formation. Moreover, according to Shi et. al. (SHI et al., 2014), the MG-63 play a positive role in HUVEC cells proliferation. It can be observed tubule formation within the HUVECs clusters indicated by arrows at Figure 66 (D), which increases the cellular crosstalk within the HUVEC clusters. Interesting, the same elongated structures were not observed at the HUVEC monocultures on GelMA (Figure 66 (A)). Thus, when co-cultured in 3D GelMA hydrogels, HUVECs and MG-63 will assembly into particular 3D structures thanks to their synergistic crosstalk and interaction, and this behavior was expected when both cells lineages were co-cultured by the dynamic seeding with the tubular scaffold/GelMA system.

Figure 66. 3D culture in GelMA construct of: A. HUVEC cells, with their characteristic tubule formation; B. MG-63 osteoblasts-like, forming circular colonies; C. HUVEC + MG-63 co-cultures, with the association of colonies + tubular formation; D. Image from the dashed area in C, evidencing the tubular structure which connects the cell colonies. Images taken 2 days after cell seeding.

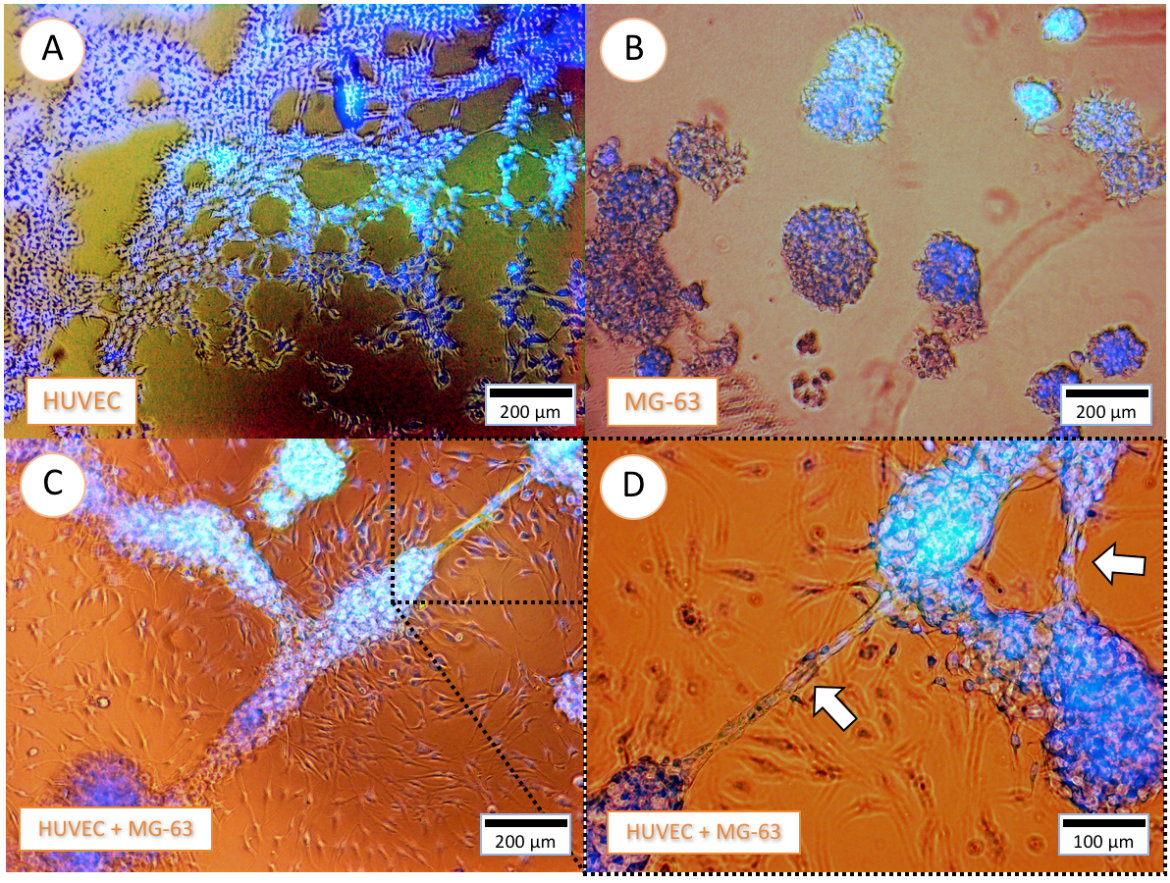

Source: Own authorship.

Dynamic seeding onto tubular scaffolds/GelMA 3D constructs

HUVEC 3D culture in porous tubular scaffolds

As we created relatively large porous by laser machining on the tubular electrospun scaffolds, allowing endothelial cell migration for rapid vascularization, we performed a dynamic seeding on the PGS-PVA scaffold/GelMA 3D construct with HUVEC only, in order to simulate the endothelial cells migration delivered through blood and to confirm the HUVEC migration over the GelMA. Moreover, the migration behavior of the HUVEC cells seeded from the porous tubular scaffold may not be the same as observed when directly cultured on the free, hydrogel surface. HUVECs were seeded inside the porous tubular scaffolds regarding the required cell amount ($2x10^4$) suspended in 15 µl of EBM-2 + bullet kit media. The cells were allowed to adhere for 30 minutes, then the wells with the 3D constructs were completed with culture media.

Even if suspended in a small quantity of cell culture media, from the gross observations of the Figure 67, we suppose HUVEC suspension immediately leaked outside the tubular structure due to capillaries created within the machined porous on the tubular scaffolds, prior to a cell migration. Therefore, the HUVEC cells successfully flowed through the scaffolds, corroborating our hypothesis of rapid vascularization from the electrospun porous scaffolds.

After 24 hours of cell culture, HUVECs spread on the external GelMA surface (Figure 67 (A)), then moved and accumulated together into cell clusters, with no particular structure, different of that observed from the culture on GelMA only (Figure 66(A)). Thus, this is the behavior we expected when seeding the HUVECs from the tubular porous scaffolds into the osteoblasts (MG-63) gradient at the external side of the tubular scaffold/GelMA construct.

Figure 67. 3D construct from the association of the PGS/PVA tubular scaffolds (with pores) and GelMA, seeded with HUVECs. The scaffolds lumen was seeded with HUVECs, which colonized the external side of the GelMA by passing through the pores of the scaffolds. A. Constructs after 24 hours of HUVECs seeding. B. After 48 hours of HUVEC seeding, the HUVEC cells moved and aggregated into clusters.

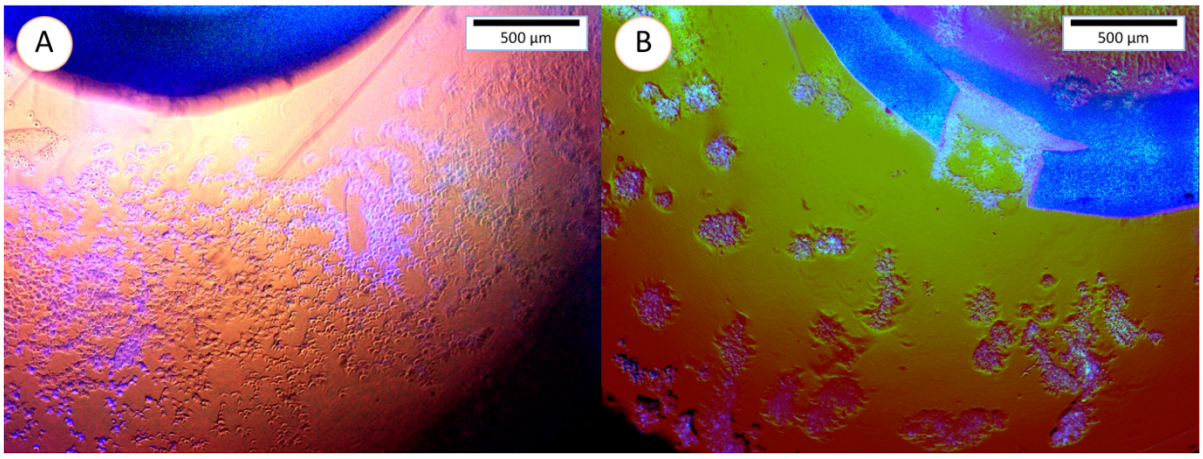

Source: Own authorship.

Dynamic co-culture of Endothelial cells/Osteoblasts in tubular scaffolds/GelMA 3D constructs: Tubular scaffolds with no laser-ablated pores

Due to the absence of pores, HUVECs remains stuck inside the tubular scaffold, as can be checked at Figure 68 (A). Inside the scaffold, the HUVECs formed some tubes (highlighted square in Figure 68 (A), amplified at Figure 68 (C)), however, due to high cell density (equally employed for all experiments), the cells preferably aggregated into large structures over capillaries (ARNAOUTOVA et al., 2009) into the scaffold lumen. At the external side of the scaffold region, over the hydrogel, it remains the MG-63 (highlighted in Figure 68 (B), which is magnified at Figure 68 (C)) aggregated into clusters with no particular structure, as observed in Figure 66 (B), for the MG-63 3D culture in scaffold-free GelMA construct. Therefore, because there are no pores to allow the endothelial cells flow/migration towards the external side of the 3D construct, where remains the osteoblasts, no interaction within these two cell types were observed. These observations emphasize the essential characteristic of the pores created in these tubular scaffolds: when a scaffold with no porous which would allow cell migration, there will may not have endothelialization/vascularization in a period which is crucial for the implant survival (ROUWKEMA; KHADEMHOSSEINI, 2016).

Figure 68. 3D construct from the association of the PGS/PVA tubular scaffolds (without pores) and GelMA. The inner (luminal) side of the scaffold (A) was seeded with HUVECs, while the exterior (B) was seeded with MG-63. At the luminal side, it can be observed tubule-like structures (C), while at the exterior it can be notice colonies with no particular shape or structure (D). Imagens taken after 48 hours of cell seeding.

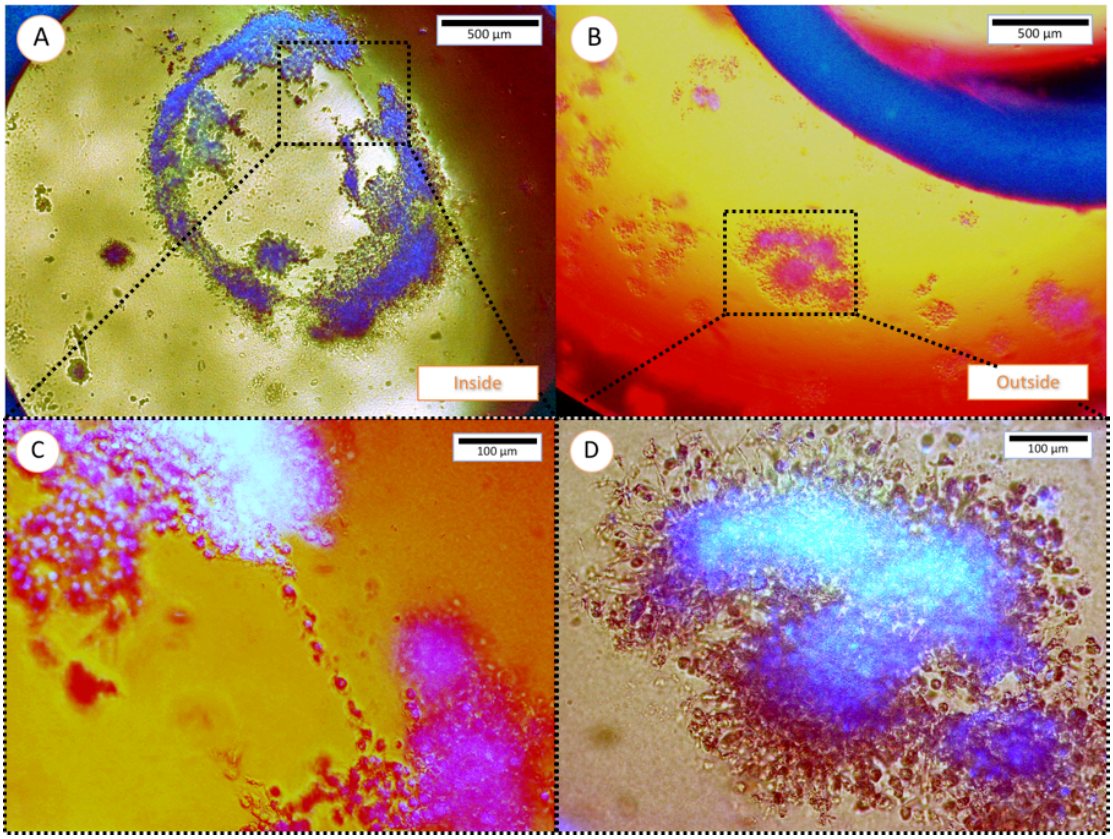

Source: Own authorship.

Dynamic co-culture of Endothelial cells/Osteoblasts in tubular scaffolds/GelMA 3D constructs: Tubular scaffolds with laser-ablated pores

When the scaffold possesses pores that allows the endothelial cell to flow, these cells can permeate the external surface of the hydrogel and, then, interact with the osteoblasts at the external side, as can be seen at Figure 69. Close cell–cell contacts could be observed, suggesting the formation of specialized unions (Figure 69 (B)). At the same figure, anastomosis within HUVECs/MG-63 clusters and the graft can be observed. This is the key point the rapid vascularization: to provide an instant endothelial/blood cells into the biofabricated constructs in host, while promoting the anastomosis of the new capillary network formed.

Though this is a preliminary study regarding the *in vitro* endothelialization of 3D constructs, this rapid vascularization *in vitro* model shows the be simple and effective. Although the constructs were not stained with specific HUVEC and/or mg-63 markers, we can localize the cells type by their morphology: HUVEC are cuboid cells which organizes in clusters, while MG-63 are spindle-like cells (HOFMANN et al., 2008; PAUTKE et al., 2004; SHI et al., 2014).

From the Figure 69 (B), we can observe the MG-63 (spindle-like cells) around the HUVECs cluster. Differently from the Figure 68, we can easily identify the MG-63 by their characteristic shape (PAUTKE et al., 2004) because, when around the HUVEC cluster, they sprout. The same phenomena can be observed at the Figure 66. Endothelial cells are known to secret osteogenic growth factors which enhance the survival and the proliferation of osteoblasts (VILLARS et al., 2000). Osteoblasts, on the other hand, secrets VEGF in enough quantities to increase the cell proliferation and survival of endothelial cells (FURUMATSU et al., 2003). Moreover, it has been reported that not only growth factors, but also direct contact with endothelial cells, has a positive effect on the alkaline phosphatase activity of osteoblasts (STAHL et al., 2004). This complex crosstalk occurs in a complex way in the organism, with hundreds of cell types regulating each other in harmony (ALBERTS et al., 2013). The importance to reproduce these crosstalks on *in vitro* models leads to an increasing in the employment of co-culture systems (KIRKPATRICK et al., 1997). Besides, this vascular network can later serve as template for ossification, which happens thanks to the synergistic interactions between osteoblasts and endothelial cells (VATTIKUTI; TOWLER, 2004).

It is also worthy to point out that, in the lumen of the scaffolds, we can find some clusters associations of HUVECs/MG-63, though less developed than at the external side. Inevitably, during the MG-63 seeding, some cells can also get in into the lumen through the porous. In order to avoid this association, for further studies, we suggest to bioprint the bone construct from the association of GelMA and osteoblasts, embedding the tubular scaffold inside the structure and perfuse the endothelial cells by through a bioreactor.

It is likely probable the permeability of the vascular grafts allows the crosstalk of cell-secreted growth factors from MG-63 and HUVECs which stimulates the cell migrations, while the created microporous allows these cell flows/migrations. The 3D implants biofabricated with osteoblasts may improve the host vasculature, while the presence of the vascular network will increase the bone formation in a dynamic effect (KANG et al., 2013b; NGUYEN et al., 2012a). Although more research at the molecular lever (i.e. Polymerase Chain Reverse Transcription, or PCR-rt) is necessary to better understand how these crosstalk works and, thus, help to predict what will happen once the constructs were sutured into the host. This preliminary study already indicates the electrospun scaffolds architecture is ideal to permit this crosstalk, at the same time they clearly allow endothelial cell migration, which will later form vascular networks that will benefit the vascularization of the bone constructs, as other tissue engineering constructs too. Therefore, this work is an enormous step into the clinical translation of 3D biofabricated tissue constructs.

Figure 69. Images of the 3D construct from the association of the PGS/PVA tubular scaffolds (with pores) and GelMA, taken after 48 hours of cell seeding. The inner (luminal) side of the scaffold was seeded with HUVECs, while the exterior was seeded with MG-63. A. 3D structures formed from the scaffold due to the interaction with HUVECs and MG-63 cells, which happens thanks to the scaffolds pores that allows this interaction. At the left side, the osteoblasts (MG-63)/endothelial cells, formed from the tubular scaffolds, are highlighted on the right side. B. External side of the construct, evidencing the external 3D HUVEC/MG-63 structures (on the left side), where their interactions are shown on the right side.

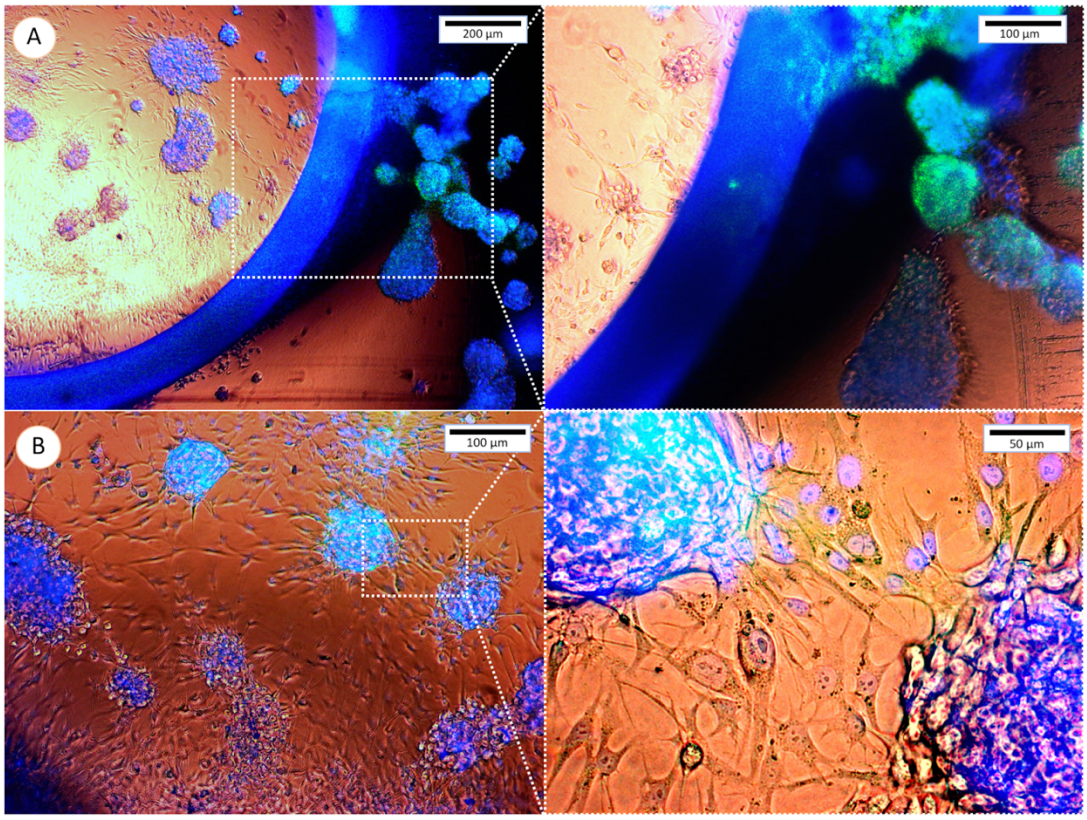

Source: Own authorship.

We maintained the tubular porous scaffold/GelMA construct with HUVECS/MG-63 in culture for 120 hours. Normally, *in vitro* 3D cultures of HUVECs tend to fall apart after 48 hours (ARNAOUTOVA et al., 2009, p. 20) as can be seen at Figure 67 and, usually, the studies regarding angiogenesis are not carried for beyond 24 hours (ARNAOUTOVA; KLEINMAN, 2010; GOODWIN, 2007). However, as can be seen at the Figure 70, the structure created from the HUVECs and MG-63 (highlighted by the dotted square) resisted for a longer time than when these cell lineages were cultured separately, which we hypothesize it was due to synergistic effect from the association of these lineages, as discussed.

Therefore, the vascularization is essential for the tissue engineering construct survival, as already outline by hundreds of research in tissue engineering (ALMUBARAK et al., 2016; GOMES et al., 2017; NOVOSEL; KLEINHANS; KLUGER, 2011; PELLEGATA; TEDESCHI; DE COPPI, 2018; ROUWKEMA; KHADEMHOSSEINI, 2016).

Through our strategy, we expect to successfully embed these tubular scaffolds and provide a suturable and permeable vascular anchor that will provide an instant blood which will enhance the biofabricated implant survival and will accelerate the clinical translation of tissue engineering.

Figure 70. Images of the 3D construct from the association of the PGS/PVA tubular scaffolds (with pores) and GelMA, taken after 120 hours of HUVECs and MG-63 osteoblasts-like seeding. The 3D structure from the interactions of the endothelial cells and the osteoblasts is highlighted.

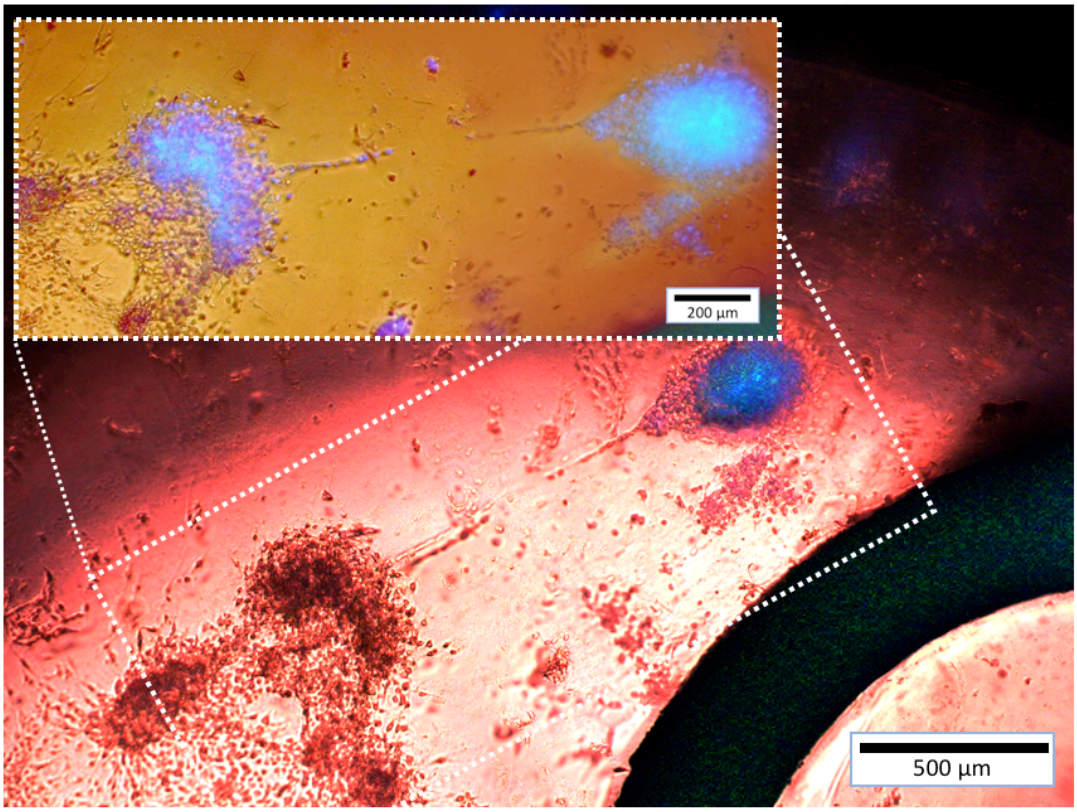

Source: Own authorship.

CONCLUSION

In order to provide an instantaneous blood supply to larger biofabricated bone constructs, we developed a new strategy based on the concept of pre-vascularization of biofabricated tissue-like constructs, employing a vascular graft strong enough to be directly

anastomosed with the host vascular networking, and porous, for vascular branching into the construct. As biomaterial, we chose the Poly (Glycerol Sebacate), a fast degrading elastomer that can remodeled into a new blood vessel. The pPGS (pre-polymer of PGS) was synthesized and coupled with Poly (Vinyl Alcohol) (PVA). As a result of the technic for fabrication of electrospun developed, it is possible to produce tubular scaffolds of various diameters, as small as 0.5 mm, diverse shapes – i.e. bifurcated, with relevant lengths (>10 cm). Thanks to the employment of the pPGS, the subsequent curing of the polymer fuses different layers of electrospun mats, which allows to employ virtually 100% of the collected fibers. The obtained tubular scaffolds have a homogenous, porous morphology that mimics the native extracellular matrix.

The post-processing of the obtained tubular scaffolds by laser ablation shows to be a relatively simple and versatile technique to create a pattern of defined pin holes of 150μm of diameter each, without fusing the fibers or damaging the scaffolds. Laser ablated and non-ablated tubular scaffolds were elastic, resistant to axial forces and suturable, as demonstrated by tensile mechanical testing. Therefore, both tubular scaffolds can be employed as biodegradable vascular grafts.

The resulting scaffolds are also autoclavable. *In vitro* analyses provided data that shows endothelial cells can attach and proliferate over PGS/PVA membranes, and no toxicity *in vitro* was found. Endothelial cells seeded inside the obtained tubular scaffolds embedded in GelMA hydrogels were able to flow and interact with the 3D culture of osteoblasts, thanks to the porous patterning fabricated over the scaffolds, creating novel 3D structures from endothelial cells/osteoblasts interaction, with improved survival of these structures in comparison with the endothelial cells and osteoblasts structures when isolated by a non-porous scaffold. This is the key-point of vascularization in bone tissue engineering, which is to improve the implant size and survivor, thanks to a positive effect in cell proliferation and survival from the interaction of osteoblasts/endothelial cells and to the potential deliver of nutrients and oxygen to the fabricated implants. Therefore, this work is an enormous step into the clinical translation of 3D biofabricated bone tissue constructs. Through our strategy, we expect to successfully embed these tubular scaffolds and provide a suturable and permeable vascular anchor that will provide an instant blood flow to the biofabricated tissue, which may enhance the biofabricated implant survival.

FUTURE PERSPECTIVES FROM THIS WORK

The objective of the first part of this work was to produce biodegradable membranes for bone tissue engineering and guided bone regeneration with improved mechanic properties, in order to better support the bone regeneration of bone defects. We employed cellulose nanocrystals as natural reinforcement to avoid possible toxic effects and the PCL as biodegradable polymer matrix, and synthesized nanocomposites from cellulose nanocrystals (CNC) and PCL. These CNC composites can potentially reinforce numerous biodegradable polymers and blends, as we previously demonstrate, in a work in collaboration with SIMÃO and BRANCIFORTI with Poly (butylene succinate-co-adipate)(PBSA) films reinforced with PCL-grafted cellulose nanocrystals (SIMÃO; BELLANI; BRANCIFORTI, 2017). Thus, this work shows the potential of PCL-grafted CNCs to be employed as non-toxic reinforcement phase of tissue engineering scaffolds manufactured by different fabrication techniques. As example, these bionanocomposites can be also applied as reinforcement in additive manufacturing, as we are, currently, collaborating with the Technology Information Center "Renato Archer", Campinas, SP, Brazil.

For the second part of the present work, we aimed to add a bioactive phase in the CNC-reinforced PCL electrospun membranes produced at the previous part, in order to potentially improve the bone formation on site. We produced novel bioactive and biodegradable composites from Biosilicate® and PCL, in order to improve the compatibility within the osteogenic phase and the polymeric phase. These achieved results highlight the potential of these membranes for guided bone regeneration and also for bone tissue engineering. Moreover, the obtained biocomposites can reinforce another biomaterials and scaffolds for bone regeneration, with improved mechanical properties and osteoconductivity. In order to complement the obtained results, the bioactivity of the membranes can be assessed by testing in simulated body fluid (SBF) and determinations of biomineralization at molecular level, optimizing the Biosilicate and CNC rate according to the application. The next phase of this work is the clinical translation of these membranes and, thus, an indispensable step will be the *in vivo* assessment of these membranes in critical bone defect models.

At the third part of this thesis, we aimed to develop vascularization strategies in bone tissue engineering, in order to improve the size and survival of tissue engineered constructs. GelMA-CNC nanocomposites were developed as reinforcement for cell-laden GelMA, to tune their mechanical properties while keeping the colloidal phase, essential for cell sprouting, of these hydrogels. An essential next step of this work is the assessment of

mechanical properties of the GelMA-CNC hydrogels, in order to stablish a correlation between the CNC rate and mechanical properties for, following, tuning the mechanical properties of these hydrogels according to the different tissues. A quite interesting application of these hydrogels is the emerging technique of 4D bioprinting: because the CNC has a high content of hydroxyl groups all over its surface, and can be self-oriented in aqueous environment. Employing advanced bioprinting, which is already available, it can be printed hydrogels with oriented CNC segments interlaced with non-oriented CNC segments. Once these 3D printed constructs are submerged in aqueous media, the oriented segments can interact with each other, creating a 4D shape.

Finally, we aimed to improve the concept of rapid vascularization in 3D biofabrication previously developed. Biodegradable and suturable scaffolds, with various diameters and shapes, were designed and manufactured, with improved porosity through post-processing by laser ablation. The suturable scaffolds were embedded inside GelMA biofabricated constructs, and the porous pattern assisted endothelial cell migration towards the bone-like structures. Through our strategy, we expect to successfully embed these tubular scaffolds and provide a suturable and permeable vascular anchor that will provide an instant blood which will enhance the biofabricated implant survival and will accelerate the clinical translation of bone tissue engineering.

As further steps, we propose to assess the gene expression of osteoblasts and endothelial cells of molecular markers of cell proliferation and mineralization, in order to understand how the resulting interaction from the cells can improve the vascularization and bone formation. Immunofluorescence with specific cells markers for endothelial cells and osteoblast and observation at confocal microscopy are essential in order to distinguish and visualize where each cell type is placed and how they interact and anastomose from the 3D GelMA to the vascular graft, by visualizing all the construct in a 3D manner. Another required step is to soak these tubular scaffolds in heparin, an anticoagulant that prevents blood coat formation as natural response from the organism at the implant site and also enhances endothelial cell recruitment. Finally, a further assessment that must be carried from this work, in order to clinical translate the pre-vascularized bone grafts produced here, is the *in vivo* assessment. Thanks to the small diameter suturable grafts produced, the animal model of choice can be smaller, being required less space and structures for the *in vivo* testing.

Though the possibilities we discussed in this work was related to bone tissue engineering and regeneration, it is undeniable the potential of these suturable grafts to treat

vascular diseases: currently, vascular diseases are the primary cause of dead, and a considerable number of these deaths could be avoided by employing the proper materials. The most employed vascular grafts for vascular bypass are made of TPFE, that does not degrade and are not remodeled into a new graft. For example, vascular bypass in children may require more than one surgery along its life in order to change the graft as they grow. Thus, by developing and employing the PGS suturable grafts, the comfort and the life expectation of these children can be improved. As product development step, we also propose the manufacturing of longer grafts. From this thesis, we only fabricated prototypes for testing, but it is possible to produce longer grafts by assembling and fusing various layers, as demonstrated. Then, the surgeon can cut and employ these grafts according to the injury site. Another suggestion is to submit the vascular grafts in association with cells into bioreactors, resulting in more mature vascular grafts. Also, it is possible to take more advantages of the laser ablation processing to create, besides porous, grooves that can enhance smooth cells proliferation, in order to create pulsatile vessels (arteries). Other interesting employment of these grafts is to simulate the epithelium in lab-on-chip technologies, in order to produce devices that requires the simulated blood flow. Finally, because all organs are interlaced with blood vessels, these suturable scaffolds can be employed for rapid vascularization in a variety of tissues, accelerating the clinical translation of many other tissues biofabricated.

GENERAL ABSTRACT AND RESEARCH TRAJECTORY (ENGLISH)

Bone tissue regeneration is still an important challenge in orthopedics and traumatology. Despite the natural ability of bone repair, a trauma beyond the critical limit (critical fracture) cannot be regenerated. Due to many traumas and pathologies, and rise in the ageing population worldwide, there is an increasing need for new treatments for patients with musculoskeletal diseases as evidenced by bone being the next most transplanted tissue after blood. Autologous bone graft, the most commonly used procedure for reconstruction of defects and bone fractures, has various disadvantages, such as limited availability, graft loss or resorption, short-term instability in the case of large areas affected, complications associated with the second surgery, and failure rates exceeding 50% in sites of difficult consolidation. Although many artificial prosthetic devices are available, few can completely replace all complex biological functions. Currently, the idea of reconstruction of laboratory-created organs and tissues is widely disseminated and investigated worldwide. As a multidisciplinary science in regenerative medicine, these studies involve knowledge in the fields of biology, health sciences, engineering and materials science.

Tissue Engineering is a multidisciplinary field that applies the principles of engineering and biological sciences to the development of biological substitutes that restore, maintain or improve the tissue function or of an organ as a whole. The development of tissue engineering is based on the *in vitro* culture of scaffolds associated progenitor bone cells, which must mimic the extracellular matrix (ECM), forming a suitable medium or microenvironment for the cells to organize into structures functionally similar to the tissue. In this context, the aim of bone tissue engineering is to create clinically relevant grafts that can be used therapeutically. An essential component in tissue engineering is the development of porous 3D structures - scaffolds - that will provide to the cells the necessary support to guide bone formation.

There are many physical and biological properties that an ideal scaffold for bone tissue engineering needs to possess, among them: a porous matrix with interconnected pores and surface suitable for cell growth and proliferation and transport of nutrients and metabolic waste; reabsorption rate and remodeling synchronized with osteogenic activity, with the production of only metabolically acceptable substances; mechanical properties appropriate to those of the host tissue by means of a concise and stable material-tissue interface which must persist during the time of resorption of the implant; have no risk of rejection or reaction of the immune system by foreign body; and have good adaptation with the host tissue environment.

Many materials and fabrication techniques have been investigated. however, despite significant advances in the area, the development of synthetic structures capable of fully sustaining the capacity for bone regeneration and self-remodeling is still a major challenge. Only the manufacturing process of the scaffold itself is not enough to manufacture an ideal scaffold. In this sense, nanotechnology may provide some characteristics to project the internal surfaces of the scaffolds. In this context, one objective of this work was to produce poly (caprolactone) (PCL) membranes for bone tissue engineering and guided bone regeneration by electrospinning. The electrospinning process allows to produce nanofibrous membranes with structural similarity with the native extracellular matrix. PCL is biodegradable semi-crystalline approved by the Food and Drug Administration (FDA). However, some challenges regarding the mechanical properties of PCL, as its brittleness, in order to extended the use of PCL as bone tissue engineering material, need to be resolved.

First, the cellulose nanocrystals (CNC) were investigated as reinforcement phase because they are natural, low-cost and biocompatible, with excellent mechanical properties. Nevertheless, the most important drawback related to the use of cellulose nanocrystals for polymer nanocomposites is their inherent difficulty to disperse in non-polar medium, because of their polar surface. Thus, in order to create a PCL interface to improve the compatibility of the reinforcement and the polymer phase, the PCL was graft-from the CNC by ring-opening. This procedure was executed in partnership with the Institute of Polymers and Chemistry for the Energy, Environment and Health (ICPEES), in collaboration with Dr. Guy Schlatter and Dr. Luc Avérous, at Strasbourg, France. It was investigated how different ratios of CNC can affect the thermomechanical properties of PCL electrospun membranes in to stablish a relation between the reinforcement ratio and the mechanical properties improvements in order to tune these properties according to tissue site and/or application. Homogeneous electrospun mats of bionanocomposites formed of PCL with PCL-grafted CNC were produced. There was a significant increase in the melting temperature and in the crystallization temperature of the electrospun PCL nanofibers with the addition of the grafted CNC. Also, an increase in the degree of crystallinity of the PCL mats with the addition of the grafted CNC indicated that a good compatibility between the matrix and the filler occurred. The incorporation of the PCL-grafted CNC, even in small amounts, increased considerably the mechanical properties of the nanofiber mats, with significant improvements in the Young's modulus and the tension at break. Therefore, it becomes clear the potential use of cellulose nanocrystals as a reinforcement phase in electrospun PCL mats, and the mechanical properties can be tuned according to the CNC ratio.

Second, as we aimed to develop biodegradable membranes for guided bone regeneration, after overcome the issue with the mechanical properties of the PCL electrospun membranes, we needed to improve the osteogenicity of the membranes, in order to stimulate bone formation at the host site. To accomplish this, I needed to add a bioactive phase in the PCL mats. After some investigation, it was found that Biosilicate®, a glass ceramic, presents an excellent bioactivity. Studies had shown Biosilicate® significantly improved the osteoblasts proliferation *in vitro* and osteoconduction *in vivo* and is currently being applied in medical and dental areas. Besides, because Biosilicate® is a ceramic glass system, it presents superior mechanical properties compared to hydroxyapatite. Thus, the CNC would confer improved mechanical properties, while the Biosilicate® would provide a bioactive on biodegradable PCL membranes. This work was also performed together with the ICPEES. However, as for the CNC, we needed to perform the PCL graft-from on Biosilicate® in order to improve the compatibility of the Biosilicate® with the polymeric phase and, therefore, improve the dispersion and mechanical adhesion in the composite interface.

Biosilicate®, as received, had a particle size distribution ranging from 25 to 54μm, which is considerably larger than the nanofiber mats diameter (0,637 μm). Then, we performed a Biosilicate® milling in order to decrease the particle size range from 0.2 to 8μm), with the largest particle distributions around 2.33μm and 2μm (about 14% of the particles for both diameters). Following, the Biosilicate® grafting was performed, as for the CNCs. Because, to the date, this is the first time the PCL grafting from Biosilicate® is reported, we had to perform a deeper investigation of the obtained particles. Transmission Electronic Microscopy (TEM) with X-Ray diffraction analysis had shown that PCL-Biosilicate® composites were successfully fabricated. FT-IR spectra demonstrated that the typical of Si-O-Si type bonds to Biosilicate® were no longer accessible to IR radiation, indicating that the surface was functionalized and, thus, there was polymerization of PCL from Biosilicate®. The PCL grafting-from CNC was also performed and confirmed by FT-IR spectra. These composites were then successfully dispersed into PCL matrix, and electrospun PCL + CNC + Biosilicate were manufactured. Their morphology was evaluated by Scanning Electron Microscopy (SEM). The micrographs revealed homogeneous, bead-free nanofibers for all scaffolds, though It could be also observed the formation of structures where the PCL-grafted Biosilicate® (BioSiO-g-PCL) larger particles were inserted. Therefore, the grafting with PCL was fundamental to improve the dispersion of both CNC and Biosilicate® PCL biocomposites in the PCL membranes. Regarding the mechanical properties, the Young's modulus and the stress at break of the PCL electrospun mats increased when the PCL-grafted CNC was added.

The same effect was observed for the BioSiO-g-PCL composites. Moreover, when both CNC and Biosilicate were employed together, the Young's Modulus increased three times in comparison with the neat PCL membranes, and doubled in comparison with the CNC-g-PCL (the PCL-grafted CNCs) ones. These findings highlight the importance to improve the compatibility of the matrix-particles in nanocomposites in order to proper predict and tune their mechanical properties. Again, because these membranes were developed for bone regeneration, *in vitro* essays were performed. Cell proliferation essays with human osteoblasts-like MG-63 cultured on the samples PCL, PCL + CNC, PCL + Biosilicate® and PCL + CNC + BioSiO showed increasing proliferation throughout the time of analysis. There were no significant differences in osteoblasts proliferation in comparison with the control and the with the different samples along the essay. Therefore, from the cell viability essays, we concluded all samples were biocompatible, support cell proliferation, and thus do not show *in vitro* toxicity. From fluorescent images, it was possible to visualize that MG-63 cultured on composite electrospun membranes. MG-63 were able to proliferate and attach over all samples during the period of essay. Osteoblasts cultured on PCL + Biosilicate® samples shown increased nuclei size and orientation in comparison with other samples. The same effect was not observed at samples with CNC + Biosilicate®, which it was attributed to the smaller fibers diameter effect, which lead to a smaller projected area available for cells to binding and spread (smaller pore size effect). Biomineralization essays performed for osteoblasts cultured for 21 days overs the mats shown mineral deposits in red over all the membranes, and thus, we could conclude all the membranes supports *in vitro* mineralization. However, quantitative analysis seems to be necessary in order to stablish a correlation between the composites and the biomineralization *in vitro* to further predict the *in vivo* mineralization and, thus, the bone formation. Therefore, all the obtained PCL/CNC/Biosilicate composites possessed improved mechanical properties, supports osteoblasts proliferation and biomineralization *in vitro*, and they can be potentially employed as membranes for guided bone regeneration. Moreover, the obtained CNC-g-PCL and the Biosilicate®-g-PCL composites developed can be further employed as reinforcement fillers in other fabrication approaches for scaffolds for bone tissue engineering, as additive manufacturing (3D printing), citing, as example, a parallel project in collaboration with Renato Archer Information Technology Center (CTI, acronym in Portuguese), Brazil.

However, despite all the advances in materials, fabrication and cell manipulation techniques, to date, bone tissue engineering constructs still not possess a clinically relevant size in order to be applied to regenerate critical size bone defects. Vascularization remains the

principle obstacle that impedes the translation of most bone tissue engineered constructs to clinical practice. Thus, if we aimed to develop potential new technologies for bone tissue engineering, we had to learn how to improve these constructs/materials, regarding learning and developing new techniques. Currently, bioengineering studies of vascular networks have been widely used employing natural hydrogel scaffolds. Several microfabrication techniques lead to the creation of vascular capillaries from Gelatin Methacrylate (GelMA), which consists of a biocompatible hydrogel platform, capable of interacting with and encapsulating cells during photopolymerization, allowing tissue formation in three dimensions. GelMA mechanical properties can be tailored according to the tissue and application target by increasing the time of photopolymerization, density and chemistry of the crosslinks and the concentration, and molecular weight of the precursors. However, highly cross-linked 3D hydrogel environments that have high stiffnesses will provide limited cell proliferation, migration, and morphogenesis. Therefore, a method that enhances the mechanical properties of hydrogels without affecting their beneficial properties is needed for advanced engineered tissue constructs. Because we hypothesized cellulose nanocrystals (CNC) could be easily incorporated in GelMA hydrogels, since the polar nature of both hydrogel and CNC, we aimed to produce GelMA-CNC hybrids in order to modify the mechanical properties of hydrogels without affecting their beneficial properties for cell sprout (the liquid phase of GelMA). CNC can be used as anchors sites for cells to spread, while maintaining a soft environment that allow the cells to spread and proliferate. Them, GelMA-CNC hydrogels were developed in partnership with the Harvard-MIT Health Sciences and Technologies and the Brigham's and Women Hospital, at Boston, MA, United States, in collaboration with Dr. Ali Khademhosseini. However, due to the presence of gelatin, nanocrystals precipitated in the matrixes, resulting in agglomeration of the nanoparticles. In order to improve the dispersion of the CNC, the CNC was methacrylated with the gelatin, resulting in the production of GelMA-CNC hybrid composites. Human Umbilical Vein Endothelial Cells (HUVEC) were successfully encapsulated with these hydrogels, they sprout and formed the typical HUVEC tubules structures, in a 3D manner. Though the GelMA-CNC showed to be potential composites for vascular network microfabrication, which can be employed in advanced techniques for microfabrication of blood vessels, the main question regarding this approach is how to connect this delicate vascular network into the host tissue, in order to provide an instantaneous blood perfusion inside the 3D engineered constructs?

Then, we had been presented to the concept of embedding a more resistant tubular scaffold inside the GelMA hydrogels. The idea was to provide a suturable biodegradable

anchor site inside the GelMA that could be directly anastomosed with the blood system of the host. As microfabrication technique to produce the vascular scaffold, we chose Electrospinning, which is widely employed to produce tubular scaffold with an architecture that mimics the native extracellular matrix of blood vessels. Moreover, by using a fast-degrading elastomer, the poly (glycerol sebacate), or PGS, the suturable graft could be remodeled into a new artery. However, since electrospinning creates a dense fibers network, we needed to improve cell migration and vascularization from the suturable graft, by employing the concept of laser ablating the obtained electrospun tubular grafts, in order to create a capillary network from the vascular graft that can potentially anastomosis with the new formed/fabricated capillary network at GelMA constructs. PGS electrospinning is challenge, because it is insoluble. Thus, it is required the employment of the pPGS. However, due to short molecular chains of the pPGS, it does not form enough molecular entanglements to form fibers and, thus, it requires the use of carrier polymers. The lab group proposed to employ the PCL as carrier polymer. We had obtained some electrospun pPGS/PCL tubes by directly electrospinning over gelatin-coated mandrels, connected to a motor. However, obtaining tubular scaffolds from this approach was challenging due to many reasons: the diameter of the tubular scaffold it is limited by the diameter of the mandrel, which cannot be too small, or there will not possess an enough surface charge to attract the fibers; because the pPGS has a glass transition temperature below the room temperature, it is required its crosslink into PGS. However, the PCL melting point is below the one required for the PGS crosslink and, thus, the obtained tubular scaffold has not been crosslinked. Besides, the process was difficulty to reproduce. In any manner, we obtained electrospun pPGS/PCL fibrous sheets and created porous over then by laser ablation, in a laser printer. From the generated processed matts, cell transmigration essays were performed. HUVECs were grown on pieces of electrospun membranes mounted on a small device containing a plastic frame filled with GelMA. The objective was to evaluate if the created porous structures facilitates endothelial migration. HUVEC cells multiplied and presented good morphology on the face of the nanofibrilic mats. However, the cells not migrate from the membranes to the GelMA because we still needed to adjust the methacrylation degree and the photoinitiator rate of the GelMA we have employed.

As the PhD trainee that allowed this collaboration finished, and we still wanted to develop this potential project, we contacted the ICPEES in order to improve it. Because most of the challenges it was encountered during the PhD trainee at United States was related to the optimization of the electrospinning, and the ICPEES possess a large structure dedicated to

electrospinning, the project was continued under the supervision of the Dr. Guy Schlatter, the current co-supervisor of this project. We had overcome the issue with the PCL by employing poly (vinyl alcohol) (PVA) as carrier polymer, in order to crosslink the PGS: PVA does not melt during thermal crosslinking, and it is highly water-soluble, enabling its safe removal by dissolution in water. Additionally, PVA is approved by the US Food and Drug Administration for applications in food chemistry and pharmaceuticals (FDA). The pPGS was synthesized by microwave and, then, electrospun with PVA. During the optimization of the electrospinning parameters, we started to electrospun over plate collectors, covered with aluminum foil. However, it was hard to detach the obtained samples from the aluminum without tear them. To resolve this issue, the fibers were collected in parchment paper and, then, we could detach virtually 100% of the fibers. The morphology of these fibers, visualized by Scanning Electron Microscopy (SEM), showed smooth and uniform fibers. Moreover, since the employment of the pPGS provide an interesting feature, that is the ability to stick different layers together, we performed some tubular scaffold assembly experiments around PTFE (also known as Teflon®) mandrels, by rolling layers of electrospun matts around then. Immediately from this assembly step, the final tube was very stable. From this technique, we were able to fabricate tubular scaffolds of different diameters, including super small tubular grafts of 0.75mm and bifurcated scaffolds, with an important length ratio (at least 10 cm length, which is considerate a clinically relevant size). The assembled scaffolds obtained from the electrospun mats were then crosslinked in vacuum oven. Cured scaffolds were purified by washing in water, to remove the PVA, and in ethanol, to remove non-crosslinked PGS. After the characterization of the purification, we concluded some PVA remained. However, as PVA is also a biodegradable and biocompatible polymer, this will not be a constraint for the application of these scaffolds as bioabsorbable vascular grafts. Following, we characterized the morphology of the tubular scaffolds by SEM. From the abluminal side SEM pictures (the external side of the scaffold), it was noticed the fibrous architecture and the preserved porosity, typical features for crosslinked electrospun membranes. From the luminal side (inside), it was possible to observe a smooth, though porous, surface, in comparison with the abluminal side, which may be an attractive feature to facilitate smooth blood flow. Transversal SEM images shown the layers connections which happened thanks to the pPGS flow and crosslinking during curing. These connections created a unique scaffold from the electrospun membranes stacked. Moreover, the SEM images of the scaffolds transversal section shown the inner porosity of the wall, which is crucial for water, physiological signaling and nutrients exchange. Delamination essays were performed to determine the interlayer connection strength. The results shown that laminated scaffolds, when properly

manufactured, can stand the same forces as the directly electrospun ones. Still, as these tubular grafts were designed for rapid vascularization in tissue engineering, to create porous structures with a relevant porous size that allows endothelial cell migration and anastomosis from the new formed vascular network was the key step. To create these pores, we contacted the IREPA laser™, located at Ilkirch, France, which had stablished a collaboration with Guy Schlatter already. Thanks to their high specialized laser ablation machines, we could create patterned porous along all the tubular scaffolds. The morphology of the obtained laser ablated tubular scaffolds was visualized by SEM, which presented a highly structured and patterned tubular scaffold. The pore diameter was 150 μm, while the porous distances obtained are 0.45 mm for the parallel pores, and 0.6 mm for the congruent pores. Moreover, the pores itself presented an inner porous structure, which may improve endothelial cell adhesion and migration, since it can provide attaching sites for the cells. Therefore, we have successfully obtained tubular scaffolds from electrospun membranes of bioabsorbable and biodegradable polymers, with an architecture that resembles the native extracellular matrix. Thanks to the employment of the pre-PGS and its ability to stick the layers together, these layers were successfully fused during the crosslink of the assembled scaffolds. This allows the free-form fabrication of scaffolds in a diversity of forms, for a diversity of applications. In order to determine the mechanical properties of the obtained PGS/PVA tubular scaffolds, establish their suturability and verify the scaffold layers bond, comparing different samples and evaluating the influence of the laser ablation processing on these properties, we performed various mechanical tests by uniaxial tensile strength. Non-machined and machined samples did not presented differences regarding their ultimate tensile strain at rupture. All scaffolds are highly elastic, and elongated for more than 100% their original size. Only the elongation at the rupture of the ablated scaffolds varied from the control scaffold (non-ablated) and this can be attributed to the presence of holes changed the stress distribution and thus decreased the strength of the scaffolds. Consequently, the elastic modulus was smaller for the machined scaffolds. Both non-machined and machined tubular scaffolds shown to be suturable. However, the suturability was smaller for the laser ablated scaffolds. We believed the porous structure facilitated the tearing due to force from the suture. Still, the suture retention strength for the machined scaffolds is $4N/mm^2$, indicating they can retain the suture forces. Thus, all scaffolds, non-ablated and ablated, can be potentially employed as suturable vascular grafts. When embedded them in fabricated tissue engineering constructs, the machined tubular scaffold can serve as anchor for their proper attachment by suture, while instantly providing a blood flow inside the biofabricated construct. To determine if the scaffolds could be sterilized by autoclaving, TGA analysis were performed. The material degradation started at 200˚C, and

its carbonization begins at around 430˚C. As the autoclave sterilize materials under a vapor temperature of 120˚C, the TGA analysis indicated the scaffolds were suitable for autoclaving and, thus, this was our sterilization method of choice prior to the *in vitro* essays. From converging the promising techniques of electrospinning and laser micro-ablation, we successfully produced a porous pattern in tubular fibrous scaffolds, without damaging the fibrous structures of the scaffold. The porous structure will potentially improve the cell migration and angiogenesis from a prospected vascular graft to a biofabricated tissue, enhancing its viability and survival. Therefore, the PGS/PVA tubular scaffolds machined by laser possess two major levels of porosity: the micro-porosity allows the nutrients and growth factors, while the porous of 150μm allows cell migration. The next step was to incorporate the scaffold into GelMA 3D fabricated constructs. These *in vitro* experiments were performed at Federal University of São Carlos, SP, Brazil, in collaboration with the Dr. Heloísa Selistre de Araujo. Prior to the scaffold incorporation, the cell proliferation and viability were assessed by culturing HUVEC cells with extracts of PGS/PVA scaffolds. HUVECs proliferated over time with both PGS extracts and cell culture media, concluding the PGS did not release armful compounds and, therefore, has no cytotoxic effects. After 5 days, HUVECs cells proliferation cultured in PGS medium extracts was significantly higher than for the HUVECs cultured with the cell medium alone. Fluorescent images of HUVEC cells cultured over the electrospun mats shows the HUVEC proliferated and attached over the PGS/PVA membranes. The porous created by laser machining on the tubular electrospun scaffolds were relatively large, allowing endothelial cell migration for rapid vascularization, we performed a dynamic seeding on the PGS-PVA scaffold/GelMA 3D construct with HUVEC only, in order to simulate the endothelial cells migration delivered through blood and to confirm the HUVEC migration over the GelMA, and also to stablish the HUVEC structure pattern cluster created after HUVEC flow. After 24 hours of cell culture, HUVECs spread on the external GelMA, then moved and accumulated together into cell clusters, with no particular structure. Following, a dynamic co-culture of Endothelial cells/Osteoblasts was performed in tubular scaffolds/GelMA 3D constructs, employing tubular scaffolds with no laser-ablated pores first. Due to the absence of pores, HUVECs remained stuck inside the tubular scaffold and aggregated into large structures, instead of tubules. MG-63 remained at the external side of the scaffold region, over the hydrogel, which aggregated into clusters with no particular structure. Thus, no interaction within these two cell types were observed. However, when the same dynamic co-culture seeding of endothelial cells/Osteoblasts in tubular scaffolds/GelMA 3D constructs with tubular scaffolds with laser-ablated pores, close cell–cell contacts could be observed, suggesting the formation of specialized unions. Anastomosis within HUVECS/MG-

63 clusters and the graft can be observed. This is the key point the rapid vascularization: to provide an instant endothelial/blood cells into the biofabricated bone-like constructs in host, while promoting the anastomosis of the new capillary network formed. The 3D implants biofabricated with osteoblasts may stimulate the formation of a vascular network, as various studies demonstrated that osteoblasts produce growth factors that stimulate the recruitment of endothelial cells from the host vasculature, while the presence of the vascular network will increase the bone formation in a dynamic effect. Although more research at the molecular lever (i.e. Polymerase Chain Reverse Transcription, or PCR-rt) is necessary to better understand how these crosstalk works and, thus, help to predict what will happen once the constructs were sutured into the host, this preliminary co-seeding investigations already indicates the electrospun scaffolds architecture is ideal to permit this crosstalk, at the same time they clearly allow endothelial cell migration, which will later form vascular networks that will benefit the vascularization of the bone constructs, as other tissue engineering constructs as well. Therefore, this work is an enormous step into the clinical translation of 3D biofabricated tissue constructs. Through our strategy, we expect to successfully embed these tubular scaffolds and provide a suturable and permeable vascular anchor that will provide an instant blood which will enhance the biofabricated implant survival and will accelerate the clinical translation of tissue engineering.

RESUMO GERAL E TRAJETÓRIA DE PESQUISA (PORTUGUÊS)

A regeneração do tecido ósseo ainda é um desafio importante em ortopedia e traumatologia. Apesar da capacidade natural de reparo ósseo, um trauma além do limite crítico (fratura crítica) não pode ser regenerado. Devido a muitos traumas e patologias, assim como o aumento da expectativa de vida em todo o mundo, há uma necessidade crescente de novos tratamentos para pacientes com doenças musculoesqueléticas, sendo o osso o segundo tecido mais transplantado, após o sangue. O enxerto ósseo autólogo, que é o procedimento mais utilizado para a reconstrução de defeitos e fraturas ósseas, apresenta várias desvantagens, como disponibilidade limitada, perda ou reabsorção do enxerto, instabilidade a curto prazo no caso de grandes áreas afetadas, complicações associadas à uma segunda cirurgia, e taxas de falha superiores a 50% em locais de difícil consolidação. Embora muitos dispositivos protéticos artificiais estejam disponíveis, poucos podem substituir completamente todas as funções biológicas complexas. Atualmente, a ideia de reconstrução de órgãos e tecidos criados em laboratório é amplamente disseminada e investigada em todo o mundo. Como uma ciência multidisciplinar em medicina regenerativa, estes estudos envolvem conhecimentos nas áreas de biologia, ciências da saúde, engenharia e ciência dos materiais.

A engenharia de tecidos é um campo multidisciplinar que aplica os princípios da engenharia e ciências biológicas para o desenvolvimento de substitutos biológicos que restauram, mantêm ou melhoram a função do tecido ou de um órgão como um todo. Assim como para a maioria dos tecidos, o desenvolvimento da engenharia de tecidos ósseos baseia-se na cultura *in vitro* de células ósseas progenitoras associadas a *scaffolds*, que devem imitar a matriz extracelular (ECM), formando um meio ou microambiente adequado para as células se organizarem em estruturas funcionalmente semelhantes ao tecido. Neste contexto, o objetivo da engenharia do tecido ósseo é criar enxertos clinicamente relevantes que possam ser usados terapeuticamente. Um componente essencial na engenharia de tecidos é o desenvolvimento de estruturas 3D porosas - *scaffolds* - que fornecerão às células o suporte necessário para guiar a formação óssea.

Existem muitas propriedades físicas e biológicas que um scaffold ideal para engenharia de tecidos ósseos precisa possuir, dentre elas: uma matriz porosa com poros interconectados e superfície adequada para o crescimento e proliferação celular e transporte de nutrientes e resíduos metabólicos; taxa de reabsorção e remodelamento sincronizada com atividade osteogênica, apenas com a produção de substâncias metabolicamente aceitáveis; propriedades mecânicas adequadas às do tecido hospedeiro por meio de uma interface tecido-

material concisa e estável que deve persistir durante o tempo de reabsorção do implante; não apresentar risco de rejeição ou reação do sistema imunológico por corpo estranho; e ter boa adaptação com o ambiente do tecido hospedeiro. Muitos materiais e técnicas de fabricação estão sendo investigados atualmente. No entanto, apesar dos avanços significativos na área, o desenvolvimento de estruturas sintéticas capazes de sustentar totalmente a capacidade de regeneração autorremodelação óssea ainda é um grande desafio. Somente o processo de fabricação do scaffold em si não é suficiente para fabricar um scaffold ideal. Nesse sentido, a nanotecnologia pode fornecer algumas das características para projetar as superfícies internas dos *scaffolds*. Nesse contexto, um dos objetivos deste trabalho foi produzir membranas de poli (caprolactona)(PCL) para engenharia de tecidos ósseos e regeneração óssea guiada, por eletrofiação. Basicamente, o processo de eletrofiação permite a produção de membranas nanofibrosas com similaridade estrutural com a matriz extracelular nativa. O PCL é um polímero biodegradável semicristalino e aprovado pela Food and Drug Admnistration (FDA). No entanto, alguns desafios relacionados às propriedades mecânicas para que seja possível ampliar o uso de PCL como material de engenharia de tecido ósseo ainda precisam ser resolvidos.

Primeiro, avaliou-se o uso dos nanocristais de celulose (CNCs) como fase de reforço porque eles são naturais, de baixo custo e biocompatíveis, com excelentes propriedades mecânicas. No entanto, a desvantagem mais importante relacionada ao uso de nanocristais de celulose para nanocompósitos poliméricos é a dificuldade inerente dos CNC de se dispersar em meio não polar, devido à sua superfície polar. Assim, realizei o PCL-grafting por abertura do anel a partir dos CNC, para criar uma interface em PCL, com o intuito de melhorar a compatibilidade do reforço e da fase polimérica. Este trabalho foi realizado em parceria com o Instituto de Química e Polímeros para a Energia, o Ambiente e a Saúde (ICPEES, acrônimo em francês), em colaboração com o Dr. Guy Schlatter e o Dr. Luc Avérous, em Estrasburgo, França. Investigou-se como diferentes concentrações de CNC podem afetar as propriedades termomecânicas de membranas de PCL obtidas por eletrofiação, para estabelecer uma relação entre o teor de CNCs e as melhorias das propriedades mecânicas, a fim de ajustar essas propriedades de acordo com o local e/ou aplicação do tecido. Membranas eletrofiadas homogêneas de bionanocompósitos formadas de PCL, incorporadas com CNC-g-PCL (ou os CNC graftizados com PCL). Houve um aumento significativo na temperatura de fusão e na temperatura de cristalização das nanofibras de PCL, com a adição dos CNC. Além disso, um aumento no grau de cristalinidade da matriz de PCL com a adição dos CNCs indicou uma boa compatibilidade entre a matriz e as partículas. A incorporação do CNCs, mesmo em pequenas

quantidades, aumentou consideravelmente as propriedades mecânicas das membranas nanofibrosas, com melhorias significativas no módulo de Young e na tensão na ruptura. Portanto, torna-se claro o potencial dos nanocristais de celulose como uma fase de reforço em membranas de PCL obtidas por eletrofiação, e as propriedades mecânicas podem ser ajustadas de acordo com a proporção dos CNC.

Em segundo lugar, como objetivou-se o desenvolvimento de membranas biodegradáveis para a regeneração óssea guiada, após melhorar as propriedades mecânicas das membranas de PCL, melhorar a osteogenicidade dessas membranas, a fim de estimular a formação óssea no local da injúria, tornou-se um novo objetivo do presente trabalho. Para conseguir isso, eu precisava adicionar uma fase bioativa nas membranas de PCL. Após algumas pesquisas, descobriu-se o Biosilicato®, uma vitrocerâmica com excelente bioatividade. Estudos mostram que o Biosilicato® melhorou significativamente a proliferação *in vitro* de osteoblastos e a osteoindução *in vivo*. O Biosilicato® é também amplamente aplicado em áreas médicas e odontológicas. Além disso, como o Biosilicato® é um sistema vitrocerâmico, este apresenta propriedades mecânicas superiores às da hidroxiapatita. Assim, enquanto que os CNCs confeririam melhores propriedades mecânicas, estabeleceu-se a hipótese de que o Biosilicato® forneceria um elemento bioativo em membranas biodegradáveis de PCL. Este trabalho também foi realizado em conjunto com o ICPEES. No entanto, assim como para os CNCs, o Biosilicato® também necessitava ser graftizado com o PCL, visando aumentar a compatibilidade do Biosilicato com a matriz de PCL, melhorando a dispersão e a adesão mecânica na interface polimérica.

O Biosilicato®, conforme recebido, possuía uma distribuição de tamanho de partícula entre 25 e 54µm, o qual é consideravelmente maior do que o diâmetro das nanofibras (0,637 µm). Assim, realizou-se moagens do Biosilicato, o que diminuiu consideravelmente o tamanho das partículas, para em torno de 0,2 µm a 8µm, com a maior concentração das partículas em torno de 2,33µm e 2µm (cerca de 14% das partículas para ambos os diâmetros). Em seguida, a graftização do Biosilicato® foi realizada assim como para os nanocristais de celulose.

Pela razão de esta ser a primeira vez que o enxerto de PCL a partir do Biosilicato® é relatado, uma investigação mais profunda das partículas obtidas foi realizada. Análises em Microscopia Eletrônica de Transmissão (MET), utilizando um módulo de análises de difração de Raios-X, mostraram que os biocompósitos de PCL-Biosilicato® foram desenvolvidos com sucesso. Os espectros de FT-IR demonstraram que as típicas ligações do tipo Si-O-Si do

Biosilicato® não estavam mais acessíveis à radiação Infravermelha, indicando que a superfície foi funcionalizada e, assim, houve polimerização do PCL a partir do Biosilicato®. A enxertia de PCL (grafting) a partir dos CNCs também foi realizado e confirmado pelos espectros de FT-IR. Ambos os compósitos foram então dispersos com sucesso em matriz de PCL, e seus respectivos compósitos foram fabricados por eletrofiação. A morfologia dos PCL + CNC + Biosilicato® foi avaliada por microscopia eletrônica de varredura. As micrografias revelaram nanofibras homogêneas, sem grânulos (ou *beads*), para todos as membranas, embora também possa ser observada a formação de estruturas onde são inseridas partículas maiores de BioSiO-g-PCL.

Portanto, o grafting com PCL foi fundamental para melhorar a dispersão dos biocompósitos de CNC e Biosilicato® nas membranas de PCL. Com relação às propriedades mecânicas, o módulo de Young e o Stress na Ruptura das membranas aumentaram quando os CNC-g-PCL foram adicionados. O mesmo efeito foi observado para os compósitos BioSiO-g-PCL. Além disso, quando o CNC e o Biosilicato® foram empregados juntos, o Módulo de Young aumentou três vezes em comparação com as membranas PCL puras e duplicou em comparação com os CNC-g-PCL. Estes resultados destacam a importância de melhorar a compatibilidade das partículas da matriz em nanocompósitos, a fim de prever e ajustar suas propriedades mecânicas adequadamente. Novamente, por conta de essas membranas terem sido desenvolvidas para a regeneração óssea, estas também foram avaliadas por testes *in vitro* com osteoblastos. Ensaios de proliferação celular com MG-63 (osteoblastos humanos) cultivados nas amostras PCL, PCL + CNC, PCL + BioSiO e PCL + CNC + BioSiO mostraram proliferação crescente ao longo do tempo de análise. Não houve diferenças significativas na proliferação de osteoblastos em comparação com o controle e com as diferentes amostras ao longo do ensaio. Portanto, a partir do ensaio de viabilidade celular, conclui-se que todas as amostras são biocompatíveis, suportam a proliferação celular e, portanto, não apresentam toxicidade *in vitro*. A partir de imagens fluorescentes, foi possível visualizar que os osteoblastos cultivados em membranas eletrofiadas foram capazes de aderir e proliferar em todas as amostras durante o período de ensaio. Contudo, para as amostras de PCL + Biosilicato®, os osteoblastos cultivados em amostras de PCL + Biosilicato® mostraram maior tamanho e orientação dos núcleos em comparação com outras amostras. O mesmo efeito não foi observado nas amostras com CNC + Biosilicato®, o que foi atribuído ao efeito do menor diâmetro das fibras, que levou a uma menor área projetada disponível (menor tamanho de poro) para as células se aderirem e se espalharem. Ensaios de biomineralização realizados para osteoblastos cultivados durante 21 dias sobre as membranas mostraram

depósitos minerais sobre todas as membranas, e assim, pudemos concluir que todas as membranas suportam a mineralização *in vitro*. Entretanto, sugere-se análises quantitativas para estabelecer uma correlação entre os compósitos e a biomineralização *in vitro*, para que seja possível predizer ainda mais a mineralização *in vivo* e, consequentemente, a formação óssea. Portanto, todos os compósitos PCL/CNC/Biosilicato obtidos possuem propriedades mecânicas melhoradas, suportam proliferação e biomineralização de osteoblastos *in vitro*, e podem ser potencialmente utilizados como membranas para regeneração óssea guiada. Além disso, os compósitos de partículas CNC-g-PCL e Biosilicato®-g-PCL obtidos podem também ser empregados como fase de reforço em outras técnicas de fabricação de *scaffolds* para engenharia de tecidos ósseos, como manufatura aditiva (impressão 3D), a exemplo do que foi realizado em um projeto em paralelo com o Centro de Tecnologia da Informação Renato Archer (Brasil).

No entanto, apesar de todos os avanços em materiais, na fabricação e nas técnicas de manipulação celular, até o momento, os tecidos obtidos por engenharia de tecido ósseo ainda não possuem um tamanho clinicamente relevante para serem aplicadas na regeneração de fraturas ósseas de tamanho crítico. A vascularização continua sendo o principal obstáculo que impede a tradução da maioria destes implantes para a prática clínica. Assim, um outro objetivo deste trabalho foi desenvolver novas tecnologias potenciais para a engenharia do tecido ósseo, com o intuito de acelerar a aplicação clínica destes implantes por meio da vascularização destes tecidos/materiais. Atualmente, estudos de bioengenharia de redes vasculares têm sido amplamente utilizados empregando-se *scaffolds* naturais de hidrogel. Diversas técnicas de microfabricação permitem a criação de capilares vasculares utilizando Gelatina Metacriloil (GelMA), que consiste em uma plataforma de hidrogel biocompatível, capaz de interagir com e encapsular células durante a sua fotopolimerização, permitindo a formação de tecidos em três dimensões (3D). As propriedades mecânicas de GelMA podem ser adaptadas de acordo com o tecido e a aplicação, por meio do ajuste do tempo de fotopolimerização, da densidade, da química das ligações cruzadas e da concentração do fotopolimerizador, assim como pelo peso molecular dos precursores. No entanto, hidrogéis 3D altamente reticulados apresentam microambientes que possuem alta rigidez, limitando a proliferação celular migração e morfogênese. Portanto, é necessário um método que melhore as propriedades mecânicas dos hidrogéis sem afetar sua fase líquida. Assim, supôs-se que os nanocristais de celulose (CNC) poderiam ser facilmente incorporados em hidrogéis GelMA, visto a natureza polar do hidrogel e do CNC. Desta maneira, investigou-se a produção de hidrogéis híbridos de GelMA-CNC para modificar as propriedades mecânicas dos hidrogéis

sem afetar suas propriedades benéficas para as células se aderirem e se espalhar (*sprout*). Além disso, os CNCs podem ser usados como um local de ancoragem para as células aderirem, mantendo um ambiente líquido que permite que as células se espalhem e proliferem. Assim, hidrogéis GelMA-CNC foram desenvolvidos em parceria com o Harvard-MIT Health Sciences and Technologies e o Brigham and Women's Hospital, em Boston, MA, Estados Unidos, em colaboração com o Dr. Ali Khademhosseini. No entanto, devido à presença de gelatina, os nanocristais precipitaram no GelMA, resultando na aglomeração das nanopartículas. Com o intuito de melhorar a dispersão do CNC, o CNC foi metacrilado com a gelatina durante a síntese do GelMA, resultando na produção de compósitos híbridos GelMA-CNC. Células Endoteliais da Veia Umbilical Humana (HUVEC) foram encapsuladas com sucesso nestes estes hidrogéis, se espalharam e formaram as estruturas típicas dos túbulos HUVEC, de uma maneira 3D.

Embora os GelMA-CNCs tenham se mostrado como compósitos potencial para a microfabricação da rede vascular, a principal questão dessa abordagem é como conectar essa delicada rede vascular ao tecido hospedeiro, a fim de fornecer uma perfusão sanguínea instantânea dentro das tecidos biofabricados em 3D? Assim, o conceito de incorporar um scaffold tubular mais resistente dentro dos hidrogéis GelMA foi apresentado. A ideia seria fornecer um local de ancoragem biodegradável suturável dentro do GelMA que pudesse ser diretamente anastomizado com o sistema sanguíneo do hospedeiro. Como técnica de microfabricação do scaffold tubular, escolheu-se o *electrospinning*. O *Electrospinning* é amplamente utilizado para produzir *scaffolds* vasculares com uma arquitetura que imita a matriz extracelular nativa dos vasos sanguíneos. Empregando um elastômero de degradação rápida, o poli (sebacato de glicerol), ou PGS, o enxerto suturável pode ser remodelado em uma nova artéria/vaso. Entretanto, como a eletrofiação cria uma rede de fibras densas, a fim de melhorar a migração e vascularização celular do enxerto suturável, empregamos o conceito de usinagem a laser dos enxertos tubulares obtidos, a fim de criar uma rede capilar a partir do enxerto vascular que potencialmente ligue-se com a nova rede capilar formada/fabricada nos enxertos biofabricados em GelMA. Porém, a eletrofiação de PGS é um desafio porque ele é insolúvel. Assim, é necessário o emprego do pPGS (pré-polímero). No entanto, devido às cadeias moleculares curtas do pPGS, ele não forma enredamentos moleculares suficientes para formar fibras e, portanto, requer o uso de polímeros carreadores. O grupo do Dr. Khademhosseini propôs empregar o PCL como polímero carreador. Obtivemos alguns tubos pPGS/PCL por eletrofiação direta sobre mandris revestidos de gelatina, conectados a um motor. Entretanto, a obtenção de *scaffolds* tubulares a partir dessa abordagem foi desafiadora

devido a muitas razões: o diâmetro do scaffold tubular é limitado pelo diâmetro do mandril, que não pode ser muito pequeno, ou não possuirá carga superficial suficiente para atrair as fibras; porque o pPGS tem uma temperatura de transição vítrea abaixo da temperatura ambiente, causando a fusão das fibras, é necessária sua reticulação em PGS. No entanto, o ponto de fusão do PCL está abaixo do necessário para a reticulação do PGS e, assim, o scaffold tubular obtido não foi reticulado. Além disso, o processo foi difícil de reproduzir. De qualquer maneira, obteve-se membranas fibrosas de pPGS/PCL e, com o auxílio de uma impressora a laser, criou-se os poros. A partir das membranas usinadas geradas, os ensaios de transmigração celular foram realizados. HUVECs foram cultivadas em pedaços de membranas eletrofiadas e montadas em um pequeno dispositivo contendo uma armação de plástico preenchida com GelMA. O objetivo foi avaliar se as estruturas porosas criadas facilitariam a migração endotelial. As células HUVEC se multiplicaram e apresentaram boa morfologia na face das mantas nanofibrílicas. No entanto, as células não migraram das membranas, provavelmente porque ainda necessitava-se ajustar o grau de metacrilação e a taxa de fotoiniciadores do GelMA utilizados.

Como o estagiário de doutorado que permitiu esta colaboração terminou, este projeto potencial ainda precisava ser desenvolvido, realizou-se uma parceria com o ICPEES, na França, para melhorá-lo. Como a maioria dos desafios encontrados durante o estágio de doutorado nos Estados Unidos estava relacionada à otimização da eletrofiação, e o ICPEES possui uma estrutura de ponta dedicada à pesquisa em *electrospinning*, continuou-se o projeto sob a supervisão do Dr. Guy Schlatter, que se tornou também co-orientador deste projeto. Resolveu-se a questão da reticulação do PGS substituindo o PCL e empregando o PVA como polímero carreador para a eletrofiação. O PVA não funde durante a reticulação térmica do PGS, e é altamente solúvel em água, permitindo sua remoção de maneira segura. Além disso, o PVA é aprovado pela Food and Drug Administration dos EUA para aplicações em química de alimentos e produtos farmacêuticos. O pPGS foi sintetizado por micro-ondas e, em seguida, membranas de pPGS/PVA foram eletrofiadas. Durante as etapas de otimização dos parâmetros de eletrofiação, as mantas foram eletrofiadas sobre coletores planos, cobertos com papel alumínio. No entanto, foi difícil remover as amostras obtidas do papel alumínio sem rasgá-las, já que estas aderiam ao substrato. Para resolver esse problema, eletrofiou-se as fibras em papel vegetal e, assim, conseguiu-se separar praticamente 100% das fibras do substrato. A morfologia dessas fibras, visualizadas por Microscopia Eletrônica de Varredura (MEV), mostrou fibras lisas e uniformes. Além disso, como o emprego do pPGS fornece a interessante característica às membranas de unir diferentes camadas. Foram realizadas

experiências de montagem de *scaffolds* tubulares em torno de hastes em PTFE (também conhecido como Teflon®), rolando camadas das membranas obtidas ao redor destas hastes. Imediatamente a partir desta etapa de montagem, o tubo final ficou muito estável. Graça a esta técnica, foi possível fabricar *scaffolds* tubulares de diferentes diâmetros, incluindo enxertos tubulares bem pequenos, de 0,75 mm de diâmetro interno, e *scaffolds* bifurcados, com uma importante relação de comprimento de pelo menos 10 cm de comprimento, o que é considerado um tamanho clinicamente relevante. Os *scaffolds* montados obtidos a partir das membranas eletrofiadas foram então reticulados em um forno a vácuo. Em seguida, os *scaffolds* curados foram purificados por lavagem com água, para remover o PVA e em etanol, para remover PGS não reticulado. Após a caracterização da purificação, concluiu-se que ainda havia resquícios de PVA. Contudo, como o PVA também é um polímero biodegradável e biocompativel, este não será um impedimento para a aplicação destes *scaffolds* como enxertos vasculares bioabsorvíveis. A seguir, a morfologia dos *scaffolds* tubulares foi caracterizada por MEV. A partir das imagens do lado abluminal (o lado externo do scaffold), notou-se a arquitetura fibrosa e a porosidade preservada, características típicas das membranas eletrofiadas reticuladas. Do lado luminal (interior), foi possível observar uma superfície lisa, porém porosa, em comparação com o lado abluminal, que pode ser uma característica atrativa para facilitar o fluxo sanguíneo.

Imagens MEV de cortes transversais dos *scaffolds* mostram as conexões das camadas que aconteceram graças ao fluxo de pPGS e sua respectiva reticulação durante a cura. Essas conexões, consequentemente, estabeleceram uma união das membranas umas sobre as outras. Além disso, essas imagens também mostraram a porosidade interna da parede, que é crucial para o fluxo de água, sinalizadores fisiológicos e troca de nutrientes. Ensaios de delaminação foram realizados para determinar a força da conexão entre camadas. Os resultados mostraram que os *scaffolds* laminados, quando adequadamente manufaturados, podem suportar as mesmas forças que quando diretamente eletrofiados. Ainda assim, como pretendia-se utilizar esses enxertos tubulares para vascularização rápida em engenharia de tecidos, necessitou-se criar estruturas porosas de tamanhos suficiente para permitir a migração e anastomose de células endoteliais da nova rede vascular formada, o que constituiu em um passo fundamental. Contatou-se a empresa IREPA laser ™, localizada em Ilkirch, na França, que já estabeleceu anteriormente uma colaboração com o Dr. Schlatter. Graças às suas máquinas de usinagem a laser altamente especializadas, foi possível criar poros padronizados ao longo de todos os *scaffolds* tubulares. A morfologia dos *scaffolds* tubulares usinados a laser foi visualizada por MEV, que mostrou uma estrutura porosa altamente estruturada e padronizada. As distâncias

dos poros obtidos foram de 0,45 mm para os poros paralelos e 0,6 mm para os poros congruentes, enquanto que o diâmetro do poro foi de 150 µm. Além disso, os próprios poros apresentavam uma estrutura porosa interna, que pode melhorar a adesão e a migração das células endoteliais, uma vez que fornece locais de fixação para as células. Portanto, obteve-se com sucesso estruturas tubulares de membranas eletrofiadas de polímeros bioabsorvíveis e biodegradáveis, com uma arquitetura que se assemelha à matriz extracelular nativa. Graças ao emprego do pré-PGS e à capacidade de ligação dessas camadas, estas foram unidas com sucesso durante a reticulação dos *scaffolds*. Com isto, é possível a fabricação de forma livre de *scaffolds* de uma diversidade de formas, para uma diversidade de aplicações. Para determinar as propriedades mecânicas dos *scaffolds* tubulares PGS/PVA obtidos, estabelecer a sua suturabilidade e verificar a ligação das camadas do scaffold, comparar diferentes amostras e avaliar a influência do processamento por usinagem a laser nestas propriedades, realizamos vários ensaios mecânicos por tração uniaxial. Amostras não usinadas e usinadas não apresentaram diferenças em relação ao stress na ruptura. Todos os *scaffolds* são altamente elásticos e alongaram-se por mais de 100% do tamanho original. Contudo, o alongamento na ruptura dos *scaffolds* usinados variou em relação ao scaffold controle (não usinado).

Acredita-se que a presença dos poros alterou a distribuição de tensões e, assim, diminuiu a rigidez dos *scaffolds*. Consequentemente, o módulo elástico é menor para os *scaffolds* usinados. Todos os *scaffolds* tubulares, não usinados e usinados, demonstraram ser suturáveis. No entanto, a suturabilidade é menor para os *scaffolds* usinados a laser, e atribui-se esse fato à estrutura porosa, que facilitou o rompimento quando submetido à força da sutura. Por outro lado, a força de retenção da sutura para os *scaffolds* usinados é de $4N/mm^2$, indicando que estes retêm a sutura. Assim, todos os *scaffolds*, não-usinados e usinados, podem ser potencialmente utilizados como enxertos vasculares suturáveis. Quando incorporado em enxertos biofabricados, o scaffold tubular usinado pode servir como âncora para sua fixação adequada por sutura, enquanto fornece instantaneamente um fluxo de sangue dentro do enxerto biofabricada.

Para determinar se os *scaffolds* poderiam ser esterilizados por autoclavagem, realizou-se uma análise em TGA, que mostrou que a degradação do material inicia a 200°C, e sua carbonização começa em torno de 430°C. Como a autoclave esteriliza os materiais sob uma temperatura de vapor de 120˚C, a análise da TGA indicou que os enxertos tubulares são, portanto, adequados para a autoclavagem e, então, este foi o método de esterilização escolhido para a realização dos ensaios *in vitro*. Portanto, a partir da convergência das promissoras técnicas de eletrofiação e usinagem a laser, produziu-se com sucesso um padrão

poroso em estruturas fibrosas tubulares, sem danificar as estruturas eletrofiadas do scaffold. A estrutura porosa potencializará a migração celular e a angiogênese a partir do enxerto vascular para um tecido ósseo biofabricado, aumentando sua viabilidade e sobrevivência. Desta maneira, os *scaffolds* tubulares de PGS/PVA usinados a laser possuem dois níveis principais de porosidade: a microporosidade, que permite a circulação dos nutrientes e fatores de crescimento, enquanto que o macro poroso permite a migração celular. O próximo passo foi incorporar o scaffold em hidrogéis de GelMA 3D. Esta etapa de incorporação, assim como os ensaios *in vitro*, foram realizados na Universidade Federal de São Carlos, SP, em colaboração com a Dra. Heloísa Selistre de Araújo. Antes da incorporação do scaffold, avaliou-se a proliferação celular e a viabilidade de células HUVEC cultivadas com extratos de membranas de PGS/PVA. As HUVECs proliferaram ao longo do tempo com extratos de PGS e meio de cultura de células, concluindo que os *scaffolds* não liberam compostos nocivos e, portanto, não possuem efeitos citotóxicos. Após 5 dias, a proliferação de células HUVEC cultivadas em extratos dos *scaffolds* foi significativamente mais elevada do que para as HUVEC cultivadas apenas com o meio celular. Imagens fluorescentes de células HUVEC cultivadas sobre as membranas mostraram que as HUVECs proliferaram e fixaram-se sobre as membranas de PGS/PVA.

Com o intuito de testar a hipótese de que os poros gerados por usinagem a laser permitem a migração celular, a fim de simular a migração das células endoteliais que fluem através de sangue, além de confirmar a migração de HUVEC sobre o GelMA e também para estabelecer o de padrão de estrutura das HUVEC criado após o fluxo das mesmas, realizou-se um *seeding* dinâmico na estrutura PGS-PVA/ + hidrogéis GelMA 3D apenas com as HUVECs. Como criamos poros relativamente grandes por usinagem a laser nos *scaffolds* tubulares, permitindo a migração de células endoteliais para rápida vascularização, após 24 horas, as HUVECs se espalharam no GelMA externo, e depois se moveram e se acumularam juntas em aglomerados de células, sem estrutura particular. A seguir, realizou-se uma cocultura dinâmica de células endoteliais/osteoblastos em estruturas tubulares de *scaffolds*/GelMA 3D, empregando primeiro estruturas tubulares sem poros usinados a laser. Devido à ausência de poros, as HUVECs (células endoteliais) permaneceram presas dentro do scaffold tubular e agregadas em grandes estruturas, em vez de formarem túbulos. As MG-63 (osteoblastos) permaneceram no lado externo da região do scaffold, sobre o hidrogel, que também se agregaram em aglomerados sem estrutura particular. Assim, nenhuma interação dentro destes dois tipos de células foi observada. No entanto, quando a mesma cocultura dinâmica de células endoteliais/osteoblastos foi realizada em hidrogéis de GelMA 3D com os

scaffolds com poros usinados a laser, as células endoteliais puderam migrar do tubo em direção aos osteoblastos, graças aos poros. Assim, observou-se contatos célula-célula próximos, sugerindo a formação de uniões especializadas. Ademais, a anastomose destes agrupamentos de células endoteliais/osteoblastos com o enxerto pode ser observada. Este é o ponto-chave da rápida vascularização: fornecer células endoteliais/sanguíneas de uma maneira instantânea para os implantes ósseos biofabricados a partir do enxerto, enquanto promove a anastomose da nova rede capilar formada. Os implantes 3D biofabricados com osteoblastos podem estimular a formação de uma rede vascular a partir do paciente, já que estudos indicam que osteoblastos segregam fatores de crescimento que estimulam o recrutamento de células endoteliais, enquanto a presença da rede vascular aumentará a formação óssea em um efeito dinâmico. Contudo, mais estudos à nível molecular (ou seja, Transcrição Reversa da Polimerase em Cadeia, ou PCR-rt) são necessárias para entender melhor como esse "*crosstalk*" funciona e, assim, ajudar a prever o que acontecerá quando os implantes forem suturados no hospedeiro. De qualquer maneira, estes estudos preliminares já indicam que a arquitetura dos *scaffolds* obtidos permite este *crosstalk* entre as duas linhagens celulares, ao mesmo tempo em que permite claramente a migração de células endoteliais, que posteriormente formará redes vasculares que beneficiarão a vascularização dos implantes ósseos bioconstruídos, assim como outros tipos de implantes obtidos de engenharia de tecidos. Através desta estratégia, espera-se incorporar com sucesso esses *scaffolds* tubulares nos implantes biofabricados, agregando uma âncora vascular suturável e permeável que proverá uma circulação sanguínea instantânea, aumentando, por conseguinte a sobrevivência de tecidos biofabricados, o que pode potencialmente acelerar a translação clínica da engenharia de tecidos.

RESUME GENERALE ET TRAJECTOIRE DE RECHERCHE (FRANÇAIS)

La régénération du tissu osseux reste un défi important en orthopédie et traumatologie. Malgré la capacité naturelle de la réparation osseuse, un traumatisme trop important (fracture critique) ne peut pas être régénéré. En raison de nombreux traumatismes et pathologies de l'os, et du vieillissement de la population dans le monde entier, il existe un besoin croissant de nouveaux traitements pour les patients souffrant de maladies musculo-squelettiques. Aujourd'hui le transplant d'os est le plus nombreux, après le sang. La greffe osseuse autologue, la procédure la plus couramment utilisée pour la reconstruction des défauts et des fractures osseuses, présente divers inconvénients, tels qu'une disponibilité limitée, une perte ou une résorption du greffon, une instabilité à court terme dans les zones greffés, des complications associées à une seconde intervention chirurgicale, et des taux d'échec supérieurs à 50% dans les sites de consolidation difficile. Bien que des nombreux dispositifs prothétiques artificiels soient disponibles, peu d'entre eux peuvent complètement remplacer toutes les fonctions biologiques complexes. Actuellement, l'idée de reconstruction d'organes et de tissus créés en laboratoire est largement diffusée et étudiée dans le monde entier. Comme une science pluridisciplinaire en médecine régénérative, ces études impliquent des connaissances dans les domaines des sciences biologiques, de la santé, de l'ingénierie et des matériaux.

L'ingénierie tissulaire est un domaine multidisciplinaire qui applique les principes de l'ingénierie et des sciences biologiques au développement de substituts biologiques qui restaurent, maintiennent ou améliorent la fonction tissulaire ou d'un organe dans son ensemble. Le développement de l'ingénierie tissulaire osseuse repose sur la culture *in vitro* de *scaffolds* associés à des cellules osseuses progénitrices, qui doivent imiter la matrice extracellulaire (ECM), formant un milieu ou microenvironnement approprié pour que les cellules s'organisent en structures fonctionnellement similaires au tissu. Dans ce contexte, le but de l'ingénierie des tissus osseux est de créer des greffes cliniquement pertinentes qui pouvant être utilisées dans la médecine régénérative. Un élément essentiel dans l'ingénierie tissulaire osseuse est, portant, le développement de structures 3D poreuses - *scaffolds* - qui fourniront aux cellules le support nécessaire pour guider la formation osseuse.

Il existe de nombreuses propriétés physiques et biologiques qu'un scaffold idéal pour l'ingénierie des tissus osseux doit posséder, parmi lesquels: une matrice poreuse avec des pores interconnectés et une surface appropriée pour la croissance et la prolifération cellulaire, ainsi que le transport des nutriments et des déchets métaboliques; taux de réabsorption et de

remodelage synchronisé avec l'activité ostéogénique, avec la production seulement de substances métaboliquement acceptables; des propriétés mécaniques appropriées à celles du tissu hôte dans le contexte d'une interface matériau-tissu concise et stable qui doit persister pendant la durée de la résorption de l'implant; ne pas avoir de risque de rejet ou de réaction du système immunitaire par un corps étranger; et avoir bonne adaptation avec l'environnement tissulaire de l'hôte.

Des nombreux matériaux et techniques de fabrication ont été étudiés. Cependant, malgré des progrès significatifs dans ce domaine, le développement de structures synthétiques capables de maintenir pleinement la capacité d'auto-remodelage et de régénération osseuse reste un défi majeur. Seul le processus de fabrication du scaffold lui-même n'est pas suffisant pour fabriquer un scaffold idéal. En ce sens, la nanotechnologie peut fournir des outils pour projeter les surfaces internes des *scaffolds*. Dans ce contexte, un des objectifs de ce travail était de produire des membranes de poly (caprolactone) pour l'ingénierie tissulaire osseuse et la régénération osseuse guidée par *electrospinning*. L'*electrospinning* permet de produire des membranes fibreuses présentant une similarité structurelle avec la matrice extracellulaire native. La policaprolactone (PCL) est un polymère semi-cristallin, biodégradable, approuvé par FDA. Cependant, certains défis concernant les propriétés mécaniques du PCL, comme sa fragilité par exemple, afin d'étendre l'utilisation de PCL en tant que matériau d'ingénierie tissulaire osseuse doivent être résolus.

Dans un premier moment, les nanocristaux de cellulose (CNC) en tant que phase de renforcement, ont été investigués, car ils sont naturels, peu coûteux et biocompatibles, et ont d'excellentes propriétés mécaniques. Néanmoins, l'inconvénient le plus important lié à l'utilisation de nanocristaux de cellulose pour les nanocomposites polymériques est qui ils sont difficiles à être dispersés dans un milieu non polaire, en raison de leur surface polaire. Ainsi, la greffe en PCL depuis la surface des CNC, par ouverture de cycle, a été réalisé, afin de créer une interface en PCL pour améliorer la compatibilité entre les particules et la phase polymère, en partenariat avec l'Institut des Chimie et Polymères pour l'énergie, l'environnement et la Santé (ICPEES), en collaboration avec le Dr. Guy SCHLATTER et le Dr. Luc AVÉROUS, à Strasbourg, France. Nous avons étudié le rapport avec CNC et les propriétés thermomécaniques des membranes électrofilées en PCL pour établir une relation entre le rapport de renforcement et les améliorations des propriétés mécaniques, afin de régler ces propriétés en fonction du site tissulaire et/ou selon l'application. Des membranes homogènes avec des bionanocomposites avec les CNC greffées en PCL ont été produits. Il y eu une augmentation significative de la température de fusion et de la température de

cristallisation des membranes de PCL avec les CNC. De même façon, une augmentation du degré de cristallinité des membranes en PCL avec l'ajout de les CNCs greffée a indiqué une bonne compatibilité entre la matrice et les CNC. L'incorporation de la CNCs greffés avec le PCL, même en petites quantités, a considérablement augmenté les propriétés mécaniques des membranes en PCL, avec des améliorations significatives du module d'Young et de la tension à la rupture. Par conséquent, il devient clair l'utilisation potentielle de nanocristaux de cellulose comme une phase de renforcement dans les membranes en PCL électrofilées, et leurs propriétés mécaniques peuvent être ajustées en fonction du rapport des CNC.

Deuxièmement, comme le développement des membranes biodégradables pour la régénération osseuse guidée était visé, après avoir surmonté le problème des propriétés mécaniques des membranes en PCL, nous avions besoin d'améliorer l'ostéogénicité de ces membranes, afin de stimuler la formation osseuse. Pour accomplir ceci, il fallait ajouter une phase bioactive dans les membranes en PCL. Après quelques recherches, nous avons trouvé que la vitrocéramique Biosilicate® possède une excellente bioactivité. Des études ont montré que le Biosilicate® améliore significativement la prolifération *in vitro* des ostéoblastes in et l'ostéoinduction *in vivo*. De plus, le Biosilicate® est actuellement appliquée dans les domaines médicaux et dentaires. En outre, parce que Biosilicate® est un système de vitrocéramique, il présente des propriétés mécaniques supérieures à celles de l'hydroxyapatite. Ainsi, les CNCs confèreraient des propriétés mécaniques améliorées, tandis que le Biosilicate® fournirait un caractère bioactif à des membrane biodégradables en PCL. Ce travail a également été réalisé en collaboration avec l'ICPEES, en collaboration avec le Dr. Guy Schlatter et la Dr. Anne Hébraud.

Cependant, ainsi comme pour le CNC, il fallait greffer le PCL à partir du Biosilicate®, afin d'améliorer la compatibilité du Biosilicate® avec la phase polymérique (PCL) et, par conséquent, améliorer la dispersion et l'adhérence mécanique à l'interface du composite. Le Biosilicate®, comme a été reçu, avait une taille des particules d'environ 25-54µm, considérablement plus grand que le diamètre des nanofibres (637µm). Ainsi, le Biosilicate a été broyé, ce qui a diminué la taille des particules, entre 0,2 et 8µm, avec une valeur modale entre 2,33µm et 2µm (14% des particules environ). Ensuite, le greffe en PCL a été réalisé pour le Biosilicate®, ainsi comme pour les CNCs. Parce que, à ce jour, c'est la première fois que la greffe PCL de Biosilicate® est rapportée, une recherche plus approfondie sur les particules obtenues a été effectuée. La microscopie électronique à transmission avec analyse par diffraction des rayons X a montré qu'une interface PCL-Biosilicate® a été créé avec succès. Les spectres FT-IR ont démontré que les liaisons de type Si-O-Si du

Biosilicate® n'étaient plus accessibles aux rayonnements IR, ce qui indique que la surface de la vitrocéramique était fonctionnalisée et qu'il y avait donc une polymérisation de PCL sur le Biosilicate®. La greffe du PCL sur les CNCs a également été réalisée et confirmée par les spectres FT-IR. Ensuite, ces deux composites ont été dispersés avec succès dans une matrice en PCL, et des membranes électrofilées en PCL + CNC + Biosilicate® ont été fabriqués. Leur morphologie a été évaluée par microscopie électronique à balayage (MEB). Les micrographies ont révélé des nanofibres homogènes, sans *beads*, pour toutes les *scaffolds*, bien que nous ayons pu également observer la formation de structures dans lesquelles des particules plus grosses de BioSiO-g-PCL sont insérées. Par conséquent, le greffage avec le PCL était fondamental pour améliorer la dispersion des biocomposites aux CNC et au Biosilicate® dans les *scaffolds*. Nous attendions que ces biocomposites allaient améliorer les propriétés mécaniques et le bioactivité par l'incorporation de ces composites dans les membranes en PCL.

En ce qui concerne les propriétés mécaniques, le module de Young et le stress à la rupture des membranes en PCL ont augmenté grâce aux CNC ajoutées. Le même effet a été observé pour les composites BioSiO-g-PCL. De plus, lorsque le CNC et le Biosilicate étaient utilisés ensemble, le stress à la rupture a augmenté trois fois par rapport aux membranes PCL seules, et a doublé par rapport aux membranes CNC-PCL. Ces découvertes soulignent l'importance d'améliorer la compatibilité des particules utilisés comme particules de renforcement dans les nanocomposites afin de prédire et d'ajuster correctement leurs propriétés mécaniques.

Parce que ces membranes ont été développées pour la régénération osseuse, elles ont été également évaluées par des tests *in vitro*. Des essais de prolifération cellulaire avec des ostéoblastes humains MG-63 cultivés sur les échantillons PCL, PCL + CNC, PCL + BioSiO et PCL + CNC + BioSiO ont montré une prolifération croissante tout au long de l'analyse. Il n'y eu pas de différences significatives dans la prolifération des ostéoblastes en comparaison avec le contrôle et avec les différents échantillons au long de l'essai. Par conséquent, à partir de l'essai de viabilité cellulaire, nous avons conclu que tous les échantillons sont biocompatibles, soutiennent la prolifération cellulaire, et ne montrent donc pas de toxicité *in vitro*.

A partir d'images fluorescentes, il a été possible de visualiser les ostéoblastes (MG-63) cultivés sur des membranes électrofilées composites. Les MG-63 ont pu proliférer et se fixer sur tous les échantillons pendant la période d'essai. Les ostéoblastes cultivés sur des

échantillons de PCL + Biosilicate® ont montré une augmentation de la taille et de l'orientation des noyaux en comparaison avec d'autres échantillons. Le même effet n'a pas été observé sur les échantillons avec CNC + Biosilicate®, qui a été attribué à l'effet de diamètre plus petit des fibres, ce qui a réduit la surface projetée disponible pour l'adhésion et la dissémination des cellules. Des essais de bio-minéralisation effectués pour des ostéoblastes cultivés pendant 21 jours sur les membranes ont montré des dépôts minéraux en rouge sur toutes les membranes, et ainsi, nous pouvons conclure que toutes les membranes supportent la minéralisation *in vitro*. Cependant, une analyse quantitative semble nécessaire pour établir une corrélation entre les composites et la biominéralisation *in vitro* afin de mieux prédire la minéralisation *in vivo* et, par conséquent, la formation osseuse.

Nous avons conclu que tous les composites PCL/CNC/Biosilicate obtenus possèdent des propriétés mécaniques améliorées, supportent la prolifération des ostéoblastes et la biominéralisation *in vitro*, et peuvent être potentiellement utilisés en tant que membranes pour la régénération osseuse guidée. De plus, les composites de particules CNC-PCL et Biosilicate®-CNC obtenus peuvent être utilisés comme charges de renforcement dans d'autres approches de fabrication des *scaffolds* pour l'ingénierie des tissus osseux, comme la fabrication additive (impression 3D), comme, par exemple, un projet en parallèle en collaboration avec le Centre pour des Technologies Numériques « Renato Archer » (Brésil).

Cependant, malgré toutes les avancées dans le domaine des biomatériaux, des techniques de fabrication, et de manipulation de cellules, les tissus obtenus pour l'ingénierie tissulaire osseuse ne possèdent pas encore une taille pertinente pour être cliniquement appliquées à la régénération des fractures osseuses de taille critique. La vascularisation reste le principal obstacle qui entrave la traduction de la plupart des greffons produits pour le tissu osseux en pratique clinique. Ainsi, si l'objectif de ce travail était de développer des technologies pertinentes pour l'ingénierie des tissus osseux, il fallait chercher comment améliorer la vascularisation de ces greffons/matériaux. Actuellement, les études de bio-ingénierie des réseaux vasculaires ont été largement utilisées avec des *scaffolds* en hydrogels naturels. Plusieurs techniques de microfabrication aboutissent à la création de capillaires vasculaires à partir de gélatine méthacrylate (GelMA), qu'est constitué d'une plateforme d'hydrogel biocompatible, capable d'interagir et d'encapsuler des cellules pendant la photopolymérisation de l'hydrogel, permettant la formation de tissus en trois dimensions. Les propriétés mécaniques de la GelMA peuvent être adaptées en fonction du tissu et de la cible d'application en augmentant le temps de photopolymérisation, sa densité, sa chimie et sa concentration des réticulants, bien comme le poids moléculaire des précurseurs. Cependant,

des hydrogels fortement réticulés peuvent limiter la prolifération, la migration et la morphogenèse cellulaires. Par conséquent, une méthode qui améliore les propriétés mécaniques des hydrogels sans affecter leurs propriétés bénéfiques pour les cellules est nécessaire pour des greffons performants obtenus par l'ingénierie tissulaire.

Parce que nous avions l'hypothèse que les nanocristaux de cellulose (CNC) pourraient être facilement incorporés dans les hydrogels GelMA, grâce la nature polaire de l'hydrogel et des CNC, nous avons visé la fabrication des hydrogels hybrides GelMA-CNC pour améliorer les propriétés mécaniques des hydrogels, sans affecter sa phase liquide, ce qui pouvait empêcher les cellules de proliférer. Les CNCs peuvent être utilisés comme sites d'ancrage pour la propagation des cellules, tout en maintenant un environnement colloïdal qui permet aux cellules de se propager et de proliférer. En collaboration avec le Dr. Ali Khademhosseini, nous avons développé des hydrogels GelMA-CNC en partenariat avec le Harvard-MIT Health Sciences and Technologies et le Brigham and Women's Hospital à Boston, États-Unis. Cependant, en raison de la présence de gélatine, les nanocristaux ont précipité dans les matrices, entraînant l'agglomération des nanoparticules. Afin d'améliorer la dispersion des CNC, les CNC ont été méthacrylés avec la gélatine, résultant en la production de composites hybrides GelMA-CNC. Les cellules endothéliales de la veine ombilicale humaine (HUVEC) ont été encapsulées avec succès dans ces hydrogels, et ont formé des structures tubulaires typiques, d'une manière 3D.

Bien que les GelMA-CNC se sont révélée des composites potentiels pour la microfabrication de réseaux vasculaires, qui peuvent être utilisés dans des techniques avancées de microfabrication de vaisseaux sanguins, la question principale était comment connecter ce délicat réseau vasculaire dans le tissu de l'hôte, en fournissant une perfusion sanguine instantanée à l'intérieur des greffons 3D ? Ainsi le concept d'intégration d'un scaffold tubulaire plus résistant à l'intérieur des hydrogels en GelMA a été présenté. L'idée était de fournir un site d'ancrage biodégradable et suturable à l'intérieur du GelMA qui pourrait être directement anastomisé avec le système sanguin de l'hôte. Comme technique en biofabrication du greffon suturable, l'*electrospinning* a été choisi. L'*electrospinning* est largement utilisé pour produire des *scaffolds* tubulaires avec une architecture qui imite la matrice extracellulaire native des vaisseaux sanguins. En utilisant un élastomère à dégradation rapide, le poly (sébacate de glycérol) (PGS), le scaffold suturable peut être remodelée en une nouvelle artère. Cependant, comme l'électrospinning crée un réseau de fibres denses, que peut empêcher les cellules de migrer, nous avons utilisé le concept de l'usinage à laser sur les *scaffolds* tubulaires obtenus, afin d'améliorer la migration cellulaire et la vascularisation du

greffe suturable et, par conséquent, créer un réseau capillaire à partir du greffon vasculaire qui peut potentiellement être anastomisé avec le nouveau réseau capillaire formé/fabriqué dans des greffons 3D. Cependant, l'électrospinning du PGS est un défi, car il est insoluble. Ainsi, il est nécessaire l'emploi du pré-polymère de PGS (pPGS), qui peut être dissolu. En raison des courtes chaînes moléculaires du pPGS, il ne forme pas suffisamment d'enchevêtrements moléculaires pour former des fibres et, par conséquent, il nécessite l'utilisation de polymères porteurs. Le groupe du Khademhosseini a proposé d'utiliser le PCL en tant que polymère porteur. Nous avons obtenu des tubes en pPGS/PCL par *electrospinning* directement sur des mandrins revêtus de gélatine, reliés à un moteur. Cependant, l'obtention des *scaffolds* tubulaires à partir de cette approche était difficile pour plusieurs raisons : le diamètre du scaffold tubulaire était limité par le diamètre du mandrin, qui ne peut pas être trop petit, ou il ne possède pas une charge de surface suffisante pour attirer les fibres ; parce que le pPGS a une température de transition vitreuse inférieure à la température ambiante, il est nécessaire sa réticulation en PGS. Malgré cela, le point de fusion PCL est inférieur à celui requis pour la réticulation de PGS et, ainsi, le scaffold tubulaire obtenu n'a pas été réticulé. En outre, le processus était difficile à reproduire. De quelque manière que ce soit, nous avons obtenu des membranes fibreuses électrofilées en pPGS/PCL et des pores ont été créés par usinage à laser avec l'assistance d'une imprimante laser. Des essais de transmigration cellulaire ont été réalisés avec les membranes usinées. Les HUVECs ont été cultivées sur des morceaux de membranes électrofilées montées sur un petit dispositif contenant un cadre en plastique rempli de GelMA. L'objectif était d'évaluer si les structures poreuses créées facilitent la migration endothéliale. Les cellules HUVEC se sont multipliées et présentent une bonne morphologie sur la face des membranes. Cependant, les cellules n'ont pas migré vers le GelMA parce qu'il avait encore besoin d'ajuster le degré de méthacrylation et le taux de photo-initiateur du GelMA employé.

Comme le stage de recherche qui a permis cette collaboration a terminé, et il avait toujours ce projet potentiel, nous avons établi un partenariat avec l'ICPEES afin de l'améliorer. Parce que la plupart des défis rencontrés pendant le stage de doctorat aux États-Unis étaient liés à l'optimisation de l'électrospinning, et que l'ICPEES possède une grande structure dédiée au électrospinning, ce projet a été continué sous la supervision du avec Dr. Guy Schlatter, qui est le co-superviseur de ce projet. D'abord, le problème avec l'utilisation du PCL comme polymère porteur, qu'a permettrait le PGS d'être réticulé, a été surmonté en employant le poly (alcool vinylique) (PVA) en tant que polymère porteur. Le PVA ne fondre pas pendant la réticulation thermique, et il est hautement soluble dans l'eau, permettant son

élimination de façon facile. En outre, le PVA est approuvé par la Food and Drug Administration des États-Unis pour des applications dans la chimie alimentaire et les produits pharmaceutiques.

Le pPGS a été synthétisé par micro-ondes. Ensuite, des membranes de pPGS/PVA ont été électrofilées. Au cours des étapes d'optimisation des paramètres d'électrofilage, de membranes ont été fabriquées sur des collecteurs plats, recouverts par des feuilles d'aluminium. Cependant, il était difficile de détacher les échantillons obtenus de l'aluminium sans les déchirer. Pour résoudre ce problème, les fibres ont été collectées sur le papier sulfurisé et, ainsi, il était possible de détacher pratiquement 100% des fibres. La morphologie de ces membranes, visualisée par microscopie électronique à balayage (MEB), a été composée des fibres lisses et uniformes.

De plus, l'utilisation du pPGS fournit une caractéristique intéressante à ces membranes, qui est leur capacité à solder des différentes couches ensemble. Ainsi, des expériences d'assemblage d'échafaudages tubulaires autour des tubes en PTFE (également connu sous le nom de Téflon®) ont été réalisés en roulant des couches de membranes électrofilées. Immédiatement à partir de cette étape d'assemblage, le tube final était très stable. Avec cette technique, des échafaudages tubulaires de diamètres différent ont été fabriqués, y compris des *scaffolds* tubulaires super petits, de 0,75 mm de diamètre, et des greffons bifurqués, avec un rapport de longueur important (au moins 10 cm de longueur, considéré une taille cliniquement pertinente). Les *scaffolds* assemblés obtenus à partir des membranes électrofilées ont été réticulés dans un four sous-vide, à 150˚C pendant 48 heures. Les *scaffolds* réticulés ont été purifiés par lavage à l'eau, pour éliminer le PVA, et par l'éthanol, pour éliminer le PGS non réticulé. Après la caractérisation de la purification, nous avons conclu qu'il a resté du PVA. Malgré cela, comme le PVA est également un polymère biodégradable et biocompatible, nous espérons que ceci ne constituera pas une contrainte pour l'application de ces *scaffolds* tubulaires en tant que greffons vasculaires bioabsorbables. Ensuite, la morphologie des *scaffolds* tubulaires a été caractérisé par MEB. A partir des images MEB du côté abluminal (le côté externe de l'échafaudage), il était possible remarquer l'architecture fibreuse et la porosité préservée, caractéristiques typiques des membranes électrofilées réticulées. Du côté luminal (à l'intérieur), une surface lisse, bien que poreuse, en comparaison avec le côté abluminal, a été observée ce qui peut être une caractéristique attrayante pour faciliter le flux sanguin. Des images MEB transversales ont montré les connexions de couches qui se sont produites grâce au flux de pPGS et à sa consécutive réticulation pendant le durcissement. Ces connexions ont créé des *scaffolds* uniques à partir

des membranes électrofilées. De plus, les images MEB de la section transversale des *scaffolds* montrent la porosité interne de la paroi, qui est cruciale pour la circulation de l'eau, la signalisation physiologique et l'échange des nutriments. Des essais de délamination ont été effectués pour déterminer la force de connexion de l'intercouche. Les résultats ont montré que les *scaffolds* laminés, lorsqu'ils sont correctement fabriqués, peuvent supporter les mêmes forces que les *scaffolds* directement électrofilés.

Cependant, comme nous avons l'intention d'utiliser ces greffes tubulaires pour une vascularisation rapide en ingénierie tissulaire, créer des structures poreuses avec une taille poreuse pertinente qui permet la migration des cellules endothéliales et l'anastomose du nouveau réseau vasculaire formé a été l'étape clé. Nous avons contacté l'IREPA laser ™, situé à Ilkirch, en France, qui avait déjà établi une collaboration avec Guy Schlatter. Grâce à leurs machines d'usinage laser spécialisées, nous avons pu créer des structures poreuses tout au long des *scaffolds* tubulaires. La morphologie de ces tubes usinés a été visualisée par MEB, qui a montré des *scaffolds* tubulaire très structurés, avec des motifs poreux. Les distances des pores obtenus sont de 0,45 mm pour les pores parallèles et de 0,6 mm pour les pores congrus. Le diamètre des pores était de 150 µm. De plus, les pores présentent eux-mêmes des structures internes poreuses, qui peuvent améliorer l'adhésion et la migration des cellules endothéliales, car elles fournissent des sites de fixation pour les cellules.

Par conséquent, nous avons réussi à obtenir des *scaffolds* tubulaires à partir de membranes électrofilées de polymères bioabsorbables et biodégradables, avec une architecture qui ressemble à la matrice extracellulaire native. Grâce à l'utilisation du pré-PGS, les couches électrofilées ont été fusionnées avec succès pendant la réticulation des *scaffolds* assemblés. Cela permet la fabrication sous forme libre des *scaffolds* d'une grande diversité de formes, pour une diversité d'applications.

Afin de déterminer les propriétés mécaniques des *scaffolds* tubulaires obtenus, établir leur suturabilité et vérifier la force de liaison entre les couches, ainsi que comparer les différents échantillons et évaluer l'influence de l'usinage par laser sur ces propriétés, nous avons effectué divers tests mécaniques par traction uniaxial. Les échantillons non usinés et usinés n'ont pas présenté de différences quant à leur stress à la rupture. Tous les deux types de *scaffolds* obtenus sont très élastiques et sont allongés pour plus de 100% de leur taille d'origine. Cependant, l'allongement à la rupture des *scaffolds* usinés a varié des *scaffolds* non usinés. Nous avons attribué cette caractéristique à la présence de trous, qui a modifié la répartition des forces et, donc, a diminué la résistance des *scaffolds*. Par conséquent, le

module d'élasticité (module d'Young) est plus petit pour les *scaffolds* usinés. Tous les deux types de *scaffolds* tubulaires, non usinés et usinés, ont montré qu'ils étaient suturables. Cependant, la suturabilité est plus petite pour les *scaffolds* usinées par laser. Nous croyons que la structure poreuse a facilité le déchirement dû à la force de la suture. En revanche, la résistance à la rétention des sutures pour les tubes usinés est de $4N/mm^2$, indiquant qu'ils retiennent la suture. Ainsi, tous les *scaffolds*, non usinés et usinés, peuvent être potentiellement employés en tant que greffons vasculaires suturables. Lorsqu'ils sont incorporés dans des greffons obtenus par l'ingénierie tissulaire, le scaffold tubulaire usiné peut servir d'ancrage pour leur fixation correcte par suture, tout en fournissant un flux sanguin instantanément à l'intérieur du tissu biofabriqué.

Pour déterminer si les échafaudages pourraient être stérilisés par autoclavage, nous avons fait une analyse TGA, qui a montré que la dégradation du matériau commence à 200˚C, et sa carbonisation commence à environ 430˚C. Comme l'autoclave est opéré à une température de vapeur de 120˚C, l'analyse TGA indique que les échafaudages sont donc appropriés pour l'autoclavage et, ensuite, c'était notre méthode de stérilisation de choix avant les essais *in vitro*.

L'étape suivante consistait à incorporer les *scaffolds* dans des structures fabriquées en 3D dans la GelMA. Les expériences *in vitro* ont été réalisées à l'Université Fédérale de São Carlos, SP, Brésil, en collaboration avec Dr. Heloísa Selistre de Araujo. Avant l'incorporation du scaffold, la prolifération cellulaire et la viabilité des cellules HUVEC cultivées avec des extraits des membranes ont été évaluées. Les HUVEC ont proliféré au fil du temps avec des extraits de PGS et des milieux de culture cellulaire seule, concluant que le PGS ne libère pas de composés nocifs et, par conséquent, n'a aucun effet cytotoxique. Après 5 jours, la prolifération des cellules HUVEC cultivées dans des extraits de PGS était significativement plus élevée que pour les cellules HUVEC cultivées avec le milieu cellulaire seul. Des images fluorescentes de cellules HUVEC cultivées sur les membranes électrofilées montrent que les cellules HUVEC ont proliféré et se sont adhérés sur les membranes PGS/PVA.

Comme nous avons créé des pores relativement grands par l'usinage à laser sur les greffons tubulaires, permettant donc la migration des cellules endothéliales pour vascularisation rapide, nous avons effectué un ensemencement dynamique sur les constructions 3D en GelMA intégrées avec les *scaffolds* tubulaires usinées. Dans un premier moment, on a utilisé seulement les HUVECs, afin de simuler la migration des cellules endothéliales administré par voie sanguine et pour confirmer s'il y a la migration des HUVEC

vers le GelMA, et également pour établir le structure 3D organisé avec les HUVEC après ce flux de cellules.
Après 24 heures de culture cellulaire, les HUVECs se sont étalées vers la surface externe de la GelMA, puis se sont déplacées et accumulées ensemble en grappes cellulaires, sans structure particulière.

Ensuite, nous avons effectué une co-culture dynamique avec des cellules endothéliales et ostéoblastes dans des *scaffolds* tubulaires/constructions 3D en GelMA, en employant des *scaffolds* tubulaires sans les pores ablatés par laser, d'abord. En raison de l'absence de pores, les HUVECs sont restés bloqués à l'intérieur du scaffold tubulaire et agrégés en grandes structures, au lieu de tubules. Les MG-63 sont restés du côté externe de la région du scaffold, au-dessus de l'hydrogel, et se sont agrégés en grappes sans structure particulière. Ainsi, aucune interaction au sein de ces deux types de cellules n'a été observée.

Cependant, lorsque la même co-culture dynamique avec des cellules endothéliales/ostéoblastes dans des *scaffolds* tubulaires/GelMA 3D hybrides, avec des *scaffolds* tubulaires usinés par laser, des interactions entre les différentes ont pu être observés, suggérant la formation d'unions spécialisées. L'anastomose au sein des grappes HUVECs/MG-63 et la greffe a pu être observée. Et portant, celui c'est le point clé de la vascularisation rapide : fournir un fluxe des cellules endothéliales/sanguines instantanées vers les greffons osseux biofabriqués, tout en favorisant l'anastomose du nouveau réseau capillaire formé. Les implants 3D biofabriqués avec des ostéoblastes peuvent stimuler une formation d'un réseau vasculaire depuis l'hôte, vue qu'il a des études démontrant que les ostéoblastes produisent des facteurs de croissance qui stimulent le recrutement des cellules endothéliales, tandis que la présence du réseau vasculaire augmentera la formation osseuse dans un effet dynamique. Bien que plus de recherche au niveau moléculaire (Polymérase Chain Reverse Transcription ou PCR-rt) est nécessaire pour mieux comprendre comment fonctionne cette diaphonie cellulaire et, ainsi, aider à prédire ce qui se passera une fois que les greffons sont suturés dans l'hôte, cette expérience préliminaire indique déjà que l'architecture des *scaffolds* obtenus par *electrospinning* permettre cette diaphonie, tout en permettant aussi la migration des cellules endothéliales, qui formeront plus tard des réseaux vasculaires qui bénéficieront la vascularisation des constructions osseuses, comme d'autres tissus obtenues par l'ingénierie tissulaire. Par conséquent, ce travail est une étape énorme dans la traduction clinique des greffons tissulaires biofabriqués en 3D. Grâce à notre stratégie, nous prévoyons d'intégrer avec succès ces échafaudages tubulaires et fournir une ancre vasculaire suturable et perméable

qui fournira un sang instantané qui améliorera la survie de l'implant biofabriqué et accélérera la recherche translationnelle de l'ingénierie tissulaire osseuse.

REFERENCES

ADOMAVIČIŪTĖ, E.; MILAŠIUS, R. The influence of applied voltage on poly (vinyl alcohol)(PVA) nanofibre diameter. **Fibres & Textiles in Eastern Europe**, v. 15, n. 5–6, p. 63, 2007.

AGARWAL, S.; WENDORFF, J. H.; GREINER, A. Progress in the field of electrospinning for tissue engineering applications. **Advanced Materials**, v. 21, n. 32–33, p. 3343–3351, 2009.

ALBERTS, B. et al. **Essential cell biology**. Oxford: Garland Science, 2013.

ALGE, D. L.; ANSETH, K. S. Bioactive hydrogels: Lighting the way. **Nature Materials**, v. 12, n. 11, p. 950, 2013.

ALMUBARAK, S. et al. Tissue engineering strategies for promoting vascularized bone regeneration. **Bone**, v. 83, p. 197–209, 2016.

AMINI, A. R.; LAURENCIN, C. T.; NUKAVARAPU, S. P. Bone tissue engineering: recent advances and challenges. **Critical Reviews™ in Biomedical Engineering**, v. 40, n. 5, p. 363-408, 2012.

ANNABI, N. et al. Hydrogel-coated microfluidic channels for cardiomyocyte culture. **Lab on a Chip**, v. 13, n. 18, p. 3569–3577, 2013.

ANNABI, N. et al. 25th anniversary article: Rational design and applications of hydrogels in regenerative medicine. **Advanced materials**, v. 26, n. 1, p. 85–124, 2014.

ARMENTANO, I. et al. Biodegradable polymer matrix nanocomposites for tissue engineering: a review. **Polymer degradation and stability**, v. 95, n. 11, p. 2126–2146, 2010.

ARNAOUTOVA, I. et al. The endothelial cell tube formation assay on basement membrane turns 20: state of the science and the art. **Angiogenesis**, v. 12, n. 3, p. 267–274, 2009.

ARNAOUTOVA, I.; KLEINMAN, H. K. In vitro angiogenesis: endothelial cell tube formation on gelled basement membrane extract. **Nature protocols**, v. 5, n. 4, p. 628, 2010.

ARONSON, J. Temporal and Spatial Increases in Blood Flow During Distraction Osteogenesis. **Clinical Orthopaedics and Related Research**, v. 301, 1994.

ASGHARI, F. et al. Biodegradable and biocompatible polymers for tissue engineering application: a review. **Artificial Cells, Nanomedicine, and biotechnology**, v. 45, n. 2, p. 185–192, 2017.

ASHAMMAKHI, N. et al. Tissue engineering: a new take-off using nanofiber-based scaffolds. **Journal of Craniofacial Surgery**, v. 18, n. 1, p. 3–17, 2007.

ATTIA, A. C. et al. A Review of Nanofiber Shish Kebabs and Their Potential In Creating Effective Biomimetic Bone Scaffolds. **Regenerative Engineering and Translational Medicine**, v. 4, n. 3, p. 107-119, Sept. 2018.

BAJAJ, A. K.; WONGWORAWAT, A. A.; PUNJABI, A. Management of alveolar clefts. **Journal of Craniofacial Surgery**, v. 14, n. 6, p. 840–846, 2003.

BAKER, B. M. et al. The potential to improve cell infiltration in composite fiber-aligned electrospun scaffolds by the selective removal of sacrificial fibers. **Biomaterials**, v. 29, n. 15, p. 2348–2358, 2008.

BAKER, M. I. et al. A review of polyvinyl alcohol and its uses in cartilage and orthopedic applications. **Journal of Biomedical Materials Research Part B: Applied Biomaterials**, v. 100, n. 5, p. 1451–1457, 2012.

BALAJI, S. et al. The role of endothelial progenitor cells in postnatal vasculogenesis: implications for therapeutic neovascularization and wound healing. **Advances in wound care**, v. 2, n. 6, p. 283–295, 2013.

BARNES, C. P. et al. Nanofiber technology: designing the next generation of tissue engineering scaffolds. **Advanced drug delivery reviews**, v. 59, n. 14, p. 1413–33, Dec. 2007.

BASHUR, C. A.; DAHLGREN, L. A.; GOLDSTEIN, A. S. Effect of fiber diameter and orientation on fibroblast morphology and proliferation on electrospun poly(d,l-lactic-co-glycolic acid) meshes. **Biomaterials**, v. 27, n. 33, p. 5681–5688, 1 nov. 2006.

BELLANI, C. F. et al. Morphological, thermal, and mechanical properties of poly(ε-caprolactone)/poly(ε-caprolactone)-grafted-cellulose nanocrystals mats produced by electrospinning. **Journal of Applied Polymer Science**, p. n/a-n/a, fev. 2016.

BENTON, J. A. et al. Photocrosslinking of gelatin macromers to synthesize porous hydrogels that promote valvular interstitial cell function. **Tissue Engineering Part A**, v. 15, n. 11, p. 3221–3230, 2009.

BERTASSONI, L. E. et al. Hydrogel bioprinted microchannel networks for vascularization of tissue engineering constructs. **Lab on a Chip**, v. 14, n. 13, p. 2202–2211, 2014.

BERTHIAUME, F.; MAGUIRE, T.; YARMUSH, M. Tissue engineering and regenerative medicine: history, progress, and challenges. **Annual Review of chemical and biomolecular engineering**, v. 2, p. 403–430, 2011.

BETTINGER, C. J. Biodegradable elastomers for tissue engineering and cell–biomaterial interactions. **Macromolecular Bioscience**, v. 11, n. 4, p. 467–482, 8 abr. 2011.

BILLIET, T. et al. The 3D printing of gelatin methacrylamide cell-laden tissue-engineered constructs with high cell viability. **Biomaterials**, v. 35, n. 1, p. 49–62, 2014.

BOSE, S.; ROY, M.; BANDYOPADHYAY, A. Recent advances in bone tissue engineering scaffolds. **Trends in biotechnology**, v. 30, n. 10, p. 546–54, out. 2012.

BOSKEY, A. L. Biomineralization: conflicts, challenges, and opportunities. **Journal of cellular biochemistry**, v. 72, n. S30–31, p. 83–91, 1998.

BOSSINI, P. S. et al. Biosilicate® and low-level laser therapy improve bone repair in osteoporotic rats. **Journal of Tissue Engineering and Regenerative Medicine**, v. 5, n. 3, p. 229–237, mar. 2011.

BROWDER, T.; FOLKMAN, J.; PIRIE-SHEPHERD, S. The hemostatic system as a regulator of angiogenesis. **Journal of Biological Chemistry**, v. 275, n. 3, p. 1521–1524, 2000.

BROWN, J. M. Vasculogenesis: a crucial player in the resistance of solid tumours to radiotherapy. **The British journal of radiology**, v. 87, n. 1035, p. 20130686, 2014.

BURG, K. J. .; PORTER, S.; KELLAM, J. F. Biomaterial developments for bone tissue engineering. **Biomaterials**, v. 21, n. 23, p. 2347–2359, dez. 2000.

BURSTEIN, N. L. Corneal cytotoxicity of topically applied drugs, vehicles and preservatives. **Survey of ophthalmology**, v. 25, n. 1, p. 15–30, 1980.

CANCEDDA, R. Cartilage and bone extracellular matrix. **Current pharmaceutical design**, v. 15, n. 12, p. 1334–1348, 2009.

CARMELIET, P. Mechanisms of angiogenesis and arteriogenesis.**Nature medicine**, v. 6, n. 3, p. 389-395, Mar. 2000.

CASTILLO-DALI, G. et al. In vivo comparative model of oxygen plasma and nanocomposite particles on PLGA membranes for guided bone regeneration processes to be applied in pre-prosthetic surgery: a pilot study. **Journal of dentistry**, v. 42, n. 11, p. 1446–1457, 2014.

CHA, C. et al. Microfluidics-assisted fabrication of gelatin-silica core–shell microgels for injectable tissue constructs. **Biomacromolecules**, v. 15, n. 1, p. 283–290, 2014.

CHANDRA, R.; RUSTGI, R. Biodegradable polymers. **Progress in polymer science**, v. 23, n. 7, p. 1273–1335, 1998.

CHAOUAT, M. et al. A Novel Cross-linked Poly(vinyl alcohol) (PVA) for Vascular Grafts. **Advanced Functional Materials**, v. 18, n. 19, p. 2855–2861, out. 2008.

CHAPPUIS, V. et al. Effectiveness of contour augmentation with guided bone regeneration: 10-year results. **Journal of dental research**, p. 0022034517737755, 2017.

CLAVERO, J.; LUNDGREN, S. Ramus or chin grafts for maxillary sinus inlay and local onlay augmentation: comparison of donor site morbidity and complications. **Clinical Implant Dentistry and Related Research**, v. 5, n. 3, p. 154–160, 2003.

CLOVER, J.; GOWEN, M. Are MG-63 and HOS TE85 human osteosarcoma cell lines representative models of the osteoblastic phenotype? **Bone**, v. 15, n. 6, p. 585–591, 1994.

CORREIA, C. et al. In Vitro Model of Vascularized Bone: Synergizing Vascular Development and Osteogenesis. **PLoS ONE**, v. 6, n. 12, p. e28352, 2 dez. 2011.

CRESCENZI, V. et al. Thermodynamics of fusion of poly-β-propiolactone and poly-ϵ-caprolactone. comparative analysis of the melting of aliphatic polylactone and polyester chains. **European Polymer Journal**, v. 8, n. 3, p. 449–463, mar. 1972.

CROVACE, M. C. et al. Biosilicate®—A multipurpose, highly bioactive glass-ceramic. In vitro, in vivo and clinical trials. **Journal of Non-Crystalline Solids**, v. 432, p. 90–110, 2016.

CROWDER, S. W. et al. Poly(ε-caprolactone)–carbon nanotube composite scaffolds for enhanced cardiac differentiation of human mesenchymal stem cells. **Nanomedicine**, v. 8, n. 11, p. 1763–1776, out. 2013.

CUI, H. et al. Hierarchical fabrication of engineered vascularized bone biphasic constructs via dual 3D bioprinting: integrating regional bioactive factors into architectural design. **Advanced healthcare materials**, v. 5, n. 17, p. 2174–2181, 2016.

CZEKANSKA, E. M. Assessment of cell proliferation with resazurin-based fluorescent dye. In: STODDART, M.J. (Ed.). **MammalianCell Viability**. [s.l.]: Springer, 2011. p. 27–32.

D. DESHPANDE, H. et al. Carbon Nanofiber Reinforced Polycaprolactone Fibrous Meshes by Electrostatic Co-spinning. **Current Nanoscience**, v. 8, n. 5, p. 753–761, 2012.

DAHL, S. L. M. et al. Readily Available Tissue-Engineered Vascular Grafts. **Science Translational Medicine**, v. 3, n. 68, p. 68ra9-68ra9, 2 fev. 2011.

DAI, X. et al. Coaxial 3D bioprinting of self-assembled multicellular heterogeneous tumor fibers. **Scientific reports**, v. 7, n. 1, p. 1457, 2017.

DAMIEN, C. J.; PARSONS, J. R. Bone graft and bone graft substitutes: a review of current technology and applications. **Journal of Applied Biomaterials**, v. 2, n. 3, p. 187–208, 1991.

DE MESQUITA, J. P. et al. Hybrid layer-by-layer assembly based on animal and vegetable structural materials: multilayered films of collagen and cellulose nanowhiskers. **Soft Matter**, v. 7, n. 9, p. 4405–4405, abr. 2011.

DE SOUZA LIMA, M. M.; BORSALI, R. Rodlike cellulose microcrystals: structure, properties, and applications. **Macromolecular rapid communications**, v. 25, n. 7, p. 771–787, 2004.

DE VOLDER, M. F. L. et al. Carbon Nanotubes: Present and Future Commercial Applications. **Science**, v. 339,

p. 535–539, 2013.

DELLOYE, C. et al. Bone allografts: what they can offer and what they cannot. **Bone & Joint Journal**, v. 89, n. 5, p. 574–580, 2007.

DEMERLIS, C. C.; SCHONEKER, D. R. Review of the oral toxicity of polyvinyl alcohol (PVA). **Food and Chemical Toxicology**, v. 41, n. 3, p. 319–326, 2003.

DERBY, B. Printing and prototyping of tissues and scaffolds. **Science**, v. 338, n. 6109, p. 921–926, 2012.

DIBA, M. et al. Preparation and characterization of polycaprolactone/forsterite nanocomposite porous scaffolds designed for bone tissue regeneration. **Composites Science and Technology**, v. 72, n. 6, p. 716–723, mar. 2012.

DO, A.-V. et al. 3D printing of scaffolds for tissue regeneration applications. **Advanced healthcare materials**, v. 4, n. 12, p. 1742–1762, 2015.

DOSHI, J.; RENEKER, D. H. Electrospinning process and applications of electrospun fibers. **Journal of electrostatics**, v. 35, n. 2–3, p. 151–160, 1995.

EHRBAR, M. et al. Enzymatic formation of modular cell-instructive fibrin analogs for tissue engineering. **Biomaterials**, v. 28, n. 26, p. 3856–3866, 2007.

EICHHORN, S. J. et al. current international research into cellulose nanofibres and nanocomposites. **Journal of materials science**, v. 45, n. 1, p. 1, 2010.

ENAYATI, M. S. et al. Development of electrospun poly (vinyl alcohol)-based bionanocomposite scaffolds for bone tissue engineering. **Journal of Biomedical Materials Research Part A**, v. 106, n. 4, p. 1111–1120, 2018.

ENGLER, A. J. et al. Matrix elasticity directs stem cell lineage specification. **Cell**, v. 126, n. 4, p. 677–689, 2006.

ERRINGTON, R. J. **Advanced practical inorganic and metalorganic chemistry**. [s.l.]: CRC, 1997.

FATIH CANBOLAT, M. et al. Mammalian Cell Viability in Electrospun Composite Nanofiber Structures. **Macromolecular Bioscience**, v. 11, n. 10, p. 1346–1356, 2011.

FERNANDEZ-YAGUE, M. A. et al. Biomimetic approaches in bone tissue engineering: Integrating biological and physicomechanical strategies. **Advanced drug delivery reviews**, v. 84, p. 1–29, 2015.

FERRIS, C. J.; GILMORE, K. G.; WALLACE, G. G. Biofabrication: an overview of the approaches used for printing of living cells. **Applied microbiology and biotechnology**, v. 97, n. 10, p. 4243–4258, 2013.

FRAISL, P. et al. Regulation of angiogenesis by oxygen and metabolism. **Developmental cell**, v. 16, n. 2, p. 167–179, 2009.

FREED, L. et al. Biodegradable polymer scaffolds for tissue engineering. **Biotechnology (N Y)**, v. 12, p. 689–693, 1994.

FUCHS, S.; HOFMANN, A.; KIRKPATRICK, C. J. Microvessel-like structures from outgrowth endothelial cells from human peripheral blood in 2-dimensional and 3-dimensional co-cultures with osteoblastic lineage cells. **Tissue engineering**, v. 13, n. 10, p. 2577–2588, 2007.

FURUMATSU, T. et al. Vascular endothelial growth factor principally acts as the main angiogenic factor in the early stage of human osteoblastogenesis. **Journal of biochemistry**, v. 133, n. 5, p. 633–639, 2003.

GAHARWAR, A. K. et al. Nanoclay-enriched poly (ε-caprolactone) electrospun scaffolds for osteogenic differentiation of human mesenchymal stem cells. **Tissue Engineering Part A**, v. 20, n. 15–16, p. 2088–2101, 2014.

GARIPCAN, B. et al. Image analysis of endothelial microstructure and endothelial cell dimensions of human arteries–a preliminary study. **Advanced Engineering Materials**, v. 13, n. 1-2, 2011.

GAUVIN, R. et al. Microfabrication of complex porous tissue engineering scaffolds using 3D projection stereolithography. **Biomaterials**, v. 33, n. 15, p. 3824–3834, 2012.

GHASEMI-MOBARAKEH, L. et al. Electrospun poly(epsilon-caprolactone)/gelatin nanofibrous scaffolds for nerve tissue engineering. **Biomaterials**, v. 29, n. 34, p. 4532–9, dez. 2008.

GIBBS, D. M. et al. Hope versus hype: what can additive manufacturing realistically offer trauma and orthopedic surgery? **Regenerative medicine**, v. 9, n. 4, p. 535–549, 2014.

GOMES, M. E. et al. Tissue Engineering and Regenerative Medicine: New Trends and Directions—A Year in Review. **Tissue Engineering Part B: Reviews**, v. 23, n. 3, p. 211–224, 2017.

GOODWIN, A. M. In vitro assays of angiogenesis for assessment of angiogenic and anti-angiogenic agents. **Microvascular research**, v. 74, n. 2–3, p. 172–183, 2007.

GOTTLIEB, D. et al. In vivo monitoring of function of autologous engineered pulmonary valve. **The Journal of thoracic and cardiovascular surgery**, v. 139, n. 3, p. 723–731, 2010.

GOUSSÉ, C. et al. Stable suspensions of partially silylated cellulose whiskers dispersed in organic solvents. **Polymer**, v. 43, n. 9, p. 2645–2651, 2002.

GRANITO, R. N. et al. Effects of biosilicate and bioglass 45S5 on tibial bone consolidation on rats: a biomechanical and a histological study. **Journal of Materials Science: Materials in Medicine**, v. 20, n. 12, p. 2521–2526, 2009.

GREGORY, C. A. et al. An Alizarin red-based assay of mineralization by adherent cells in culture: comparison with cetylpyridinium chloride extraction. **Analytical biochemistry**, v. 329, n. 1, p. 77–84, 2004.

GREINER, A.; WENDORFF, J. H. Electrospinning: a fascinating method for the preparation of ultrathin fibers. **Angewandte Chemie (International ed. in English)**, v. 46, n. 30, p. 5670–703, jan. 2007.

GRIFFITH, L. G.; NAUGHTON, G. Tissue engineering--current challenges and expanding opportunities. **science**, v. 295, n. 5557, p. 1009–1014, 2002.

GRIGORE, A. et al. Behavior of encapsulated MG-63 cells in RGD and gelatine-modified alginate hydrogels. **Tissue Engineering Part A**, v. 20, n. 15–16, p. 2140–2150, 2014.

GROLL, J. et al. Biofabrication: reappraising the definition of an evolving field. **Biofabrication**, v. 8, n. 1, p. 013001, 2016.

GUESS, G.; KRATCHMAN, S.; KIM, S. Guided Tissue Regeneration in Endodontic Microsurgery. **Microsurgery in Endodontics, First Edition**, p. 193–203, 2018.

HABIBI, Y. et al. Bionanocomposites based on poly(ε-caprolactone)-grafted cellulose nanocrystals by ring-opening polymerization. **Journal of Materials Chemistry**, v. 18, n. 41, p. 5002–5002, out. 2008.

HABIBI, Y. Key advances in the chemical modification of nanocelluloses. **Chemical Society reviews**, v. 43, n. 5, p. 1519–42, mar. 2014.

HAJIALI, F.; TAJBAKHSH, S.; SHOJAEI, A. Fabrication and properties of polycaprolactone composites containing calcium phosphate-based ceramics and bioactive glasses in bone tissue engineering: a review. **Polymer Reviews**, v. 58, n. 1, p. 164–207, 2018.

HASAN, A. et al. Electrospun scaffolds for tissue engineering of vascular grafts. **Acta biomaterialia**, v. 10, n. 1, p. 11–25, jan. 2014.

HASHI, C. K. et al. Antithrombogenic Modification of Small-Diameter Microfibrous Vascular Grafts. **Arteriosclerosis, Thrombosis, and Vascular Biology** , v. 30, n. 8, p. 1621–1627, 1 ago. 2010.

HASSAN, C. M.; PEPPAS, N. A. Structure and applications of poly (vinyl alcohol) hydrogels produced by conventional crosslinking or by freezing/thawing methods. In: **Biopolymers· PVA Hydrogels, Anionic Polymerisation Nanocomposites**. [s.l.] Springer, 2000. p. 37–65.

HENCH, L. L. Glass and genes: The 2001 W. E. S. Turner Memorial Lecture. **Glass Technology**, v. 44, n. 1, p. 1–10, 2003.

HEO, D. N. et al. Enhanced bone regeneration with a gold nanoparticle–hydrogel complex. **Journal of Materials Chemistry B**, v. 2, n. 11, p. 1584–1593, 2014.

HEYDARI, P. et al. Preparation and evaluation of poly glycerol sebacate/poly hydroxy butyrate core-shell electrospun nanofibers with sequentially release of ciprofloxacin and simvastatin in wound dressings. **Polymers for Advanced Technologies**, 2018.

HILLIER, M. L.; BELL, L. S. Differentiating human bone from animal bone: a review of histological methods. **Journal of forensic sciences**, v. 52, n. 2, p. 249–263, 2007.

HOERSTRUP, S. P. et al. Functional living trileaflet heart valves grown in vitro. **Circulation**, v. 102, n. suppl 3, p. Iii-44- Iii–49, 2000.

HOFMANN, A. et al. The effect of human osteoblasts on proliferation and neo-vessel formation of human umbilical vein endothelial cells in a long-term 3D co-culture on polyurethane scaffolds. **Biomaterials**, v. 29, n. 31, p. 4217–4226, 1 nov. 2008.

HOLLISTER, S. J. Porous scaffold design for tissue engineering. **Nature materials**, v. 4, n. 7, p. 518, 2005.

HOREJS, C.-M. et al. Mimicking the extracellular matrix–a biomaterials approach to inhibit tissue fibrosis. 2016.

HOSSEINI, V. et al. Fiber-Assisted Molding (FAM) of Surfaces with Tunable Curvature to Guide Cell Alignment and Complex Tissue Architecture. **Small**, v. 10, n. 23, p. 4851–4857, 2014.

HOTZA, D. et al. Influência da adição de defloculante, ligante e partículas de alumina no comportamento reológico de suspensões a base de frita e caulim. **Química Nova**, v. 21, n. 4, p. 526–528, 1998.

HRISTOV, V. et al. Organic/inorganic bioactive materials Part I: Synthesis, structure and in vitro assessment of collagen/silicocarnotite biocoatings. **Central European Journal of Chemistry**, v. 7, n. 4, p. 702, 2009.

HU, J. et al. Electrospinning of poly (glycerol sebacate)-based nanofibers for nerve tissue engineering. **Materials Science and Engineering: C**, v. 70, p. 1089–1094, 2017.

HUANG, H. et al. Avidin–biotin binding-based cell seeding and perfusion culture of liver-derived cells in a porous scaffold with a three-dimensional interconnected flow-channel network. **Biomaterials**, v. 28, n. 26, p. 3815–3823, 2007.

HULSART-BILLSTRÖM, G. et al. A surprisingly poor correlation between in vitro and in vivo testing of biomaterials for bone regeneration: results of a multicentre analysis. 2017.

HUTMACHER, D. W.; WOODFIELD, T. B.; DALTON, P. D. Scaffold design and fabrication. In: **Tissue Engineering (Second Edition)**. [s.l.] Elsevier, 2015. p. 311–346.

HUTSON, C. B. et al. Synthesis and characterization of tunable poly (ethylene glycol): gelatin methacrylate composite hydrogels. **Tissue Engineering Part A**, v. 17, n. 13–14, p. 1713–1723, 2011.

HYNES, R. O. The extracellular matrix: not just pretty fibrils. **Science**, v. 326, n. 5957, p. 1216–1219, 2009.

INGAVLE, G. C.; LEACH, J. K. Advancements in electrospinning of polymeric nanofibrous scaffolds for tissue engineering. **Tissue Engineering Part B: Reviews**, v. 20, n. 4, p. 277–293, 2013.

ISENBERG, B. C.; WILLIAMS, C.; TRANQUILLO, R. T. Small-Diameter Artificial Arteries Engineered In Vitro. **Circulation Research** , v. 98, n. 1, p. 25–35, 6 jan. 2006.

JACKSON, J. K. et al. The use of nanocrystalline cellulose for the binding and controlled release of drugs. **International Journal of Nanomedicine**, v. 6, p. 321–330, fev. 2011.

JAFARIAN, M. et al. Marrow-derived mesenchymal stem cells-directed bone regeneration in the dog mandible: a comparison between biphasic calcium phosphate and natural bone mineral. **Oral surgery, oral medicine, oral pathology, oral radiology, and endodontics**, v. 105, n. 5, p. e14-24, maio 2008.

JAIN, R. K. et al. Engineering vascularized tissue. **Nat Biotech**, v. 23, n. 7, p. 821–823, jul. 2005.

JANG, J.-H.; CASTANO, O.; KIM, H.-W. Electrospun materials as potential platforms for bone tissue engineering. **Advanced drug delivery reviews**, v. 61, n. 12, p. 1065–1083, 2009.

JEFFRIES, E. M. et al. Highly elastic and suturable electrospun poly(glycerol sebacate) fibrous scaffolds. **Acta biomaterialia**, v. 18, p. 30–9, maio 2015.

JIA, L. et al. Stem cell differentiation on electrospun nanofibrous substrates for vascular tissue engineering. **Materials science & engineering. C, Materials for biological applications**, v. 33, n. 8, p. 4640–50, 1 dez. 2013.

JIANG, S. et al. Electrospun nanofiber reinforced composites: a review. **Polymer Chemistry**, 2018.

JOSHI, M. K. et al. In situ generation of cellulose nanocrystals in polycaprolactone nanofibers: effects on crystallinity, mechanical strength, biocompatibility, and biomimetic mineralization. **ACS applied materials & interfaces**, v. 7, n. 35, p. 19672–19683, 2015.

KANG, Y. et al. Osteogenic and angiogenic potentials of monocultured and co-cultured human-bone-marrow-derived mesenchymal stem cells and human-umbilical-vein endothelial cells on three-dimensional porous beta-tricalcium phosphate scaffold. **Acta biomaterialia**, v. 9, n. 1, p. 4906–15, jan. 2013a.

KANG, Y. et al. Osteogenic and angiogenic potentials of monocultured and co-cultured human-bone-marrow-derived mesenchymal stem cells and human-umbilical-vein endothelial cells on three-dimensional porous beta-tricalcium phosphate scaffold. **Acta biomaterialia**, v. 9, n. 1, p. 4906–15, jan. 2013b.

KANG, Y. et al. Engineering a vascularized collagen-β-tricalcium phosphate graft using an electrochemical approach. **Acta biomaterialia**, v. 11, p. 449–58, jan. 2015.

KANNAN, R. Y. et al. The roles of tissue engineering and vascularisation in the development of micro-vascular networks: a review. **Biomaterials**, v. 26, n. 14, p. 1857–1875, maio 2005.

KAUSHAL, S. et al. Functional small-diameter neovessels created using endothelial progenitor cells expanded ex vivo. **Nature medicine**, v. 7, n. 9, p. 1035–1040, 2001.

KAYAT, J. et al. Pulmonary toxicity of carbon nanotubes: a systematic report. **Nanomedicine : nanotechnology, biology, and medicine**, v. 7, n. 1, p. 40–9, fev. 2011.

KENAR, H.; KOSE, G. T.; HASIRCI, V. Design of a 3D aligned myocardial tissue construct from biodegradable polyesters. **Journal of Materials Science: Materials in Medicine**, v. 21, n. 3, p. 989–997, 2010.

KIM, E.-S.; KIM, J.-J.; PARK, E.-J. Angiogenic factor-enriched platelet-rich plasma enhances in vivo bone formation around alloplastic graft material. **J Adv Prosthodont**, v. 2, n. 1, p. 7–13, mar. 2010.

KIM, G.-M. et al. Electrospinning of PCL/PVP blends for tissue engineering scaffolds. **Journal of materials**

science. Materials in medicine, v. 24, n. 6, p. 1425–42, jun. 2013.

KIM, H.-W.; KIM, H.-E. Nanofiber generation of hydroxyapatite and fluor-hydroxyapatite bioceramics. **Journal of Biomedical Materials Research Part B: Applied Biomaterials**, v. 77, n. 2, p. 323–328, 2006.

KIM, H.-W.; LEE, H.-H.; CHUN, G.-S. Bioactivity and osteoblast responses of novel biomedical nanocomposites of bioactive glass nanofiber filled poly (lactic acid). **Journal of biomedical materials research Part A**, v. 85, n. 3, p. 651–663, 2008.

KIRKPATRICK, C. J. et al. Physiology and cell biology of the endothelium: a dynamic interface for cell communication. **International Journal of Microcirculation**, v. 17, n. 5, p. 231–240, 1997.

KISHAN, A. P.; COSGRIFF-HERNANDEZ, E. M. Recent advancements in electrospinning design for tissue engineering applications: a review. **Journal of Biomedical Materials Research Part A**, 2017.

KLENKE, F. M. et al. Impact of pore size on the vascularization and osseointegration of ceramic bone substitutes in vivo. **Journal of Biomedical Materials Research Part A**, v. 85A, n. 3, p. 777–786, 1 jun. 2008.

KLOTZ, B. J. et al. Gelatin-Methacryloyl Hydrogels: Towards Biofabrication-Based Tissue Repair. **Trends in Biotechnology**, v. 34, n. 5, p. 394–407, 1 maio 2016.

KNESER, U. et al. Evaluation of processed bovine cancellous bone matrix seeded with syngenic osteoblasts in a critical size calvarial defect rat model. **Journal of Cellular and Molecular Medicine**, v. 10, n. 3, p. 695–707, 1 jul. 2006.

KOKUBO, T. et al. Apatite formation on non-woven fabric of carboxymethylated chitin in SBF. **Biomaterials**, v. 25, n. 18, p. 4485–8, ago. 2004.

KOONS, K. C. et al. **Turbulence in Saphenous Vein Bypass Grafts by Duplex Ultrasound Imaging**. [s.l.] Am Heart Assoc, 2015.

KROUIT, M.; BRAS, J.; BELGACEM, M. N. Cellulose surface grafting with polycaprolactone by heterogeneous click-chemistry. **European Polymer Journal**, v. 44, n. 12, p. 4074–4081, dez. 2008.

KUMACHEV, A. et al. High-throughput generation of hydrogel microbeads with varying elasticity for cell encapsulation. **Biomaterials**, v. 32, n. 6, p. 1477–1483, 2011.

KÜMMERER, K. et al. Biodegradability of organic nanoparticles in the aqueous environment. **Chemosphere**, v. 82, n. 10, p. 1387–92, mar. 2011.

KURIEN, T.; PEARSON, R. G.; SCAMMELL, B. E. Bone graft substitutes currently available in orthopaedic practice: the evidence for their use. **Bone Joint Journal**, v. 95, n. 5, p. 583–597, 2013.

KYRIAKIDOU, K. et al. Dynamic co-seeding of osteoblast and endothelial cells on 3D polycaprolactone scaffolds for enhanced bone tissue engineering. **Journal of bioactive and compatible polymers**, v. 23, n. 3, p. 227–243, 2008.

LABET, M.; THIELEMANS, W. Synthesis of polycaprolactone: a review. **Chemical Society Reviews**, v. 38, n. 12, p. 3484–3504, 2009a.

LABET, M.; THIELEMANS, W. Synthesis of polycaprolactone: a review. **Chemical Society Reviews**, v. 38, n. 12, p. 3484–3504, 2009b.

LAM, E. et al. Applications of functionalized and nanoparticle-modified nanocrystalline cellulose. **Trends in biotechnology**, v. 30, n. 5, p. 283–90, maio 2012.

LANGER, R.; VACANTI, J. P. Tissue engineering. **Science**, v. 260, n. 5110, p. 920–926, maio 1993.

LEACH, J. K.; MOONEY, D. J. Bone engineering by controlled delivery of osteoinductive molecules and cells.

Expert opinion on biological therapy, v. 4, n. 7, p. 1015–1027, 2004.

LEE, B. L.-P. et al. Femtosecond laser ablation enhances cell infiltration into three-dimensional electrospun scaffolds. **Acta Biomaterialia**, v. 8, n. 7, p. 2648–2658, 1 jul. 2012.

LEVATO, R. et al. Biofabrication of tissue constructs by 3D bioprinting of cell-laden microcarriers. **Biofabrication**, v. 6, n. 3, p. 035020, 2014.

L'HEUREUX, N. et al. Human tissue-engineered blood vessels for adult arterial revascularization. **Nat Med**, v. 12, n. 3, p. 361–365, mar. 2006a.

L'HEUREUX, N. et al. Human tissue-engineered blood vessels for adult arterial revascularization. **Nat Med**, v. 12, n. 3, p. 361–365, mar. 2006b.

LI, X. et al. Nanostructured scaffolds for bone tissue engineering. **Journal of Biomedical Materials Research Part A**, v. 101, n. 8, p. 2424–2435, 2013.

LI, X. et al. Criteria for Quick and Consistent Synthesis of Poly(glycerol sebacate) for Tailored Mechanical Properties. **Biomacromolecules**, v. 16, n. 5, p. 1525–1533, 11 maio 2015.

LIM, Y. C. et al. Micropatterning and characterization of electrospun poly (ε-caprolactone)/gelatin nanofiber tissue scaffolds by femtosecond laser ablation for tissue engineering applications. **Biotechnology and bioengineering**, v. 108, n. 1, p. 116–126, 2011.

LIN, H. et al. Cartilage tissue engineering application of injectable gelatin hydrogel with in situ visible-light-activated gelation capability in both air and aqueous solution. **Tissue Engineering Part A**, v. 20, n. 17–18, p. 2402–2411, 2014.

LIN, N.; DUFRESNE, A. Nanocellulose in biomedicine: Current status and future prospect. **European Polymer Journal**, v. 59, p. 302–325, ago. 2014.

LIN, R.-Z. et al. Transdermal regulation of vascular network bioengineering using a photopolymerizable methacrylated gelatin hydrogel. **Biomaterials**, v. 34, n. 28, p. 6785–6796, 2013.

LIND, J. U. et al. Instrumented cardiac microphysiological devices via multimaterial three-dimensional printing. **Nature materials**, v. 16, n. 3, p. 303, 2017.

LIU, Y. et al. Understanding the Toxicity of Carbon Nanotubes. **Accounts of Chemical Research**, v. 46, n. 3, p. 702–713, mar. 2013.

LJUNGBERG, N. et al. New nanocomposite materials reinforced with cellulose whiskers in atactic polypropylene: effect of surface and dispersion characteristics. **Biomacromolecules**, v. 6, n. 5, p. 2732–2739, 2005.

LÖNNBERG, H. et al. Synthesis of Polycaprolactone-Grafted Microfibrillated Cellulose for Use in Novel Bionanocomposites–Influence of the Graft Length on the Mechanical Properties. **ACS Applied Materials & Interfaces**, v. 3, n. 5, p. 1426–1433, maio 2011.

LU, H. et al. Electrospun submicron bioactive glass fibers for bone tissue scaffold. **Journal of Materials Science: Materials in Medicine**, v. 20, n. 3, p. 793–798, 2009.

LUCIANI, A. et al. PCL microspheres based functional scaffolds by bottom-up approach with predefined microstructural properties and release profiles. **Biomaterials**, v. 29, n. 36, p. 4800–4807, 2008.

LUKOWIAK, A. et al. Bioactive glass nanoparticles obtained through sol-gel chemistry. **Chemical communications (Cambridge, England)**, v. 49, n. 59, p. 6620–2, 2013.

LUO, C. J.; STRIDE, E.; EDIRISINGHE, M. Mapping the influence of solubility and dielectric constant on

electrospinning polycaprolactone solutions. **Macromolecules**, v. 45, n. 11, p. 4669–4680, 2012.

LUO, Y.; LODE, A.; GELINSKY, M. Direct Plotting of Three-Dimensional Hollow Fiber Scaffolds Based on Concentrated Alginate Pastes for Tissue Engineering. **Advanced healthcare materials**, v. 2, n. 6, p. 777–783, 2013.

LUTOLF, M. P.; HUBBELL, J. A. Synthetic biomaterials as instructive extracellular microenvironments for morphogenesis in tissue engineering. **Nature biotechnology**, v. 23, n. 1, p. 47, 2005.

MADDEN, L. R. et al. Proangiogenic scaffolds as functional templates for cardiac tissue engineering. **Proceedings of the National Academy of Sciences** , v. 107, n. 34, p. 15211–15216, 24 ago. 2010.

MAHMOUD, K. A. et al. Effect of Surface Charge on the Cellular Uptake and Cytotoxicity of Fluorescent Labeled Cellulose Nanocrystals. **ACS Applied Materials & Interfaces**, v. 2, n. 10, p. 2924–2932, out. 2010.

MANSOUR, A. et al. Extracellular matrices for bone regeneration: a literature review. **Tissue Engineering Part A**, v. 23, n. 23–24, p. 1436–1451, 2017.

MARRAZZO, C.; DI MAIO, E.; IANNACE, S. Conventional and nanometric nucleating agents in poly (ϵ-caprolactone) foaming: Crystals vs. bubbles nucleation. **Polymer Engineering & Science**, v. 48, n. 2, p. 336–344, 2008.

MASOUMI, N. et al. Electrospun PGS: PCL microfibers align human valvular interstitial cells and provide tunable scaffold anisotropy. **Advanced healthcare materials**, v. 3, n. 6, p. 929–939, 2014.

MASTERS, J. R. Human cancer cell lines: fact and fantasy. **Nature reviews Molecular cell biology**, v. 1, n. 3, p. 233, 2000.

MATHEWS, D. T. et al. Vascular cell viability on polyvinyl alcohol hydrogels modified with water-soluble and -insoluble chitosan. **Journal of Biomedical Materials Research Part B: Applied Biomaterials**, v. 84B, n. 2, p. 531–540, 2008.

MATTIOLI-BELMONTE, M. et al. Tuning polycaprolactone–carbon nanotube composites for bone tissue engineering scaffolds. **Materials Science and Engineering: C**, v. 32, n. 2, p. 152–159, mar. 2012.

MCCULLEN, S. D. et al. Laser Ablation Imparts Controlled Micro-Scale Pores in Electrospun Scaffolds for Tissue Engineering Applications. **Annals of Biomedical Engineering**, v. 39, n. 12, p. 3021, 17 ago. 2011.

MCKEON-FISCHER, K. D.; FLAGG, D. H.; FREEMAN, J. W. Coaxial electrospun poly(ε-caprolactone), multiwalled carbon nanotubes, and polyacrylic acid/polyvinyl alcohol scaffold for skeletal muscle tissue engineering. **Journal of Biomedical Materials Research Part A**, v. 99A, n. 3, p. 493–499, 2011.

MEHTA, M. et al. Biomaterial delivery of morphogens to mimic the natural healing cascade in bone. **Advanced drug delivery reviews**, v. 64, n. 12, p. 1257–1276, 2012.

MELCHELS, F. P. et al. Development and characterisation of a new bioink for additive tissue manufacturing. **Journal of Materials Chemistry B**, v. 2, n. 16, p. 2282–2289, 2014.

MORELLI, C. L. et al. **Extraction and characterization of cellulose nanowhiskers from balsa wood**. Macromolecular Symposia. **Anais**...Wiley Online Library, 2012

MORONI, L. et al. Polymer hollow fiber three-dimensional matrices with controllable cavity and shell thickness. **Biomaterials**, v. 27, n. 35, p. 5918–5926, 2006.

MORONI, L. et al. Biofabrication strategies for 3D in vitro models and regenerative medicine. **Nature Reviews Materials**, v. 3, n. 5, 2018.

MOURA, J. et al. In vitro osteogenesis on a highly bioactive glass-ceramic (Biosilicate®). **Journal of**

Biomedical Materials Research Part A, v. 82A, n. 3, p. 545–557, set. 2007.

MURPHY, S. V.; ATALA, A. 3D bioprinting of tissues and organs. **Nature biotechnology**, v. 32, n. 8, p. 773, 2014.

NAGHIZADEH, F. et al. The fabrication and characterization of PCL/rice husk derived bioactive glass-ceramic composite scaffolds. **Journal of Nanomaterials**, v. 2014, p. 4, 2014.

NAIR, L. S.; LAURENCIN, C. T. Biodegradable polymers as biomaterials. **Progress in polymer science**, v. 32, n. 8–9, p. 762–798, 2007.

NAM, J. et al. Improved cellular infiltration in electrospun fiber via engineered porosity. **Tissue engineering**, v. 13, n. 9, p. 2249–2257, 2007.

NEDJARI, S. et al. Electrospun Honeycomb as Nests for Controlled Osteoblast Spatial Organization. **Macromolecular Bioscience**, v. 14, n. 11, p. 1580–1589, nov. 2014.

NGADIMAN, N. H. A. et al. A review of evolution of electrospun tissue engineering scaffold: From two dimensions to three dimensions. **Proceedings of the Institution of Mechanical Engineers, Part H: Journal of Engineering in Medicine**, v. 231, n. 7, p. 597–616, 2017.

NGUYEN, L. H. et al. Vascularized Bone Tissue Engineering: Approaches for Potential Improvement. **Tissue Engineering Part B: Reviews**, v. 18, n. 5, p. 363–382, jul. 2012a.

NGUYEN, L. H. et al. Vascularized Bone Tissue Engineering: Approaches for Potential Improvement. **Tissue Engineering Part B: Reviews**, v. 18, n. 5, p. 363–382, 6 jul. 2012b.

NICHOL, J. W. et al. Cell-laden microengineered gelatin methacrylate hydrogels. **Biomaterials**, v. 31, n. 21, p. 5536–44, jul. 2010.

NICHOL, J. W.; KHADEMHOSSEINI, A. Modular tissue engineering: engineering biological tissues from the bottom up. **Soft matter**, v. 5, n. 7, p. 1312–1319, 2009.

NIKKHAH, M. et al. Directed endothelial cell morphogenesis in micropatterned gelatin methacrylate hydrogels. **Biomaterials**, v. 33, n. 35, p. 9009–9018, 2012.

NIKLASON, L. E. et al. Functional Arteries Grown in Vitro. **Science**, v. 284, n. 5413, p. 489–493, 16 abr. 1999.

NIRMALA, R. et al. Structural, thermal, mechanical and bioactivity evaluation of silver-loaded bovine bone hydroxyapatite grafted poly(ε-caprolactone) nanofibers via electrospinning. **Surface and Coatings Technology**, v. 205, n. 1, p. 174–181, set. 2010.

NISHINO, T.; TAKANO, K.; NAKAMAE, K. Elastic modulus of the crystalline regions of cellulose polymorphs. **Journal of Polymer Science Part B**: polymer physics, v. 33, n. 11, p. 1647–1651, 1995.

NOVOSEL, E. C.; KLEINHANS, C.; KLUGER, P. J. Vascularization is the key challenge in tissue engineering. **Advanced drug delivery reviews**, v. 63, n. 4–5, p. 300–311, 2011.

O'BRIEN, C. M. et al. Three-dimensional printing of nanomaterial scaffolds for complex tissue regeneration. **Tissue Engineering Part B: Reviews**, v. 21, n. 1, p. 103–114, 2014.

OCCHETTA, P. et al. VA-086 methacrylate gelatine photopolymerizable hydrogels: A parametric study for highly biocompatible 3D cell embedding. **Journal of Biomedical Materials Research Part A**, v. 103, n. 6, p. 2109–2117, 2015.

OKADA, M. Chemical syntheses of biodegradable polymers. **Progress in polymer science**, v. 27, n. 1, p. 87–133, 2002.

OKSMAN, K. et al. Manufacturing process of cellulose whiskers/polylactic acid nanocomposites. **Composites**

Science and Technology, v. 66, n. 15, p. 2776–2784, dez. 2006.

OLSZTA, M. J. et al. Bone structure and formation: a new perspective. **Materials Science and Engineering: R: Reports**, v. 58, n. 3–5, p. 77–116, 2007.

ORYAN, A. et al. Bone regenerative medicine: classic options, novel strategies, and future directions. **Journal of orthopaedic surgery and research**, v. 9, n. 1, p. 18, 2014.

OSTADAL, B. et al. Ontogenetic differences in cardiopulmonary adaptation to chronic hypoxia. **Physiological research**, v. 44, n. 1, p. 45–51, 1995.

O'SULLIVAN, A. C. Cellulose: the structure slowly unravels. **Cellulose**, v. 4, n. 3, p. 173–207, 1997.

PAN, L. et al. Multiwall carbon nanotubes/polycaprolactone composites for bone tissue engineering application. **Colloids and surfaces. B, Biointerfaces**, v. 93, p. 226–34, maio 2012.

PARK, S. H. et al. Development of dual scale scaffolds via direct polymer melt deposition and electrospinning for applications in tissue regeneration. **Acta biomaterialia**, v. 4, n. 5, p. 1198–207, set. 2008.

PATEL, P. N. et al. Poly (ethylene glycol) hydrogel system supports preadipocyte viability, adhesion, and proliferation. **Tissue engineering**, v. 11, n. 9–10, p. 1498–1505, 2005.

PATEL-HETT, S.; D'AMORE, P. A. Signal transduction in vasculogenesis and developmental angiogenesis. **The International journal of developmental biology**, v. 55, p. 353, 2011.

PAUTKE, C. et al. Characterization of osteosarcoma cell lines MG-63, Saos-2 and U-2 OS in comparison to human osteoblasts. **Anticancer research**, v. 24, n. 6, p. 3743–3748, 2004.

PECK, M. et al. Tissue engineering by self-assembly. **Materials Today**, v. 14, n. 5, p. 218–224, 2011.

PELLEGATA, A. F.; TEDESCHI, A. M.; DE COPPI, P. Whole organ tissue vascularization: engineering the tree to develop the fruits. **Frontiers in Bioengineering and Biotechnology**, v. 6, p. 56, 2018.

PEPPAS, N. A.; MERRILL, E. W. Differential scanning calorimetry of crystallized PVA hydrogels. **Journal of Applied Polymer Science**, v. 20, n. 6, p. 1457–1465, 1976.

PHAM, Q. P.; SHARMA, U.; MIKOS, A. G. Electrospinning of polymeric nanofibers for tissue engineering applications: a review. **Tissue engineering**, v. 12, n. 5, p. 1197–1211, 2006.

PHNG, L.-K.; GERHARDT, H. Angiogenesis: a team effort coordinated by notch. **Developmental cell**, v. 16, n. 2, p. 196–208, 2009.

PIATTELLI, A.; SCARANO, A.; PAOLANTONIO, M. Bone formation inside the material interstices of e-PTFE membranes: a light microscopical and histochemical study in man. **Biomaterials**, v. 17, n. 17, p. 1725–1731, 1996.

QIAO, R.; BRINSON, L. C. Simulation of interphase percolation and gradients in polymer nanocomposites. **Composites Science and Technology**, v. 69, n. 3–4, p. 491–499, 2009.

RAI, R. et al. Synthesis, properties and biomedical applications of poly(glycerol sebacate) (PGS): A review. **Progress in Polymer Science**, v. 37, n. 8, p. 1051–1078, ago. 2012.

RENNO, A. C. M. et al. Effect of 830 nm laser phototherapy on osteoblasts grown in vitro on Biosilicate® scaffolds. **Photomedicine and laser surgery**, v. 28, n. 1, p. 131–133, 2010.

RENNO, A. C. M. et al. Characterization and in vivo biological performance of biosilicate. **BioMed research international**, v. 2013, 2013.

RESCIGNANO, N. et al. PVA bio-nanocomposites: a new take-off using cellulose nanocrystals and PLGA

nanoparticles. **Carbohydrate polymers**, v. 99, p. 47–58, jan. 2014.

RETZEPI, M.; DONOS, N. Guided bone regeneration: biological principle and therapeutic applications. **Clinical oral implants research**, v. 21, n. 6, p. 567–576, 2010.

REZWAN, K. et al. Biodegradable and bioactive porous polymer/inorganic composite scaffolds for bone tissue engineering. **Biomaterials**, v. 27, n. 18, p. 3413–3431, 2006.

RIDLEY, A. J. et al. Cell migration: integrating signals from front to back. **Science**, v. 302, n. 5651, p. 1704–1709, 2003.

RISAU, W.; FLAMME, I. Vasculogenesis. **Annual review of cell and developmental biology**, v. 11, n. 1, p. 73–91, 1995.

RODAN, G. A. **Introduction to bone biology**. [s.l.] Elsevier, 1992.

ROSE, F. R.; OREFFO, R. O. Bone tissue engineering: hope vs hype. **Biochemical and biophysical research communications**, v. 292, n. 1, p. 1–7, 2002.

ROUWKEMA, J.; KHADEMHOSSEINI, A. Vascularization and angiogenesis in tissue engineering: beyond creating static networks. **Trends in biotechnology**, v. 34, n. 9, p. 733–745, 2016.

ROUWKEMA, J.; RIVRON, N. C.; VAN BLITTERSWIJK, C. A. Vascularization in tissue engineering. **Trends in biotechnology**, v. 26, n. 8, p. 434–41, ago. 2008.

RUCKH, T. T. et al. Osteogenic differentiation of bone marrow stromal cells on poly(epsilon-caprolactone) nanofiber scaffolds. **Acta biomaterialia**, v. 6, n. 8, p. 2949–59, ago. 2010.

SAJESH, K. M. et al. Sequential layer-by-layer electrospinning of nano SrCO3/PRP loaded PHBV fibrous scaffold for bone tissue engineering. **Composites Part B: Engineering**, v. 99, p. 445–452, 15 ago. 2016.

SALEHI, S. et al. Generation of PGS/PCL Blend Nanofibrous Scaffolds Mimicking Corneal Stroma Structure. **Macromolecular Materials and Engineering**, v. 299, n. 4, p. 455–469, 1 abr. 2014.

SALGADO, A. J.; COUTINHO, O. P.; REIS, R. L. Bone Tissue Engineering: State of the Art and Future Trends. **Macromolecular Bioscience**, v. 4, n. 8, p. 743–765, 9 ago. 2004.

SANT, S. et al. Hybrid PGS–PCL microfibrous scaffolds with improved mechanical and biological properties. **Journal of tissue engineering and regenerative medicine**, v. 5, n. 4, p. 283–291, 2011a.

SANT, S. et al. Hybrid PGS–PCL microfibrous scaffolds with improved mechanical and biological properties. **Journal of Tissue Engineering and Regenerative Medicine**, v. 5, n. 4, p. 283–291, abr. 2011b.

SANT, S. et al. Effect of biodegradation and de novo matrix synthesis on the mechanical properties of valvular interstitial cell-seeded polyglycerol sebacate-polycaprolactone scaffolds. **Acta biomaterialia**, v. 9, n. 4, p. 5963–73, abr. 2013.

SARKAR, S. et al. Addressing thrombogenicity in vascular graft construction. **Journal of Biomedical Materials Research Part B: Applied Biomaterials**, v. 82, n. 1, p. 100–108, 2007.

SCHNEIDER, D. et al. A randomized controlled clinical multicenter trial comparing the clinical and histological performance of a new, modified polylactide-co-glycolide acid membrane to an expanded polytetrafluorethylene membrane in guided bone regeneration procedures. **Clinical oral implants research**, v. 25, n. 2, p. 150–158, 2014.

SCHOEN, B. et al. Electrospun Extracellular Matrix: Paving the Way to Tailor-Made Natural Scaffolds for Cardiac Tissue Regeneration. **Advanced Functional Materials**, v. 27, n. 34, 2017.

SCHROERS, M.; KOKIL, A.; WEDER, C. Solid polymer electrolytes based on nanocomposites of ethylene

oxide–epichlorohydrin copolymers and cellulose whiskers. **Journal of Applied Polymer Science**, v. 93, n. 6, p. 2883–2888, 2004.

SCHUURMAN, W. et al. Gelatin-methacrylamide hydrogels as potential biomaterials for fabrication of tissue-engineered cartilage constructs. **Macromolecular bioscience**, v. 13, n. 5, p. 551–561, 2013.

SEGAL, L. et al. An Empirical Method for Estimating the Degree of Crystallinity of Native Cellulose Using the X-Ray Diffractometer. **Textile Research Journal**, v. 29, n. 10, p. 786–794, 1959.

SHI, B. et al. The angiogenic behaviors of human umbilical vein endothelial cells (HUVEC) in co-culture with osteoblast-like cells (MG-63) on different titanium surfaces. **Dental Materials**, v. 30, n. 8, p. 839–847, 2014.

SHI, F. N.; NAPIER-MUNN, T. J. Estimation of shear rates inside a ball mill. **International Journal of Mineral Processing**, v. 57, n. 3, p. 167–183, 1999.

SHI, Q. et al. Mechanical properties and in vitro degradation of electrospun bio-nanocomposite mats from PLA and cellulose nanocrystals. **Carbohydrate polymers**, v. 90, n. 1, p. 301–8, set. 2012.

SHIN, H.; JO, S.; MIKOS, A. G. Biomimetic materials for tissue engineering. **Biomaterials**, v. 24, n. 24, p. 4353–4364, 2003.

SHIN, N. G. R. AND C. S. S. AND H. Current approaches to electrospun nanofibers for tissue engineering. **Biomedical Materials**, v. 8, n. 1, p. 14102, 2013.

SHIN, S. R. et al. Carbon Nanotube Reinforced Hybrid Microgels as Scaffold Materials for Cell Encapsulation. **ACS Nano**, v. 6, n. 1, p. 362–372, jan. 2012.

SIKAVITSAS, V. I.; TEMENOFF, J. S.; MIKOS, A. G. Biomaterials and bone mechanotransduction. **Biomaterials**, v. 22, n. 19, p. 2581–2593, 2001.

SILL, T. J.; VON RECUM, H. A. Electrospinning: applications in drug delivery and tissue engineering. **Biomaterials**, v. 29, n. 13, p. 1989–2006, maio 2008.

SIMÃO, J. A.; BELLANI, C. F.; BRANCIFORTI, M. C. Thermal properties and crystallinity of PCL/PBSA/cellulose nanocrystals grafted with PCL chains. **Journal of Applied Polymer Science**, v. 134, n. 8, 2017.

SIMIAN, M. et al. Effect of different microstructures of e-PTFE membranes on bone regeneration and soft tissue response: a histologic study in canine mandible. **Clinical oral implants research**, v. 10, n. 2, p. 73–84, 1999.

SIQUEIRA, G. et al. Thermal and mechanical properties of bio-nanocomposites reinforced by Luffa cylindrica cellulose nanocrystals. **Carbohydrate polymers**, v. 91, n. 2, p. 711–7, jan. 2013.

SMITH, M. K. et al. Locally enhanced angiogenesis promotes transplanted cell survival. **Tissue engineering**, v. 10, n. 1–2, p. 63–71, 2004.

SOHRABI, A. et al. A new design for electrospinner collecting device facilitates the removal of small diameter tubular scaffolds and paves the way for tissue engineering of capillaries. **Experimental Cell Research**, v. 347, n. 1, p. 60–64, 10 set. 2016.

SOLIMAN, S. et al. Controlling the porosity of fibrous scaffolds by modulating the fiber diameter and packing density. **Journal of Biomedical Materials Research Part A**, v. 96, n. 3, p. 566–574, 2011.

SRINIVASAN, R. Ablation of polymers and biological tissue by ultraviolet lasers. **Science**, v. 234, n. 4776, p. 559–565, 1986.

STAHL, A. et al. Bi-directional cell contact-dependent regulation of gene expression between endothelial cells and osteoblasts in a three-dimensional spheroidal coculture model. **Biochemical and biophysical research**

communications, v. 322, n. 2, p. 684–692, 2004.

STEVENS, M. M. Biomaterials for bone tissue engineering. **Materials today**, v. 11, n. 5, p. 18–25, 2008.

STOREY, R. F.; SHERMAN, J. W. Kinetics and mechanism of the stannous octoate-catalyzed bulk polymerization of ε-caprolactone. **Macromolecules**, v. 35, n. 5, p. 1504–1512, 2002.

SUN, B. et al. Advances in three-dimensional nanofibrous macrostructures via electrospinning. **Progress in Polymer Science**, v. 39, n. 5, p. 862–890, maio 2014.

TAMAYOL, A. et al. Fiber-based tissue engineering: Progress, challenges, and opportunities. **Biotechnology advances**, v. 31, n. 5, p. 669–87, jan. 2013.

TAMAYOL, A. et al. Hydrogel templates for rapid manufacturing of bioactive fibers and 3D constructs. **Advanced healthcare materials**, v. 4, n. 14, p. 2146–2153, 2015.

TAN, G. et al. Biomimetically-mineralized composite coatings on titanium functionalized with gelatin methacrylate hydrogels. **Applied Surface Science**, v. 279, p. 293–299, 2013.

TANG, D. et al. Biofabrication of bone tissue: approaches, challenges and translation for bone regeneration. **Biomaterials**, v. 83, p. 363–382, 1 mar. 2016.

TAYLOR, G. Electrically driven jets. **Proc. R. Soc. London, Ser. A**, v. 313, n. 1515, p. 453–475, 1969.

TEJEDA-ALEJANDRE, R. et al. Electrospinning Complexly-shaped, Resorbable, Bifurcated Vascular Grafts. **Procedia CIRP**, v. 65, p. 207–212, 2017.

TEO, W.-E.; INAI, R.; RAMAKRISHNA, S. Technological advances in electrospinning of nanofibers. **Science and technology of advanced materials**, v. 12, n. 1, p. 013002, 2011.

TEODORO, K. B. R. et al. Whiskers de fibra de sisal obtidos sob diferentes condições de hidrólise ácida: efeito do tempo e da temperatura de extração. **Polímeros**, v. 21, n. 4, p. 280–285, 2011.

THOMAS, V. et al. Mechano-morphological studies of aligned nanofibrous scaffolds of polycaprolactone fabricated by electrospinning. **Journal of Biomaterials Science, Polymer Edition**, v. 17, n. 9, p. 969–984, jan. 2006.

TIAN, H. et al. Biodegradable synthetic polymers: Preparation, functionalization and biomedical application. **Progress in Polymer Science**, v. 37, n. 2, p. 237–280, fev. 2012.

TIELENS, S. et al. Gelatin-based microcarriers as embryonic stem cell delivery system in bone tissue engineering: an in-vitro study. **Biomacromolecules**, v. 8, n. 3, p. 825–832, 2007.

TURNER, C. H.; WANG, T.; BURR, D. B. Shear strength and fatigue properties of human cortical bone determined from pure shear tests. **Calcified tissue international**, v. 69, n. 6, p. 373–378, 2001.

UNGER, R. E. et al. Tissue-like self-assembly in cocultures of endothelial cells and osteoblasts and the formation of microcapillary-like structures on three-dimensional porous biomaterials. **Biomaterials**, v. 28, n. 27, p. 3965–76, set. 2007a.

UNGER, R. E. et al. Tissue-like self-assembly in cocultures of endothelial cells and osteoblasts and the formation of microcapillary-like structures on three-dimensional porous biomaterials. **Biomaterials**, v. 28, n. 27, p. 3965–76, set. 2007b.

VAN DEN BULCKE, A. I. et al. Structural and rheological properties of methacrylamide modified gelatin hydrogels. **Biomacromolecules**, v. 1, n. 1, p. 31–38, 2000.

VATTIKUTI, R.; TOWLER, D. A. Osteogenic regulation of vascular calcification: an early perspective. **American Journal of Physiology-Endocrinology And Metabolism**, v. 286, n. 5, p. E686–E696, 2004.

VENUGOPAL, J. et al. Electrospun-modified nanofibrous scaffolds for the mineralization of osteoblast cells. **Journal of biomedical materials research Part A**, v. 85, n. 2, p. 408–417, 2008.

VILLARS, F. et al. Effect of human endothelial cells on human bone marrow stromal cell phenotype: role of VEGF? **Journal of cellular biochemistry**, v. 79, n. 4, p. 672–685, 2000.

VISSER, J. et al. Endochondral bone formation in gelatin methacrylamide hydrogel with embedded cartilage-derived matrix particles. **Biomaterials**, v. 37, p. 174–182, 2015.

WANG, M. et al. In vitro and in vivo study to the biocompatibility and biodegradation of hydroxyapatite/poly (vinyl alcohol)/gelatin composite. **Journal of Biomedical Materials Research Part A**, v. 85, n. 2, p. 418–426, 2008.

WANG, X.; DING, B.; LI, B. Biomimetic electrospun nanofibrous structures for tissue engineering. **Materials today (Kidlington, England)**, v. 16, n. 6, p. 229–241, jun. 2013.

WANG, Y. et al. A tough biodegradable elastomer. **Nat Biotech**, v. 20, n. 6, p. 602–606, jun. 2002.

WEINBERG, C. B.; BELL, E. A blood vessel model constructed from collagen and cultured vascular cells. **Science**, v. 231, n. 4736, p. 397–400, 24 jan. 1986.

WINKLER, T. et al. A review of biomaterials in bone defect healing, remaining shortcomings and future opportunities for bone tissue engineering: The unsolved challenge. **Bone & Joint Research**, v. 7, n. 3, p. 232–243, 2018.

WOODRUFF, M. A.; HUTMACHER, D. W. The return of a forgotten polymer—Polycaprolactone in the 21st century. **Progress in Polymer Science**, v. 35, n. 10, p. 1217–1256, out. 2010.

WU, W.; ALLEN, R. A.; WANG, Y. Fast-degrading elastomer enables rapid remodeling of a cell-free synthetic graft into a neoartery. **Nat Med**, v. 18, n. 7, p. 1148–1153, jul. 2012a.

WU, W.; ALLEN, R. A.; WANG, Y. Fast-degrading elastomer enables rapid remodeling of a cell-free synthetic graft into a neoartery. **Nat Med**, v. 18, n. 7, p. 1148–1153, jul. 2012b.

WU, Y. et al. Preparation of hydroxyapatite fibers by electrospinning technique. **Journal of the American Ceramic Society**, v. 87, n. 10, p. 1988–1991, 2004.

XIA, W.; ZHANG, D.; CHANG, J. Fabrication and in vitro biomineralization of bioactive glass (BG) nanofibres. **Nanotechnology**, v. 18, n. 13, p. 135601, 2007.

XIANG, C.; JOO, Y. L.; FREY, M. W. Nanocomposite fibers electrospun from poly(Lactic Acid)/cellulose nanocrystals. **Journal of Biobased Materials and Bioenergy**, v. 3, n. 2, p. 147–155, 2009.

XU, C. et al. Electrospun nanofiber fabrication as synthetic extracellular matrix and its potential for vascular tissue engineering. **Tissue engineering**, v. 10, n. 7–8, p. 1160–1168, 2004.

YAO, Q. et al. Three dimensional electrospun PCL/PLA blend nanofibrous scaffolds with significantly improved stem cells osteogenic differentiation and cranial bone formation. **Biomaterials**, v. 115, p. 115–127, 2017.

YI, F.; LAVAN, D. A. Poly(glycerol sebacate) Nanofiber Scaffolds by Core/Shell Electrospinning. **Macromolecular Bioscience**, v. 8, n. 9, p. 803–806, 9 set. 2008.

YIXIANG, D. et al. Degradation of electrospun nanofiber scaffold by short wave length ultraviolet radiation treatment and its potential applications in tissue engineering. **Tissue Engineering Part A**, v. 14, n. 8, p. 1321–1329, 2008.

YOSHIMOTO, H. et al. A biodegradable nanofiber scaffold by electrospinning and its potential for bone tissue

engineering. **Biomaterials**, v. 24, n. 12, p. 2077–2082, 2003.

YU, H. et al. Improved tissue-engineered bone regeneration by endothelial cell mediated vascularization. **Biomaterials**, v. 30, n. 4, p. 508–17, fev. 2009.

YUE, K. et al. Synthesis, properties, and biomedical applications of gelatin methacryloyl (GelMA) hydrogels. **Biomaterials**, v. 73, p. 254–271, 2015.

ZAMANIAN, B. et al. Interface-directed self-assembly of cell-laden microgels. **Small**, v. 6, n. 8, p. 937–944, 2010.

ZEIN, I. et al. Fused deposition modeling of novel scaffold architectures for tissue engineering applications. **Biomaterials**, v. 23, n. 4, p. 1169–1185, 2002.

ZHANG, D.; CHANG, J. Electrospinning of three-dimensional nanofibrous tubes with controllable architectures. **Nano letters**, v. 8, n. 10, p. 3283–3287, 2008.

ZHANG, Y. et al. Enhanced biomineralization in osteoblasts on a novel electrospun biocomposite nanofibrous substrate of hydroxyapatite/collagen/chitosan. **Tissue Engineering Part A**, v. 16, n. 6, p. 1949–1960, 2010a.

ZHANG, Y. et al. The proliferation and differentiation of osteoblasts in co-culture with human umbilical vein endothelial cells: an improved analysis using fluorescence-activated cell sorting. **Cellular & molecular biology letters**, v. 15, n. 4, p. 517, 2010b.

ZHAO, X.; LIU, R. Recent progress and perspectives on the toxicity of carbon nanotubes at organism, organ, cell, and biomacromolecule levels. **Environment International**, v. 40, p. 244–255, abr. 2012.

ZHOU, L. et al. Biomimetic mineralization of anionic gelatin hydrogels: effect of degree of methacrylation. **Rsc Advances**, v. 4, n. 42, p. 21997–22008, 2014.

ZOPPE, J. O. et al. Reinforcing poly(epsilon-caprolactone) nanofibers with cellulose nanocrystals. **ACS applied materials & interfaces**, v. 1, n. 9, p. 1996–2004, set. 2009a.

ZOPPE, J. O. et al. Reinforcing poly(epsilon-caprolactone) nanofibers with cellulose nanocrystals. **ACS applied materials & interfaces**, v. 1, n. 9, p. 1996–2004, set. 2009b.

ZUO, Y. et al. Photo-cross-linkable methacrylated gelatin and hydroxyapatite hybrid hydrogel for modularly engineering biomimetic osteon. **ACS applied materials & interfaces**, v. 7, n. 19, p. 10386–10394, 2015.